

# USAMBARA

Quiet Autonomous Aerial Surveillance  
System For Environmental Protection

*Spring DSE Group 11*

*Delft, June 21st 2022*

"If we can teach people about wildlife, they will be touched. Share my wildlife with me, because humans want to save things that they love."  
- Steve Irwin

# USAMBARA

## Quiet Autonomous Aerial Surveillance System For Environmental Protection

### DSE Group 11

June 21, 2022

<b>Last Name</b>	<b>Name</b>	<b>Student Number</b>
Chassagnette	Hugo	4770897
Compagne	Lars	4998537
Onorato	Lorenzo	4816455
Padrón Tardáguila	Mario	5007933
Slobbe	Matthijs	5051096
Staleman	Maxime	4843525
Domínguez Larrabeiti	Mikel	5003385
Levin	Nathan	5107873
Schellinx	Noa	5019060
Marín Petersen	Sergio	5073723

<b>Last Name</b>	<b>Name</b>	<b>Role</b>
Merino-Martinez	Dr. Roberto	Tutor
Solanki	Prashant	Coach
Freire Guimarães	Manoel	Coach

Cover image: Wallpaper Cave (URL:<https://wallpapercave.com/w/wp7161796>)

# Executive Overview

## Mission Definition

### Project Objectives

For the design synthesis exercise, the team has been tasked to design an unmanned aerial vehicle (UAV) to monitor natural reserves for poachers, wildfires, and litter. A mission need statement has thus been made for the exercise given. The mission need statement is:

***Protect and monitor the wildlife and environment with minimum disturbance and zero emissions.***

The objective of the project is:

***Design a zero-emissions, unmanned, autonomous aerial surveillance system to monitor wildlife and the environment with a team of ten students by June 21st, for a cost of less than 100,000 and 50,000 euros per vehicle and ground station respectively.***

An essential aspect of this project is sustainability, and the UAV design will thus take this into special consideration. As a case study, the UAV will fly in the Kruger National Park in South Africa, with multiple UAVs surveying an area of 50 km by 50 km.

### Requirements

The UAV has to be designed according to several requirements, which are divided into stakeholder and system requirements. From all requirements, some key requirements were identified which are of utmost importance to the design since they can drive the design to an unacceptable level (killer requirements), drive the design more than others (driving requirements), and bring high risks if not met (high-risk requirements), or are of particular importance to the stakeholder. No killer requirements were identified. The following driving requirements were identified:

- SYS-SUSN-01 - The system shall provide a noise reduction of 6 dB from commercially available drones at ground level (thus a noise output of 75dB)
- SYS-SUSM-01 - The UAV shall consist of 75% of recyclable or processable materials (excluding sensors)
- SYS-SUSEM-01 - The UAV shall not emit carbon oxides, nitrogen oxides, nor particulates during operation
- SYS-PER-03 - The UAV shall endure flights of at least 2hrs
- SYS-PER-05 - The system shall be able to reach any location within its monitoring zone in less than 2 minutes
- SYS-PER-06 - The UAV shall have a maximum take-off and landing distance of 25 m

The high risks requirements identified are:

- SYS-MAI-01 - The payload shall be easily replaceable by trained staff
- SYS-SUSEC-02 - In the case of an accident, the UAV shall not release polluting substances
- SH-PER-02 - The vehicle shall detect poachers in the National Park
- SYS-PER-08 - The UAV shall have a minimum range of 150 km
- SH-SR-01 - The system shall be able to avoid damage from poacher attacks

The requirements important to the stakeholder are identified to be:

- SH-BU-01 - Each aerial vehicle shall cost less than 100,000 euros
- SH-BU-02 - Each ground station shall cost less than 50,000 euros
- SH-PER-01 - The vehicle shall detect wildfires in the National Park
- SH-PER-02 - The UAV shall detect poachers in the National Park
- SH-PER-03 - The vehicle shall identify litter in the National Park
- SYS-SUSN-01 - The system shall provide a noise reduction of 6dB compared to commercially available

drones at ground level (thus a noise output of 75dB)

- SYS-SUSEM-01 - The UAV shall not emit carbon oxides, nitrogen oxides, nor particulates during operation

The product will be verified and validated such that all requirements are met. The product will be verified using four methods: inspection, demonstration, test, and analysis. The validity of all requirements has also been checked. This was done using the VALID method, checking if each requirement is verifiable, achievable, logical, integral, and definitive. It was found that all requirements are indeed valid.

## Sustainable Development Strategy

Since sustainability is crucial during this project, a sustainable development strategy has been made. This strategy ensures that sustainability is accounted for during the UAV and ground station design. The focus of the sustainable development strategy are the goal 7 (affordable and clean energy), goal 13 (climate action), and goal 15 (life on land) of the sustainable development goals as defined by the United Nations<sup>1</sup>. Sustainability is measured in three objectives: economic, environmental, and social sustainability.

The economic objectives defined are:

- Jobs for local authorities need to be created and be fairly paid
- Variable costs need to be as low as possible
- Cheap renewable energy sources need to be used for low operational costs
- Material costs need to be low
- End-of-life costs must be as low as possible
- The system must be universal
- Good project management and system engineering must be used to keep development costs low

The environmental objectives are:

- Renewable energy must be used
- The renewable energy must be produced locally
- The production of energy must cause minimum harm to the surrounding environment
- A certain amount of the UAV material must be of recyclable material
- Material of the UAV should not be toxic to the environment
- The noise level produced by the UAV must be constrained

The social objectives are:

- Local authorities and residents must control and reduce the detected poachers, wildfires, and litter
- Local residents must be educated on the risks of poaching, wildfires, and littering

## Design Concept Selection

During the midterm report a UAV configuration has been chosen. Four configurations have been investigated:

- N-copter
- Fixed-wing propeller UAV
- Fixed-wing VTOL UAV
- Fixed-wing turbojet UAV

Two different propulsion methods have also been investigated for the N-copter, fixed-wing propeller UAV, and the fixed-wing VTOL UAV, namely hydrogen fuel cells and batteries. A trade-off has been done for these configurations using the Analytical Hierarchy Process (AHP), using the selection criteria of cost, Reliability, Availability, and Maintainability (RAMS), performance, and sustainability. For each configuration, their design characteristics were examined, a market research was done, and their reliability was investigated. The trade-off was won by the fixed-wing VTOL UAV powered by a hydrogen fuel cell, and this configuration was thus chosen to be further designed in this report.

---

<sup>1</sup>URL: <https://sdgs.un.org/goals> [03/05/2022]

## Design Methodology and Iterative Design Structure

To design the configurations chosen for the UAV, the group was divided into eight design groups: payload sizing, operation and logistics, aircraft configuration, aerodynamic design, stability and controllability, propulsion and power systems, noise considerations, and structural design. An N2 chart has been made to ensure a smooth working between the design groups and to ensure all variables needed for the final design iteration loop are determined.

### Payload Sizing

In order to perform the mission of the UAV, it needs to have a payload. Components whose mass or function do not change with the UAV design and configuration are considered payload. Cameras are needed to detect the poachers, wildfires, and litter in the area. An autopilot is needed to let the UAV fly autonomously. The chosen autopilot includes accelerometers, gyroscopes, and magnetometers to determine the orientation of the UAV and includes GNSS and a pitot-static system to determine the position of the UAV. LiDAR sensors will also be equipped to sense and avoid nearby objects.

Additional equipment is needed for the UAV to communicate with the ground station. The UAV has to transmit a livestream of the footage taken by the cameras to the ground station. This livestream has a bit rate of 20.38 Mbps. The location of the UAV will also be transmitted to the ground station, which has a bit rate of about 1.023 Mbps. A transceiver was chosen to transmit these signals. The UAV and the ground station will be equipped with this transceiver, so they can both transmit and receive signals from one another. The transceiver will need antennas to help transmit and receive signals to the ground station. Since the chosen transceiver uses Multiple-Input and Multiple-Output (MIMO) technologies, two antennas will be equipped to the UAV, as well as an antenna that receives GNSS signals.

A collision with a bird poses a significant risk for the UAV since it may mean the end of its life and mission. Therefore, the UAV will be equipped with a speaker which will produce sounds of predators and two Passive Infrared (PIR) sensors. If the PIR sensors sense that a bird is approaching, the speaker will turn on and produce sound. These sounds will scare away the birds and avoid a collision.

All the payload and sensors that will be equipped to the UAV are stated in Table 1, this also includes the costs, mass, power consumption, and sizes of the payload.

**Table 1:** Budget for the payload and sensors that will be equipped on the UAV.

Sensor type	Mass [kg]	Power consumption [W]	Cost [Euro]	Size [mm]
Camera & long range LiDAR <sup>1</sup>	0.88	45	~ 15,000	161 x 178 x 135
Short range LiDAR <sup>2</sup>	0.9	16	~ 8,100	87 x 103 dia
Bird repellant speaker <sup>3</sup>	0.15	10	~ 90	68 x 55 x 65
PIR <sup>4</sup>	-	0.034	~ 40	20 x 25 x 25
Autopilot <sup>5</sup>	0.19	5	~ 5,800	63 x 67.9 x 39.6
GNSS antenna <sup>6</sup>	0.1	0.29	~ 200	15 x 57 dia
Transceiver <sup>7</sup>	0.09	10	3,000	90.5 x 70.7 x 18.2
Antenna (2x) <sup>8</sup>	0.05	-	~ 9	L: 195
<b>Total</b>	2.36	86.3	~ 32,250	-

### Operation and Logistics

The logistics and operations are defined for the UAV to assess how the UAV will operate during its mission. First, it was determined that the UAV would fly in the Kruger National Park as a case study. The climate of this park defines the temperature at which the UAV has to operate. Due to this climate, the UAV must also be cleaned during each flight due to the dust in the area. Second, the mission profile of the UAV has been

defined. After start-up, the UAV will take-off vertically to 50 m with a rate of climb (ROC) of 3 m/s. Then it will climb further to its cruise altitude of 600 m using its fixed wings. When the cruise altitude is reached, the UAV will further monitor the area at a cruise speed of 22 m/s. The cruise altitude was constrained to a minimum of 120 m and a maximum of 855 m. This maximum constraint is set by the quality of the chosen camera and the number of pixels a poacher must have to be detected, equal to 30 pixels. Once this surveillance is done, it will fly back to the ground station, slow down to stall speed, and then land vertically with a rate of descent of 2 m/s. During cruise, the UAV will fly in a zigzag pattern in order to monitor the whole area. The distance that the UAV has to cover to monitor this area is dependent on the swath width of the narrow-angle thermal camera at the cruise altitude, equal to 272 m. To surveil an area of 35.3 km<sup>2</sup>, the UAV will have to fly for 101.3 minutes.

The general layout and refueling operation have also been defined. The ground station is composed of an elevated platform with two hinged hatches that open when the UAV returns to the ground station or leaves it. Once the UAV has returned to the ground station, it must be refueled. The platform the UAV lands on in the ground station is rotatable. Due to several sensors, the UAV will be correctly positioned to align with the refueling pipe. This pipe will come out and connect with the UAV using a quick disconnect. Due to the pressure difference in the onboard hydrogen tank of the UAV and the hydrogen storage tank of the ground station, the tank of the UAV will be refueled.

## Aircraft Configuration

During the midterm report, a trade-off was performed and it was decided that the UAV would be a VTOL hydrogen fuel cell (HFC) powered fixed-wing UAV. However, a configuration of the geometric design layout still needed to be chosen. Four options were considered for this configuration:

- Conventional configuration
- Blended wing body
- Canard configuration
- Twin-boom configuration

From these configurations, it was chosen that the UAV will have a twin-boom configuration. The fuselage shape of the UAV was based on the housing of the hydrogen tank, payload, and parasitic drag. The hydrogen tank will be located within the fuselage; this is beneficial for the aerodynamics, reduces noise production, and is safer since the tank is not exposed to the environment.

For the tail, four commonly used tail configurations for UAVs have been analyzed. These tail configurations are:

- Inverted U-shape
- U-shape
- Inverted V-shape
- Semi-inverted V-shape

Each tail configuration has been analyzed based on lift, critical angle, stability, and maneuverability performance. The analysis found that the most convenient tail configuration for the UAV is the inverted U-shape. This tail configuration performed well in the lift force and longitudinal stability. In the other categories, it performed above or on average. However, it should be noted that this tail configuration does not have very good directional and lateral stability.

A trade-off of the placement of the wing has been made. Three wing placements configurations have been considered:

- High wing
- Mid wing
- Low wing

The placement of the wing heavily affects the stability, aerodynamic performance, and RAMS of the UAV. The high wing performs best in stability RAMS, while in aerodynamic performance, the low wing config-

uration is best and the high wing the worst. Regarding all these aspects, the high wing configuration was determined to be the best for the UAV and will thus be chosen.

Four configurations have been considered for the UAV to handle the transition between vertical take-off and landing to forward flight. These configurations are:

- Tilt-rotor
- Tilt-wing
- Tail-sitter
- Dual-system

The dual-system VTOL configuration will be used for the design because of its simplicity and reliability.

## **Aerodynamic Design**

The wing must be sized to ensure the UAV produces sufficient lift during its mission. Besides this, the characteristics of the wing influence the drag, stability, and structural weight of the UAV as well. The preliminary sizing began with estimating the wing loading, which was found to be  $129 \text{ N/m}^2$ . The desired lift coefficient at cruise could be determined from this wing loading. This lift coefficient was the basis for selecting an airfoil for the wing. The airfoil was selected from a vast database of available airfoils. The NACA 64<sub>2</sub>-415 was selected; this airfoil suits the mission requirements and was chosen over other airfoils within its family due to its higher lift coefficient, lift-to-drag ratio, and stall speed.

After the airfoil was selected, the geometry of the wing was defined. This geometry is mainly influenced by the aspect ratio and the taper ratio, which were set to 6 and 0.6 respectively. The aspect ratio influences the lift-to-drag ratio, the maximum lift coefficient of the wing, the UAV's lateral and longitudinal stability, and the wing's structure. The taper ratio's function is mainly to simulate elliptical lift distribution, which produces the least induced drag. Besides the aspect ratio and taper ratio, the sweep of the wing at a quarter chord was set to zero. This was decided since the speed of the UAV does not exceed Mach 0.3, and no sweep is thus needed to delay drag created by shock waves. The surface area of the wing was determined by the wing loading, and using this surface area, the taper ratio, aspect ratio along the span, root chord, and tip chord of the wing could be established as well as the location of the mean aerodynamic chord (MAC).

The tail of the UAV has also been sized. The purpose of the tail is to provide static and dynamic and lateral and longitudinal stability. For the design of the tail, an airfoil was selected. A symmetric airfoil is desired since the design lift coefficient should be able to change based on the configuration. Based on stall angle, stall behavior, maximum lift coefficient, and lift-to-drag ratio, it was chosen that the NACA 0015 will be used as airfoil for both the horizontal and vertical tails. Besides the airfoil, it was chosen that the sweep at the quarter chord will be zero, like the main wing. Since an inverted U-tail was chosen, the tips chords of the vertical and horizontal tails must be equal; this influences the choice of taper ratio of the tail. There is also no structural reason to implement taper for the horizontal tail and the uneven downwash distribution is reduced due to the vertical tail acting as winglets. Due to these reasons, it was chosen that the horizontal tail will have a taper ratio of 1. The aspect ratios of the tail were sized according to recommendations in literature. The aspect ratio of the horizontal tail will be 6 and the aspect ratio of the vertical tail will be 1.3.

## **Stability & Controllability Design**

The tail design is an essential part of the design that will define and controllability of the UAV during forward flight. The center of gravity of the UAV will not change much during its flight since the payload is fixed to the UAV. The only mass that changes during the flight is the hydrogen that is being used. The tail surface area was plotted against the center of gravity location along the mean aerodynamic chord (MAC) of the wing, as seen in Figure 1. With this plot, the surface area of the horizontal tail could be selected, which would make the UAV both stable and controllable.

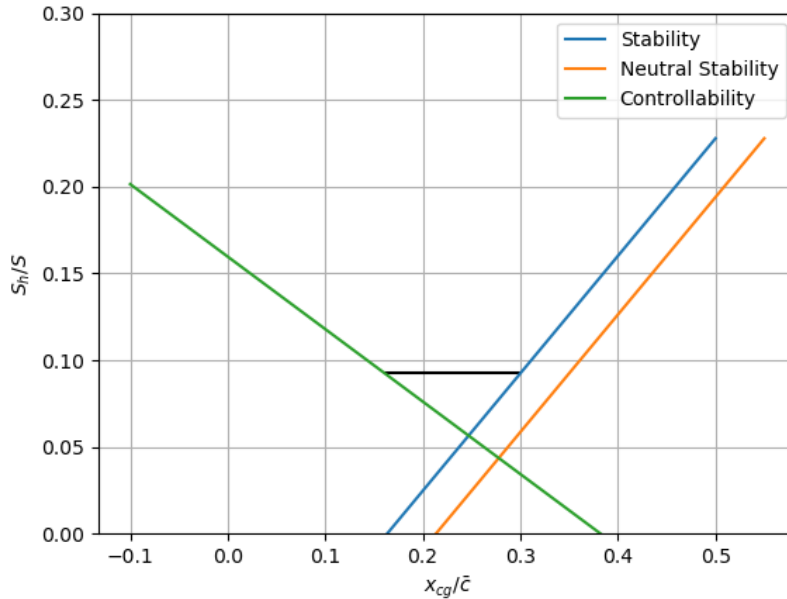


Figure 1: UAV controllability and stability scissor plot

The ailerons were sized so that the UAV could roll along its longitudinal axis. Since the UAV has to surveil natural reserves, it is not required to do aggressive movements or sudden maneuvers during normal operations, and thus the ailerons were designed only to fulfill the basic requirements. These basic requirements are set by the category the UAV is in, which is class II, which are medium weight aircraft. The roll requirement for this class is to bank 45 degrees in 1.4 seconds.

## Propulsion and Power Systems Design

The UAV has to be powered to ensure it can fly during its mission. The power required by the rotors and the thrust needed to be generated by the rotors has been determined for each flight stage. These flight stages are vertical take-off, forward climb, cruise, sprint (which is flying at max speed), hovering, and vertical landing. From the determined thrust that needs to be generated, the propellers were sized. The amount of thrust a propeller generates is dependent on the diameter, the pitch, and the number of rotations per minute (RPM) of the propeller. The diameter and pitch are fixed once a propeller is chosen, but the RPM can be changed throughout the flights, so the thrust can be varied according to the flight stage the UAV flies in at that moment. Once the propellers were sized, their position was determined. The propellers were positioned just so that they do not collide with each other or with the main wing or horizontal tail wing, a clearance of 0.1 m was also used as a safety margin. From the determined power that the UAV requires during flight and the power required by the payload, the energy was calculated that the UAV uses during one flight. With this energy, the hydrogen tank was sized using the low heating value (LHV) of hydrogen, the efficiency of the hydrogen fuel cell (HFC), and the ideal gas law. Lastly, the fuel cell that will produce the electricity from the hydrogen was selected to support the power required by the UAV.

## Noise Considerations

Unwanted sounds produced by the UAV must be limited to avoid disturbing wildlife. The sound produced by the UAV will be analyzed using the Sound Pressure Level (SPL). With this analysis, the UAV was assumed to be a point source for sound, meaning the wavefronts are spheres. During the analysis, propeller noise was considered, the effect due to wind was left out, and the airframe noise was assumed to be negligible. The propellers produce a significant amount of noise due to their high rotational speeds and their size. Propellers produce two types of noise: broadband and tonal noise. However, only tonal noise was analyzed for the propellers since this is the main component of noise produced by the propellers. For the analysis,

it was assumed that the data used to assess the disturbance of humans applies to animals as well, an A weighting was used for this. The distance to the observer and the atmospheric absorption were addressed as factors that could decrease the noise of the propellers. It is desired that during cruise the noise generated is less than 35 dB measured at the ground. This is desired since the ambient background noise in the area at night is also 35 dB on average<sup>2</sup>. During take-off and landing, the noise produced by the propellers will be the largest. To take this into account, the sound exposure level has been calculated to estimate the effect on wildlife.

## Structural Design

For the structure of the UAV, a material has been selected. This material supports the critical load cases the wing is subjected to and is desired to be lightweight. Recyclability must also be considered when selecting a material to meet the requirement that states that 75% of the UAV shall be recyclable. It was chosen that the entire airframe of the UAV will be made of only one material to simplify the design process, decrease manufacturing costs, and allow ease of recyclability. Due to recyclability reasons, aluminum alloys were chosen over carbon fiber reinforced polymers (CFRPs). Al6061 has been chosen to be used as the material for the airframe due to its corrosion and fatigue resistance while still providing enough strength to withstand the loads. The properties of the Al6061 are stated in Table 2.

**Table 2:** Material properties of Al6061.

Al Alloy	$\rho$ [kg/m <sup>3</sup> ]	$\sigma_y$ [MPa]	E [GPa]
6061	2710	325	70

The loads present on the wing and tail during flight must be carried by the structure of the wing and tail. A wing box has been sized to carry these maximum stresses, primary failure modes, and loads that occur during VTOL and forward flight. A simple rectangular wing box was designed to carry these loads. This wing box contains thick rectangular spars to carry bending loads, ribs to help prevent buckling of the skin, and a single stringer to reduce torsional deformation.

## Iterative Design Process

The calculations performed by the various subsystem design departments have been integrated into one Python script to perform an iteration to find the best final design of the UAV that meets the requirements. The values that were used by the individual departments as constants have been put into one file, and these were used as the inputs for the iteration. The Python script was looped until the weight of the UAV did not change more than 0.01% from iteration to iteration.

The models made in Python to facilitate the iteration process have been verified and validated. For verification of the code, inspection and analysis have been used. For inspection, the formulas and their inputs were checked by the person who made the code. For analysis, the models were reproduced on paper to ensure the correct implementation of the equations. The primary method used for verification was the use of unit tests; a separate file for unit testing was created to verify each function independently. To validate the model, the results obtained were compared to verified data from tests or independent models. Sanity checks were also done throughout the making of the model. Finally, once the data of the final design was known, this data was compared with known correct data.

A sensitivity analysis was performed on two different levels; by changing the initial conditions or by changing other parameters. With this analysis, it was found that the code would produce a convergent design for all the tested conditions below an initial mass below 22 kg. It does not converge for higher initial masses. The power required for masses above 22 kg is very high, and the fuel cell selected does not allow for any more decrease in weight. For a second analysis, the parameter of power was changed. It was found that a

<sup>2</sup>URL: <https://www.airbonedrones.co/drone-noise-levels/> [15/06/2022]

slight change in the power can lead to a significant change in mass and even to divergence.

## Complete Final Design

At the end of the iteration process, a converged final design was achieved. The most important final design values of the UAV are stated in Table 3.

**Table 3:** Most important final values of the UAV design

Parameter	Value [unit]
S	1.3 [m <sup>2</sup> ]
b	3.2 [m]
S <sub>h</sub>	0.12 [m <sup>2</sup> ]
b <sub>h</sub>	0.84 [m]
d <sub>VTOL</sub>	0.8 [m]
d <sub>cruise</sub>	0.5 [m]
Diameter H2 tank	0.143 [m]
Length H2 tank	0.546 [m]
SPL at cruise distance using cruise propellers	27.249 [dBA]
Total mass	16.85 [kg]
Total power required	541.67 [W]

Most of the UAV parts will be produced from AI6061 sheets that will have to be cut to the correct dimensions before being bent into the right shape. The ribs of the UAV will be produced using punching and deep drawing, while for the complex shapes, casting will be used. The parts and structures of the UAV are assembled together using welding, soldering, riveting, and bonding.

The performance of the final UAV has been analyzed to also check if some design requirements are met. These performance parameters are stated in Table 4 and Table 5.

**Table 4:** Maximum and minimum performance considerations.

Parameter	Value [unit]
max range	160 [km]
max endurance	2:30 [hr:min]
max speed	26.4 [ms]
max operative ceiling <sup>1</sup>	840
max surface covered per flight	35 [km <sup>2</sup> ]
max flights per day <sup>2</sup>	11 [-]
max $w_{ct}$ at $h_{cruise}$	277 [m]
min $w_{ct}$ at $h_{cruise}$	38 [m]
max $w_{ct}$ at 120 m	54 [m]
min $w_{ct}$ at 120 m	8 [m]
min px swath width $h_{cruise}$ <sup>3</sup>	0.06 [m]
max $px_{pp}$ at $h_{cruise}$	196 [-]
min SPL at max ceiling	24 [dBA]
max SPL at sl	91 [dBA]

<sup>1</sup> In order to still be able to provide more than  $px_{pp}$ ;

<sup>2</sup> for a single drone;

<sup>3</sup> ground width that each pixel covers;

**Table 5:** Regular flight performance data.

Parameter	Value [unit]
operative range	160 [km]
operative endurance	2 [hr]
cruise speed	22.22 [m]
$h_{cruise}$	610[m]
surface covered per flight	35 [km <sup>2</sup> ]
flights per day	8 [-]
operative swath width	38 [m]
operative px swath width	0.06 [m]
SPL at $h_{cruise}$	27 [dBA]
$px_{frame}$	1920 x 1080 [-]
drone number for surveilled area <sup>1</sup>	18 [-]

<sup>1</sup> Number of drones required to cover a 50x50 area as stated in the requirements.

## **RAMS**

To ensure a reliable UAV, it was chosen to design a simple UAV since complex systems have a higher chance of failure. Besides this, specific components were oversized in order to assure superior reliability. To ensure the availability of the UAV, it was designed for the harsh environmental condition of the Kruger National Park. To reduce the environmental impact on the UAV and its mission, the ground station will serve as a shield for the UAV. For easy maintenance, the UAV has a modular design to make it simple to change smaller portions of the UAV when necessary. For the safety of the environment special attention has been paid to the noise and emissions generated by the UAV; these have been minimized. To reduce the risk of crashing or hurting wildlife, the stability was prioritized over the maneuverability.

## **Compliance matrix**

To check that the final design meets all the requirements, a compliance matrix was made. All requirements that could be analyzed at this point were met. However, for some requirements, the UAV has not been tested or no complete analysis could be made at this stage of the design. The requirements that could not be tested or completely analyzed are:

- SYS-MOV-06 The UAV shall be flight dynamically stable through control mechanisms
- SYS-SR-01 The system shall abide by the relative EASA regulations
- SYS-SR-02 The system shall be 90% reliable for 500 hours of operational time
- SYS-MAI-01 The payload shall be easily replaceable by trained staff

## **Post design risks**

All the post-design risks have been identified and assessed based on their likelihood and estimated impact on the UAV. For the risks that are medium-high or medium risks, a mitigation strategy has been developed. The medium-high risks and medium risks identified are

- R-OP-02 Maintenance is not performed correctly
- R-PRO-03 Off-the-shelf parts are not available
- R-OP-01 Maintenance is not performed regularly
- R-PRO-01 Production falls behind
- R-OP-05 Failed delivery of hydrogen to the ground station
- R-EX-02 Demand is overestimated
- R-PRO-02 Aluminum price increases

With a mitigation strategy for each of these risks, the likelihood or impact of the risks was reduced. With this, the risks have been reduced to medium-low or even low risks.

## **Economic Considerations**

### **Market Analysis**

A market analysis has been done to have a good understanding of the market the UAV is competing in. UAVs could be used for multiple applications. There are ones available for logistics, public safety, consumer use, enterprises, and to use for defense. The to-be-designed UAV will monitor natural reserves and will thus have to compete with other UAVs that are used for public safety. In this specific field of applications, various types of UAVs are already on the market: vertical take-off and landing (VTOL), fixed-wing UAVs, and multicopters. The performance of these types differs in cruise speed and endurance. Since drag increases significantly for a multicopter design at high speeds, more battery mass is needed, significantly increasing its total mass. Therefore, only fixed-wing and VTOL UAVs are selected for more considerable distances and higher cruise speeds. The leading competitor that has a cruise speed and an endurance that meets the requirements set for the to-be-designed UAV is the Helvetis VTOL UAV that runs on fuel. However, this product is not yet commercially available. The other UAVs that are in the market do not meet the requirements for cruise

speed and endurance that have been set for the to-be-produced UAV; this indicates that the technology is not sufficiently mature yet.

The current market share for UAVs is the largest in North America and Asia. These two continents make up two-thirds of the global market share. It is estimated that this share, which was 18 billion US dollars in 2020, will more than double by 2030 and that the market share of UAVs used for public safety will grow from 0.7 billion US dollars in 2020 to 5 billion US dollars in 2030. Additionally to the market share, three potential customers were identified: natural parks, the government, and non-profit organizations.

## Cost Analysis

The development and manufacturing costs of the UAV design have been estimated based on known prices of the subsystems and unit costs estimations based on data of the Boeing 777-200. These costs are stated in Table 6.

**Table 6:** Final development and manufacturing cost breakdown for the UAV

	Development costs [EUR]	Manufacturing costs [EUR]	Purchase price [EUR]
Wing	~165,000	~ 12,250	-
Empennage	~82,000	~ 6,400	-
Fuselage	~23,000	~ 800	-
Landing gear	~2,500	~ 160	-
Systems	~ 2,200	~ 40	-
Final assembly	-	~ 3,200	-
Payload	-	-	~ 32,000
Propulsion	-	-	~2,200
Power	-	-	12,600
<b>Total</b>	<b>~ 274,700</b>	<b>22,850</b>	<b>47,000</b>
<b>Grand total</b>	<b>274,700</b>	<b>69,850</b>	

## Return on Investment

The return on investment has been based on the product of one UAV and one ground station and has been established using the market price, the market volume, the achievable market share, the development costs, the production cost, and the operational cost. The market price of one UAV and ground station is 100,000 and 50,000 euros respectively. The market volume and share are stated in Table 7. The return on investment is stated in Table 8.

**Table 7:** Products to be sold

Estimation future product sold	
Market volume	422
Market share	9.1%
Estimate of to be sold products	38 products

**Table 8:** Return on Investment

Return on Investment	
Sold products	38
Market price per product	100,000 euro
Total price for sold products	3,800,000 euro
Total investment cost	€2,929,000
<b>Return on Investment</b>	<b>29.7%</b>

# Summary

Current methods for monitoring and protecting wildlife and the environment have consistently proven insufficient. National parks and wildlife reserves worldwide have experienced an ever-increasing number of species driven to the brink of extinction and their habitats ruined. At a number of these parks, animals are poached with impunity despite the severe consequences which are typical. A large part of the reason for this is that park rangers are overburdened, limiting the area they can surveil. This report discusses the design of an unmanned aerial vehicle (UAV) which aims to complement the deployment of park rangers by providing autonomous surveillance for the detection of poachers, wildfires, and litter. A single UAV is capable of covering a 35 km<sup>2</sup> area in a single flight, and flying 8 missions daily, vastly expanding the area which can be protected. In order to minimize the impact of these UAVs, low-noise and zero-emissions concepts were designed. Out of a number of feasible concepts, a hydrogen-powered fixed wing VTOL (vertical take-off and landing) aircraft was chosen for its superior performance in the context of an extended endurance autonomous mission. This report contains the design methodology for the six design groups which comprise the final detailed design: the aircraft configuration, aerodynamic design, stability and controllability design, propulsion and power system design, noise considerations, and structural design.

Extensive analysis and trade-offs are performed within the context of hydrogen-powered fixed wing VTOL aircraft to provide a viable design that meets numerous requirements on performance aspects in varied categories such as range, noise, and UAV reliability. A detailed trade-off was performed for the overall aircraft, fuselage, empennage, and wing configurations. Next, an airfoil was sized for both the wing and tail to achieve efficient cruise flight and stable operations. Afterward, the sizing of the wing and parameters such as the aspect ratio, taper ratio, and additional wing dimensions are given with optimal lift and minimum drag in mind. Additionally, a stability and controllability analysis ensures the UAV can recover from minor disturbances and can perform the transition from VTOL flight mode to forward flight mode autonomously. Included is the static stability and control of the UAV, as well as the aileron sizing for the aircraft's maneuverability.

The aircraft is designed with a mission requirement of two hours of flight without refueling while producing zero emissions. A hydrogen fuel cell provides power to the aircraft. By determining the power and duration of each stage of the mission profile, the total energy needs and peak power of the UAV are estimated, and a lightweight hydrogen fuel cell and tank are chosen accordingly. Moreover, to minimize the disturbance of UAV operation on the wildlife it seeks to protect, the noise of the UAV was minimized throughout the design. An extensive literature review on this subject was done to provide insight into the mechanisms of noise and the impact UAV sound may have on wildlife. Finally, the UAV design is concluded with a structural design and analysis. This includes the material selection, which is driven by a requirement mandating the structure is 75% recyclable by weight. Additionally, the loads and stresses on the wing and tail are analyzed, which results in a weight-efficient wing box design.

These six systems share a number of design inputs and outputs. The final configuration, therefore, resulted from an iterative process, where the interdependencies between groups flowed between systems until the UAV design converged. This process required substantial optimization of each system to reach a feasible concept. A final take-off weight, wing and tail dimensions, selection of an off-the-shelf hydrogen tank, hydrogen fuel cell sizing, estimates of noise, and the wing structural components were produced in the final design which resulted. Additionally, the report presents the payload sizing for a dual thermal and optical camera system to enable autonomous surveillance. The operations and logistics of the surveillance mission are also discussed, with a detailed explanation of the ground station provided. Lastly, the economic feasibility of the design is analyzed. The final concept, USAMBARA, provides an effective platform for the aerial monitoring and protection of wildlife, offering autonomous, scalable, surveillance capabilities with the potential to act as a vital tool in the fight to protect endangered species and their environments.

# Nomenclature

## Abbreviations

---

ACAI	Available Control Authority Index	NGO	Non-Governmental Organization
AHP	Analytic Hierarchy Process	OSPL	Overall Sound Pressure Level
BPF	Blade-passing Frequency	PIR	Passive Infrared
BPP	Bits Per Pixel	RAMS	Reliability, Availability, Maintainability, and Safety
CFRP	Carbon Fiber Reinforcer Polymers	ROI	Return On Investment
CI	Consistency Index	RTK	Real-Time Kinematic
COPV	Composite Overwrapped Pressure Vessel	SEL	Sound Exposure Level
CR	Consistency Rate	SPL	Sound Pressure Level
CTT	Collective Thrust Transition	SPOT	Systematic POacher deTector
DSE	Design Synthesis Exercise	STOL	Short Take-Off and Landing
DTT	Differential Thrust Transitioning	SWOT	Strengths, Weaknesses, Opportunities and Threats
EO	Electro-Optical	TRL	Technology Readiness Level
FPS	Frames Per Second	UAV	Unmanned Aerial Vehicle
GFRP	Glass Fiber Reinforced Polymers	US	United States
HFC	Hydrogen Fuel Cell	VTOL	Vertical Take-Off and Landing
IR	Infrared	WAO	Wide Angle Optical
ISA	International Standard Atmosphere	WATH	Wide Angle Thermal
MAC	Mean Aerodynamic Chord	WOT	Wide-Open Throttle
MAI	Manufacturing, assembly, and integration	WWF	World Wide Fund
MIMO	Multiple input multiple output		
MTT	Mono Thrust Transition		
MTOW	Maximum Take-Off Weight		
NAO	Narrow Angle Optical		
NATH	Narrow Angle Thermal		

## Symbols

---

Symbol	Definition	Unit
A	Surface area	m <sup>2</sup>
AR	Aspect ratio	-
AR <sub>h</sub>	Aspect ratio horizontal tail	-
AR <sub>v</sub>	Aspect ratio vertical tail	-
b	Wingspan	m
b <sub>h</sub>	Horizontal tail span	m
b <sub>v</sub>	Vertical tail span	m
c	Chord	m
$\bar{c}$	Mean aerodynamic chord	m
c <sub>r</sub>	Root chord	m
c <sub>r<sub>h</sub></sub>	Horizontal tail root chord	m
c <sub>r<sub>v</sub></sub>	Vertical tail root chord	m
c <sub>t</sub>	Tip chord	m
c <sub>t<sub>h</sub></sub>	Horizontal tail tip chord	m
c <sub>t<sub>v</sub></sub>	Vertical tail tip chord	m
C <sub>D</sub>	Drag coefficient	-
C <sub>D0</sub>	Zero lift drag coefficient	-
C <sub>l</sub>	2D lift coefficient	-
C <sub>l<sub>i</sub></sub>	Ideal 2D lift coefficient	-

Symbol	Definition	Unit
$C_{l_{max}}$	Maximum 2D lift coefficient	-
$C_L$	Lift coefficient	-
$C_{Lc}$	Lift coefficient at cruise	-
$C_{Lc_w}$	Lift coefficient of wing at cruise	-
$C_{L_\alpha}$	Lift coefficient gradient	-
$C_m$	Moment coefficient	-
$C_{m,ac}$	Moment coefficient around aerodynamic center	-
$C_{m,cg}$	Moment coefficient around center of gravity	-
$C_{m_\alpha}$	Moment coefficient gradient	-
$C_N$	Normal force coefficient	-
$C_{N_\alpha}$	Normal force moment coefficient	-
$d$	Diameter	m
$d_{VTOL}$	VTOL propellers diameter	m
$d_{cruise}$	Cruise propellers diameter	m
DL	Disk loading	N/m <sup>2</sup>
E	Young's modulus	GPa
e	Oswald efficiency factor	-
FM	Figure of Merit	-
FOV	Field of View	deg
h	Altitude	m
$h_{cruise}$	Cruise altitude	m
I	Moment of inertia	mm <sup>4</sup>
$I_{xy}$	Second moment of area	mm <sup>4</sup>
$K_s$	Safety factor	-
$K_c$	Thin-sheet buckling coefficient	-
l	Length	m
$L_{DN}$	Day-night exposure level	dba
LE	Leading edge	m
$l_f$	Fuselage length	m
$l_h$	distance between c/4 of the wing and horizontal tail	m
LHV	Low heating value	Wh/g
M	Flying mach number	-
m	mass	kg
MAC	mean aerodynamic chord	kg
MOS	Margin of safety	-
$N_p$	Number of propellers	-
$n_{ult}^+$	Positive ultimate limit load factor	-
$n_{ult}^-$	Negative ultimate limit load factor	-
P	Power	W
$P_a$	Power available	W
$P_{br}$	Engine power	kW
PL	Power loading	N/W
pos	position	m
$P_r$	Required power	W
$px$	pixel count	-
$px_{pp}$	amount of pixels per an average person	-
q	Dynamic pressure	Pa
Re	Reynolds number	-
ROC	Rate of Climb	m/s
RPM	Revolutions per Minute	-
S	Wing surface area	[m <sup>2</sup> ]

Symbol	Definition	Unit
$S_h$	Horizontal tail surface area	$[m^2]$
sl	sea level	-
$S_v$	Vertical tail surface area	$[m^2]$
T	Thrust	N
TE	Trailing edge	-
TOM	Take-off mass	kg
T/W	Thrust to weight ratio	-
$T_{WOT}$	Thrust at wide open throttle	-
V	Velocity	m/s
$\nu$	Poisson ratio	-
W	Weight	N
w	Width	m
$w_{ct}$	Cross-track width	m
$w_s$	Effective thin sheet width	m
W/S	Wing loading	$N/m^2$
$x_{ac}$	Longitudinal position of aerodynamic center	m
$x_{cg}$	Longitudinal position of center of gravity	m
$x_{cgw}$	Longitudinal position of wing center of gravity	m
$x_c$	position in chord percentage from the LE of the MAC	m
$\alpha$	Angle of attack	deg
$\alpha_0$	Zero-lift angle of attack	deg
$\alpha_s$	Stall angle of attack	deg
$\Delta C_L$	Lift coefficient margin	-
$\eta$	Efficiency	-
$\theta$	Angle	deg
$\phi^e$	Material shape factor for elastic bending	-
$\lambda$	Taper ratio	-
$\Lambda$	Wing sweep	deg
$\Lambda_{c/2}$	Half-chord wing sweep	deg
$\Lambda_{c/4}$	Quarter-chord wing sweep	deg
$\sigma$	Tensile/compressive maximum allowable stress	Pa
$\sigma_{cr}$	Tensile/compressive buckling stress	Pa
$\sigma_{failure}$	Tensile/compressive failure stress	Pa
$\sigma_y$	Tensile/compressive yield stress	Pa
$\rho$	Density	$kg/m^3$
$\tau$	Shear stress	Pa
$\tau_{cr}$	Critical shear buckling stress	Pa

# Contents

Executive overview	ii
Summary	xii
Nomenclature	xiii
1 Introduction	1
2 Mission Definition	2
2.1 Project Objectives . . . . .	2
2.2 Risk Analysis . . . . .	6
2.3 Sustainable Development Strategy . . . . .	8
3 Design Concept Selection	10
3.1 Design Options . . . . .	10
3.2 Design Trade-Off and Selection . . . . .	10
3.3 Selected Final Concept. . . . .	12
4 Design Methodology and Iterative Design Structure	14
5 Payload Sizing	17
5.1 Detection System Selection . . . . .	17
5.2 Autopilot System Selection . . . . .	17
5.3 Communication System Sizing . . . . .	19
5.4 Bird Repellent. . . . .	20
5.5 Payload Budget . . . . .	22
6 Operations and Logistics	23
6.1 Climate Considerations . . . . .	23
6.2 Flight Operations. . . . .	24
6.3 Footage Processing. . . . .	28
6.4 Ground Station Layout. . . . .	29
6.5 Refueling Operations. . . . .	29
6.6 Types of Hydrogen . . . . .	30
6.7 Scalability. . . . .	31
6.8 Emergency Operational Profile . . . . .	32
6.9 Communications. . . . .	32
6.10 Certification of the UAV . . . . .	35
6.11 End-of-Life . . . . .	35
7 Aircraft Configuration	37
7.1 Overall Aircraft Configuration . . . . .	37
7.2 Fuselage Configuration . . . . .	37
7.3 Empennage Configuration . . . . .	38
7.4 Wing Configuration . . . . .	41
7.5 Vertical Take-off and Landing Transition . . . . .	43
8 Aerodynamic Design	48
8.1 Wing Aerodynamic Design . . . . .	48
8.2 Wing Geometry. . . . .	53
8.3 Wing Lift Coefficient & Stall . . . . .	56
8.4 Moment Coefficients & Aerodynamic Center . . . . .	57
8.5 Drag Estimation . . . . .	58
8.6 Tail Geometric Design . . . . .	60
9 Stability & Controllability Design	63
9.1 Static Longitudinal Stability & Control at Cruise Flight . . . . .	63
9.2 Aileron Sizing. . . . .	65

10	Propulsion and Power Systems Design	67
10.1	Propulsion . . . . .	67
10.2	Propeller sizing . . . . .	68
10.3	Propeller positioning. . . . .	69
10.4	Power & Energy . . . . .	70
11	Noise Considerations	72
11.1	Background Sound Theory . . . . .	72
11.2	Propeller Noise . . . . .	72
11.3	Consequences of Noise Pollution on Wildlife . . . . .	75
11.4	Airframe Noise . . . . .	76
12	Structural Design	77
12.1	Material Selection process. . . . .	77
12.2	Wing and Tail Structural Design. . . . .	81
12.3	Fuselage, Booms and Landing Gear Design Sizing. . . . .	87
13	Iterative Design Process	89
13.1	Iteration Dependencies . . . . .	89
13.2	Verification and Validation . . . . .	91
13.2.1	Model Verification . . . . .	91
13.2.2	Model Validation . . . . .	91
13.2.3	Sensitivity Analysis . . . . .	92
14	Complete Final Design	95
14.1	Finalized Design . . . . .	95
14.2	Mass and Power Budget Breakdown . . . . .	96
14.3	Production Plan . . . . .	98
14.4	Performance Analysis . . . . .	99
14.5	Reliability, Availability, Maintenance, Safety . . . . .	100
14.6	Compliance Matrix. . . . .	100
14.7	Post Design Risk Analysis . . . . .	102
15	Economic Considerations	105
15.1	Market Analysis. . . . .	105
15.2	Cost Analysis . . . . .	111
15.3	Return on Investment . . . . .	114
16	Project Design and Development Logic	116
17	Conclusion	119
	References	123
A	Catia Technical Drawings	124

# Introduction

The digital revolution has made life for many people more accessible, but with good also comes evil. Since the turn of the century, the rapid proliferation of organized crime syndicates dedicated to poaching rare wildlife has driven numerous species to extinction. At least one rhino<sup>1</sup> and ninety-six elephants are killed daily for their ivory horns and tusks, and an average of two park rangers are killed weekly while honoring their wildlife conservation duties<sup>2</sup>. Despite harsh regulations punishing poaching, the illegal wildlife trading industry remains and is even estimated to be worth around 70 billion each year<sup>3</sup>. The potential for enormous profits, the low regard for human and animal life, and the rise of high-tech equipment, such as the GPS to locate animals and avoid ranger detection, give the poachers a considerable advantage over the often under-equipped rangers fighting against the illegal wildlife trade. Usambara, named after the African eagle owl that soars above the forests of Tanzania, aims to provide a technical solution and tip the scales back in favor of wildlife protection programs.

Usambara, an autonomous aerial vehicle equipped with high-fidelity thermal imaging, is designed to monitor and protect wildlife and the environment. It will be an effective partner to park rangers in the fight to protect national parks, allowing rangers to locate and apprehend poachers more efficiently and safely. Additionally, Usambara will produce zero emissions and cause minimum disturbance to the surrounding wildlife and habitat. Finally, as the UAV monitors large swathes of natural reserves for poachers, the existing sensors also provide the capability for early detection of wildfires.

This report will adhere to the following structure. The mission objectives are stated in Chapter 2 followed by a requirement analysis and the sustainable development strategy. The selection of the design concepts is stated in Chapter 3. Chapter 4 contains the design methodology and iterative design structure, as well as some block diagrams such as communication and data handling. The payload sizing and budget of the camera, autopilot, communication, and bird repeller are in Chapter 5. Chapter 6 explains operations and logistics of the mission once the UAV is in use. This contains sections such as the flight and refueling operations, the ground system logistics, the scalability of the system, and the end-of-life operation. The aircraft configuration can be found in Chapter 7, the sections include the geometric design, the body, tail, and wing configuration, the stability performance and the Vertical Take-Off and Landing (VTOL) transition. In Chapter 8, the wing design and airfoil trade-off are given, as well as the wing geometry and drag estimation. The stability and controllability design of the UAV can be found in Chapter 9. This chapter includes both the forward and VTOL flight stability, and the aileron sizing. Chapter 10 presents the propeller sizing and positioning, and the power required for the mission profile. The noise considerations based on the relevant sound theory are explained in Chapter 11. Then Chapter 12 presents the material choice, and the wing and tail structural design. The iterative design process, including the sensitivity analysis and verification and validations methods is shown in Chapter 13. Chapter 14 shows the finalized design, and the mass and power budget breakdown. In Chapter 14, the production plan, performance analysis and compliance matrix of the finalized design, the Reliability, Availability, Maintenance, and Safety (RAMS), and the risk analysis for post-DSE activities is also presented. The Economic considerations of the design are addressed in Chapter 15. The return on investment closes this chapter. The project design and development logic is presented in Chapter 16. Finally, the conclusion and recommendations of the project are in Chapter 17.

---

<sup>1</sup>URL: <https://www.savetherhino.org/rhino-info/poaching-stats/?cn-reloaded=1> [8/06/2022]

<sup>2</sup>URL: <https://petpedia.co/poaching-statistics/> [8/06/2022]

<sup>3</sup>URL: <https://www.poachingfacts.com> [8/06/2022]

# Mission Definition

This chapter introduces the fundamental aspects of this report. Initially, the project objectives are explained in Section 2.1 to lay the foundation thoughts and needs are carried out to establish the frame that the system will be designed into. This section also contains the requirements the UAV is designed to fulfill. The technical risk and operational risks present during the operation and design of the UAV are addressed in Section 2.2. Finally, a sustainable development strategy is laid in Section 2.3.

## 2.1. Project Objectives

The aim of this chapter is to give an overview of the project objectives of the design synthesis exercise (DSE). For the DSE the team has been asked to design an unmanned aerial vehicle (UAV) for monitoring natural reserves. More and more threats endanger the natural reserves and habitats of wildlife. These areas are prone to wildfires, littering, as well as poachers. Thus, the following mission need statement was defined by the team to address these threats:

*Protect and monitor the wildlife and environment with minimum disturbance and zero emissions.*

Since limited resources are available for the team, the following project objective has been given to them:

*Design a zero-emissions, unmanned, autonomous aerial surveillance system to monitor wildlife and the environment with a team of ten students by June 21st, for a cost of less than 100,000 and 50,000 euros per vehicle and ground station respectively.*

From the mission need statement and project objective, it is clear that the most important aspects are with regard to sustainability. The UAV must be friendly to the surrounding environment by not producing any emissions during its operation, it should be very low noise to avoid disturbing the wildlife while it is monitoring the environment. To test the concept, a case study will be performed for the Kruger National Park in South Africa. The total system will monitor an area of 50 km by 50 km in this national park using several UAV. Each individual UAV will be assigned a smaller area to monitor and will record footage of that area to detect poachers, fires or litter.

## Requirements Verification & Validation

In this section, a brief plan regarding the verification and validation procedures that will happen during and after the DSE will be presented [1]. The methods of verification and validation will be explained.

### Verification methods

There are four methods that one can use to verify a product. They are as follows:

- **Inspection:** This involves examining the product and its documentation to display compliance with its requirement.
- **Demonstration:** By means of operation or adjustment, it is shown that the product complies with its requirement.
- **Test:** Test an (accurate) model of the product with its requirement under representative conditions.
- **Analysis:** By means of analysis techniques, such as mathematical, establish that the product meets its requirements.

## Requirement Validation

Validating a requirement has the purpose of ensuring that the requirement meets requirements on itself, such that it can unambiguously be met. This, conveniently, can be checked with the acronym VALID [1]:

- **Verifiable:** The requirement must be objective, preferably quantitative .
- **Achievable:** The requirement must be realistically attainable in the situation.
- **Logical:** It must be possible to check that the requirement is achieved, and is traceable.
- **Integral:** The requirement must be complete and address a relevant topic.
- **Definitive:** The requirement must be simple to understand by the group of readers it is intended for. For example for a stakeholder.

With these requirements on requirements, the validation process can occur. By reviewing the requirements it was found that they indeed follow the VALID philosophy, therefore being validated.

## Stakeholder Requirements

The primary stakeholders driving the requirements for the design of the autonomous wildlife surveillance system, are the customer and the DSE Group 11. The customer drives the stakeholder requirements by imposing specific tasks the system needs to be able to complete and by imposing constraints within sustainability and budget. The DSE Group 11 drives the requirements by discussing the system's feasibility with the customer. The secondary stakeholders are all external entities that are impacted by the development and operation of the system; these entities are also considered when designing the requirements. The external entities include:

- Local, regional and national governments within the operating area
- Sponsors and investors of the project
- the TU Delft
- Park rangers
- Conservationists
- Local communities
- External suppliers

Hereafter, the location in which the UAV operates will be referred to as the National Park. The stakeholder requirements are divided into four sections, each with its own identifier. These sections are performance, sustainability, budget, and safety & reliability. All stakeholder requirements can be found in Table 2.1, and are derived from the project guide<sup>1</sup>. These requirements include the killer, driving (D), and high-risk requirements(Hr), as well as the most important requirements to the stakeholder (SH).

**Table 2.1:** Stakeholder requirements

Identifier	Requirement	Verification Method	Key
Performance			
SH-PER-01	The vehicle shall detect wildfires in the National Park.	Demonstration	SH
SH-PER-02	The vehicle shall detect poachers in the National Park.	Demonstration	Hr, SH
SH-PER-03	The vehicle shall identify litter in the National Park.	Demonstration	SH
SH-PER-04	The vehicle shall be able to operate in low visibility conditions.	Demonstration	
SH-PER-05	The vehicle shall be autonomous.	Test	
SH-PER-06	The system shall be easily deployable in remote areas.	Demonstration	
SH-PER-07	The system shall provide a livestream between the UAV and ground station.	Demonstration	
Sustainability			
SH-SUS-01	The vehicle shall have zero emissions during operation.	Test	

<sup>1</sup>URL:[https://brightspace.tudelft.nl/d2l/common/viewFile.d2lfile/Database/MjgzMjI3Mw/Project\\_Guide\\_2022\\_Spring%20DSE\\_Team11.pdf?ou=397908&display=1](https://brightspace.tudelft.nl/d2l/common/viewFile.d2lfile/Database/MjgzMjI3Mw/Project_Guide_2022_Spring%20DSE_Team11.pdf?ou=397908&display=1) [29/04/2022]

SH-SUS-02	The installation of the ground stations shall disturb wildlife as least as possible.	Analysis	
SH-SUS-03	The noise emissions shall be a minimum of 6 dB less than industry standard for commercially available drones.	Test	
Budget			
SH-BU-01	Each aerial vehicle shall cost less than 100,000 euros.	Analysis	SH
SH-BU-02	Each ground station shall cost less than 50,000 euros.	Analysis	SH
Safety & Reliability			
SH-SR-01	The system shall be able to avoid damage from poacher attacks.	Demonstration	Hr
SH-SR-02	The system shall not obstruct or interfere with other aircraft.	Analysis	

## System Requirements

The system requirements follow from the stakeholder requirements and dive deeper into the technical aspects required, as well as some requirements with the external entities in mind. The system requirements give a clear overview of the scope that the system needs to adhere to. By defining which are the key requirements, it is clear where extra attention needs to be given, such that difficult situations are avoided. The system requirements are divided into seven subsections: performance, movement, detection, communication, safety & reliability, sustainability - including noise, materials, emissions, and ecosystem - and maintenance. Again all requirements and sections have their own identifier. The system requirements can be found in Table 2.2.

**Table 2.2:** System requirements with verification method and requirement type

Identifier	Requirement	Verification Method	Key
Performance			
SYS-PER-01	The system shall surveil an area of 50 km x 50 km at least twice a day.	Demonstration	
SYS-PER-02	The UAV shall reach a cruise speed of at least 80 kmh.	Test	
SYS-PER-03	The UAV shall have an endurance of at the least 2 hrs.	Test	D
SYS-PER-04	The UAV shall have a minimum cruise altitude of 120 m.	Demonstration	
SYS-PER-05	The system shall be able to reach any location within its monitoring zone in less than 2 minutes.	Demonstration	D
SYS-PER-06	The UAV shall have a maximum take-off and landing distance of 25 m.	Demonstration	D
SYS-PER-07	A single UAV shall be able to monitor an area of at least 5 km <sup>2</sup> in one single flight.	Demonstration	
SYS-PER-08	The UAV shall have a minimum range of 150 km.	Demonstration	Hr
Movement			
SYS-MOV-01	The UAV shall fly and manage recharging/refueling autonomously.	Demonstration	
SYS-MOV-04	The UAV shall be able to carry out regular operations with headwinds of up to 5.7 m/s.	Demonstration	
SYS-MOV-05	The UAV shall be flight statically stable.	Test	
SYS-MOV-06	The UAV shall be flight dynamically stable through control mechanisms.	Test	
SYS-MOV-07	The system shall detect poachers with a maximum rainfall of 7.6 mm/hr.	Demonstration	

SYS-MOV-08	The system shall detect poachers within fog of maximum CAT II fog <sup>2</sup> .	Demonstration	
Detection			
SYS-DET-01	The system shall allow detection a wildfire affecting an area larger than 100 m <sup>2</sup> .	Demonstration	
SYS-DET-02	During daytime, the system shall allow detection of litter covering a ground area no smaller than 2 m <sup>2</sup> .	Demonstration	
SYS-DET-03	The UAV cameras shall be able to provide footage of human figures with a resolution no-lower than 30 pixels.	Analysis	
Communication			
SYS-COMM-01	The system shall have an alert response time of maximum TBD seconds.	Test	
SYS-COMM-02	The UAV shall provide its position to the ground station at a data rate of 1.02 Mbps or more.	Test	
SYS-COMM-03	The aerial vehicle shall provide a continuous data budget of at least 21.4 Mbps downlink.	Test	
SYS-COMM-04	The system shall receive a continuous data budget of at least 2 Mbps uplink.	Test	
SYS-COMM-05	The ground station shall record the received livestream data.	Demonstration	
Safety & Reliability			
SYS-SR-01	The system shall abide by the relative EASA regulations.	Demonstration	
SYS-SR-02	The system shall be 90% reliable for 500 hours of operational time.	Test	
Sustainability: Noise			
SYS-SUSN-01	The system shall provide a noise reduction of 6dB compared to commercially available drones, measured at ground level (thus a noise output of 75dB).	Test	D, SH
Sustainability: Materials			
SYS-SUSM-01	The UAV shall consist of 75% of recyclable or reprocessible materials (excluding sensors).	Inspection	D
Sustainability: Emissions			
SYS-SUSEM-01	The UAV shall not emit carbon oxides, nitrogen oxides nor particulates during operation.	Demonstration	D, SH
Sustainability: Ecosystem			
SYS-SUSEC-02	In the case of an accident, the UAV shall not release polluting substances.	Analysis	Hr
Maintenance			
SYS-MAI-01	The payload shall be easily replaceable by trained staff.	Demonstration	Hr

## Key Requirements

From the system and stakeholder requirements given above, key requirements are identified. Key requirements should be tracked throughout the project and given additional consideration during trade-offs. These include killer requirements, defined as requirements driving the design to an unacceptable extent, and driving requirements, which drive the design more than average. Key requirements also include requirements paramount to the stakeholder and requirements expected to be a risk item.

<sup>2</sup>URL:<https://www.flir.com/discover/rd-science/can-thermal-imaging-see-through-fog-and-rain/>

No killer requirements were identified at this stage of the design process. The stakeholder requirements that are given and the resulting system requirements defined all require performance comparable with current competitors on the market within the budget given.

The driving requirements identified all drive the design more than the other requirements. These requirements are driving since they decide the particular configuration that must be chosen for the UAV or have a great influence on multiple subsystems of the UAV. SYS-SUSN-01, SYS-SUSM-01, SYS-SUSEM-01, SYS-PER-03, SYS-PER-05, SYS-PER-06 are all identified as driving requirements since they have a great influence on the performance of the UAV and the design of multiple subsystems.

The requirements that propose a threat with high risk on the mission or design were defined as high risk requirements. These requirements are key since they have severe consequences when not met. SYS-MAI-01 and SH-SR-01 are defined as high risk since the UAV can be out of operation if this happens, which will spoil the mission of surveilling the national park. SYS-SUSEC-02 is high risk, since risk to the environment is present if this requirement is not met. The current technology and software to detect poachers is still developing. This causes a risk to the UAV mission since the team that will design the UAV is not in charge of making this technology. Thus SH-PER-02 is also defined as a high risk requirement. Lastly, SYS-PER-08 is a high risk requirement since this requirement will be most difficult to be met and will require a highly efficient design.

Requirements important to the stakeholder are also key requirements. Since the stakeholder is very fond of its money the requirements SH-BU-01 and SH-BU-2 were identified as requirements important to the stakeholder. Additionally, the customer would like that the UAV performs the mission set by the customer. Thus, SH-PER-01, SH-PER-02 and SH-PER-03 were also identified as requirements important to the stakeholder. Furthermore, the stakeholder emphasizes that the UAV is low noise (SYS-SUSN-01) and produces zero emissions during operation (SYS-SUSEM-01). These two requirements have also been identified as driving requirements.

## 2.2. Risk Analysis

Risks can be the cause of an early ending of the mission of the product. Risks must thus be identified and assessed, such that they can be mitigated. The aim of this chapter is to update the risks of the system and project and to explain how to mitigate them if necessary. Firstly, all of the risks are identified by the team and assessed based on their likelihood and estimated impact. Following this, the methods to reduce or mitigate the medium-high risks and medium risks are presented.

### Risk Assessment

The risks identified by the team are outlined in Table 2.3. The risks have been divided into ten different categories. These categories are: communication, extreme environment, external interactions, propulsion, sensors, power, software, movement, budget and structure. These categories cover various stages of the operation of the UAV. Table 2.3 only provides the reader with insight on the high and medium risks. For more detail about the low risk assessed, the reader is directed to previous work[2].

**Table 2.3:** Risk list and breakdown of the values

Identifier	Risk	Likelihood	Estimated Impact	Total Value
Extreme environment				
R-XTR-01	Failure due to high winds	3	4	12
R-XTR-04	Overheating of the system due to high temperatures	4	3	12
External interactions				
R-EXT-01	Damage to the UAV due to animal or human interactions	3	4	12

R-EXT-05	The UAV emits sounds that animals are sensitive to, but humans can not perceive	4	3	16
Propulsion				
R-PRP-03	One propeller inactive	3	4	12
Power				
R-PWR-04	Hydrogen fuel cell catching fire during flight	3	5	15
R-PWR-05	System catching fire during crash	3	5	15
Movement				
R-MOV-05	UAV collision with wildlife	3	4	12
Budget				
R-BUD-01	Unforeseen/unexpected costs that bring the system above budget	3	4	12
R-BUD-02	Unacceptable increase of mass due to the snowball effect	4	4	16
Structure				
R-STR-02	Structure damage due to fatigue stress	4	4	16
R-STR-03	Structure damage due to crack propagation	3	4	12

The likelihood and estimated impact uses a ranking system ranging from 1 to 5, corresponding to two different categorizations. The categories are: low, medium-low, medium, medium-high, and high for the likelihood. For estimated impact, the categories are: catastrophic, critical, moderate, marginal, and negligible. The total value, or the likelihood and estimated impact values multiplied with one another, is presented in the final column of Table 2.3. This total value determines the section in which the risk is present in the risk matrix, as presented in Table 2.5.

The severity of potential setbacks is visualized with the risk matrix in Table 2.5. The total values as stated in Table 2.3 are used for the color labeling. It is considered that the values of the likelihood and the estimated impact are equally important. No additional weights were thus calculated for these values. The ranking used is as follows:

- 1-5: Green color means lowest level risk
- 5-10: Yellow color means medium-low level risk
- 10-15: Orange color means medium level risk
- 15-20: Dark orange means medium-high level risk
- 20-25: Red means high level risk

**Table 2.4:** Risk matrix

		Likelihood				
		Low	Medium Low	Medium	Medium High	High
Estimated Impact	<b>Negligible</b>					
	<b>Marginal</b>					
	<b>Moderate</b>				R-XTR-04, R-EXT-05	
	<b>Critical</b>			R-XTR-01, R-EXT-01, R-PRP-03, R-MOV-05, R-BUD-01, R-STR-03	R-BUD-02, R-STR-02	
	<b>Catastrophic</b>			R-PWR-04, R-PWR-05		

The lowest level risks do not require a mitigation strategy, since they are very unlikely to affect the project significantly. The medium-low risk will not need a mitigation strategy as well. The level of these risks is still too low to have a significant effect on the project. From the medium level risks onward, a mitigation strategy will be necessary. These risks may affect the project in such a way that setbacks may occur, therefore for a

risk that ranks 10 or higher a mitigation assessment is performed. Below only the mitigation strategy for medium-high risks is given, for more detail on the medium risks the reader is directed to [2].

### Medium-High Risks

**R-BUD-02 Unacceptable increase of mass due to the snowball effect** The UAV can very quickly increase in mass due to the snowball effect if no attention is paid to this. An increase in mass means more power is needed, which will add extra weight and so on. To decrease this risk, the mass of the UAV will be kept track of, using a mass budget. This mass budget will be updated each time a subsystem or other part adds weight to the UAV. When this method is used, no unexpected mass is suddenly added to the UAV.

**R-STR-02 Structure damage due to fatigue stress** Since the UAV is powered by hydrogen, it can make around 10 flights a day. This results in a more efficient coverage of the area. However, this increases the fatigue compared with if the UAV would only do two flights a day. Because of this increase in fatigue, it is recommended to do maintenance every month to prevent unfortunate events from happening.

Table 2.5: Mitigated Risk matrix

		Likelihood				
		Low	Medium Low	Medium	Medium High	High
Estimated Impact	Negligible					
	Marginal					
	Moderate		R-EXT-05	R-PRP-03, R-BUD-01, R-XTR-04		
	Critical		R-BUD-02, R-STR-02, R-XTR-01, R-MOV-05, R-STR-03, R-PWR-05			
	Catastrophic		R-PWR-04			

### 2.3. Sustainable Development Strategy

In this section, the sustainable development strategy is presented for this project. The presence of this strategy ensures that sustainability is taken into account in the design as well as in the operation of the system. To do so, three objectives are defined to measure sustainability. These are economic, environmental, and social sustainability. These three objectives need to be balanced to optimize the sustainability for all stakeholders and to meet the sustainable development targets. The basis used for this sustainable development strategy are the seventeen sustainable development goals as defined by the United Nations<sup>3</sup>. The three goals mainly focused on are goal 7 (affordable and clean energy), goal 13 (climate action), and goal 15 (life on land).

First of all, the economic sustainability objectives will be defined. Economic sustainability can be defined as practices that support long-term economic growth without negatively impacting social, environmental, and cultural aspects of the community<sup>4</sup>. Since a lot of parties are involved in the project, there must be some economic considerations. Local authorities are the ones responsible to take action in case of a detected threat. This means that jobs are created for the local communities, which need to be fairly paid. Since the case study focuses on the Kruger National park in South Africa, a minimum wage of 23.19 South African Rand per hour is required (1.48 US Dollar)<sup>5</sup>. However, since costs of living are a lot higher<sup>6</sup>, a wage of 56.15 South African Rand per hour will be the standard. Moreover, variable costs need to be as low as possible. This indicates that the system must be very reliable so that maintenance is as rare as possible. Additionally, cheap renewable energy sources must be used so that costs of operation are also kept to a minimum. The

<sup>3</sup>URL: <https://sdgs.un.org/goals> [03/05/2022]

<sup>4</sup>URL: <https://sustainability.umw.edu/areas-of-sustainability/economic-sustainability/> [03/05/2022]

<sup>5</sup>URL: <https://mywage.co.za/salary/minimum-wages/6226-national-minimum-wage> [25/05/2022]

<sup>6</sup>URL: [https://www.numbeo.com/cost-of-living/country\\_result.jsp?country=South+Africa](https://www.numbeo.com/cost-of-living/country_result.jsp?country=South+Africa) [25/05/2022]

current price of 1 kg green hydrogen is 19.12 US Dollar<sup>7</sup> but is expected to be 1.60 US Dollar in 2030<sup>8</sup>. This can be taken into account for future investments. Moreover, material costs need to be low such that the system can be manufactured for a cheap and competitive price. Moreover, end-of-life costs must be as low as possible by using easily reusable materials like metals. Also, since the system must be scalable to bigger and different areas, a universal system must be developed. This reduces the costs to adapt the system to different environments. Lastly, a very important economic objective to consider is the development costs in the design phase since an aerospace engineer has an average salary of 38 US Dollars an hour<sup>9</sup>. By applying good project management and system engineering, an efficient collaboration is ensured and fewer repetitive tasks have to be done.

Subsequently, environmental sustainability has to be considered. This can be defined as the management of our physical environment in a way that supports living within ecological limits, protection of natural resources, and meeting the needs of communities without compromising the ability of future generations to meet their own needs<sup>10</sup>. To meet this objective, the use of affordable and clean energy must be ensured. This means that both for the production, and for the UAV during operation, renewable energy must be the power source. For the latter, this renewable energy will either be produced by the UAV or the ground station itself, or it will be bought from local energy producers. In case the UAV or ground station produces its energy, it must be taken into account that the production of the energy will cause minimum harm to the surrounding environment. For instance, the presence of large solar panels must be avoided in natural reserves. Additionally, the system must be produced from a certain amount of recyclable materials and preferably materials that do not harm the environment. For instance, bamboo, wood, or bio plastics are possibilities. Another very important consideration is that the system should not harm wildlife, during operation. This puts constraints on the noise level of the UAV itself, just like the presence of the ground station.

This continues into the post operation of the UAV and ground station. Irrespective of the quality of the system, at some point it will need to be replaced, or the need for the materials may be elsewhere. A responsible reuse, disposal or recycling strategy is vital in the current age. The materials on the planet are finite, and despite the UAV and ground station having a relatively small impact compared to other operations, it is important that all establishments, without regard to the size, contribute to a cleaner future. Choosing materials that are reusable, recyclable or at worst safely disposable is critical. Not only this, once the material is definitively decided on, a strategy must be determined and carried out.

Lastly, social sustainability objectives need to be defined. Social sustainability encourages communities to promote social interaction and foster community investment while respecting social diversity<sup>11</sup>. For these social sustainability objectives, an important development is awareness for wildlife preservation being created by the system. Education is key for the preparation of current and future tourists, locals, and rangers, for the threat of poachers, wildfires, and litter. Furthermore, the consequences of poaching, wildfires, and littering will become clearer, causing the community to encourage each other to preserve the environment. In addition, having the locals appreciate the presence of the UAVs is very beneficial. In the future, when the chosen materials need to be sourced, making use of local companies is an ideal way to create a positive relationship between the UAV operating organization and the local people.

---

<sup>7</sup>URL: [https://www.investec.com/en\\_za/focus/beyond-wealth/hydrogen-the-fuel-of-south-africas-green-future.html](https://www.investec.com/en_za/focus/beyond-wealth/hydrogen-the-fuel-of-south-africas-green-future.html) [25/05/2022]

<sup>8</sup>URL: <https://www.csis.org/analysis/south-africas-hydrogen-strategy> [25/05/2022]

<sup>9</sup>URL: <https://www.salary.com/research/salary/benchmark/aerospace-engineer-ii-salary> [25/05/2022]

<sup>10</sup>URL: <https://sustainability.umw.edu/areas-of-sustainability/environmental-sustainability/> [03/05/2022]

<sup>11</sup>URL: <https://sustainability.umw.edu/areas-of-sustainability/social-sustainability/> [03/05/2022]

# Design Concept Selection

This chapter will briefly cover the process followed in a previous report [2] to decide which configuration of UAV is the best for the mission. Section 3.1 describes the shortlist of valid options, following this the trade off method and criteria are defined in Section 3.2. Lastly, in Section 3.3 the trade off is completed, and the final configuration is decided upon.

## 3.1. Design Options

A broad range of UAV configurations is suitable for surveillance missions. Within the UAV market, several designs were considered based on the requirements for the mission. The first design category was the N-copter, which consists of a set amount of propellers producing vertical lift, making this design versatile in real-world applications. The second category was the fixed-wing propeller UAV which can fly for long periods due to the significant amounts of lift that the wing produces without needing too much power. The final design that is considered is a fixed-wing turbojet aircraft with a speed advantage.

The group realized that the N-copter category was strongly advantageous in terms of take off and landing. However, the fixed wing design is advantageous for lift production capabilities. Choosing one over the other would have created a great loss of efficiency. Therefore, it was chosen to add another category of plane design, the fixed-wing VTOL. With this addition, it can be tested that compromising for being able to comfortably take off and land and being efficient in lift creation would outperform conventional designs.

Apart from the aircraft configuration and type, the propulsion method was also important as it influences sustainability and noise creation. Carbon-based fuels were clearly not an option, leaving two options: hydrogen and batteries. With hydrogen, in the case of the propeller-driven concepts, power is delivered through a fuel cell. Hydrogen could also be used to power a turbojet engine. In the case of a battery, electrical motors would be directly powered by the batteries.

## 3.2. Design Trade-Off and Selection

The Analytic Hierarchy Process (AHP) is a popular method of multi-objective decision making in the engineering industry as a whole [3]. The reason behind its popularity is the ability to break down complex problems with multiple goals into a more straightforward hierarchy between the goals [4]. This is done by comparing pairs of selection criteria individually instead of comparing all of them simultaneously, which might lead to imprecise or unsatisfactory criteria weights or complicated arguments between the decision makers.

Following this thought process, each pair is scored on importance relative to the overall mission according to the Saaty scale (Figure 3.1<sup>1</sup>), with the most important criterion of each pair being assigned an integer between 1 and 9 (with some exceptions for when the criteria are too close in importance, see Figure 3.1).

<sup>1</sup>URL: [https://en.wikipedia.org/wiki/Analytic\\_hierarchy\\_process\\_%E2%80%93\\_leader\\_example](https://en.wikipedia.org/wiki/Analytic_hierarchy_process_%E2%80%93_leader_example) [16/05/2022]

**Figure 3.1:** Saaty's scale for establishing a relationship between priorities in AHP.

The Fundamental Scale for Pairwise Comparisons		
Intensity of Importance	Definition	Explanation
1	Equal importance	Two elements contribute equally to the objective
3	Moderate importance	Experience and judgment moderately favor one element over another
5	Strong importance	Experience and judgment strongly favor one element over another
7	Very strong importance	One element is favored very strongly over another; its dominance is demonstrated in practice
9	Extreme importance	The evidence favoring one element over another is of the highest possible order of affirmation
Intensities of 2, 4, 6, and 8 can be used to express intermediate values. Intensities of 1.1, 1.2, 1.3, etc. can be used for elements that are very close in importance.		

These comparison results are then entered into a matrix, where each node of the matrix reflects the importance of one criterion concerning another. The nodes in the diagonal are always one since the criteria are compared to themselves in the diagonal nodes. A node value higher than one means that the criteria on the row are more important than the criteria on the column. Therefore, the matrix's upper triangle contains the lower side's reciprocals.

The matrix is then mathematically processed to obtain the relative weight of each criterion, whose sum must add to 1 (it is normalized). To do this, the nodal value is first averaged with respect to its column. Then, the normalized nodes of a row are averaged to obtain the final weight of the criterion. These relationships are synthesized in Equations 3.1 and 3.2 for a  $M \times N$  matrix.

$$\overline{e_{i,j}} = \frac{e_{i,j}}{\sum_{k=1}^M e_{k,j}} \quad (3.1)$$

$$\overline{w_i} = \frac{\sum_{k=1}^N \overline{e_{i,k}}}{N} \quad (3.2)$$

One of the main advantages of AHP is also one of its weaknesses: the fact that the pairwise comparisons are unrelated introduces many redundancies in weighing the criteria. On the one hand, this helps to reach more complete and even weights for the criteria, as parallel characteristics are contrasted, leading to different valuations later averaged. On the other hand, if the pairwise comparisons are very different, it can lead to inconsistency and, therefore, to a failed trade-off. To check if there is bias in the found weights, the consistency index (CI) and consistency rate (CR) can be determined using Equation 3.4 and Equation 3.5. In these formulas,  $N$  is the total number of selection criteria used, equal to six,  $\lambda_{max}$  is the maximum eigenvalue (Equation 3.3) and  $RI$  is the random consistency index<sup>2</sup>. To pass the bias test, the CR should be less than 0.1.

$$\lambda_{max} = \sum_{i=1}^M \frac{w_i}{\sum_{j=1}^N \overline{e_{j,i}}} \quad (3.3)$$

$$CI = \frac{\lambda_{max} - N}{N - 1} \quad (3.4)$$

$$CR = \frac{CI}{RI} \quad (3.5)$$

Apart from this, another factor should be taken into account for the trade-off weight determination: since the group is comprised of ten people, it is impossible to agree on the importance of the relationships between each of the criteria. As a result, each team member voted on their personal valuation of the criteria, and the average was used to obtain the final weights. Since AHP works with integers and their reciprocals, a logarithmic average is the best estimation of the overall feeling of the group; otherwise, scores larger than one would dominate the averaging. The logarithmic average equation is illustrated in Equation 3.6. Furthermore, the personal valuations will be used in the analysis of the trade-off to analyze its consistency.

<sup>2</sup>URL: <https://www.pmi.org/learning/library/analytic-hierarchy-process-prioritize-projects-6608> [05-02-2022]

$$e_{i,j}^{team} = \exp \frac{\ln \left( \prod_{m=1}^{10} e_{i,j}^m \right)}{10} \quad (3.6)$$

Once the selection methodology has been chosen, the objectives of the mission must be explored to compose a list of selection criteria against which the design options will be weighed.

Four selection criteria have been chosen based on several key requirements of the system: Cost, RAMS (Reliability, Availability, Maintainability, and Safety), Performance, and Sustainability. Each has its own sub-criteria, compiled below with their respective requirements. For a more detailed explanation of each criterion and their motivations, the reader is referred to [2].

- |   |   |
|---|---|
| <ul style="list-style-type: none"> <li>1. Cost (<b>SH-BU-01/02</b>) <ul style="list-style-type: none"> <li>1.1. Development</li> <li>1.2. Manufacturing</li> <li>1.3. Operation</li> <li>1.4. End-of-Life Processing (<b>SYS-SUSM-01/02</b>)</li> </ul> </li> <li>2. RAMS (<b>SYS-SR-04</b>) <ul style="list-style-type: none"> <li>2.1. TRL</li> <li>2.2. Reliability</li> <li>2.3. Maintainability</li> </ul> </li> </ul> | <ul style="list-style-type: none"> <li>2.4. Safety</li> <li>2.5. Availability</li> <li>3. Performance <ul style="list-style-type: none"> <li>3.1. STOL (<b>SYS-PER-06</b>)</li> <li>3.2. Range (<b>SYS-PER-08</b>)</li> <li>3.3. Endurance (<b>SYS-PER-03</b>)</li> <li>3.4. Speed (<b>SYS-PER-02</b>)</li> </ul> </li> <li>4. Sustainability <ul style="list-style-type: none"> <li>4.1. Emission (<b>SYS-SUSEM-01</b>)</li> <li>4.2. Noise (<b>SYS-SUSN-01/03</b>)</li> </ul> </li> </ul> |
|---|---|

### 3.3. Selected Final Concept

The scores for each concept are assigned by thoroughly examining the characteristics of the designs, conducting market research, and investigating their reliability. The weighted scores of the lower level trade-offs are then compiled on the main trade-off (Table 3.2), where the final winner is highlighted. The weight of each criterion can be seen below their labels. The scores of the concepts use a different scale than AHP, from 1 to 5. These have been color-coded to make the performance of each design easily identifiable.

Perhaps the easiest criteria to evaluate are the numerical ones. In Table 3.1, many parameters of the concepts are displayed, which allows to compare with the requirements and evaluate the score. If the parameter meets the requirement barely, it receives a 3. If it exceeds it positively, a 4 or 5 is given depending on the margin; the opposite is true if it does not fulfill the requirement. Apart from the apparent performance requirements, other less evident requirements such as noise can be evaluated by observing the rated maximum power and assuming that power and noise are proportional to compare the relative noise of the designs.

The performance in terms of cost is also estimated. Manufacturing costs are directly estimated by the components sized for each design. The sensors, autopilot, and transmitter are shared between each concept and form a majority of the total UAV cost for all designs. Development costs were predicted using the TLR of the concepts and the availability of similar products in the market. Designs with lower TLR or commercially available variants were designated a higher development cost. Operational cost is primarily considered the cost of fueling the UAVs, with batteries scoring better than hydrogen due to the loss of efficiency in both producing and reacting hydrogen compared to electrical storage and propulsion. However, maintenance costs were an additional consideration. Finally, end-of-life costs were estimated in the discarding criteria, with battery variants scoring slightly worse due to the low recyclability of Li-ion batteries and the high cost of extracting the constituent minerals. Fuel cells also present relatively high costs at the end of life, but this is required less frequently than batteries, and recycling is more feasible.

The RAMS trade-off judges the design concepts' reliability, availability, maintainability, safety, and TRL. These considerations are somewhat subjective and were scored according to the research into the technologies used performed in a prior report [5]. The TRL score was heavily influenced by the existence of

commercially available variants of shared technologies. As a result, the hydrogen turbojet performed poorly, given that large scale commercial developments are still ongoing, and no existing projects exist producing this means of propulsion at a smaller scale. PEMFC UAVs exist but are significantly less researched compared to battery-powered UAVs and therefore score worse. Reliability describes the likelihood of both technological failure and operational failure. In terms of operational failure, design variants with VTOL were scored as more reliable, given the elevated risk for crashes during conventional landings in an unmanned flight, particularly if the runway may not be level or clear given the environments where the UAV will be deployed. Maintainability favors hydrogen fuel-cell designs, given their long service lives compared to batteries if operated nominally. For the same reason, the turbojet concept scores poorly, with frequent and difficult maintenance required. The primary safety risk identified was a crash causing combustion, and therefore VTOL designs were favored due to the judgment that crashes are less likely. However, the presence of a fixed-wing also increased scoring in safety, given that this prevents a rapid fall from high altitude if the electrical system fails. No distinction was made between hydrogen and battery systems in terms of safety. Finally, battery variants were judged to perform best on availability due to the higher reliability. Moreover, non-VTOL concepts scored better, as the more complex system used for VTOL, high power requirements, and a larger number of motors increase the chance of a mechanical or electrical failure.

Observing these trade-offs, it can be determined that the winner of the trade-off is the hydrogen-powered VTOL fixed-wing, with a mean score of 3.95, with the battery VTOL fixed-wing concept version ranked second, scoring 3.90. This difference is small enough to be reasonably interpreted as within the margin of error of the weights and scores assigned. Therefore it was judged that the trade-off result is insufficient to choose between the two concepts. Further analysis was completed in a previous report [2] which resulted in the hydrogen option being the best. A large contributor to this is that hydrogen refueling is faster than recharging batteries.

**Table 3.1:** Performance estimates for design variants.

Concept	m [kg]	Range [km]	Endurance [hrs]	V <sub>cruise</sub> [m/s]	Cost [10 <sup>3</sup> ]	P <sub>prop,max</sub> [W]	TO/LND strip [m]
Hydrogen powered VTOL	8.2	160	2.5	22.2	23	1150	0
Battery powered VTOL	14.2	160	2.5	22.2	19	4100	0
Hydrogen powered quadcopter	14.1	53.5	3	20	26	1100	0
Battery powered quadcopter	10.3	20.5	1.2	19	21	600	0
Hydrogen powered fixed wing	5.9	160	2	22.2	20	264	25
Battery powered fixed wing	8.0	160	2.5	22.2	21	420	25
Hydrogen turbojet	39.7	160	2.5	22.2	25	10 000	140

**Table 3.2:** Main trade-off of UAV concepts

Criteria	Cost	RAMS	Performance	Sustainability	Score
	0.048	0.131	0.508	0.312	
Turbojet H2	1.91 (r)	2.30 (o)	3.27 (y)	1.54 (r)	2.54
VTOL Hybrid Battery	3.88 (lg)	4.18 (dg)	3.72 (lg)	4.09 (dg)	3.90
VTOL Hybrid H2	2.71 (o)	3.87 (lg)	3.72 (lg)	4.54 (dg)	3.95 (b)
N-copter Battery	4.03 (dg)	3.35 (y)	2.07 (r)	3.63 (lg)	2.82
N-copter H2	2.56 (o)	3.42 (y)	3.74 (lg)	3.63 (lg)	3.61
Propeller Battery	4.53 (dg)	3.57 (y)	3.44 (y)	4.54 (dg)	3.85
Propeller H2	2.71 (o)	3.20 (y)	3.00 (o)	5.00 (dg)	3.64

# Design Methodology and Iterative Design Structure

The design process of the concept selected in Chapter 3 was developed according to a specific process structure. The group carried out concurrent design of different sectors starting from the initial estimations used in the trade-off selection (treated in Section 3.2, documented in [2]).

Table 4.1 summarises the eight design sectors involved in the design process with a brief explanation of the area of competence. Design sectors are divided based on the disciplines involved.

**Table 4.1:** List of design sectors, chapter of reporting and area of competence.

Design Sector	Chapter	Competence
Payload Sizing	Chapter 5	Choice of the instruments for detection (e.g. camera system), communication system, and autopilot
Operations and Logistics	Chapter 6	Climate considerations, flight operations, ground station operations, data handling, ground station layout, end-of-life operations
Aircraft Configuration	Chapter 7	Choices over general body, wing, tail, engine positioning, stability/manoeverability
Aerodynamic Design	Chapter 8	Choice of airfoil, design of wing planform, tail geometry, measuring of the aerodynamic performance
Stability and Controllability	Chapter 9	Ensuring longitudinal (flight) static stability, aileron design
Propulsion and Power Systems	Chapter 10	Sizing of propeller, motors and power system
Noise Considerations	Chapter 11	Propeller and airframe noise considerations
Structural Design	Chapter 12	Material selection, wingbox, tail, fuselage and landing gear structural design

All the design sectors have in common the dependency on both constant values and parameters sized by other sectors. While decisions were taken and shared during the design process, common values were only used at the end.

The N2 chart on page 19 portrays the design dependencies between the different sectors. The top three lines contain the overall initial inputs coming from Class I, literature, existing designs, and requirements. The cells in different colors indicate design areas with special reciprocal dependency. The red color indicates the dependency between payload sizing, divided in the chart into "sensing", "communication", and "operations & logistics". These two design sectors have a sizing based on requirements that do not depend on other subsystems but do set requirements for most of them. For this reason, the design of these sectors was carried out initially and not iterated. The green color highlights the design iteration loop involving the specific aircraft-design-related design sectors. The designs begin with initial guesses/values from preliminary sizing but is iterated until convergence is reached. This iteration process is portrayed in Figure 4.1 and the specific dependencies are dealt with in Chapter 13. Furthermore, three more steps of the design are indicated in the bottom right corner. These design/analyses were planned to be carried out only after the "green loop" would find convergence.

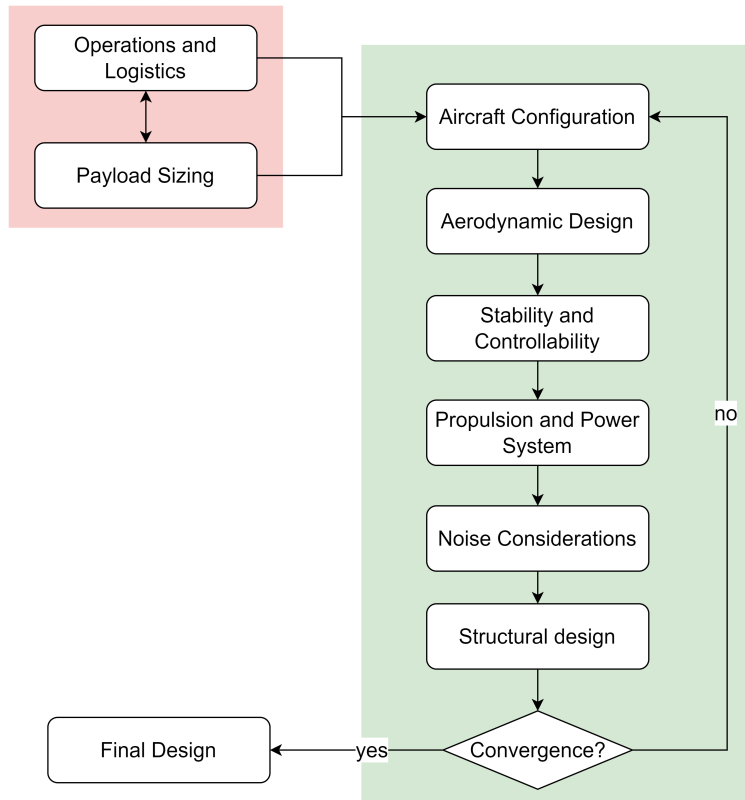


**Figure 4.1:** Design sectors iteration loop.

<b>Outcomes of Class I estimation</b>	- Preliminary sensor pack		- Preliminary cruise altitude - Flight paths and duration - Preliminary operations design	- Configuration from trade-off - Conceptual propulsion system	- W/S - Preliminary cruise altitude			- Fuel type - W/S						
<b>Literature or existing aircraft</b>	- Commercially available sensors	- Commercially available components - Conventional communication system architecture	- Environmental data	- Commercially available and currently operating UAVs - Optimal positioning of payload	- Existing airfoil profiles - Wing planform design methods	- Conventional aerodynamic surfaces architecture	- Existing aircraft with analogous mission profiles	- Commercially available hydrogen systems		- Available engineering materials - Experience with aerospace materials - Recyclability considerations	- Commercially available components			
<b>Requirements</b>	- SYS-DET-01, SYS-DET-02, SYS-DET-03; (- SYS-DET-04, SYS-DET-05); (- SYS-MOV-01, SYS-MOV-02); (- SYS-MOV-03, SYS-MOV-04); (- SYS-MOV-05, SYS-MOV-06); (- SYS-MOV-07, SYS-MOV-08); (- SYS-SR-01, SYS-SR-02)	- SYS-COMM-01, SYS-COMM-02, SYS-COMM-03, SYS-COMM-04, SYS-COMM-05; (- SYS-SR-02)	-SYS-PER-01, SYS-PER-02, SYS-PER-03, SYS-PER-04, SYS-PER-05, SYS-PER-06, SYS-PER-07, SYS-PER-08, SYS-PER-09; (- SYS-MOV-01, (- SYS-MOV-02); (- SYS-SR-01; (- SYS-SR-02; (- SYS-MAI-01	- SYS-PER-06, - SYS-MAI-01	- SYS-MOV-07; (- SYS-SUSN-01	- SYS-PER-6; (- SYS-MOV-05, SYS-MOV-06	- SYS-PER-05, SYS-PER-02; (- SYS-MOV-04; (- SYS-SR-02, SYS-SUSN-01; (- SYS-SUSEM-01, (- SYS-SUSEM-01	- SYS-PER-05; (- SYS-SR-02; (- SYS-SUSEM-01; (- SYS-SUSEM-01	- SYS-SUSN-01	- SYS-PER-09; (- SYS-SR-02; (- SYS-SUSEM-01; (- SYS-MAI-01	- SYS-COMM-01, SYS-COMM-05	- SYS-COMM-01, SYS-COMM-05		- Budget
	<b>Sensing</b>	- Required min bitrate for sensed data transmission	- Optimal cruise altitude range for sensors	- Optimal position for sensors - Sensors mass		- Attitude sensors specs		- Sensors power consumption - Sensors required voltage				- Reliability of sensors	- Sensors cost	
		<b>Communication</b>		- Optimal position for communication system based on communication quality - Communication system mass				- Communication system power consumption - Communication system required voltage			- UAV to ground station distance constraints - Data rate	- Reliability of communication system	- Communication system cost	
	- Operational cruise and maximum speed	- Cruise altitude - Max UAV to ground station operational distance	<b>Operations &amp; Logistics</b>		- Cruise altitude		- Cruise altitude	- Flight time - Flight profiles - Cruise altitude	- Take-off approach and ROC - Landing approach and ROD - Cruise altitude	- Operative environment conditions	- Refueling operations	- Operative safety procedures		
	- Actual location of sensors	- Actual positioning of communication system	- Type of power system	<b>Aircraft Configuration</b>		- Tail configuration - Types of possible control surfaces	- Engine location	- Type of power system		- Payload mass and shape	- General design of UAV			
				- Wing planform design	<b>Aerodynamics</b>	- Aerodynamic moments and forces - Wing design characteristics	- Wing surface area - Wing loading			- Wing force and moment coefficients distribution - Wing design characteristics				
				- Required tail sizing and positioning - Control surfaces size & shape		<b>Stability &amp; Control</b>				- Position of landing gear - Required tail sizing and positioning	- Position of landing gear	- Reliability of control mechanisms and algorithms	- Control mechanisms costs	
			- Cruise and maximum speed	- Propeller design and configuration			<b>Propulsion</b>	- Propulsion system power consumption	- Propeller and motor design and operational RPMs	- Mass and design parameters of the propulsion system - Loads introduced by propulsion system into the airframe		- Reliability of propulsion system	- Propulsion system cost	
			- Achievable range and endurance - Available total stored energy					- Available voltage - Available power	<b>Power &amp; Energy</b>	- Mass, and design parameters of the power system	- Total energy capacity UAV - Charge/refuel rate	- Reliability of power & energy systems - Safety measures	- Power and energy system cost	
			- Implementations to cruise altitude				- Propeller design implementations		<b>Noise</b>					
				- Wing box design - Position of payload	- Total aircraft mass - Wing loading	- Total aircraft mass - Airframe design - Design groups masses and relative locations	- Total aircraft mass - Wing loading			<b>Materials &amp; Structures</b>	- Size and mass of UAV - Landing gear design	- Flight envelope - Material degradation considerations	- Airframe cost	
			- Effective UAV to ground station distance limit					- Total energy capacity ground station			<b>Ground Station</b>	- Reliability of ground station systems		
			- Required safety procedures					- Required safety procedures		- Structural safety margins	- Required safety procedures	<b>Reliability &amp; Safety</b>	- Safety costs	
	- Cost budget for payload	- Cost budget for payload					- Cost budget for propulsion system	- Cost budget for power and energy system		- Cost constraints for airframe manufacturing	- Cost constraints for ground station		<b>Cost</b>	

# Payload Sizing

This chapter aims to select and size the payload and sensors equipped on the UAV. Section 5.1 presents the chosen camera present on the UAV. This camera can sense poachers, wildfires, and litter. In Section 5.2 a suitable autopilot is selected for the UAV for its autonomous flight, the communication subsystem is sized in Section 5.3. Resulting in a transceiver and antennas for the UAV and the ground station. Section 5.4 presents how the UAV mitigates a bird collision. Lastly, Section 5.5 shows the payload and sensors' mass, power consumption, costs, and size budget.

## 5.1. Detection System Selection

Usambara is equipped with a visual and a thermal camera to significantly increase the detection rate of poachers, wildfires, and litter. These are the only sensors that are needed and fitted on the UAV to detect these threats so that no unnecessary weight is added to the UAV. The Zenmuse H20N<sup>1</sup> is the top-scoring camera after the trade-off in the midterm report between various camera systems with a thermal and visual camera. The Zenmuse H20N has two visual and two thermal cameras; both have a zoom camera and a narrow angle camera. The visual cameras also have a Starlight sensor, making them perfect to use at night. The UAV can easily detect predefined threats using these four types of cameras. Besides these cameras, the Zenmuse H20N has a LiDAR sensor, which has a range of 1200 m. Some general technical specifications of this system can be found in Table 5.1. In addition, the resolution and frames per second of the four camera types can be found in Table 5.4.

**Table 5.1:** General data of the Zenmuse H20N

	Zenmuse H20N
Mass [kg]	0.883
Size [mm]	178 x 135 x 161
Power consumption [W]	45
Operating temperature range [°C]	-20 to +50
Cost [Euro]	14,999

## 5.2. Autopilot System Selection

As per requirement SH-PER-05, the vehicle shall be autonomous; an autopilot is selected to control the UAV autonomously. Sensors that can determine the attitude and altitude of the UAV have already been identified in the midterm report. With Figure 5.1 giving an overview of these sensors. After a quick study, three autopilots, specifically designed for VTOL UAVs and including most of the attitude and position sensors defined in Figure 5.1 are chosen to compare. The autopilots are: the Vector-600<sup>2</sup>, the Veronte Autopilot 1x<sup>3</sup> and the Veronte Autopilot 4x<sup>4</sup>. The three chosen autopilots have a three-axis accelerometer, a three-axis gyroscope, a three-axis magnetometer, GNSS navigation, and a pitot-static system. They can support external sensors such as a LiDAR sensor and a camera with a gimbal. However, the Veronte Autopilot was discarded and will not be part of a trade-off due to the significantly higher cost of this autopilot and the similar capabilities to the other two autopilots.

<sup>1</sup>URL: <https://www.dji.com/nl/zenmuse-h20n> [05/04/2022]

<sup>2</sup>URL: [https://www.uavnavigation.com/sites/default/files/docs/2021-11/UAV%20Navigation%20VECTOR-600%20Brochure\\_0.pdf](https://www.uavnavigation.com/sites/default/files/docs/2021-11/UAV%20Navigation%20VECTOR-600%20Brochure_0.pdf) [18/05/2022]

<sup>3</sup>URL: <https://www.embention.com/product/autopilot-for-drone/> [20/05/2022]

<sup>4</sup>URL: <https://www.embention.com/product/professional-autopilot-4x/> [18/05/2022]

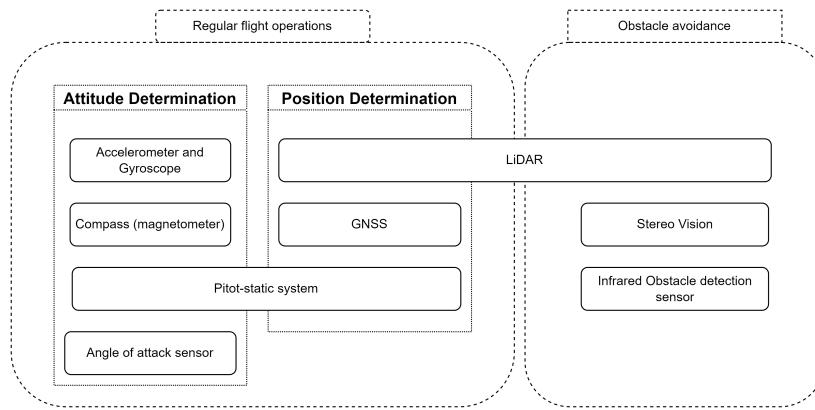


**Figure 5.1:** Sensor that can be used to determine the attitude and altitude of the UAV

A trade-off was performed for the other two autopilots using the analytic hierarchy process described in the midterm report [2]. The selection criteria used for the trade-off are mass, size, power, and cost. Each autopilot has been given a score from unacceptable to excellent, as described in Table 5.2, for all criteria. The trade-off can be seen in Table 5.3. Table 5.3 shows the autopilot data for each criterion, the second row shows the weights of each criterion, and the colors indicate the score. The Veronte Autopilot 1x has won the trade-off with a score of 3.725 against 2.990.

**Table 5.2:** Trade-off weights description

Weight	Description
red (r)	Unacceptable
orange (o)	Poor
yellow (y)	Acceptable
light green (lg)	Good
dark green (dg)	Excellent
blue (b)	Winning score

**Table 5.3:** Trade-off table of the autopilots for the UAV

Criteria	Mass [kg]	Size [mm]	Power [W]	Cost [Euro]	Final trade-off score
Weights of the criteria	0.169	0.052	0.275	0.505	-
Vector-600	0.18 (lg)	45 x 68 x 74.5 (lg)	2.5 (lg)	11,848 (o)	2.990
Veronte Autopilot 1x	0.19 (lg)	63 x 39.6 x 67.9 (lg)	5 (y)	5,750 (lg)	3.725 (b)

The Veronte Autopilot 1x still needs an antenna to receive GNSS signals that the autopilot will process. The GNSS antenna chosen is the GPS Antenna Advanced SSMA<sup>5</sup>. This antenna was chosen for its compatibility with the Veronte Autopilot 1x as it is from the same supplier as the autopilot.

To better the autonomous flight and decrease changes with static objects, the UAV is equipped with a LiDAR sensor which can detect objects in the vicinity of the UAV. The Zenmuse H20N already has a long-range LiDAR sensor which will be used for long ranges from 3 to 1200 m. For the short range, a short-range LiDAR is needed that can detect objects during take-off and landing. For this short range, the M8-1 Ultra LiDAR Sensor has been chosen. The choice for the M8-1 Ultra LiDAR Sensor was based on its horizontal field of view of 360 degrees. This is ideal for landing since it can sense any object or animal at the landing place/ground station. This LiDAR sensor can be used for ranges of 0.5 m to 20 m and has a range accuracy of plus min 3 cm<sup>6</sup>. More general data about this sensor can be found in Table 5.7<sup>7</sup>.

<sup>5</sup>URL: <https://www.embention.com/product/gps-antenna-advanced-ssma/> [30/05/2022]

<sup>6</sup>URL: <https://www.robotshop.com/nl/en/m8-1-ultra-lidar-sensor.html> [31/05/2022]

<sup>7</sup>URL: [https://quanergy.com/wp-content/uploads/2019/12/M8-Datasheet\\_QPN-98-00037-Rev-M.pdf](https://quanergy.com/wp-content/uploads/2019/12/M8-Datasheet_QPN-98-00037-Rev-M.pdf) [31/05/2022]

### 5.3. Communication System Sizing

The UAV must constantly communicate with the ground station during its flight; per requirement SH-PER-07: the system shall provide a livestream between the UAV and the ground station. Thus the UAV is, for instance, required to provide a constant live stream of its video footage during its flight. To communicate, a transmitter and receiver, as well as antennas, are needed. First, however, it must be known how much data the UAV must transmit to the ground station. Most of the data that must be transmitted is the live video stream. The amount of data transmitted can thus be calculated as the bit rate, which is the number of bits transmitted per second. To calculate the bit rate needed for a good quality livestream, the resolution, frames per second, and the bits per pixel of the video need to be known. The Zenmuse H20N has multiple camera types, with each a different resolution and frames per second of the video; these values are stated in Table 5.4. The bits per pixel are estimated to be 0.1, this value is based on literature<sup>89</sup>. The bit rate is calculated using Equation 5.1, where  $w$  is the resolution width,  $h$  is the resolution height,  $\text{fps}$  is the frames per second and  $\text{bpp}$  is the bits per pixel of the video<sup>10</sup>. The calculated bit rate can also be found in Table 5.4. The UAV will record multiple videos simultaneously using all four camera types. Thus, all video streams must be transmitted to the ground station; a total bit rate of 20.38 Mbps is needed to transmit this.

$$\text{bit rate} = \frac{w \cdot h \cdot \text{fps} \cdot \text{bpp}}{10^6} \quad (5.1)$$

**Table 5.4:** The maximum video resolution, frame per seconds and bit rate of each camera type of the Zenmuse H20N

Camera type	Resolution width [px]	Resolution height [px]	Frames per second	Bit rate [Mbps]
WAO	1920	1080	30	6.22
NAO	2688	1512	30	12.19
WATh	640	512	30	0.98
NATh	640	512	30	0.98

#### Transceiver

It was chosen that the UAV would have a transceiver to transmit the data to the ground station. A transceiver was chosen since it can both send and receive data. Six commercially available products were found that can provide these communication functions of the UAV. These products are: pMDDL Radio data link system<sup>11</sup>, SKY HOPPERPRO<sup>12</sup>, BERTEN P6000 Transceiver<sup>13</sup>, BERTEN S-6000 Dual Transceivers<sup>14</sup>, StreamCaster LITE 4200<sup>15</sup>, StreamCaster 4200 Enhanced Plus<sup>16</sup>. The Sky HopperPRO was quickly discarded since it does not meet the system requirement SYS-PER-09; the UAV shall conduct regular operations within a temperature range of -10 to 50 degrees Celsius. The StreamCaster LITE 4200 was discarded as well since it had a lower data rate than the bit rate that must be transmitted for the video streaming. A trade-off was made between the other four transceivers to select the optimum one for the UAV. As a trade-off method, the analytical hierarchy process was used again. The results of the trade-off can be found in Table 5.5. The pMDDL Radio DATA LINK SYSTEM has won the trade-off and will be deployed on the UAV for communications. In addition to the video streaming, this transceiver can also transmit the location of the UAV to the ground sta-

<sup>8</sup>URL:<https://www.omnicalculator.com/other/streaming-bitrate> [20/05/2022]

<sup>9</sup>URL: <https://streamshark.io/blog/bpp-calculator-for-live-stream-bitrate/#:~:text=comes%20in%20handy.-,Generally%20it's%20considered%20that%20a%20BPP%20of%200.1%20is%20the,occur%20during%20your%20live%20stream.> [20/05/2022]

<sup>10</sup>URL:<https://www.omnicalculator.com/other/streaming-bitrate> [20/05/2022]

<sup>11</sup>URL:<https://www.uavos.com/products/communication-systems/pmddlradio-data-link-system/> [25/05/2022]

<sup>12</sup>URL:<https://www.skyhopper.biz/products/communication-data-links/> [25/05/2022]

<sup>13</sup>URL:[https://www.bertendsp.com/pdf/datasheet/BDS005\\_P6000\\_Datasheet\\_v3.0.pdf](https://www.bertendsp.com/pdf/datasheet/BDS005_P6000_Datasheet_v3.0.pdf) [25/05/2022]

<sup>14</sup>URL:[https://www.bertendsp.com/pdf/datasheet/BDS003\\_S6000\\_Datasheet\\_v1.2.pdf](https://www.bertendsp.com/pdf/datasheet/BDS003_S6000_Datasheet_v1.2.pdf) [30/05/2022]

<sup>15</sup>URL:<https://silvustechologies.com/wp-content/uploads/2021/04/StreamCaster-Lite-4200-SL4200-Datasheet.pdf> [30/05/2022]

<sup>16</sup>URL:<https://silvustechologies.com/wp-content/uploads/2021/04/StreamCaster-4200-SC4200-Enhanced-Plus-Datasheet.pdf> [30/05/2022]

tion, which is a signal with a data rate of about 1.023Mbps and has first been processed in the autopilot<sup>17</sup>. The transceiver must thus transmit a data rate of 21.403 Mbps. This transceiver used Multiple-Input and Multiple-Output (MIMO) technologies, which means it uses two antennas.

**Table 5.5:** The trade-off for various transceivers for the UAV

Criteria	Mass [kg]	Size [mm]	Power [W]	Data rate [Mbps]	Final trade-off score
Weights of the criteria	0.199	0.061	0.327	0.414	-
pMDDL Radio DATA LINK SYSTEM	0.09 (dg)	90.5 x 70.7 x 18.2 (lg)	10 (lg)	Up to 25 (y)	3.785 (b)
Berten P6000 Transceiver	0.7 (o)	118 x 107 x 48 (y)	19.6 (y)	Up to 120 (dg)	3.629
Berten S-6000 Dual Transceivers	0.75 (o)	165 x 110 x 37 (y)	14 (y)	Up to 78 (lg)	3.215
StreamCaster 4200 Enhanced Plus	0.425 (o)	101.6 x 66.8 x 38.35 (lg)	5 - 48 (y)	Up to 100 (lg)	3.276

## Antennas

Using the MIMO technique, the pMDDL Radio DATA LINK SYSTEM can transmit and receive signals up to 9 km, without the need of a visual line of sight using two onboard omni-directional 5dBi antennas and two LAN antennas 14dBi for the ground station. Since these kinds of antennas are desired, the UAV will be equipped with two 5dBi antennas that operate at a frequency of 2.4 GHz. This frequency range was chosen since the receiver has a frequency range of 2.402 to 2.478 GHz. The ANTGSM24. Omnidirectional antenna 2.4 Ghz 5dBi was chosen as onboard antenna for the UAV<sup>18</sup>. No trade-off was made since this antenna has the best specifications for a 2.4 GHz 5 dBi omni-directional antenna that can be deployed on a UAV.

For the ground station, the same transceiver will be used, and two LAN 44dBi antennas are desired to receive and transmit signals. These kinds of antennas are, however, all directional and must thus be mounted on a rational boom at the ground station, so that it can be pointed towards the UAV. Two suitable antennas were found: the ANT24D18 Prosafe Wireless LAN antenna<sup>19</sup> and the Antenna 2.4 GHz 14 dBi WiFi Panel Directional Long-Range<sup>20</sup>. A trade-off between the two has been made and can be seen in Table 5.6. In this table 'vert' indicates the beamwidth in the vertical plane and 'horz' indicates the beamwidth in the horizontal plane. A narrow beamwidth is desired since it increases the signal to noise ratio (SNR), which is favorable<sup>21</sup>. The mass and size of the antenna are not very important since this antenna will be deployed on the ground station. As can be seen in the trade-off the ANT24D18 Prosafe Wireless LAN antenna wins due to its narrow beamwidth and thus two of these antennas will be equipped on the ground station. Two of these antennas are needed since the transceiver uses MIMO.

**Table 5.6:** Trade-off between two 2.4 GHz 14 dBi antennas for the ground station

Criteria	Mass [kg]	Size [mm]	Beam width [deg]	Final trade-off score
Weights of the criteria	0.106	0.261	0.633	-
ANT24D18 Prosafe Wireless LAN antenna	1.5 (y)	260 x 240 x 30 (y)	vert: 30, horz: 60 (lg)	3.633 (b)
Antenna 2.4 GHz Directional Long-Range	0.75 (lg)	225 x 185 x 50 (lg)	vert: 30, horz: 80 (y)	3.367

## 5.4. Bird Repellent

Bird strikes pose a substantial operational risk to airborne vehicles. These collisions are of exceptionally high risk for the UAV compared to passenger aircraft due to its small size and non-redundant forward propulsion, as collisions are likely to cause loss of aircraft. The bird would likely also not survive. Therefore, a method is needed to avoid these collisions with birds during cruise. There exist various methods that deter birds. Some of these methods are bird spikes, sonic and ultrasonic devices, lasers and optical deter-

<sup>17</sup>URL:[https://www.researchgate.net/figure/GNSS-typical-signal-The-carrier-is-modulated-by-a-binary-code-and-with-a-far-slower\\_fig1\\_236247299](https://www.researchgate.net/figure/GNSS-typical-signal-The-carrier-is-modulated-by-a-binary-code-and-with-a-far-slower_fig1_236247299) [01/06/2022]

<sup>18</sup>URL: <https://d3.xlrs.eu/product/antgsm24-omnidirectional-antenna-2-4ghz-5dbi/> [30/05/2022]

<sup>19</sup>URL; <https://www.downloads.netgear.com/files/GDC/datasheet/en/AntennaCables.pdf> [31/05/2022]

<sup>20</sup>URL: <https://www.data-alliance.net/antenna-2-4ghz-14dbi-wifi-panel-directional-long-range/> [31/05/2022]

<sup>21</sup>URL: <https://www.data-alliance.net/blog/antenna-beamwidth/> [31/05/2022]

rents and pyrotechnics<sup>22</sup>.

Ultrasonic devices are not very practical for detecting birds, since some birds can not hear these kinds of sounds<sup>23</sup>. Pyrotechnics and spikes will not be used on the UAV to scare away birds since they may hurt the birds, what is against the mission of the UAV<sup>24</sup>. Laser and optical deterrence methods are very effective for birds. They emit laser light in the green spectrum. Birds perceive these lasers as physical objects and will trigger their natural flight or fight instinct. Due to this, the birds will flee without any harm to the bird<sup>25</sup>. Sonic devices to repel birds emit sounds of distressed bird calls or predator sounds. These kinds of sounds scare the birds away and are normal sounds to the environment, so they will not disrupt other wildlife<sup>26</sup>.

### **Sonic repellent device**

The Kruger park is inhabited by a lot of different birds that can be a threat to the UAV. It has many species of birds, from very common species like doves to large predator birds like eagles and hawks<sup>27</sup>. Sonic devices to repel birds often use the sounds of predators, which include the sounds of hawks. Thus, these sonic devices may not work for some predator birds in the Kruger park, since they will not be scared off by these sounds and may even trigger an attack. To avoid attacks by these predator birds, the wing span of the UAV must be larger than those of the birds, so the UAV is the 'bigger bird in the air'. However, this device will repel most other birds in the area. The M2E speaker, which is a specially designed speaker for drones, could be used for this repellent method<sup>28</sup>. This speaker can play up to ten custom recordings, and thus recordings of predators of the birds could be played by this speaker. This speaker has a size of 68 mm x 55 mm x 65 mm, a maximum power consumption of 10 W and costs 89 euros<sup>29,30</sup>. Additionally, the system should also have a movement sensor to work. The speaker will then be turned on once the sensor has detected movement. The B+B Thermo-Technik PIR-bewegingssensormodule PIR-STD could be used for this<sup>31</sup>. This sensor costs about 20 euros, and has a size of 20 mm x 25 mm x 25 mm and power consumption of 16.8 mW.

### **Laser repellent device**

Commercially available laser and optical bird repellants are either handheld devices or are stationed on the ground. Thus, no commercially available repellent of this kind could be equipped on the UAV. However, a simple repellent could be designed using green laser light and a movement detector. No detailed design will be given in this report, but a short description of the concept will be provided. This device will consist of a fully rotatable laser light that emits green light and a movement detector. When the movement detector detects approaching birds, the laser beam will be turned on and pointed to the target. Once the target is repelled, the laser beam will be turned off again. One disadvantage of this system is that the laser beam could never be operational with a 360 degrees view since the UAV will block the laser beam in certain cases. Thus, multiple of these systems should be applied to the UAV to function. An initial sizing has been made for this system. The sizing is based on a laser module and a movement detector. For the laser module, a laser of green light will be used with a wavelength of 532 nm with a laser rating of 2 and a power consumption of 1mW. These values are based on a commercially available bird repellent<sup>32</sup>. A small laser module with

<sup>22</sup>URL: <https://foodsafetytech.com/column/bird-problems-and-control-methods-for-food-production-facilities/> [10/05/2022]

<sup>23</sup>URL: <https://www.birdbgone.com/blog/bird-control-devices-that-work-and-those-that-dont/> [01/05/2022]

<sup>24</sup>URL: <https://www.nj.gov/agriculture/pdf/pyrotechnicsforbirdmanagement.pdf> [10/05/2022]

<sup>25</sup>URL: <https://www.birdcontrolgroup.com/> [10/05/2022]

<sup>26</sup>URL: <https://www.birdbgone.com/blog/how-sound-bird-deterrents-work-to-scare-birds-away/> [10/05/2022]

<sup>27</sup>URL: [https://www.krugerpark.co.za/information/Africa\\_Bird\\_Guide.html](https://www.krugerpark.co.za/information/Africa_Bird_Guide.html) [10/05/2022]

<sup>28</sup>URL: <https://www.dji.com/nl/mavic-2-enterprise-advanced> [10/05/2022]

<sup>29</sup>URL: <https://www.dji.com/nl/mavic-2-enterprise/specs> [10/05/2022]

<sup>30</sup>URL: <https://www.dronewinkel.eu/mavic-2-enterprise-part-05-speaker.html> [10/05/2022]

<sup>31</sup>URL: <https://www.conrad.nl/nl/p/b-b-thermo-technik-pir-bewegingssensormodule-pir-std-12-v-dc-3-12-v-dc-1-x-b-x-h-20-x-25-x-25-mm-1-stuk-s-172500.html> [10/05/2022]

<sup>32</sup>URL: <https://www.diergedrag.nl/a-61509209/vogels/laser-vogelverjager-buiten> [10/05/2022]

these specific parameters was found, the TRU COMPONENTS Lasermodule Punt Groen 1mW LM01GND<sup>33</sup>. For the detection module, a PIR sensor will be used, for a conceptual sizing the B+B Thermo-Technik PIR-bewegingssensormodule PIR-STD will be used<sup>34</sup>. Using these specific modules of the laser module and passive infrared (PIR) sensor, this bird control system will cost about 45 euros and consume about 16.9 W power, and has a size of about 70 mm by 39 mm by 39 mm. Note that these values are without a system that will make the laser module able to rotate.

## Selected repellent device

The sonic device will be used to repel birds. The sonic device has been chosen over the laser device since the sonic device can scare off multiple birds at once, while the laser can only target one bird at a time. Targeting multiple birds at once is more desired since birds often travel in flocks. The sonic device is also preferred over the laser device because a speaker for UAVs is already commercially available, which can fulfill this task. Thus, the birds will be scared of by the M2E speaker which will play sounds of predators. A PIR sensor will turn on the speaker once a bird is in the vicinity of the UAV.

## 5.5. Payload Budget

With all the sensors and payload that will be equipped on the UAV, a budget has been made. This budget keeps track of the costs, power consumption, and mass of all these parts. The size of each component is also stated since it will be used to give the location of all these components on the UAV. This budget can be seen in Table 5.7.

**Table 5.7:** Budget for the payload and sensors that will be equipped on the UAV.

Sensor type	Mass [kg]	Power consumption [W]	Cost [Euro]	Size [mm]
Camera & long range LiDAR <sup>1</sup>	0.88	45	~ 15,000	161 x 178 x 135
Short range LiDAR <sup>2</sup>	0.9	16	~ 8,100	87 x 103 dia
Bird repellent speaker <sup>3</sup>	0.15	10	~ 90	68 x 55 x 65
PIR <sup>4</sup>	-	0.034	~ 40	20 x 25 x 25
Autopilot <sup>5</sup>	0.19	5	~ 5,800	63 x 67.9 x 39.6
GNSS antenna <sup>6</sup>	0.1	0.29	~ 200	15 x 57 dia
Transceiver <sup>7</sup>	0.09	10	3,000	90.5 x 70.7 x 18.2
Antenna (2x) <sup>8</sup>	0.05	-	~ 9	L: 195
<b>Total</b>	2.36	86.3	~ 32,250	-

<sup>1</sup> Zenmuse H20N

<sup>2</sup> M8-1 Ultra

<sup>3</sup> M2E speaker

<sup>4</sup> B+B thermo-technik PIR-bewegingssensormodule (2x)

<sup>5</sup> Autopilot 1x

<sup>6</sup> GPS Antenna advanced SSMA

<sup>7</sup> pMDDL Radio DATALINK SYSTEM

<sup>8</sup> ANT GSM 2.4. Omnidirectional antenna 2.4 GHz 5dBi

<sup>33</sup>URL:<https://www.conrad.nl/nl/p/tru-components-lasermodule-punt-groen-1-mw-lm01gnd-1566747.html#productDescription> [10/05/2022]

<sup>34</sup>URL: <https://www.conrad.nl/nl/p/b-b-thermo-technik-pir-bewegingssensormodule-pir-std-12-v-dc-3-12-v-dc-1-x-b-x-h-20-x-25-x-25-mm-1-stuk-s-172500.html> [10/05/2022]

# Operations and Logistics

This chapter aims to address all topics related directly to the UAV, which are not relevant to the design. These topics do not comprise the main body of this report, but are however important to give the reader an idea of the context surrounding the UAV and how it is intended to be operated.

Firstly in Section 6.1, the climate in which the UAV will operate is discussed. Next, the flight operations are reviewed in Section 6.2, followed by a brief explanation of the processing of the camera footage in Section 6.3. The concentration is shifted to the ground station in Section 6.4 and to the refueling operations in Section 6.5. The different types of hydrogen is explained in Section 6.6. The scalability of the system is discussed in Section 6.7. The procedures in the case of an emergency situation are explored in Section 6.8. Furthermore the internal and external communication are discussed in Section 6.9. The chapter is concluded with a discussion of the UAV certification in Section 6.10 and end-of-life processing in Section 6.11.

## 6.1. Climate Considerations

As a case study, the UAV is designed for the Kruger National Park in South Africa. This case study has given some requirements to the UAV. For other environments, other considerations would need to be taken into account. Since the UAV cannot be tailored to all conditions, it has been decided that if the UAV is to be used in other extreme conditions, this study should be revised.

The temperature in the Kruger National Park can range from 10 degrees Celsius during its winter months to up to extremes of 47 degrees Celsius during hot summer days<sup>1</sup>. The UAV has to withstand this temperature range to complete the mission. The most critical systems to which this applies to are the propulsion system and the surveillance components (cameras). Besides the temperature, the UAV must also withstand the average winds speeds in the national park of 5.11 m/s<sup>2</sup>. Dust is also a big issue in the park, and may have a large impact on the lifetime of the UAV and the quality of the camera footage. In order to reduce the impact of dust on the performance of the UAV it should be cleaned regularly.

Ideally after every flight the drone should be cleaned with a water spray, however, this is unrealistic with our application. Since the UAV will land and be stored in the ground station this should reduce the amount of dust on the craft. This is due to the fact that the majority of the dust would be kicked up by the VTOL propulsion during take off and landing, the ground station will then act as a barrier between the aircraft and the ground. Furthermore, when the drone is stationary between flights the dust kicked around by the wind would be able to reach the craft depositing a layer of dust. This problem is solved by the fact that the ground station can be sealed to protect the UAV from the environmental conditions while being idle. Nonetheless, it is still required that the drone be cleaned at least once a week to reduce the degradation cause by dust. Since the ground station will need to be refueled every week in order to provide fuel for the week's mission, it would be possible to coordinate cleaning the UAV simply with water at the same time. This procedure would not require additional specialized staff therefore not increase the cost.

In the future the team would like to automate this step in a way that the drones may be cleaned after every flight. This automation would be a system integrated directly in the ground station. Two options would be available in order to achieve this, first a water tank could be added to the ground station, storing water for the week it could be filled up by non-specialized personnel every week during the hydrogen refueling. Secondly, if the ground station is installed near water sources, the water tank could be bypassed and water would directly be taken from the source to clean the UAV.

<sup>1</sup>URL:<https://www.safaribookings.com/kruger/climate>[11/05/2022]

<sup>2</sup>URL:<https://wanderlog.com/weather/79419/7/kruger-national-park-weather-in-july>[11/05/2022]

## 6.2. Flight Operations

### Mission profile

To determine the specifics of the operations during flight, the mission profile of the UAV needs to be set first. The mission profile can be seen in Figure 6.1. At the start of each flight the UAV will first start up while it is based on the ground station. After start up, the UAV will take off vertically using its VTOL propellers. It will fly to an altitude of 50 m. This altitude was determined by taking twice the height of the tallest trees in the Kruger National Park, which is about 25 m<sup>3</sup>. Based on experience, the DSE Group 11 has chosen the Rate of Climb (RoC) to be 3 m/s. Using this rate of climb and the 50 m altitude, it was found that the vertical take-off takes about 17 seconds.

After the UAV has reached the 50 m, the UAV will transition from VTOL to forward flight. The forward flight propeller will be turned on, while the VTOL propellers will be turned off once a specific climb speed is reached. This speed will be determined later in the propulsion and power system design chapter. After this transition, the UAV will climb to its cruise altitude using its wings and the forward flight propeller. The same rate of climb of 3 m/s will be used for this as for the vertical take-off<sup>4</sup>. It was chosen that the UAV will not perform the entire ascent cruise altitude in VTOL mode, since this expends significantly more power than conventional forward flight climb. Therefore, the UAV will take off vertically to a set altitude, and then transition to forward facing climb. During this climb, the cameras are already turned on and the area will already be surveilled for threats.

Once the cruise altitude is reached, the UAV will continue to surveil the area to be monitored at its cruise speed of about 22 m/s. Once the area is completely monitored, the UAV will return to the ground station. During return the UAV will slow down to its stall speed. Once the stall speed is reached, the UAV will transition back to its VTOL propellers and the landing is initiated. The UAV will land with a speed of 2 m/s from the cruise altitude. Once landed on the ground station the UAV will power down and will be refueled.

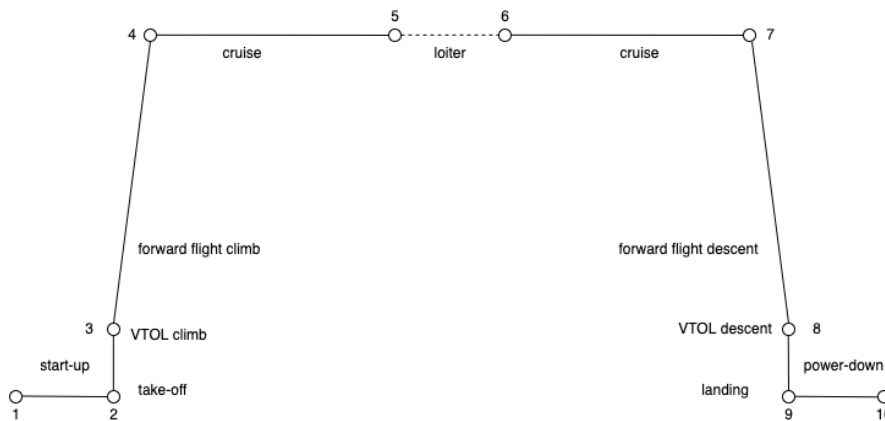


Figure 6.1: Mission profile characteristics of UAV.

### Flight altitude

The cruise flight altitude of the UAV is constrained by SYS-PER-04 (the cruise altitude is at minimum 120 m) as well as the resolution of the cameras of the Zenmuse H20N. Mission objectives include detecting poachers, litter and wildfires. Out of these three threats, the most constraining one in terms of resolution is to detect the poachers. Human beings are hard to be distinguished from animals at low resolution with a thermal camera and this will make it hard to detect poachers [6]. Wildfires are easier to detect since they have a clear thermal footprint and litter is expected to be evident during the daylight with the optical camera.

<sup>3</sup>URL:[https://www.krugerpark.co.za/Kruger\\_National\\_Park\\_Wildlife-travel/kruger-park-trees.html](https://www.krugerpark.co.za/Kruger_National_Park_Wildlife-travel/kruger-park-trees.html) [03/06/2022]

<sup>4</sup>URL: <https://www.skyeyesystems.it/products/rapier-x-25/> [03/06/2022]

To detect poachers it is required that the surface of a human being on the ground is scanned by no less than 30 pixels [6, 7]. The smallest surface area of a human being,  $A_{tot_h}$ , that needs to be considered is the area of a human standing. This area is assumed to be  $1 \text{ m}^2$ , since this encompassed a human of 2 m in height and 0.5 in chest width. However, the outline of the person would effectively only occupy the projection of its surface area on the plane perpendicular to the line connecting it to the camera. This translates to a surface area ratio total-to-effective equal to the cosine of  $\theta_{aim}$  (Figure 6.2). Therefore, the effective expected surface area occupied by a person is  $A_{eff_h} = A_{tot_h} \cdot \cos(45^\circ) = 0.707 \text{ m}^2$  when  $\theta_{aim}$  is estimated to be around 45 degrees. DSE Group 11 however feels that 30 pixels is unrealistic and hence will adopt a pixel density of 200 pixels per person of the aforementioned dimensions.

**Table 6.1:** Zenmuse H20N system camera data on FOV and resolution.

Zenmuse H20N camera	FOV [deg]	max zoom	image	
			width [px]	height [px]
wide-angle optical (WAO)	73.6	-	1920	1080
narrow-angle optical (NAO)	66.6	x20	3840	2160
wide-angle thermal (WATH)	45	x2	640	512
narrow-angle thermal (NATH)	12.5	x8	640	512

**Table 6.2:** Input variables for altitude constraint based on the Zenmuse H20N

Parameter	Value
cruise speed [m/s]	22.23
min flying altitude [m]	120
objective monitored area [km <sup>2</sup> ]	5
$A_{tot_h}$ [m <sup>2</sup> ]	1
effective human area ratio [-]	$\cos(45^\circ)$
$A_{eff_h}$ [m <sup>2</sup> ]	0.707

The specification of the four cameras of the Zenmuse H20N that will be used to determine the altitude is specified in Table 6.1. The input variables used for the calculations are specified in Table 6.2. Starting from this data, the expected resolution of human figures on the ground is computed. This allows to assess whether the pixel count drops below the critical values. First the cross track width,  $w_{ct}$ , sometimes referred as swath width, was computed using Equation 6.1. The cross track width is the ground length corresponding to the line of pixels closest to the camera. For clarity about the cross track width Figure 6.2 and Figure 6.3 can be viewed. In the calculation carried out,  $\theta_{below-horizon}$  was set to 0 for the WAO camera. This was made so that there is a constant outlook on the entire horizon, which is desirable for spotting smoke columns from wildfires. Setting  $\theta_{below-horizon}$ ,  $\theta_{aim}$  follows as the distance between the perpendicular with the ground and the middle of the WAO camera, this angle is the same for all the cameras.  $\theta_{blind}$  is specific for each camera and is especially relevant as it determines the  $w_{ct}$ .

$$w_{ct} = 2h \tan\left(\frac{FOV}{2}\right) + 2h \tan(\theta_{blind}) \tan\left(\frac{FOV}{2}\right) \quad (6.1)$$

By dividing the objective monitored area (Table 6.2) by the  $w_{ct}$ , the length of the straight strip of land to be scanned ( $l_{gr-st}$ ) is obtained. The distance that each pixel covers with its side in the width direction ( $w_{px}$ ) is computed dividing  $w_{ct}$  by the pixel count in the width direction (Table 6.1). The available resolution for human figures is obtained dividing the  $1 \text{ m}^2$   $A_{eff_h}$  times the cosines of 45 degrees by the area covered by 1 pixel ( $w_{px}^2$ ). The available resolution for human figures from the narrow-angle cameras shown in Table 6.3 is sufficient for the lowest altitude even without any zoom. To determine the maximum cruise flight altitude an iterative process was done. A maximum cruise altitude was found to be 855 m. This is due to the increased pixel density chosen by the group. At this altitude, poachers could still be detected using the thermal narrow angle camera. This means that the constraints due to the camera and the requirements lead to a cruise altitude in between 120 m and 855m. When the noise produced by the UAV is analyzed, the definitive altitude will be decided upon.

**Table 6.3:** Camera view data for minimum altitude and maximum altitude constraint by the camera

Camera	h [m]	Zoom	$w_{px}$ [cm]	av - $px_{pp}$ [-]
NATH	120	1	8.5	98
	855	8	8.4	100
NAO	120	1	5.6	226
	855	8	7.8	116
WATH	120	1	24.8	12
	855	1	176.4	0.23
WAO	120	1	12.1	48
	855	1	86.2	0.95

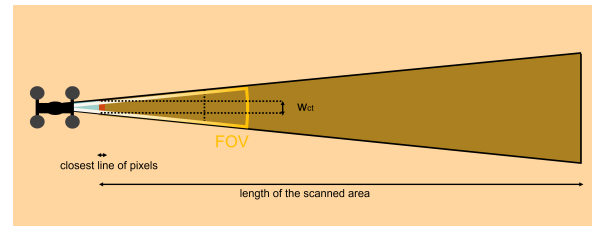
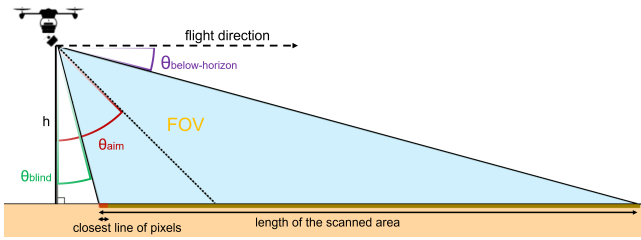


**Figure 6.2:** Side view schematic of the UAV scanning an area with an angled FOV. A number of different angles are indicated on the graph. Adjusted from [8]

**Figure 6.3:** Top view schematic of the ground area scanned by a UAV.

## Camera usage

The UAV has four different types of cameras, two visual and two thermal cameras. All these types of cameras will be used continuously. During the day, the thermal cameras will most likely be less effective to detect poachers, since the surrounding environment may heat up to the same temperature as poachers and animals. However, wildfires can still be spotted with the thermal cameras since they have a clear thermal footprint. To detect the other two threats during the day, the visual cameras will mainly be used. At night, all cameras will be used as well to record footage. The thermal cameras are especially effective during the night, since poachers could be spotted due to their thermal footprint. Most poachers will be active during the night, and it is thus of utmost importance that they will be spotted. The narrow angle thermal camera (NATH), will define the flight path during the night. This camera will define the flight path since poachers will most likely be spotted with this camera since it is a thermal camera, and it has a high average pixel per person. Thus, the swath width of the NATH will be constraining the flight path taken and the amount of kilometers that has to be flown to survey an area. The swath width of the four cameras at the minimum and maximum flight altitude can be found in Table 6.4. Note that the zoom for the NATH is at 1 for 120m and 8 for 855m.

**Table 6.4:** Swath width for the four camera types at minimum and maximum flight altitude

Camera	h [m]	$w_{ct}$ [m]
NATH	120	54
	855	54
NAO	120	215
	855	299
WATH	120	158
	855	667
WAO	120	232
	855	1714

## Flight path

An important part of the daily operations of the UAV is the flight path it will follow when surveying. In a previous report [2] it was determined that a zigzag flight path is the most efficient, when compared to other options such as circles or spirals. Since the details of the final design concept are now known, the flight path can be optimized. Firstly, the zigzag concept will be reviewed. Subsequently, details such as exact flight path, taking into account turn radius, overall efficiency and probability of poacher detection, will be determined.

Figure 6.4 intends to demonstrate the basic flight path that the UAV will follow. Importantly, this configuration ensures minimal double-coverage within the surveillance area as well as having the ground station in the corner. When the UAV will start its surveillance mission it will first go to the furthest corner of the square to scan by going along two sides of the area. This is done in order to have the maximum distance between the ground station and UAV at the earliest possible part of the mission. This permits no loss of efficiency as scanning can start immediately and means that as the UAV scans the area it will get closer to the center of its total area of operation. This is advantageous as the UAV will have the largest amount of endurance possible left when it is the furthest from the ground station and allows it to answer to emergencies with a larger safety margin of fuel. Similarly, as the UAV ends its mission close to the ground station it will be allowed to answer emergencies with a more optimal safety margin, than if it was positioned further away from the center of its total coverage area. Now that it is known that the UAV will be a hydrogen powered VTOL, it is clear that the landing-refuel-take-off cycle can be very quick. This is beneficial because if a ground station is in the corner of a surveillance zone, it in fact has the ability to cover 4 surveillance zones twice in a single day without compromised efficiency. This will greatly reduce the number of UAVs needed to cover the entire area, such as the Kruger National Park as addressed in the case study.

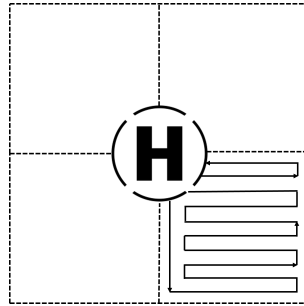


**Figure 6.4:** Visualization of the zigzag flight path the UAV will complete to survey the target area

In the optic to optimize the area covered by a UAV for each mission a more precise computation of the flight path is required. Using a python script created with the side of the square area to cover ( $L_{sidesquare}$ ) and the scanning width of a camera ( $w_{view}$ ) as input, the distance needed to be traversed by the UAV may be found. This is done by using the following equations:

$$Distance_{covered} = L_{sidesquare} + n_{lines} * (L_{sidesquare} - w_{view}) \quad (6.2)$$

$$Area_{covered} = Distance_{covered} * w_{view} \quad (6.3)$$

Equation 6.2 calculates the distance covered by the UAV by adding one side of the square with the number of lines traversed ( $n_{lines}$ ) by the UAV multiplied by the scanning width. In this case the smallest scanning width is taken in order to allow all the cameras to cover the entirety of the area. The number of lines is increased until the area covered obtained using Equation 6.3 is superior to the area of the scanned square. Once this has been obtained the final distance travelled is obtained by adding the distance between the UAV and the station. This computation depends on the number of lines used during the scanning operation. In case this number is even the UAV will end on the opposite side of the ground station so the distance added is computed with Equation 6.4. While, if the number of lines is odd the UAV will end on the same side of the ground station and the additional distance is computed by Equation 6.5.

$$Distance_{added_{even}} = \sqrt{L_{sidesquare}^2 + (L_{sidesquare} - (n_{lines} - 0.5) * w_{view})^2} \quad (6.4)$$

$$Distance_{added_{odd}} = \sqrt{w_{view}^2 + (L_{sidesquare} - (n_{lines} - 0.5) * w_{view})^2} \quad (6.5)$$

With the help of this script it is possible to find an optimal area being able to be covered while including safety margins. The limiting factor put in place is the amount of endurance left after the entire area has been scanned. This reserve should suffice to account for the take off and landing of the UAV. Furthermore it should also permit the UAV to go and come back to any corner of the total coverage area from the ground station at the end of its mission, where the lowest amount of endurance would remain. On top of the latter distance described a margin of 5% of the endurance is reserved for the take off and landing procedures. For this computations the velocity is assumed to be constant and is set at the cruise speed of 22.22 m/s. Following this, the optimal area that can be scanned in one mission is found to be 35 km<sup>2</sup>, the rest of the characteristics for the area can be found in Table 6.5.

**Table 6.5:** Optimal area to be scanned in a single mission characteristics

Scanning width [km]	Length of square side [km]	Distance covered [km]	Actual area covered [km <sup>2</sup> ]	Number of passes/lines [-]	Endurance required [mn]
0.72	5.9	130.1	35.3	21	101.3

## Threat detection

The purpose of Usambara is to protect and survey wildlife and its environment, with the three threats: poachers, fire and litter at the forefront. Three machine learning software programs are chosen to help with the detection of these threats.

First, SPOT, a near real-time AI poacher detection program [9], is chosen. SPOT uses infra-red images or live stream data to quickly and correctly detect poachers through machine learning. As previously mentioned, SPOT works best during the night as then the temperature of the surrounding area is significantly lower than that of a human. After the detection of a poacher, an alert will be sent to the park rangers and Usambara will loiter around the poachers with the help of SPOT. Second, for forest fire detection, a software method, as discussed by Hossain, Zhang and Tonima in [10] can be used. This software is based on the capture of static images where the color and texture features of smoke and flame are then analyzed. With the wide angle camera partly pointed towards the horizon, smoke and flames should be captured quite early and detected with the software. An alert will once again be sent to the rangers, who will then double check through the video live stream. Lastly, litter, as small pieces are almost impossible to detect from a UAV at 600 meters, and as it is not feasible to clean up every small piece of litter over a large terrain, only pieces that are bigger than 1 m<sup>2</sup> (or approximately the size of an oil barrel) are included. Software, as described in Knaeps is chosen for this purpose<sup>5</sup>. This software can detect large pieces of plastic in the ocean or on the beach through multi-spectral cameras and AI technology that has incorporated data of the spectral reflectance of marine plastics

## 6.3. Footage Processing

The footage recorded by the cameras has to be processed in order to detect threats in the environment. The UAV will have an algorithm that can detect poachers, litter and wildfires automatically from the video footage. It was chosen that such an algorithm will be used, since it will increase the chances of detecting a threat. Besides this, the footage will also be streamed to the ground station, which can then pass it on to an operator in a central control center. Here, immediate action can be taken by the operator in the event of the detection of a threat, by means of an alarm system. In addition to this, the footage can be stored locally for later inspection if required.

<sup>5</sup>URL: <https://vito.be/en/news/artificial-intelligence-detect-marine-plastic-litter> [15/06/2022]

## 6.4. Ground Station Layout

Despite the UAV being the central topic of this report, the ground station and its basic design will also be addressed. The goal of the ground station within the scope of this project is to serve the UAV as a refueling point and to protect the UAV when it is not in the air. A large assumption that is made at this point is that the ground station has access to a power supply, be it from a power grid or a local power source, such as hydrogen, solar or another renewable alternative. This implies that there is no power limitation for the ground station while communicating, or providing power for the UAV while it is grounded. The viability of this could be assessed in a later report.

Firstly, the protection of the UAV while on the ground will be addressed. The environments in which the UAV will be active, such as wildlife zones, can often be very dusty, and sunny during the day. Without forgetting that wildlife may interfere out of curiosity, the group decided that the UAV must be fully covered while stationed on the ground. The least invasive design appears to be one where two hinged hatches can open when the UAV intends to land and close over the UAV once it has landed. A preliminary design is included in Figure 6.5.

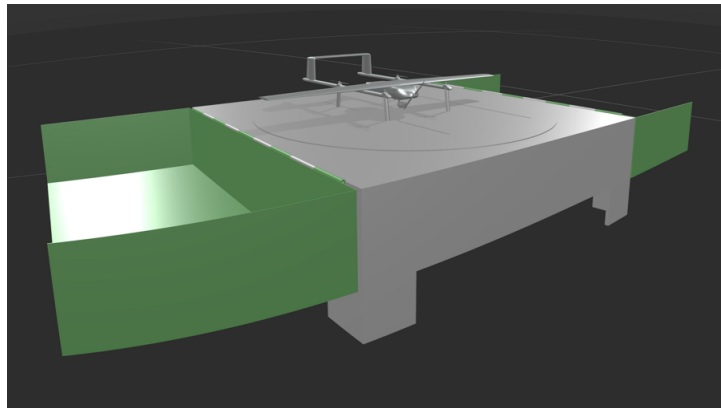


**Figure 6.5:** First design of ground station for the UAV

Given that the span of the UAV will be approximately 3 m, the ground station will require space of about 30 m<sup>2</sup>. This is because of the rotating hatches and equipment surrounding the landing pad. Despite this being fairly large, the amount of time which the ground station is active and making noise or causing vibrations that may disturb the wildlife surrounding it is very low. Therefore, the group argues that the advantages like safety and reliability are substantially higher than the disadvantages such as noise and vibrational disturbances.

The ground station is intended to be constructed out of a recycled polymer which is strong against the elements while still being able to protect the UAV from all of the environmental conditions and curious wildlife. Another benefit of the recycled polymer hatches is that they are relatively light when compared to, for example, a metal or concrete material. This ensures easy transportation of the ground station to its location, as well as easier removal if it needs to be moved or replaced. Furthermore, the actuators needed to rotate the hatches will not need to be as large, meaning that less noise and vibrations will propagate to the surroundings.

## 6.5. Refueling Operations

The UAV has to be refueled after every flight to ensure the fuel cells can provide the required energy during each flight. The UAV will have a hydrogen tank on board that will be refueled. This refueling process will be done once the UAV has landed at the ground station. At the ground station, the supplied hydrogen will be stored in a high pressure, high volume composite overwrapped pressure vessel (COPV) tank. This tank will have a higher pressure and a higher volume than the onboard hydrogen tank of the UAV. A higher pressure

and higher volume is necessary so the hydrogen will flow towards the onboard hydrogen tank. A pressure regulator will be used to ensure a proper filling pressure. Besides this the system will also have a control valve that will isolate the storage tank of the ground station. The storage tank of the ground station and the onboard hydrogen tank of the UAV will be connected with a quick disconnect.

During the refueling process, the hydrogen will warm as it expands in the onboard hydrogen tank of the UAV. To make sure some systems of the UAV will not overheat due to this heat, a cooler will be used in the filler line that cools the hydrogen once it flows towards the UAV. Once the hydrogen is in the onboard hydrogen tank the hydrogen will cool down and this will lower the pressure in the tank. For this reason, the pressure to which the tank will be filled will be approximately 5 to 10% higher than the required tank pressure to ensure the fuel cells can provide enough energy during the flight<sup>6</sup>.

In the center of the ground station platform where the UAV lands, is positioned a refuelling rod. This apparatus consists of a retractable robot arm integrated with a hydrogen refuelling system. Once the UAV lands and has lined up with the refuelling rod, the arm will extend till it makes contact with the drone's hydrogen intake. Once contact is achieved the arm will rotate in order to secure the connection. It is then possible to proceed with the refuelling of the drone. The hydrogen flow rate used is based on research on the average flow rate used currently as well as the regulation put in place by the Society of Automotive Engineers. These values reflect better rates used in the automotive industry but serve as a great guideline for the UAV. For these reason a low estimate of a flow rate of hydrogen of 0.025 kg/s is taken. [11, 12] Considering the amount of hydrogen required for each flight is roughly 80g it will taken a little over 3 seconds for the UAV to be refuelled. Consequently, this leads to no interruptions of the 8 missions a UAV has to lead every day and may even allow the number of missions to be increased in the future. Considering the currently scheduled 8 missions a day, the amount of hydrogen the ground station should provide every week will be 4.5 kg. This would require a large tank installed in the ground station that will require to be refuelled every week. This does require trained personnel and appropriate transport which does lead to a slight increase in price.

## 6.6. Types of Hydrogen

Hydrogen was selected as a fuel for this UAV due to its zero emissions capabilities as well as its relatively easy production. The only emission created by using hydrogen in conjunction with a fuel cell is water vapor. This can still be considered to be a green house gas, although due to its condensable property it is not considered to be detrimental to the environment.<sup>7</sup> Compared to other green house gas produced by humans, water vapor has a short life span and does not cause warming of the earth for extended periods of time.<sup>8</sup> However not all hydrogen is produced in the same way, and some generate more pollution than others in their production. Hydrogen is classified by different colors based on the method of production. Some of the most important classifications of hydrogen can be found in Figure 6.6<sup>9</sup>.

<sup>6</sup>URL:[https://info.ballard.com/hubfs/Premium%20Content/Hydrogen%20Fuel%20Cells%20for%20UAVs%20Refueling%20Developments/WP-Hydrogen-Fuel-Cells-for-UAVs-Refueling-Developments.pdf?\\_\\_hstc=69339407.a8cac84de3faf2becf32a079074b1f1f.1541599055665.1541599055665.1541599055665.1&\\_\\_hssc=69339407.1.1541599055665&\\_\\_hsfp=3313839345](https://info.ballard.com/hubfs/Premium%20Content/Hydrogen%20Fuel%20Cells%20for%20UAVs%20Refueling%20Developments/WP-Hydrogen-Fuel-Cells-for-UAVs-Refueling-Developments.pdf?__hstc=69339407.a8cac84de3faf2becf32a079074b1f1f.1541599055665.1541599055665.1541599055665.1&__hssc=69339407.1.1541599055665&__hsfp=3313839345) [03/06/2022]

<sup>7</sup>URL:<https://www.acs.org/content/acs/en/climatescience/climatesciencenarratives/its-water-vapor-not-the-co2.html> [19/06/2022]

<sup>8</sup>URL:<https://climatechangeconnection.org/science/what-about-water-vapour/> [19/06/2022]

<sup>9</sup>URL:<https://deeptechexpress.com/colors-of-hydrogen/> [19/06/2022]

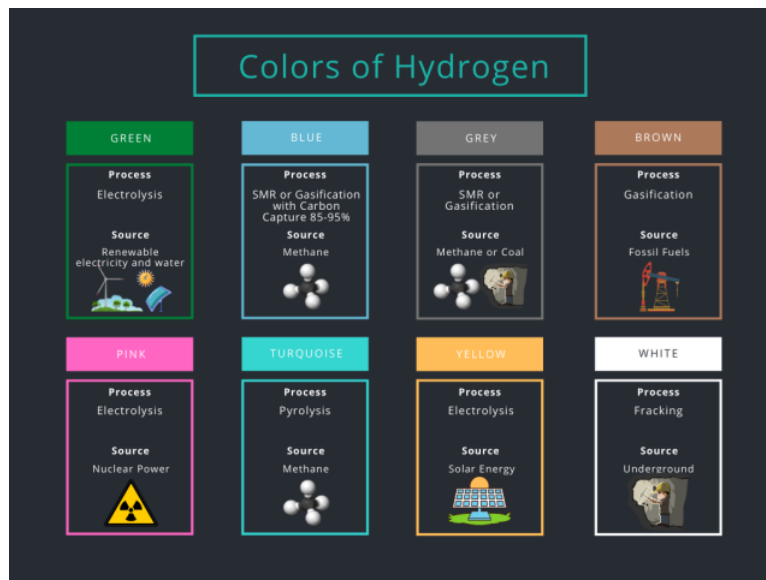


Figure 6.6: Hydrogen classification by colors

From the eight hydrogen colors seen in the figure above only two allow a zero emission production of hydrogen. These are green and yellow hydrogen produced respectively by renewable resources and solar/grid energy. Both of these uses electrolysis to turn water into clean hydrogen, another type of hydrogen that uses this technique is pink hydrogen. Pink hydrogen is produced through electrolysis but is powered by nuclear energy leading to the production of nuclear waste. The other five types of hydrogen use the refinement of fossil fuels or fracking in order to produce hydrogen. These represent the least sustainable hydrogen production methods. However, it should be highlighted that blue hydrogen, using steam methane reforming or gasification, captures and stores the carbon emissions and can therefore be considered to emit low carbon emissions. Furthermore, turquoise hydrogen uses pyrolysis to refine methane, which leads to a by-product of solid carbon that can be used in other applications. Compared to releasing carbon dioxide in the atmosphere, this solid carbon has a smaller impact on the environment, especially if it's used sustainably and is not used as a combustible.<sup>10</sup>

From this analysis and with the objective to develop a sustainable product on all different levels, the team has for goal to prioritise the use of clean hydrogen such as green and yellow hydrogen. Of course, this may be difficult since these methods of production represent a minority in the global hydrogen production. For this reason, the team has deemed acceptable to use pink, turquoise and blue hydrogen as a complementary to the previously mentioned two colors as these are the least detrimental to sustainability. The usage of green and yellow hydrogen will of course be prioritised and hopefully will be able to fully supply the project needs as they become more affordable and widespread.

## 6.7. Scalability

An extremely important functionality of the system, is that it is self-contained, but has opportunity for integration with other systems. This means that the system can be scaled up depending on the situation. This is because, like in the case study of the Kruger National Park, sometimes a large number of UAVs are necessary in order to complete the mission. However, in other cases, such as when the UAV is used to surveil smaller areas or only specific areas within a larger operating area, a system will consist of only a single UAV.

The integration of multiple UAV-ground station setups into a bigger system will be done with software. Despite this being out of the scope of this report, which is intended to design the UAV itself, an indication of how DSE Group 11 think that this can be best implemented will be given. Starting with a single unit, in the middle of a square of 4 surveillance zones, this can obviously be expanded by stacking these operational

<sup>10</sup>URL:<https://www.weforum.org/agenda/2021/07/clean-energy-green-hydrogen/> [19/06/2022]

areas next to each other. However, it is expected that this is not the most effective method to have control of an area. Ground stations can be placed in strategic locations where fire is of high risk, or where poachers are known to be active. While being close enough to each other such that in the event of a failure a UAV from a nearby ground station can still do an acceptable sweep of the area, a series of a relatively small number of UAVs can effectively cover a large area.

## **6.8. Emergency Operational Profile**

During the flight, some unexpected situations may occur that need a special operation. The UAV may be susceptible to a crash or a loss of power. The operational procedures that must happen in case of these events will be addressed in this section.

In case of a crash of the UAV, its location will be established on the last location update the UAV has sent to the ground station. Since the UAV will update its current location continuously, the UAV will most likely be close to the last location update it has sent in case of a crash. Once the location is established, the operator will alarm the person who will be in charge of UAV recovery, for example, a park ranger. This person will drive to the location of the crash and will recover the UAV if it is safe to recover. If a fire has started due to the crash, the local fire department will immediately be called. When the UAV has been safely recovered, it will be inspected to check the cause of the crash and checked if it can be repaired. In case of bad weather, the UAV may also be susceptible to a crash. To prevent crashes due to weather, the operator of the UAV mission will monitor the weather conditions in the area. If bad weather is predicted, the UAV will be instructed to return to the ground station.

A UAV may lose power during flight or may be low on power. A power module monitors the fuel cells and hydrogen tank and updates the autopilot on these systems. If the power levels are low, a signal will be sent out to the flight control system, which will order the UAV to fly back to the ground station where it will recharge. The number of times a UAV returns to the ground station to refuel even though it has not completed its surveillance will be monitored. If it is noticed that one particular UAV often ends its surveillance early to recharge, a maintenance team will be sent to check on the UAV. The maintenance team will check the power system of both the UAV and the ground station, and also the refueling system to see if there are any leaks or other deficiencies. In case the UAV has a total power loss during its flight, it will glide down and will be picked up by a recovery team once it has landed.

## **6.9. Communications**

This section aims to explain the communications within the UAV and with the UAV to external sources. Section 6.9 explains the external communications, these are the communications between the UAV and GNSS satellites that will be used to determine the location of the UAV and the communication between the UAV and the ground station. The total communication flow of the UAV, the internal and external communications, is presented in Figure 6.9.

### **External communications**

This section will explain the external communication of the UAV with the GNSS satellites and the ground station. These external communications are necessary since they determine the position of the UAV and will send and receive important data to and from the ground station.

The current location of the UAV is determined using GNSS. With GNSS multiple satellites send a signal to the UAV which gives information about the distance from the UAV to the satellites. These signals are picked up by the GNSS antenna, which sends the signals to the autopilot. In the autopilot module, these signals are being processed by the GNSS receiver unit and the location of the UAV is calculated using the distance from the UAV to the various satellites and the known location of the satellites. The communication between the

GNSS satellite and the GNSS receiver is shown in Figure 6.7<sup>11</sup>.

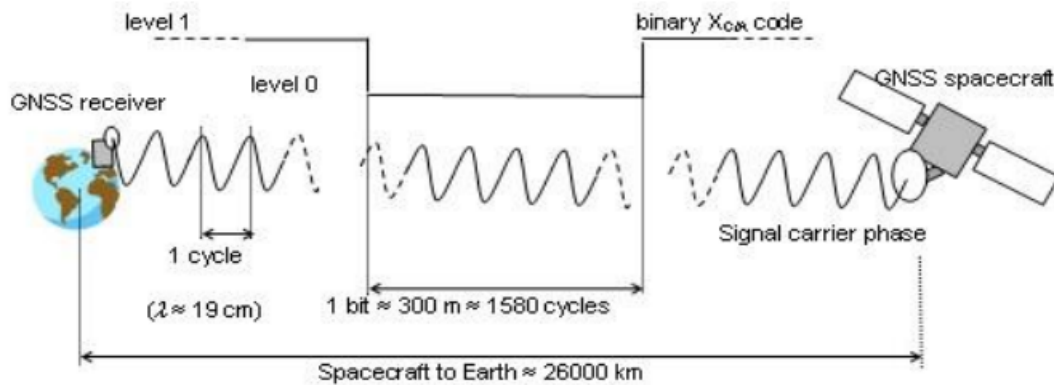


**Figure 6.7:** Typical GNSS signal communication between the GNSS satellite and the GNSS receiver

Communication between the UAV and ground station will allow them to transmit and receive signals between one another. The live footage of the cameras and the current location of the UAV has to be transmitted to the ground station. This must be done so an operator can manage the data and take action when threats are detected. On the other side, the ground station has to receive these signals and may also transmit instructions from the operator when a risk for the UAV is detected, to return to base. The UAV and the ground station will both have a transceiver, which can receive and transmit signals. The transceiver used by the UAV and ground station uses 2x2 MIMO. This means that two antennas are used on both sides to send the same data. Due to this, the communication has redundancy and the signal quality and strength are better than systems that only use one antenna<sup>12</sup>. The workings of a 2x2 MIMO system can be seen in Figure 6.8<sup>13</sup>. The transceiver will transmit these signals. These transmitted signals will be received by the two antennas of the other transceiver, which will be processed in this transceiver.

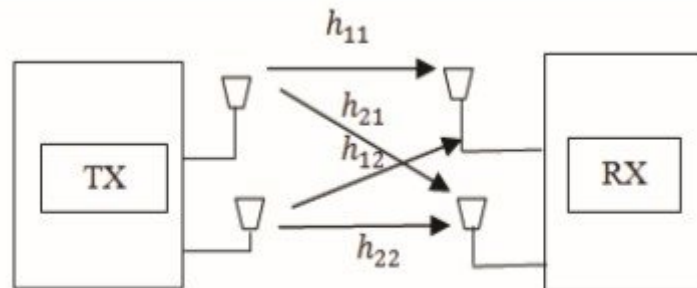


**Figure 6.8:** 2x2 MIMO diagram for UAV and ground station communication

## Communication flow

The internal communication flow of the UAV and the communication flow of the UAV with the ground station can be seen in Figure 6.9. The autopilot 1x has an accelerometer, a gyroscope, a pitot static system, an onboard data logger, a magnetometer and a flight controller in its module. The onboard data logger acts as a black box in the UAV. In the flight controller, all the received data is being processed and instructions are sent to the subsystems.

<sup>11</sup>URL:[https://www.researchgate.net/figure/GNSS-typical-signal-The-carrier-is-modulated-by-a-binary-code-and-with-a-fig1\\_236247299](https://www.researchgate.net/figure/GNSS-typical-signal-The-carrier-is-modulated-by-a-binary-code-and-with-a-fig1_236247299)[01/06/2022]

<sup>12</sup>URL:<https://www.rfmw.com/data/swa-mimo-basics.pdf>[01/06/2022]

<sup>13</sup>URL:[https://www.researchgate.net/figure/2x2-MIMO-System-Block-Diagram\\_fig1\\_330779451](https://www.researchgate.net/figure/2x2-MIMO-System-Block-Diagram_fig1_330779451)[01/06/2022]

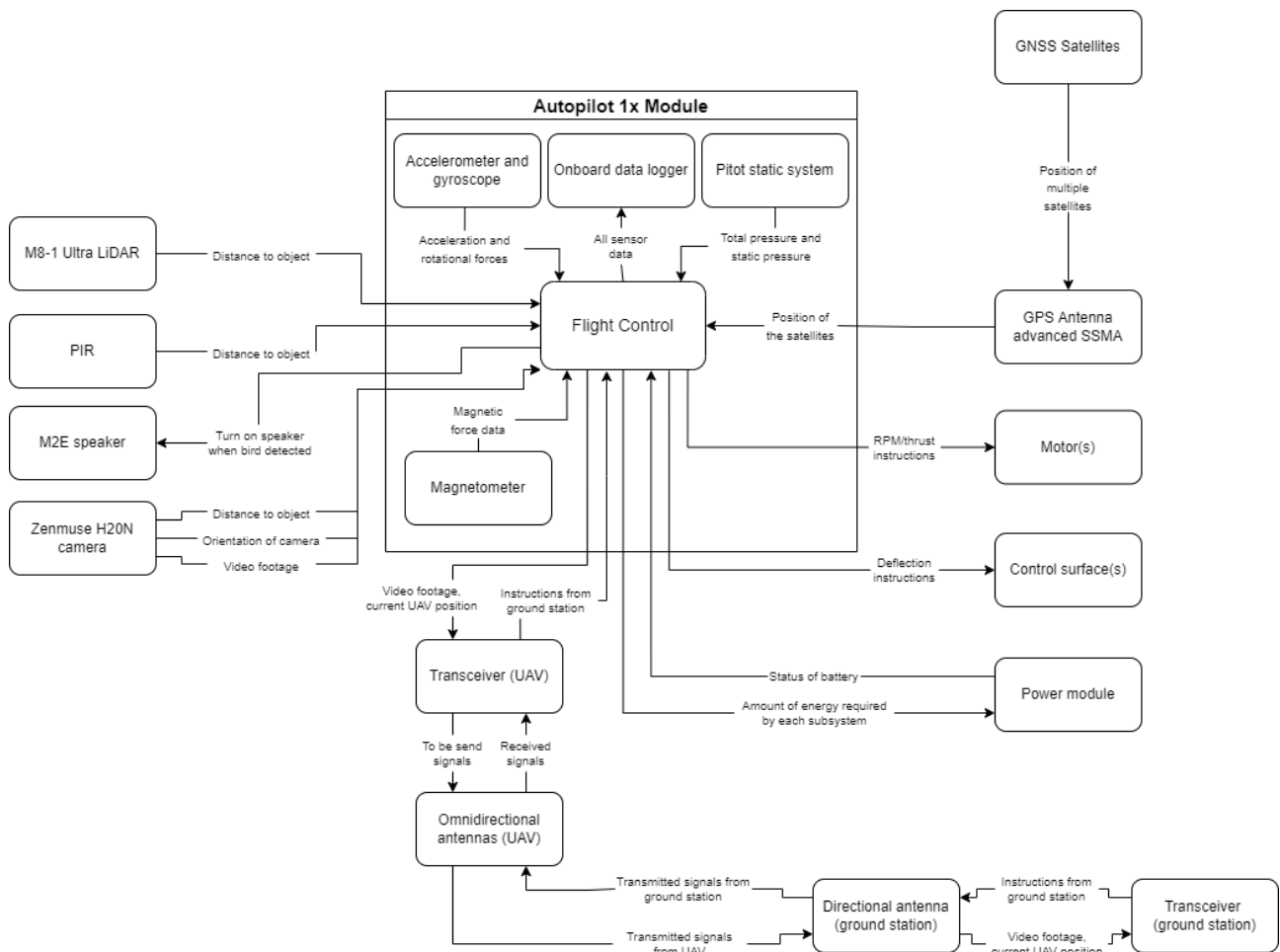


Figure 6.9: Communication flow diagram of the UAV

### Internal communication - Electronics

The internal power connections and communication paths are described in Figure 6.10 in the form of an electrical block diagram. Red arrows represent a continuous power flow while yellow arrows represent pulse shaped electrical control signals. Moreover, the green block represents a power source whereas a blue block represents a controller. The red block is the power supply to systems and payload, which are the yellow blocks. Lastly, the purple blocks are the control surfaces and propulsion systems of the UAV.

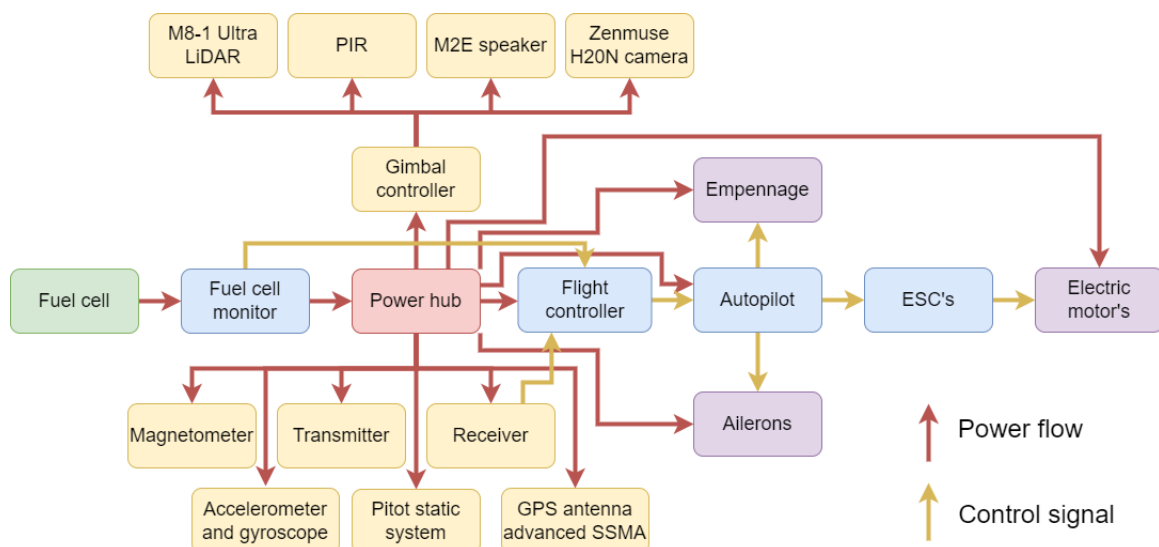


Figure 6.10: Electrical block diagram of the UAV

## Software

The principal software used in order to control the UAV are not design by the team and rely on the Veronte Autopilot 1x chosen. This autopilot was selected partially due to its high customizability allowing the team to integrate the automation of the UAV. The Veronte autopilot serves at the center brain relaying information to the various systems in the drone. In order to better understand the feedback loops that the autopilot will be operating Figure 6.11 illustrate a simplified version of the software interaction inside the aircraft.

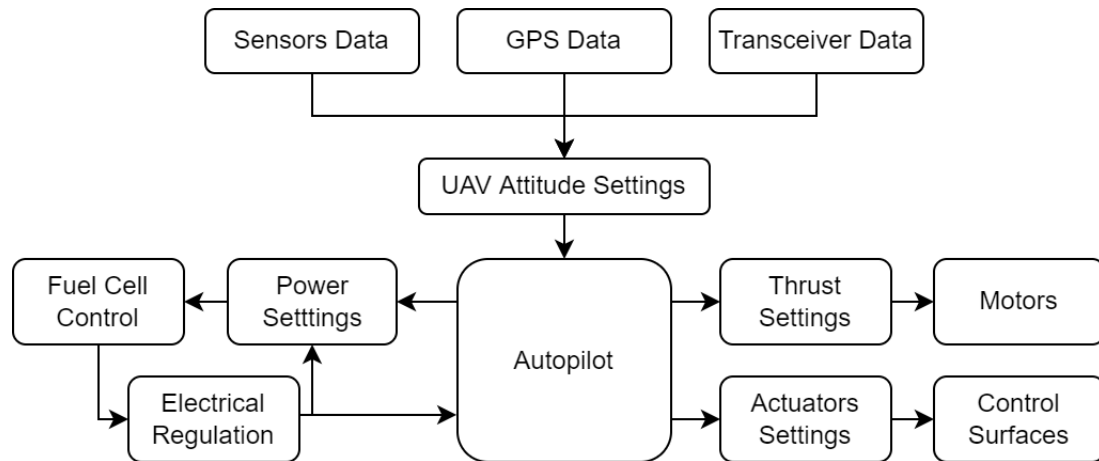


Figure 6.11: Software Diagram

## 6.10. Certification of the UAV

This section is intended to inform the reader of the class of UAV that is being designed in this report. At this point in time, it is impossible to have an autonomous UAV such as Usambara to be certified. Therefore, the standards and acceptable means of compliance to achieve those standards will not be discussed.

As non-military UAVs become increasingly common, with more data and more awareness for how safe an autonomous vehicle can be, it is expected that in the future it will be less of a challenge to get an official certification for a UAV of this class. When this happens, more concrete certification standards can be produced by bodies such as the EASA and the FAA.

The UAV will fall into the "Certified Category" of the EASA regulations. Within this, it will undergo operations labelled by EASA as type 2. EASA intended the first proposal for the amendment to be published in 2021. The authors of this report have been unable to locate this document, it has been assumed that this publishing date has been delayed.

## 6.11. End-of-Life

Once the UAV and it's ground station have fulfilled their mission and reach their end of life it is necessary to proceed with their disposal. This procedure happens on multiple levels depending on the various components of each system.

First, the UAV and ground station must be withdrawn from the environment they've been placed in and sent to a post-processing facility. In order to aim for a higher level of sustainability it is important to first establish the possibility to reuse any components of either the UAV or ground station.

Concerning the UAV, an initial inspection will be performed in order to establish if it can be reused with minimal maintenance/repairs. This would be acted out if only a few components would need replacement and the majority of the aircraft would still be functional. In case this procedure is not possible due to a high number of parts being out of commission the next step is to save the other elements that are still in working

condition. In the case of the non-structural elements, these might be either repaired by the appropriate entities, reused in UAVs or used for other applications, or they will be correctly disposed. For the structural components, the course of action would be to fully recycle all the materials in the proper facilities so that they may be used in the production of additional drones or applied for other purposes by other companies. In the event that the material might not be recyclable or reused then it is necessary to dispose of them in the most sustainable manner possible.

Furthermore, the approach for the disposal of the ground stations follows a similar procedure to the disposal of UAVs. A primary inspection is carried out to establish the possibility to reuse the station or to save only elements in good conditions. These saved components could be used when building other UAVs or sold to companies for other applications. The other portions of the drone that have not been saved will be recycled based on the proper procedures.

# Aircraft Configuration

In the midterm report [2], preliminary designs were made for four different UAV concepts. During a trade-off, the concept found to be the best for this system was the VTOL HFC powered fixed wing. The concept will be explored further in this chapter and narrowed down to a detailed design. In order to do so, a geometric layout has to be established. This will be done in Section 7.1. In Section 7.5, the VTOL technology used will be determined.

## 7.1. Overall Aircraft Configuration

A VTOL HFC powered fixed wing is the chosen concept for the UAV; there are, however, many variations of a fixed wing aircraft. Therefore, another choice needs to be made on the UAV geometry. Within the design space, four options have been chosen to consider further. These are:

- Conventional configuration
- Blended wing body
- Canard configuration
- Twin-boom configuration

In order to make a choice, aspects such as fuel tank and payload integration, mass, stability, and drag need to be considered. First of all, it has been found that the conventional configuration has the potential to host the fuel tank by making it a part of the fuselage. Also, the payload can relatively easily be mounted under the fuselage or wings. In addition, the conventional aircraft is very stable because the empennage accounts for trimming and actuating. For the blended wing body, a fuel tank is harder to install. A solution could be to make a curved wing hosting the fuel tank in the middle. Moreover, payload is hard to install as well and it is harder to achieve static stability. However, mass and drag are substantially lower [13]. As for the canard configuration, the pros and cons are comparable with the conventional aircraft. However, a canard provides positive lift, as opposed to the negative lift of an empennage, resulting in a higher  $C_{Lmax}$  and lower drag and mass [14]. However, the UAV must be designed very carefully, ensuring the canard stalls before the main wing. Lastly, the twin-boom configuration has the advantage of less structural weight and more stiffness since the mass is more distributed than in the other configurations. Moreover, less parasite drag is present since the wetted surface area is smaller. Stability is also easy to achieve since the control surfaces can be located wherever required. However, induced loads like shear and bending must be carefully watched as they can get rough in the rods. As for the fuel tank and payload, a small fuselage as large as required can be integrated.

Considering all the parameters, a twin-boom configuration was judged to be the best performing configuration for the mission profile required. A detailed design phase will determine the exact dimensions.

## 7.2. Fuselage Configuration

The shape chosen for the fuselage was based on two parameters: the housing of the hydrogen tank/payload and parasitic drag. The implementation of the hydrogen tank within the fuselage is a relatively new idea, but it has been done before. An example of this is the CW-25H Hydrogen Powered VTOL UAV [15], made in cooperation between JOUAV and Doosan companies. The design of the project's UAV is based on the CW-25H, given the layout of the fuselage with half of it being used by the hydrogen tank and the other half by the payload. For efficiency, it was a priority to have the tank inside the casing. It benefits the aerodynamics but also the noise production, and it is a safer design overall without the tank being exposed to the environment.

The shape of the fuselage and location of the instruments are positioned in terms of the parasitic drag. The following pictures demonstrate the designs explored to choose the body [16].

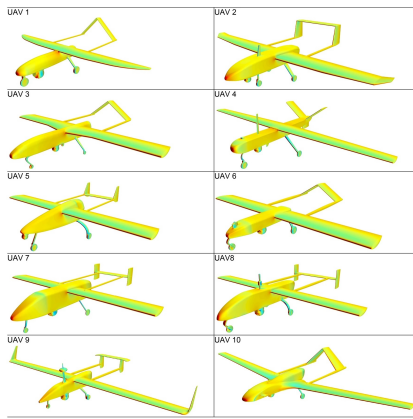


**Figure 7.1:** Twin-Boom designs based on market drones.

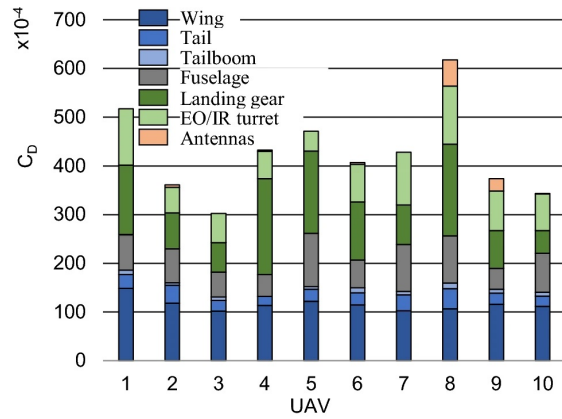


**Figure 7.2:** Parasitic drag analysis

Since the twin-boom design was already decided, the task was to decide the positioning of the instruments and the shape of the fuselage. Based on Figure 7.1, the shape of the model is chosen out of UAVs already on the market. Figure 7.2, on the other hand, provides the parasitic drag of each design, which aids the selection process. It is not intended to choose a specific model based on the pictures, the objective is to take the best performing parts in terms of parasitic drag and include them in the project's design.

From Figure 7.2, it can be concluded that the best design configuration is of UAV 3. Looking at the parasitic drag breakdown, a great factor of parasitic drag comes from the landing gear. This is advantageous regarding the project design because the landing gear will be retracted during cruise, and its parasitic drag can therefore be disregarded. Another important factor causing parasitic drag is the EO/IR (electro-optical/infra-red) turret. This will be approximately the same in all designs, therefore, the positioning of the camera turret will be taken into consideration later in the design process.

The antenna is a feature part of the UAV designed by the group. The models that have antennae are UAV 2, 4, 6, 8, and 9. Out of these models, the best performing is either 4 or 6. The antenna has a fixed design but emulating as much as possible is always beneficial for the aerodynamic efficiency. Finally, taking into account the empennage (tail and tail-boom), the design for aircraft 3 seems to perform the best. This leaves the wing to be decided, however, the wing is not decided through this qualitative method, as for the wing there is a separate analysis made more tailored to the mission requirements.

### 7.3. Empennage Configuration

The selection of the tail is based on 4 designs commonly used for drones. These are the inverted U-shape, U-shape, inverted V-shape, and semi-inverted V-shape tails shown in Figure 7.3. The analysis of the tail is based on lift, critical angle, stability, and manoeuvrability performance.

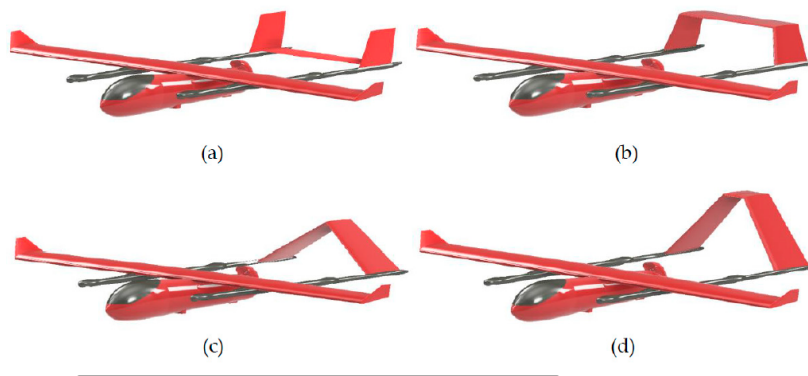


**Figure 7.3:** Tail configurations

## Lift and Efficiency Performance

The lift coefficient versus angle of attack graphs analyzes the tail's lift force, stall speed, and efficiency performance. Additionally, it can determine the stall angle and the highest lift coefficient. The stall angle is the limit angle in which increasing the angle of attack even further decreases the lift coefficient. The best performing tail configuration was the inverted U-shaped tail with a critical angle of 18 degrees at a lift coefficient of 0.8. The worst performing was the inverted V-tail with a critical angle of 12 degrees and lift coefficient of 0.76 [17].

An analysis of the lift coefficient in sideslip conditions was also performed with varying angles from 15 degrees to 30 degrees. The performance for the 15 degree sideslip was similar for all 4 configurations. The 30 degree sideslip analysis emphasized the slight advantage of the U-shaped tail, as from 4.5 degrees to 14 degrees, the lift coefficient was slightly greater than the other configurations. Since the increment was small, it can be summarized that all tail configurations perform comparably for sideslip conditions [17].

The aircraft efficiency is predominantly a product of the drag produced during cruise. The lift to drag ratio is an important parameter because it is an indicator of fuel consumption. For 0 degrees of sideslip, the best performing tail is the U-shaped with a peak lift to drag ratio of 13, for an angle of attack of 7 degrees. Conversely, the worst performing tail was the inverted U-shape, with a L/D ratio of 9, at an angle of attack of 7 degrees. The difference in performance decreases for a sideslip of 15 degrees, but the U-shaped tail still outperforms the rest slightly with an L/D ratio of about 10.2 at an angle of attack of 5 degrees. The inverted U-shape increases its performance and is no longer the worst at 6 degrees with a lift to drag ratio of 10. For the sideslip of 30 degrees, the best performing is the semi-inverted V-shape having a lift to drag ratio of around 12 at 5.5 degrees of angle of attack [17].

Another parameter analyzed was the stall speed which is the speed at which the VTOL configuration transitions to cruise speed. It was tested for 0, 15, and 30 degrees of sideslip. The results did not show a significant difference between the 4 models for 0 degree sideslip, so it can be assumed that each has a similar performance. For the 15 degree sideslip, the stall speed was 13 m/s with an angle of attack of 15 degrees. The higher the sideslip angle, the greater the stall speed velocity. This can also be seen with 30 degrees of sideslip where the stall speed is 15 m/s with an angle of attack of 15 degrees. Even though all the configurations perform similarly, the U-shaped tail had lower stall speed at lower angles of attack, which is preferable [17].

## Stability Performance

The following subsection outlines the performance of each tail with longitudinal, lateral and directional stability.

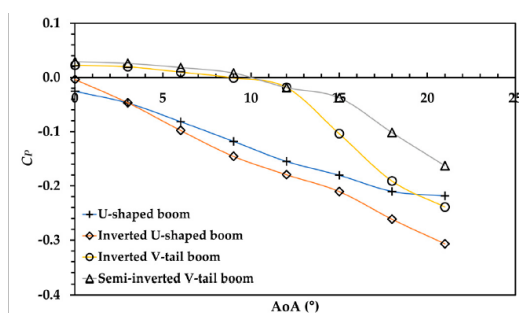


Figure 7.4:  $C_p$  vs. AoA Sideslip 0°

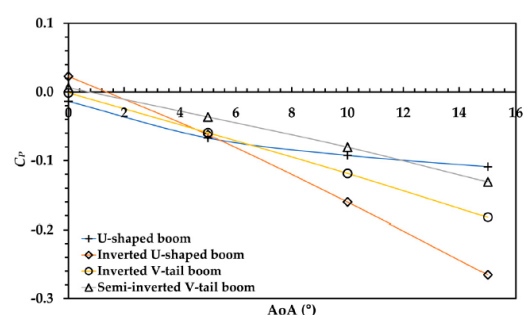


Figure 7.5:  $C_p$  vs. AoA Sideslip 30°

In Figures 7.4 and 7.5, the  $C_p$  is plotted in terms of the angle of attack. They represent how the longitudinal stability changes with different angles of sideslip. For Figure 7.4, the  $C_p$  is 0 at 0° for the inverted U-shaped boom. This means that it will not pitch up nor down during cruise, which is desirable. The worst performing tails are the inverted and semi-inverted V-shaped as they have positive  $C_p$  and would require elevators to

maintain stability. For 15° sideslip, all of the tail configurations perform very similarly except the U-shaped tail that starts with  $C_P$  at 0 for a 0° angle of attack. The graph is not shown as the difference among the tails is insignificant, with the exception of the already mentioned U-shaped tail. Finally, for 30° sideslip in Figure 7.5, the inverted U-shaped tail now has a positive  $C_P$  and inverted/semi-inverted V-tail have a  $C_P$  close to zero. The best performing is the inverted U-shaped tail for at least 0 to 15 degrees of sideslip, as 30 degrees of sideslip is an extreme and uncommon value for cruising.

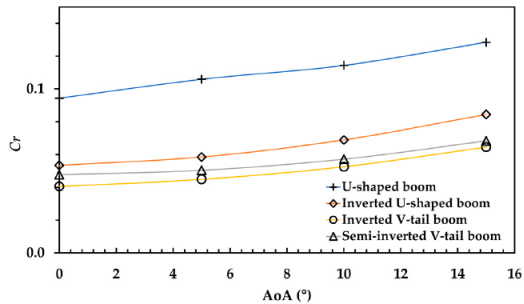


Figure 7.6:  $C_r$  vs. AoA Sideslip 15°

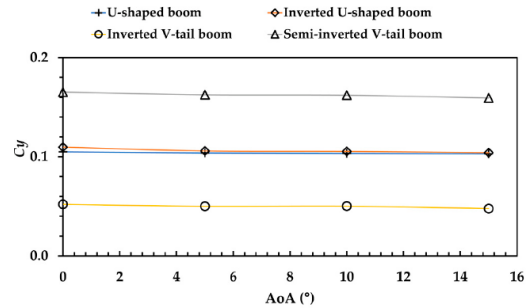


Figure 7.7:  $C_y$  vs. AoA Sideslip 15°

There are two axes left to be analyzed with regard to stability, namely lateral and directional. In Figure 7.6,  $C_r$  represents lateral stability which is in function of the angle of attack at a sideslip angle of 15°. The closer the value is to 0, the better. The inverted V-shaped tail is best performing, with the inverted U-tail and semi-inverted V-tail closely following. The U-shaped boom, however, has a positive value close to 0.1, representing significantly worse performance in terms of lateral stability [17].

Directional stability is defined by  $C_y$  and its performance is represented with Figure 7.7. The inverted V-shape offers the best performance out of the 4 configurations for directional stability. The worst performing is the semi-inverted V-shape tail, while the inverted U-shape and U-shape perform comparably to one another with a  $C_y$  of approximately 0.1 [17].

## Maneuverability Performance

Maneuverability for surveillance drones is not a priority compared to stability as the missions do not require quick changes regularly. Nevertheless, being sufficiently maneuverable is still important. This will be explored in this section.

The two best performing configurations are the inverted U-shape and the U-shape. It is evident in Figure 7.8 where at high angles of attack, the turn radius is the lowest. This example is of a banking of 40 degrees; however, the two best performing are always the same at lower banking angles. Also, from Figure 7.8 it can be seen that both V-shaped tails have a considerably higher turning radius which is undesirable for maneuverability.

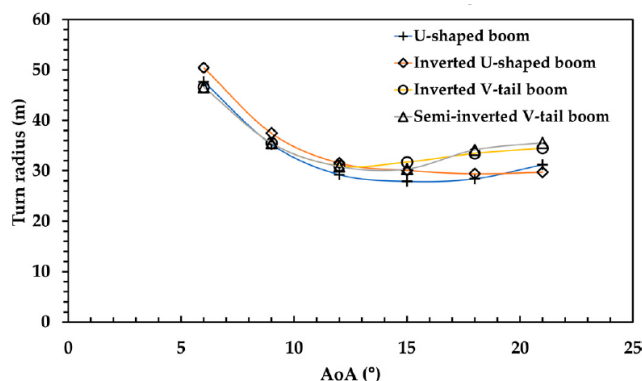


Figure 7.8: Turn radius vs. AoA - Bank Angle 40°

## Selection

The analysis has resulted in the most convenient empennage configuration for the UAV being the inverted U-shape. It performed well in the lift force and longitudinal stability. For the other categories, the inverted U-shape performed above or on average, making it the most convenient design for a surveillance mission overall. However, the directional and lateral stability is an important drawback of the inverted U-shape tail. It does not perform the worst as the semi-inverted V-shape, but it is not as good as the inverted V-tail. A ventral fin is an option to increase lateral stability as it does not affect directional stability [17]. The directional stability is easier to control than lateral stability, so the lateral stability must be increased [17].

## 7.4. Wing Configuration

A brief trade-off is presented for the wing placement, considering high wing, mid wing, and low wing configurations. The trade-off is performed according to criteria that are substantially impacted by the wing placement. These criteria are stability, aerodynamic performance, and reliability, availability, and maintainability (RAM). The three criteria are weighted equally, as the three criteria are all mission critical and therefore were judged to be approximate of equal importance. Each criterion is composed of sub-weights and sub-scores. The rationale for the selected criteria and the constituent sub-criteria and weights is given below. As well as the legend for the trade-off scores, judged from 1-5.

1. Stability
  - 1.1. Lateral stability
  - 1.2. Take-off and landing stability
2. Aerodynamic performance
  - 2.1. Aerodynamic efficiency during cruise
  - 2.2. Empennage effectiveness
  - 2.3. Maneuverability
3. Reliability, Availability, Maintainability
  - 3.1. Reliability
  - 3.2. Availability
  - 3.3. Maintainability

**Table 7.1:** Trade-off weights description

Score (greater than or equal to)	Description
1 - red (r)	Worst
2 - orange (o)	Poor
3 - yellow (y)	Acceptable
4 - light green (lg)	Good
4.5 - dark green (dg)	Excellent
- blue (b)	Winning score

### Stability

The difference in lateral stability performance between wing configurations is one point of differentiation resulting from the choice of aircraft configuration. Increased lateral stability is desired in forward flight to prevent the loss of control of the UAV in the case of disturbances. All configurations can achieve good lateral stability with either dihedral or anhedral, and stability is therefore not a crucial consideration and awarded a sub-weight of 0.2. A high-wing aircraft tends to inherently have positive lateral static stability due to the restoring moment of the center of gravity being located under the wing. Small amounts of anhedral can lessen the tendency to Dutch Roll and lead to good dynamic lateral stability for a slight reduction in lift generated. Low wing aircraft do not receive this same contribution of restoring moment but can achieve good static and dynamic lateral stability with dihedral. Finally, the mid wing aircraft typically displays the worst lateral stability, as the center of lift coincides with the center of mass, leading to neutral stability.

The wing placement also affects the stability of the UAV during take-off and landing due to the ground effect. Ground effect can be particularly dangerous for VTOL craft due to the destabilizing potential of fountain lift resulting from rotor downwash during take-off and landing, and suckdown during take-off due to the entrainment of airflow on the wings during vertical flight. The high potential and severe consequences of a crash during take-off or landing results in a weight of 0.8 for this sub-criteria. Furthermore, ground effect increases greatly with proximity to the ground, and therefore a larger distance between the wings and rotors is beneficial from the perspective of minimizing ground effect. The high wing configuration, therefore, offers clear advantages regarding the stability during take-off and landing, with the low wing aircraft most susceptible to instability.

**Table 7.2:** Trade-off on configuration stability sub-criteria of lateral stability and take-off and landing stability for high wing, mid wing and low wing configurations.

Configuration	Lateral Stability	Take-off and Landing Stability	Score
Criteria Weight	0.2	0.8	
High Wing	5.0 (dg)	5 (dg)	5.00 (b)
Mid Wing	3.0 (y)	4.0 (lg)	3.80
Low Wing	4.0 (lg)	2.0 (o)	2.40

## Aerodynamic Performance

The aerodynamic efficiency, represented by the ratio of lift-to-drag during cruise conditions, is crucial for the range and endurance performance of the UAV. The aerodynamic efficiency is the most critical category of aerodynamic performance and is, therefore, awarded a weight of 0.6. The high wing configuration suffers from slightly higher drag than the low-mounted and mid-wing configurations due to an increase in interference drag resulting from the less efficient integration of the fuselage-wing surfaces [18].

The effectiveness of the empennage is influenced by the wing downwash, which in turn depends on the wing mounting. A high mounted wing will result in the horizontal tail experiencing a greater effective downwash angle, which reduces the tail lift. Consequently, a greater tail volume must be designed to maintain stability and controllability, increasing the weight of the required design. Minimizing the structural weight of the UAV is important for performance, as well as minimizing the need for resizing, which can occur due to the snowball effect. Therefore this sub-criteria is given a weight of 0.3. The performance of the mid wing and low wing configurations were comparable, with the tail of the low wing aircraft experiencing slightly less downwash during cruise and a more substantial decrease during stall or high angle of attack maneuvers.

Finally, the maneuverability is affected by the wing placement. The UAV flies a surveillance mission where requirements for maneuverability are relatively low, and therefore this criterion is weighted with 0.1. Maneuverability is inversely related to stability; thus the mid wing craft offers the best performance, followed closely by the low wing, with the high wing the least maneuverable.

**Table 7.3:** Trade-off on configuration aerodynamic performance sub-criteria of cruise drag, empennage effectiveness and maneuverability for high wing, mid wing and low wing configurations.

Configuration	Cruise Drag	Empennage Effectiveness	Maneuverability	Score
Criteria Weight	0.600	0.300	0.100	
High Wing	3.00 (y)	2.0 (o)	3.0 (dg)	2.70
Mid Wing	4.00 (lg)	4.0 (lg)	4.0 (lg)	4.00
Low Wing	4.00 (lg)	5.0 (dg)	4.0 (lg)	4.30 (b)

## Reliability, Availability, and Maintainability

The sub-criteria of reliability, availability, and maintainability are considered equally important to the mission success, and therefore are afforded equal weights of 1/3 each. Safety was not considered as an additional sub-criteria, as the safety was not found to be dependent on the wing configuration used.

The operational reliability of the UAV is heavily dependent on the conditions of deployment. Therefore the reliability of the configurations must be considered in the context of the usage of the craft. For this assessment, the specific conditions arising from the case study of Kruger National Park in South Africa are considered. Exposure to dust and debris during take-off and landing was identified as a primary threat to the reliability of the drone operation during an interview with Robert Miller, CEO of the Eye Above, a company developing VTOL drones currently undergoing testing in the Balule Nature Reserve, part of the Kruger National Park [19]. Primary measures to counteract this include sealing of all bearings and motors, as well as maximizing the distance of the propulsion systems from the ground to minimize debris damage and exposure to dust. The wing mounting has a minimal effect on the height of forward-flight motor, but the height

of the wing dictates the height of the motors for VTOL flight, given the boom is attached to the wing. For this reason, a high mounted wing is preferable. The likelihood of crashes is also a factor for the reliability of operation. Although trends were described in the trade-off for stability, the likelihood of crashes and severity of damage in the case of a crash were difficult to quantify between configurations, and therefore this was not substantially considered.

The high cost of the UAV system necessitates a long service life to recoup the initial investment. This requires that the aircraft is maintainable. The remote deployment of the UAV, and lack of access to skilled technicians, dictates that maintenance must be simple, fast, and economical. According to Robert Miller of the Eye Above Project, one of the largest factors for maintainability considerations in the context of remote deployment is modularity [19]. This is because damage is inevitable and often technicians are unavailable, requiring park rangers perform repairs. Given this, a wing which is easily removable allows for swap repairs in the case of damage. The mounting of a high wing is most conducive to this, given it can be fastened entirely above the fuselage, while mid-wing is integrated in the fuselage, increasing the difficulty of maintenance to a large degree. Maintainability for other components are less directly reliant on the configuration, but the frequency of maintenance for the VTOL propulsion is less for the high wing configuration due to the decrease in exposure to dust and debris.

The availability of the rotorcraft during operation is largely a product of reliability and maintainability, but to a small degree also relies on additional factors influencing the inherent operational availability of the system. The mid wing aircraft scores slightly worse than the low wing design for this reason, despite comparable averaged scores across the reliability and maintainability categories, as the wing connection to the fuselage may compromise the structural life of the aircraft. The high wing design scores well in availability, due to its high performance in terms of reliability and maintainability.

**Table 7.4:** Trade-off on configuration RAM performance sub-criteria of reliability, availability and maintainability for high wing, mid wing and low wing configurations.

Configuration	Reliability	Availability	Maintainability	Score
Criteria Weight	0.333	0.333	0.333	
High Wing	5.00 (dg)	5.0 (dg)	5.0 (dg)	5.0 (b)
Mid Wing	3.00 (y)	2.0 (o)	2 (o)	2.33
Low Wing	2.00 (o)	3.0 (y)	3.0 (y)	2.66

### Selected Wing Configuration

The high wing configuration is selected as a result of the trade-off performed. The low and mid wing configurations had largely comparable performance across all three categories, while the high wing scored poorly in aerodynamic performance, but significantly outperformed the other configurations in the stability and RAM categories. The final scores resulting from the trade-off are shown in Table 7.5

**Table 7.5:** Trade-off for wing configuration selection based on stability, aerodynamic performance and reliability, availability and maintainability for high wing, mid wing and low wing configurations.

Configuration	Stability	Aerodynamic Performance	RAM	Score
Criteria Weight	0.333	0.333	0.333	
High Wing	5 (dg)	2 (o)	5 (dg)	4.23 (b)
Mid Wing	3.8 (lg)	4 (lg)	2.2 (o)	3.37
Low Wing	2.4 (o)	4.6 (dg)	2.8 (y)	3.12

## 7.5. Vertical Take-off and Landing Transition

The take-off and landing of the UAV, and the subsequent transition from hovering flight to forward flight presents several design choices in terms of configuration and control. This section details the common

take-off and landing variants of fixed-wing VTOL aircraft, and selects a mode of take-off and landing, the dual-system configuration. The sizing and position of rotors for vertical flight are given in Chapter 10.

This section details the performance of tilt-rotor, tilt-wing, tail-sitter, and dual-system variants with independent vertical and forward propulsion, and chooses a configuration. During vertical take-off, the UAV requires a thrust-to-weight (T/W) ratio in excess of 1, with typical values ranging from 1.1 to 2, compared to the values of T/W of no larger than 0.25 which are ordinarily required for conventional cruise [20]. As a result, significant excess thrust is required for the vertical take-off and landing, but not used during forward flight where aerodynamic lift is generated, which comprises the vast majority of the mission profile. The VTOL UAV therefore achieves a less weight-efficient design compared to a conventional fixed-wing configuration due to the added weight of motors and propellers which are only used in take-off and landing. The profile of the inactive motors and rotors also represents a source of additional drag, if they are not retracted. Furthermore, VTOL craft experience ground effect during take-off and landing, with the destabilizing effect of the additional lift generated presenting a particular threat to the landing. Ground effect disrupts operation of the lifting surfaces and the rotors, in terms of lift-generation as well as increasing the intensity and frequency of the noise generated [21]. Gusts can also affect the landing capabilities of a VTOL craft, particularly if precise positioning is required during landing. An overview of configurations is presented in Figure 7.9.

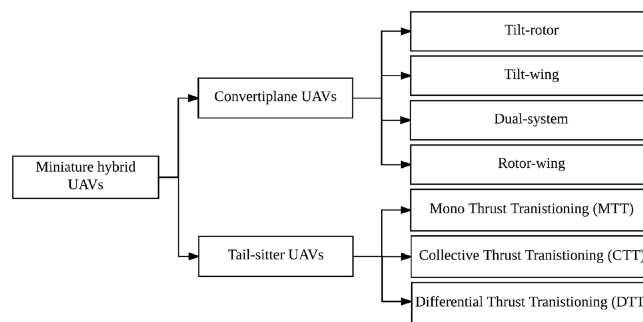


Figure 7.9: Overview of VTOL configurations [22].

### Tilt-Rotor VTOL Design Variant

The tilt-rotor variant seeks to minimize the drag and mass increases by using the same rotors used in vertical flight for cruise. As a result, the need for a dedicated forward-facing motor is eliminated, reducing the weight of the UAV. This configuration also has the added benefit of reducing drag during cruise, as the profile of the raised rotors is minimized as they are aligned with the incoming flow. Typically, between 2 and 4 rotors are used for a tilt-rotor [23]. In the case more than 2 rotors are used, generally only 2 are required for forward flight, and therefore must be tilted forward. In this case, all motors can be tilted forward to improve aerodynamic performance, but this adds weight due to additional servos required to actuate the rotation. However, the use of the same motors for cruise and VTOL significantly reduces the propulsive efficiency in forward flight, as the motors and propellers are typically sized to be most efficient for the maximum thrust condition [23]. Furthermore, the use of servos to tilt the rotors in flight adds mechanical complexity and weight, and can impact reliability as well as maintenance needs. Additionally, the off-center alignment of the tilting motors produces a large rolling torque, which dictates the use of thick wings with low aspect ratios [22]. This leads to relatively high drag for the tilt-rotor configuration, mitigating the benefits gained compared to non-tilting configurations. Finally, extensive discussion of control laws for hover and transition flight exists in literature for the tilt-rotor configuration, but is still an emerging field. Control of tilt-rotors is more simple than that of the tilt-wing configuration due to the relatively less complex aerodynamics resulting from the rotor-wing interaction, but not as simple as a dual-system multirotor, which features redundancy in thrust during transition [24]. Transition therefore still represents a significant operational risk for the operation of a tilt-rotor.

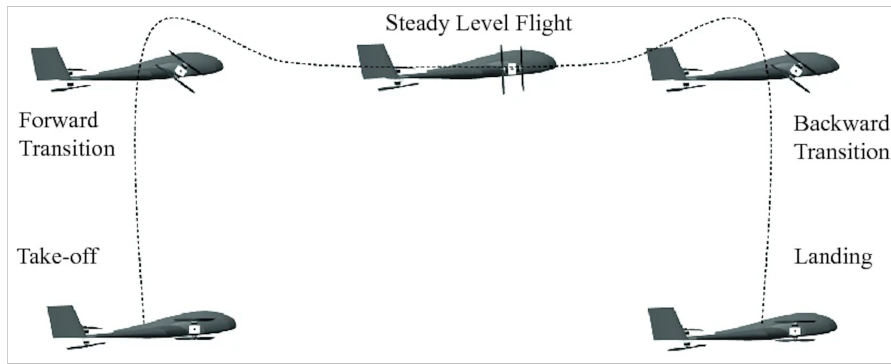


Figure 7.10: Operation of tilt-rotor VTOL in transition flight [25].

### Tilt-Wing VTOL Design Variant

The tilt-wing design variant functions in a manner similar to the tilt-rotor variant. The wing-mounted rotors are rotated to face forward as the wing swivels from a vertical to horizontal alignment during transition. This yields a number of shared advantages and drawbacks with the tilt-rotor configuration. As with the tilt-rotor, greater weight efficiency is achieved compared to a dual-system multirotor due to the lack of additional dedicated propulsion for forward flight. Furthermore, the same reduction in drag results in forward-facing flight due to the alignment of the motors with the flow. The tilt-wing also yields superior aerodynamic performance during VTOL [23]. This is because the vertically-aligned wing for take-off and landing has drag minimized in the vertical plane, leading to a lower power requirement for VTOL. This also allows for the flow around the wing to remain attached for the entirety of transition, decreasing the likelihood of aerodynamic stall during transition. However, the vertically-aligned wing during VTOL dramatically impacts the performance of the UAV in the presence of wind, generating large destabilizing forces and moments. Both the attitude and position control of the tilt-wing craft are compromised by gusts, which can be minimized by an alignment in the roll-axis with direction of the wing tips [26]. Nevertheless, this introduces an additional challenge to the VTOL operation, particularly considering precise positioning may be required for landing at the ground station. Furthermore, the tilting of the wings requires heavier actuators compared to the tilt-rotor design, diminishing the effect of the weight saved by eliminating dedicated motors for forward flight.

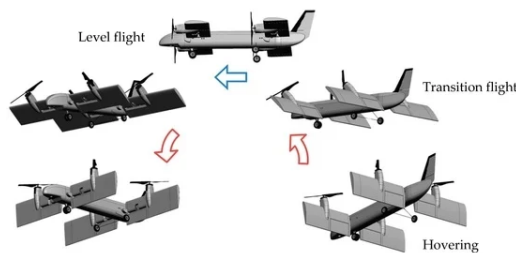
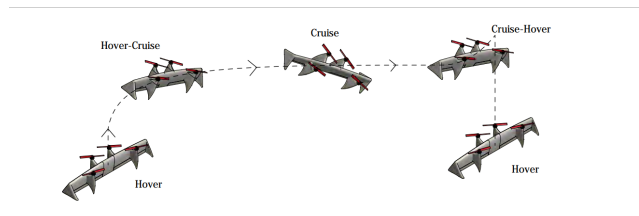


Figure 7.11: Operation of tilt-wing VTOL in transition flight [27].

### Tail-Sitter VTOL Design Variant

A tail-sitter rotates the body of the UAV during transition to and from vertical to horizontal flight, with transition pictured in Figure 7.12. Tail-sitters offer the same advantages of a tilt-wing multirotor, as well as providing a further reduction in drag during VTOL operation, achieved due to the alignment of the fuselage with the flow. Traditional tail-sitter designs employ either mono- or collective- thrust transition (MTT and CTT), taking off vertically with a single or dual rotors respectively, and transitioning using thrust vectoring. Thrust vectoring is accomplished with either the actuation of control vanes, or mounting the motors on a 2 degree of freedom servo [23]. This transition typically requires a complicated dynamic maneuver, with transition from vertical flight to forward flight often relying on an unstable stall and tumble transition ma-

neuver [23]. Control is feasible for the hover mode, but stability is poor compared to the other VTOL variants presented, suffering from similar gust issues described for the tilt-wing VTOL craft, as well as providing limited control axes [23]. Some of these issues with traditional tail-sitters are addressed with differential thrust transitioning (DTT) tail-sitter UAVs, which use 4 rotors. This configuration takes off similarly to traditional tail sitters, but typically yields superior stability in the vertical hover mode and improved transition performance. As the name suggests, DTT multirotors transition applies a thrust differential to the motors to create a pitch-up and pitch-down moment during vertical-forward and forward-vertical transition respectively. Stable transition can dictate higher thrust-to-weight ratios to generate these moments. In forward flight, either 2 or 4 rotors are active.



**Figure 7.12:** Operation of tail-sitter VTOL in transition flight [28].

### Dual-System VTOL Design Variant

Dual-system UAVs employ independent propulsion systems for vertical and horizontal flight. This provides a substantially less complex design. Typically, a dual-system craft ascends to a given altitude in VTOL mode, before increasing forward thrust and gradually decreasing VTOL thrust as aerodynamic lift is generated. Transition operation is pictured in Figure 7.13. The dual-system design allows for the independent sizing of the systems for vertical and horizontal flight, which improves the propulsive efficiency. This effect is particularly large for VTOL craft with long flight times, as the increase in the mass due to the addition of dedicated forward flight propulsion is counteracted by a lower mass of fuel required due to higher efficiency. Use of a dual-system design also greatly improves reliability and controllability during transitioning flight, providing an additional longitudinal control due to the forward propulsion, and allowing for gradual transition from hover to VTOL flight, and vice versa [22]. Furthermore, this configuration is mechanically simple. A dual-system craft does not require mechanical actuation of the rotors or wings. This leads to a reduction in maintenance needs, and also improves reliability of operation. However, the additional propulsion required for forward flight adds cost and weight. This is counteracted in part by the averted need for mechanical servos and structural reinforcement, compared to tilt-rotor or tilt-wing variants, as well as the aforementioned fuel savings. Moreover, the inactive vertical propulsion system increases drag during forward flight. This issue can be mitigated by using folding propellers, or retracting the motors, but these are mechanically complex. Alignment of the propellers parallel to the incoming flow can however lead to an order of magnitude reduction in the additional drag generated by the VTOL propellers during forward flight [29].

The dual-system VTOL variant was ultimately selected for the design largely because of its simplicity and reliability. No trade-off was performed, because the relative performance in criteria like weight and propulsive efficiency were difficult to estimate. However, other factors like RAMS and complexity of design strongly favor the dual-system design. The operational reliability of the dual-system is particularly noteworthy, as the risk of loss-of-drone during transition is less, as is the risk of damage to the UAV compared to variants with servos which are exposed to repeated wear. The limited scope of this report also limited the time that could be dedicated to the design of VTOL transition, which further drove the design selection to chose a variant with a simple transition control, also thus reducing the capabilities required of the autopilot system. Finally, the dual-system VTOL is a more developed concept for UAVs, with significantly more information available in literature in terms of both design and control compared to other VTOL variants.

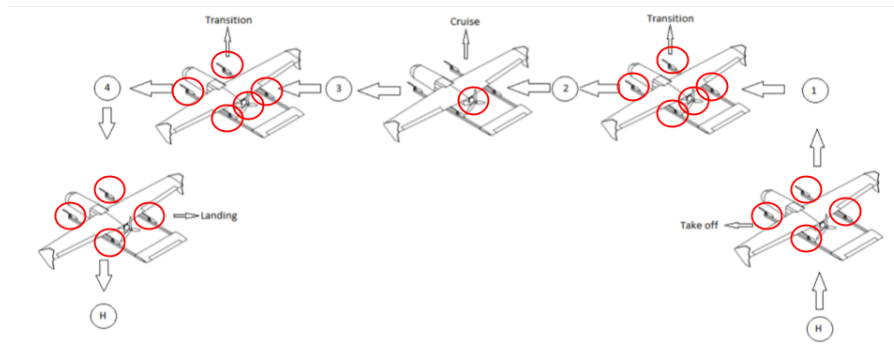


**Figure 7.13:** Operation of dual-system VTOL in transition flight, with active propeller(s) in each stage of flight highlighted [30].

# Aerodynamic Design

The aerodynamic properties of the aircraft are one of the first things to be estimated in the design loop, since it allows to calculate stability, propulsion, and structural requirements. In this chapter, the aerodynamic design of the wing is described in Section 8.1, which leads to the full planform design in Section 8.2. Following this, the main aerodynamic coefficients are provided. The lift characteristics are derived in Section 8.3, the moment coefficients in Section 8.4, and an estimate for the aircraft drag is given in Section 8.5. Finally, the planforms of the horizontal and vertical wings are selected in Section 8.6

## 8.1. Wing Aerodynamic Design

The main objective of wing sizing is to ensure that the wing ensures sufficient lift for the mission, but also that its characteristics allow for little drag, sufficient stability, and contributes to a sound structural weight. As a result, there are many aspects that need to be taken into account, such as the wing airfoil, the aspect ratio, or the tip twist, which will be discussed in this section. Examining the wing functions allows for a definition of the requirements that the wing must fulfill for a successful mission operation. These include lift, drag, dimension, and structural considerations.

### Wing, Aerodynamic Requirements

- SYS-AERO-01** The wing shall provide lift to sustain the aircraft in all stages of flight except take-off and landing.
- SYS-AERO-02** The wing shall operate at cruise at the point of maximum lift-to-drag.
- SYS-AERO-03** The wing shall ensure a smooth stall behavior.
- SYS-AERO-04** The wing shall provide support for the positioning of the ailerons.

The preliminary approach to the sizing of the wing is through a Class I weight estimation, where a plot is made of the wing loading versus the power loading as seen in Figure 8.1. In order to construct such a diagram the design space in Figure 8.1 is to the right and above of the cruise speed curve, above the rate of climb curve, and to the left of the stall speed curve. The design point was chosen where the wing loading for stall speed and the cruise speed meet, which is at  $129 \text{ N/m}^2$ .

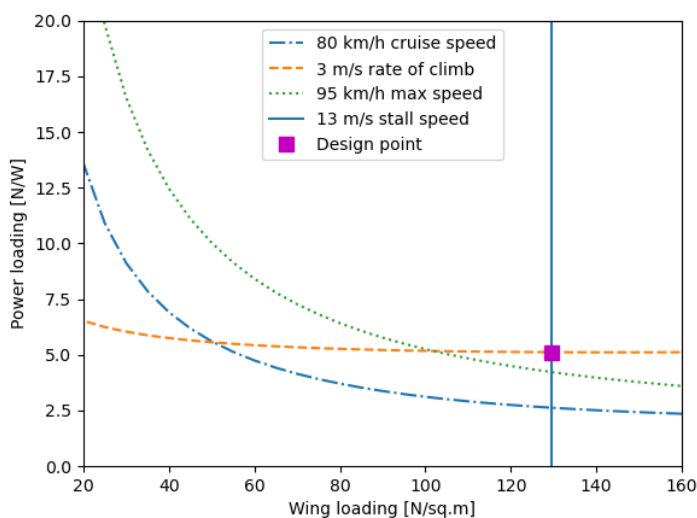


Figure 8.1: Design plot of wing loading (W/S) vs power loading (W/P)

The wing loading and mission ranges can be used to estimate the desired lift coefficient at cruise. By rearranging the terms of the lift equation in equilibrium in cruise, Equation 8.1 is obtained, where  $q$  is the dynamic pressure of the flow, and  $\frac{W}{S}$  is the estimated wing loading of the aircraft.

$$C_{Lc} = \frac{1}{q} \left( \frac{W}{S} \right) \quad (8.1)$$

By taking the resulting wing loading from the Class I estimation, 129 N/m<sup>2</sup>, and a hypothetical range of operation up to 2000 m above sea level, as 90% of the land can be found below that altitude [31], and thus is a design consideration that can make the mission more general and adaptable. The density in this range of altitudes nominally goes from 1.225 kg/m<sup>3</sup> at sea level to 1.006 kg/m<sup>3</sup> at 2000 m above it. This allows to calculate a required range of design lift coefficient of 0.4273 to 0.5203.

These values will approximately be the lift coefficients of the entire aircraft. As these values include the interference of non-lifting surfaces such as the fuselage, the required lift coefficient for cruise of the wing can be calculated through a statistical relationship as specified by Equation 8.2 [32]. In order to select the airfoil, it is necessary to calculate the required cruise lift coefficient for the 2D wing, which is obtained through another statistical relationship, as expressed in Equation 8.3 [32].

$$C_{Lc_w} = \frac{C_{Lc}}{0.95} \quad (8.2)$$

$$C_{l_i} = \frac{C_{Lc_w}}{0.9} \quad (8.3)$$

This sets the design lift coefficient of the airfoil to be between 0.4997 and 0.60853, and for the case study in Kruger Park, whose average altitude is 200 m<sup>1</sup>, and assuming an altitude of 600 m, the required airfoil lift coefficient is 0.5215. This lift coefficient value can be used to select the airfoil, aiming for a high lift-to-drag ratio to increase endurance, and a high maximum lift coefficient to decrease the stall speed, which would aid on the landing maneuver.

## Airfoil

There are many approaches to the selection of an airfoil. One option is to design the airfoil directly from mission requirements, but this is discouraged for inexperienced designers as it is complicated and the results cannot be reproduced in a test setting due to lack of resources. Fortunately, there is another option, which consists of sifting through the vast databases of available airfoils, and selecting one that suits the mission requirements. In order to do this, it helps to direct the search towards different airfoil families that generally have prospects of fulfilling the mission appropriately.

Some interesting families of airfoils are those developed by NACA; the Four and Five-Digit airfoils, and the 6-series, specifically. The Four-Digit airfoils are the most geometrically simple, but result in higher drag compared to the optimized profile of modern airfoils. Furthermore, the Five-Digit airfoils are designed for lift coefficients of approximately 0.3, which is too low for the mission, given the relatively low speeds. Lastly, the 6-series airfoils are a very interesting airfoil family to be investigated, since they are designed to maintain laminar flow over an extensive portion of the airfoil, thus greatly reducing drag. The downside of these airfoils is that, outside the range of angles of attack that ensure the laminar boundary layer, the drag increases greatly. However, as the aircraft will operate in a small range of lift coefficients, it is very likely that this drag increase does not become a big constraint. Furthermore, the expected small size of the UAV will ensure a range of Reynolds numbers that allow for laminar flow over the airfoil, as depicted in Figure 8.2<sup>2</sup>. However, the aid of laminar flow might be hindered if dirt or ice significantly alter the surface of the wing, and, for this mission, the former is a significant concern. Nonetheless, a similarly-sized aircraft with a similar airfoil was

<sup>1</sup>URL: <https://www.krugerexplorer.com/about-kruger-national-park>

<sup>2</sup>URL: [https://www.researchgate.net/figure/Drag-Coefficient-versus-Reynolds-Number-for-a-smooth-flat-plate-parallel-fig3\\_274960994](https://www.researchgate.net/figure/Drag-Coefficient-versus-Reynolds-Number-for-a-smooth-flat-plate-parallel-fig3_274960994)

built and tested in field operations, and it was noted that its performance was not greatly affected by dirt on the airfoil [33].

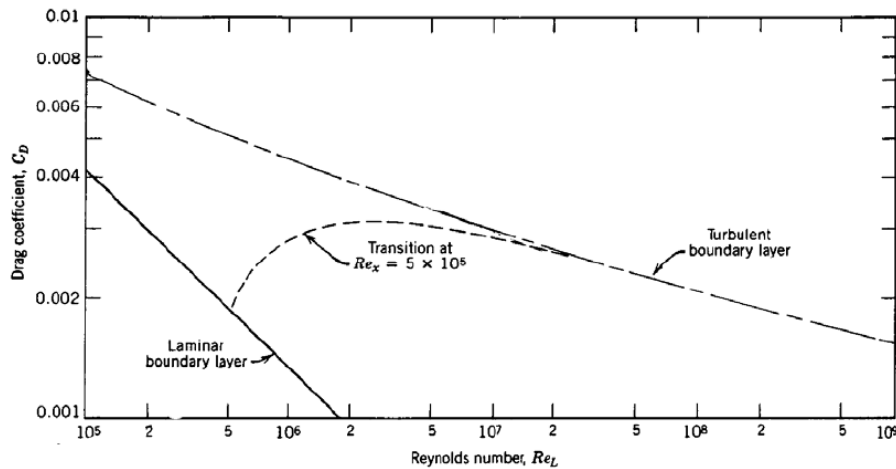
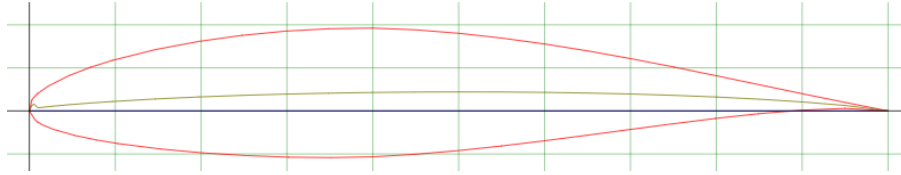


Figure 8.2: Drag Coefficient versus Reynolds Number for a smooth flat plate parallel to the flow.

Figure 8.3 shows the different airfoils for maximum lift coefficient and ideal lift coefficient [32]. As previously calculated the desired ideal lift coefficient is in the range 0.52, indicated by the purple line in Figure 8.3. However, the airfoil data in Figure 8.3 is computed for high Reynolds number, and as the aircraft operates in low Reynolds number a small shift of the airfoils in the graph can be made. Generally speaking, the maximum lift coefficient is higher, thus the airfoils should be shifted slightly down.

NACA 6-series airfoils have a particularly interesting naming system, that will be hence described [32]. Taking as an example the NACA 65<sub>3</sub>-218, the second number (5) alludes to the chordwise position of minimum pressure in tenths of chord behind the leading edge of the airfoil (hence  $0.5\bar{c}$ ) for the basic symmetrical airfoil at zero lift; the subscript number (3) refers to the range of  $C_l$  in tenths above and below the design  $C_l$  in which favourable pressure gradients exist, and therefore low drag; the third number (2) indicates the design  $C_l$  in tenths (therefore making the favourable range -0.1 - 0.5); and finally, the last two numbers (18) indicate the maximum thickness-to-chord ratio of the airfoil, which usually determines the  $C_{l_{max}}$  and stall behavior of the airfoil.





**Figure 8.4:** Normalized shape of the NACA 64<sub>2</sub> – 415, where the centerline is highlighted (produced in XFLR5).

**Table 8.1:** Trade-off table of the NACA-6 series airfoils for the UAV wing

Criteria	$C_d$ (cruise)	$C_d$ parasite	$C_l/C_d$ (cruise)	$C_l$ max	$\alpha$ max	Final trade-off score
Weights of the criteria	0.125	0.125	0.25	0.25	0.25	1.0
NACA 63(4)-412)	0.01037 (lg)	0.00414 (lg)	52.2 (y)	1.320 (dg)	10.5 (y)	3.75
NACA 64(2)-415	0.00864 (dg)	0.00294 (dg)	62.9 (dg)	1.348 (dg)	16.5 (dg)	5 (w)
NACA 64(4)-421	0.01082 (lg)	0.00444 (lg)	49.3(lg)	1.276 (lg)	9.25 (o)	3.125
NACA65(2)-415	0.00872 (dg)	0.00338 (dg)	62.1 (dg)	1.287 (lg)	14.5(lg)	4.5
NACA65(2)-415 a=0.5	0.00892 (dg)	0.0039 (lg)	61.4 (dg)	1.267 (lg)	16.5 (dg)	4.625
NACA65(4)-421	0.0111 (lg)	0.00514 (y)	48.1 (lg)	1.152 (o)	8.25 (o)	2.875
NACA65(4)-421 a=0.5	0.01142 (lg)	0.00565 (y)	46.7 (y)	1.171 (o)	9.75 (y)	2.875
NACA66(2)-415	0.01056 (lg)	0.00593 (y)	53.5 (lg)	1.211 (lg)	13.8 (lg)	3.875
NACA66(3)-418	0.01289 (y)	0.00818 (o)	43.3 (o)	1.204 (y)	17.5 (dg)	3.125

Out of this initial selection, three finalists are chosen, namely: NACA 64<sub>2</sub> – 415, 65<sub>2</sub> – 415, and 65<sub>2</sub> – 415  $a = 0.5$ , where  $a$  is a coefficient that indicates the shape of an added camber line. In the end, the NACA 64<sub>2</sub> – 415 was selected because of its higher lift coefficient, lift-to-drag ratio, and stall speed; its shape is described in Figure 8.4<sup>3</sup>. The characteristics of these three airfoils, furthermore, can be visualized in Figure 8.5.

<sup>3</sup>URL: <http://airfoiltools.com/airfoil/details?airfoil=naca642415-il>

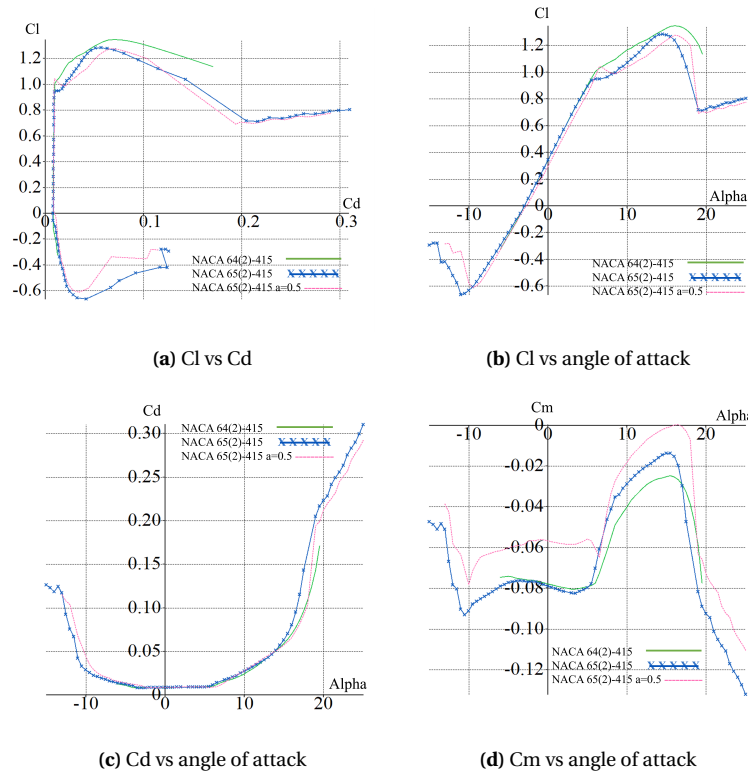


Figure 8.5: Aerodynamic graphs of the three airfoils: NACA 64(2)-415, NACA 65(2)-415, NACA 65(2)-415 a=0.5

## 8.2. Wing Geometry

The geometry of the wing is defined by a set of parameters that affect many aspects of its performance, such as stall behavior, induced drag, or structural considerations. In this section, the different geometrical parameters of the wing will be explained, and their values, selected. These will range from basic parameters, such as aspect and taper ratio, to more advanced ones, as wing twist, angle of incidence, or dihedral.

### Aspect Ratio

The aspect ratio is one of the most defining parameters of wing design. It is defined as the ratio between the span  $b$  over the chord  $c$ , for rectangular wings. However, for wings with spanwise variations in chord, the aspect ratio is defined as expressed in Equation 8.4.

$$AR = \frac{b^2}{S} \quad (8.4)$$

A wing with high aspect ratio has many advantages. For the same surface area, a wing with high aspect ratio will experience less drag induced by the generation of lift, since the longer span and smaller chord result in a smaller wing surface affected by the wingtip vortices [34]. This makes the wing more efficient (as it has a higher lift-to-drag ratio). Furthermore, since less lift is lost, wings with high aspect ratio will present a higher  $C_{l_{max}}$ .

In addition, aspect ratio influences the aircraft's lateral and longitudinal stability. In the case of lateral stability, a high aspect ratio wing presents a less concentrated lift distribution than a wing with low aspect ratio [34]. Effectively, this means that the aircraft is more laterally stable since a localized disturbance will be neutralized more quickly. On the other hand, this also means that the high aspect ratio wing will be less maneuverable. Regarding longitudinal stability, the higher lift capability of a high aspect ratio wing makes it more susceptible to gusts, as a momentary change in angle of attack will result in a bigger change of lift. This phenomenon, which is most critical during take-off and landing, must be considered during design. In addition, this same property makes the stall angle these wings to be lower as the one of their low aspect

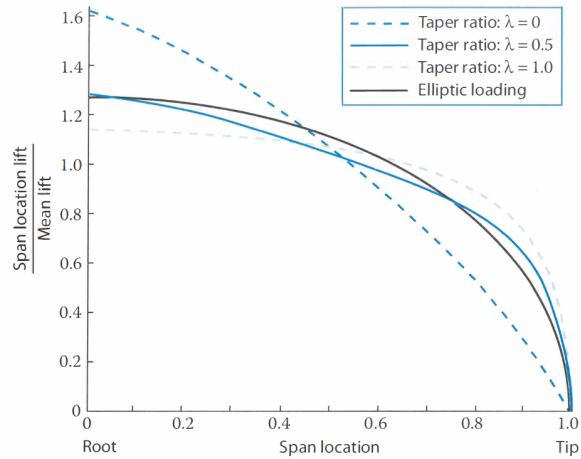


**Figure 8.6:** Effect of the taper ratio on the shape of the lift distribution of a wing.

ratio counterpart.

In deciding for aspect ratio, there are also some structural considerations to be taken in mind. The slenderness of a high aspect ratio wing makes them less stiff, resulting in higher bending at the wingtips [34]. This results in different apparent angles of attack at the extremes, which makes the high aspect ratio wing more prone to wingtip stalling. These type of stall behavior is hard to recover from, since the ailerons are usually located in the outboard sections of the span. The lesser stiffness of the wing also has the risk of inducing aileron reversal, which is the phenomenon that occurs when the bending caused by the forces at the ailerons counteract the deflection of the ailerons themselves, and thus restrict the aircraft from rolling. Apart from these complications, the longer span also results in higher structural weights, so aspect ratio is also a design consideration when considering these weights.

## Taper Ratio

The taper ratio of the wing is another major design parameter to be considered, since its implications on the wing performance are plenty. The dominant function of the taper ratio is to simulate an elliptical lift distribution, since it is the one that produces the least induced drag. In Figure 8.6 [34], the effect of the taper ratio on the lift distribution is visualized, where it can be seen that a trapezoidal wing can only approximate the elliptical shape, albeit getting very close in values of taper close to 0.5. In fact, Raymer [34] mentions that most wings with low sweep usually have a taper ratio of around 0.4-0.5; however, in small aircraft like this one, this rule is applied lightly, and some aircraft present almost rectangular wings [17].

Furthermore, taper ratio introduces sweep in the wing, with the consequences that this carries. Sweep is not discussed as a separate section since it is mostly applied to trans-sonic and supersonic aircraft in order to delay the drag created by shock waves [34]. Instead, the sweep at quarter chord location  $\Lambda_{c/4}$  is kept at zero since its speed never exceeds Mach 0.3, the point where air cannot be assumed to be incompressible anymore. Nonetheless, with taper, a slight sweep is introduced in the wing. This sweep improves dynamic lateral stability, as it creates a dihedral effect. This effect restores the aircraft to its original position when a sideslip gust induces a rolling motion.

Finally, the taper ratio also plays an important role in the structural weight of the wing, as a wing with low taper ratio will decrease its chord along the span, therefore reducing its weight and the lift it produces. This requires lighter structural elements, so taper is a major source of weight savings.

## Additional Wing Parameters

This subsection gathers other parameters that, while necessary, play a less important role in the performance of the wing. As such, they will be briefly described.

**Incidence angle** The incidence angle is defined as the angle between the fuselage axial line and the chord line of the wing. This value is usually fixed at the angle of attack at which the aircraft operates during cruise, given that, then, the parasitic drag produced by the fuselage and other protruding elements will be minimized.

**Dihedral** The dihedral of the wing is introduced for two main reasons: clearance for wing-mounted engines close to the ground, and lateral dynamic stability. The former is not a concern given the chosen design configuration, and the latter is not necessary for the moment, as the aircraft already counts with a top wing and a slight leading edge sweep, both of which induce a dihedral effect.

**Winglets** Winglets are structures that are placed at the wingtips and cleverly separate the upper and lower surfaces of the wing, reducing wing vortices, which they in turn use in order to generate extra lift. The problem with these is that they introduce extra weight, can cause vibrational problems, and their benefits are very limited for high aspect ratio wings.

**Twist** It is not uncommon for wings to have twist. There are two main methods to induce twist in a wing. The first one, and simplest, is geometrical twist. In this, the airfoil at the tip is inclined with respect to the root airfoil; it is easy to design but hard to manufacture. The second one is aerodynamic twist. This consists of using a different airfoil for the tip as compared to the root; this one introduces complications since the span in between will have to use intermediate transition airfoils, whose performance characteristics might be difficult to predict. Be that as it may, the main goals of wing twist are clear: to increase the elliptical shape of the lift distribution, and to delay tip stall, which is hard to recover from. On the other hand, it might reduce the total lift produced. Since the chosen taper ratio already produced a satisfactory lift distribution and prevents wingtip stall, it was preferred to avoid manufacturing obstacles and loss of lift.

**High Lift Devices** Despite the redundancy, it must be clarified a UAV that uses vertical take-off and landing does not need any high lift devices. They could be added as a means to lower the stall speed and therefore aid with transition to vertical flight, but this would add too much weight and complexity to the system, so they will not be considered.

## Wing Design Choices

To define the geometry first wing surface area was found by dividing the estimated take-off weight by the wing load. Once the surface area was found, the wing span  $b$  could be determined by rearranging Equation 8.4. The next step is to determine the preferred aspect and taper ratios. For this, XFLR5 was used as a design tool (as it will be used as a verification tool later on) and, taking a reference surface area, 16 wings were modelled with the NACA 64<sub>2</sub> – 418 airfoil from the combinations of four aspect ratios (0.4, 0.6, 0.8, 1.0) and four taper ratios (4, 6, 8, 10). These were analyzed through a Vortex Lattice Method (VLM) at fixed cruise speed, at operating conditions, described in Chapter 2. The analysis resulted in Figure 8.7, which plots the lift-to-drag ratios of the different wings.

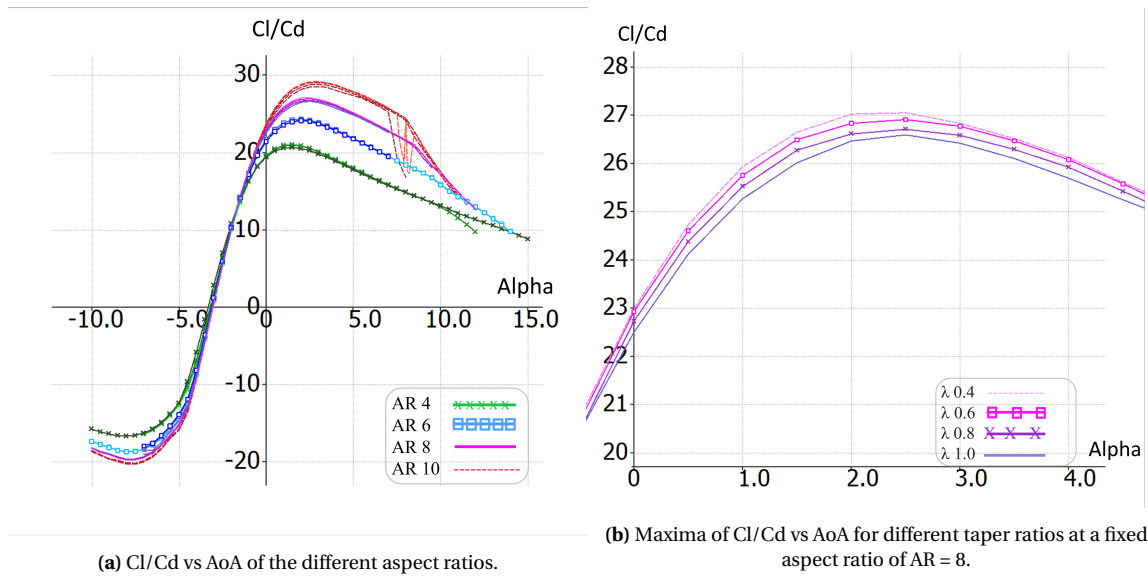


Figure 8.7: Lift-to-drag performance of the 16 simulated wings.

As it was theorized in Subsections 8.2, high aspect ratio translates to a higher efficiency, which motivated an initial choice of 10. However, iteration proved that a value of 10 was a significant toll on the structures, so it was lowered to 8, which still performed very well. As for taper ratio, the taper ratio was chosen to minimize structural weight while preserving a satisfactory lift distribution. This value of taper ratio is 0.4. With the taper ratio, the root chord,  $c_r$ , and tip chord,  $c_t$ , were found using Equation 8.5 and Equation 8.6 respectively, as well as the mean aerodynamic chord (MAC, or  $\bar{c}$ ) in Equation 8.7.

$$c_r = \frac{2S}{(1 + \lambda)b} \quad (8.5)$$

$$c_t = \lambda c_r \quad (8.6)$$

$$\bar{c} = c_r \frac{2}{3} \frac{1 + \lambda + \lambda^2}{1 + \lambda} \quad (8.7)$$

With the calculated root and tip chord, the geometry of the wing could be plotted and the location of the MAC could be determined. The location of the MAC was determined graphically with the method that can be seen in Figure 8.8. The geometry of the wing of the UAV is presented in Figure 8.9.

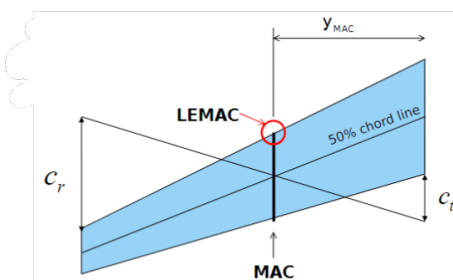


Figure 8.8: Method to determine the location of the MAC on the wing [35]

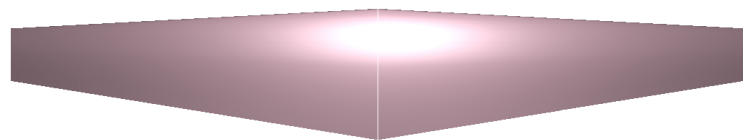


Figure 8.9: The geometry of the wing of the UAV

### 8.3. Wing Lift Coefficient & Stall

Even though XFLR5 was used for the choice of the aspect ratio and taper ratio of the wing, its precision is very limited, and therefore a secondary method needs to be introduced: the DATCOM method<sup>4</sup>. DATCOM

<sup>4</sup>URL: [https://www.esdu.com/cgi-bin/ps.pl?sess=unlicensed\\_1220615041603m xp&t=col&p=col\\_usafdatcom](https://www.esdu.com/cgi-bin/ps.pl?sess=unlicensed_1220615041603m xp&t=col&p=col_usafdatcom)[15/06/2022]

provides a summary of methods for aircraft design, it is deemed reliable for this stage of design, and it is capable of extrapolating the 2D airfoil data into 3D values. After calculating certain valuable parameters through this method, XFLR5 will be used for verification of said values.

One of the figures of greater concern is determining the lift coefficient provided by the wing  $C_L$ , since the effects of downwash and tip vortices greatly affect this value. Previously, Equation 8.3 was used as a rough estimate, considered appropriate for high aspect ratio and unswept wings (the case at hand). However, DATCOM offers a series of calculations that offer a more precise estimate of what this value might look like in real life. The first one is Equation 8.8, which estimates the derivative of the lift coefficient with respect to the angle of attack  $C_{L\alpha}$  (neglecting compressibility effects). The variable  $\eta$  is the aileron efficiency, set at 0.95 [32].

$$C_{L\alpha} = \frac{2\pi AR}{2 + \sqrt{4 + \left(\frac{AR}{\eta}\right)^2 (1 + \tan^2(\Lambda_{0.5c})}} \quad (8.8)$$

Furthermore, the angle of attack at which the lift of the airfoil is zero,  $\alpha_0$ , is the same as the one for the wing. As a result, it is possible to calculate the  $C_L$  of the wing at a certain angle of attack through Equation 8.9. The  $C_{L\alpha}$  can be obtained with the same relationship as Equation 8.3, and, finally, the stall angle of the wing can be vaguely estimated through Equation 8.10. In it,  $\Delta C_L$  is a small margin that is applied in order to account to the slope decay as it gets close to the stall angle.

$$C_L = C_{L\alpha} (\alpha - \alpha_0) \quad (8.9) \quad \alpha_s = \frac{C_{Lmax}}{C_{L\alpha}} + \alpha_0 + \Delta C_L \quad (8.10)$$

**Verification** The values output by the DATCOM method were simultaneously verified with the same values of XFLR5, with small variations. In the case of  $C_{L\alpha}$ , the value provided by DATCOM is 4.98, while for XFLR5 it is 4.94, a difference of 0.8%.

## 8.4. Moment Coefficients & Aerodynamic Center

The resultant moment acting on the wing is a key element in determining its controllability and stability. The two most important non-geometric parameters that will be used in Chapter 9 are the wing's aerodynamic center  $x_{ac}$ , and the moment coefficient around said center  $C_{m,ac}$ . These parameters are important since they are almost constant regardless of angle of attack as long as they are in the linear region of the  $C_l - \alpha$  plot, and thus allow for a direct relationship between the stability and controllability parameters and the center of gravity of the aircraft, as it will be shown in the scissor plot (Figure 9.2).

Using XFLR5 for the selected wing geometry, it is possible to obtain the lift coefficient  $C_L$ , the drag coefficient  $C_D$ , and the moment coefficient  $C_m$  calculated around the center of gravity of the wing ( $C_{m,cgw}$ ). From the plots in Figure 8.10, it is apparent that the slope of the moment curve  $C_{m\alpha}$  is positive. This means that the wing by itself is statically unstable, and thus will need a tail to compensate for it. The aerodynamic center, in addition, is defined as the point in the MAC around which the moment coefficient ( $C_{m,ac}$ ) is constant, and thus  $C_{m\alpha}$  is equivalent to zero.

It is possible to translate the moment coefficient values calculated with XFLR5 around the wing center of gravity with the normal force coefficient  $C_N$ , defined in Equation 8.11. The relationship between  $C_{m,ac}$  and  $C_{m,cgw}$  is then defined in Equation 8.12, where the normalized location of the center of gravity  $\frac{x_{cgw}}{c}$ ,  $C_N$  and  $C_{m,cgw}$  are known. Finally, the fact that  $C_{m,ac}$  is constant can be used to determine the normalized position of the aerodynamic center  $\frac{x_{ac}}{c}$ , since then  $C_{m\alpha,ac}$  is zero, which results in Equation 8.13. The derivatives of the aerodynamic coefficients can be obtained through a linear regression of the values at each angle of attack.

$$C_N = C_L \sin \alpha + C_D \cos \alpha \quad (8.11) \quad C_{m,ac} = C_{m,cgw} + C_N \frac{x_{ac} - x_{cgw}}{c} \quad (8.12)$$

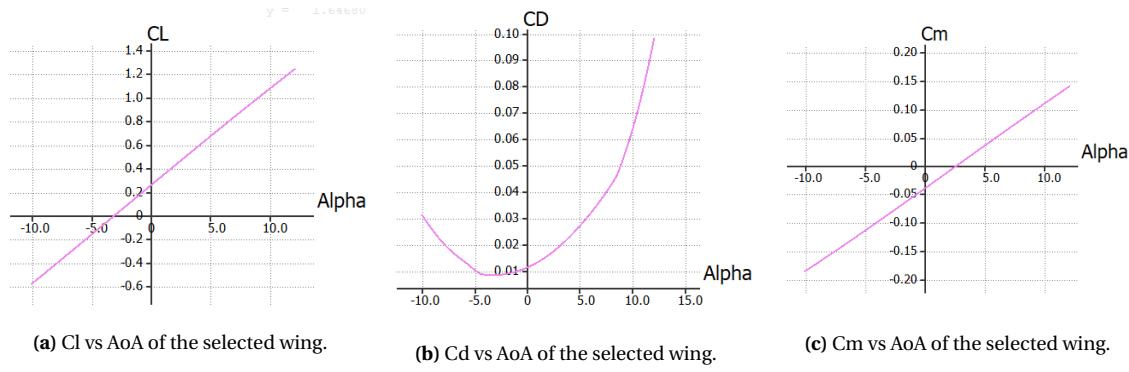


**Figure 8.10:** Simulation of the aerodynamic coefficients against angle of attack of the selected wing.

$$C_{m_{\alpha,ac}} = C_{m_{\alpha,cg_w}} + C_{N_{\alpha}} \frac{x_{ac} - x_{cg_w}}{\bar{c}} = 0 \quad (8.13)$$

## 8.5. Drag Estimation

An estimate for the total UAV drag is provided based on the drag build-up method. The drag from the wing is considered first, and given according to the aerodynamic parameters calculated in the previous sections. The wing drag is the sum skin-friction drag and the lift-induced drag, with an adjustment factor for interference drag. The tail drag is computed in a similar manner to the wing. Additionally, the fuselage drag, boom drag, and drag resulting from the VTOL propellers is estimated.

The skin-friction drag, also known as parasitic or viscous drag, is estimated using the following relation [34]. This method calculates the drag contribution of each component. For the wing, tail, and fuselage of the aircraft, the coefficient of flat-plate skin-friction drag,  $C_f$ , the component form factor,  $FF$ , and the interference factor,  $Q$ , are estimated. The component form factor adjusts the flat-plate skin-friction drag to account for pressure drag arising from viscous separation, while the interference factor accounts for the additional drag arising from the intersection of flow streamlines between components. In this case, the miscellaneous drags,  $C_{D_{misc}}$ , includes the landing gear and the booms for the VTOL propellers, as well as the inactive VTOL propellers during flight. The final term,  $C_{D_{L\&P}}$ , accounts for leakages and protuberances. This term is difficult to empirically predict, and is estimated as 5% of the total parasitic drag [34].

$$C_{D_0} = \frac{\Sigma(C_{f_c} FF_c Q_c S_{wet_c})}{S_{ref}} + C_{D_{misc}} + C_{D_{L\&P}} \quad (8.14)$$

Equation 8.5 gives the coefficient of skin friction for bodies with turbulent flow for a Reynolds number,  $Re$ , below order  $10^7$  [36]. The coefficient of skin friction for laminar flow is given by Equation 8.5. The flow was considered to be turbulent for all surfaces, with the exception of the wing. Flow over the wing was treated as 10% laminar, and 90 % turbulent.

$$C_f = \frac{0.0744}{Re^{0.2}} \quad (8.15) \quad C_f = \frac{1.328}{\sqrt{Re}} \quad (8.16)$$

First, the total wing drag was estimated. Both the viscous drag and the induced drag during the cruise condition were modeled using XFLR5. The induced drag and viscous drag polars are shown in Figure 8.11 and Figure 8.12 respectively.

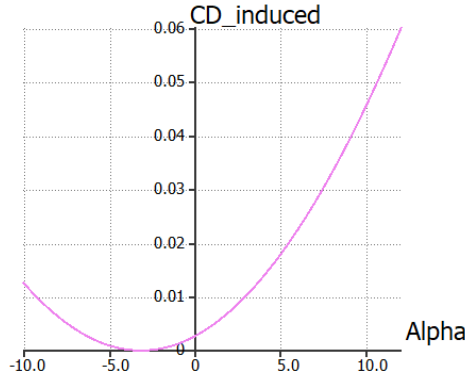


**Figure 8.11:** XFLR5 model of wing induced drag coefficient plotted against angle of attack.

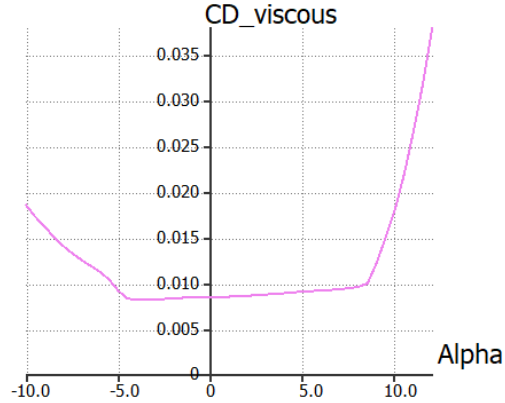


**Figure 8.12:** XFLR5 model of wing parasitic drag coefficient plotted against angle of attack.

This coefficient of induced drag was verified using an empirical relation given in Equation 8.17 [36], for the cruise lift coefficient,  $C_L$ . The planform correction factor  $k$ , calculated using Equation 8.18 [36], which compensates for the effect of taper on induced drag.

$$C_{D,i} = (1 + k) \frac{C_L^2}{\pi A} \quad (8.17)$$

$$k = A(0.0484\lambda^4 - 0.1401\lambda^3 + 0.1595\lambda^2 - 0.0703\lambda + 0.0124) \quad (8.18)$$

It can be noted that according to this equation, which does not consider winglets or twist, minimum induced drag occurs at a taper ratio  $\lambda$  of approximately 0.4, where the behavior closely approximates an elliptical wing, differing by only 1.6%. At the cruise angle of attack, this method yields an estimate for induced drag of 0.0082, approximately 8% less than the prediction of XFLR5. In order to provide a conservative estimate of drag, the higher estimate for induced drag, in this case provided from XFLR5, is used. The wing coefficient of viscous drag is calculated in XFLR5, and given in Figure 8.12. XFLR5 analysis was used in a similar manner to estimate the contributions of the empennage. Additionally, estimates for component interference factors  $Q_c$  are estimated from literature. The wing and fuselage are assumed to have a  $Q_c = 1$ , while the VTOL booms have an interference factor of 1.25, the tail an interference factor of 1.08, and the landing gear of 1.2.

The booms are narrow bodies aligned in the direction of the flow. This means the boom structures may be treated as streamlined bodies for the calculation of drag build up. The same method is used to estimate the drag contribution of the fuselage, according to the dimensions provided in Section 14.1. Equation 8.5 gives the form factor as a function of the thickness ratio  $d/l$  [36].

$$\text{Form factor} = 1 + 1.5 \left( \frac{d}{l} \right)^{\frac{3}{2}} + 7 \left( \frac{d}{l} \right)^3 \quad (8.19)$$

This allows for the calculation of drag normalized for dynamic pressure,  $\frac{D}{q}$ , where  $S_{ref}$  is the wing surface area.

$$\frac{D}{q} = S_{ref} \times C_{ref} \times \text{Form factor} \quad (8.20)$$

Finally, the drag component resulting from the inactive VTOL propellers is considered. Literature indicates that existing theoretical methods to estimate this drag using Kutta-Joukowski theory yields significant underestimates compared to data obtained in wind tunnel. A semi-empirical method for calculating the drag of the static propellers during cruise is given by Equation 8.5, where  $D_{VTOLProp}$  is the total additional drag in N,  $D_{interp}$  is the drag of a single propeller taken from wind tunnel data interpolated for flow velocity, and

$F_{scale}$  is the scaling factor for the propeller diameter, given as the ratio of the VTOL propeller diameter over that of the reference propellers measured in wind tunnel [37]. Values for  $D_{interp}$  were available for parallel and perpendicular propellers, with Equation 8.5 giving the relation for propellers oriented at an angle  $\phi$  with respect to the incoming flow. However, in order to minimize drag, the propellers are aligned parallel to the flow. This leads to a substantial reduction in additional drag resulting from the inactive VTOL propellers, which can be observed in Figure 8.13 and Figure 8.14<sup>5</sup>. Although this configuration still contributes additional drag, the alignment of the propellers with the flow nearly halves the increase in drag compared to propellers aligned perpendicular to the flow.

$$D_{VTOLProp} = 4(F_{scale})^2 D_{interp} \quad (8.21)$$

$$D(\phi) = (D_{\perp} - D_{\parallel}) \sin \phi + D_{\parallel} \quad (8.22)$$

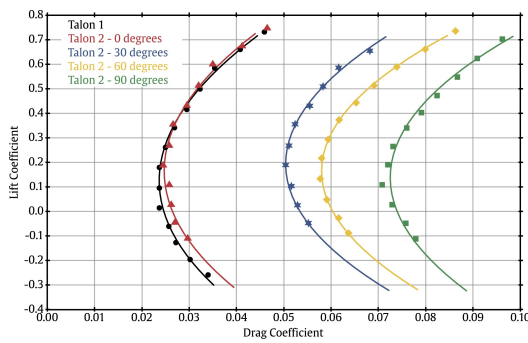


**Figure 8.13:** Forward flight drag polars with flow speed of 17.5 m/s for reference VTOL with various alignment angles of VTOL propellers.

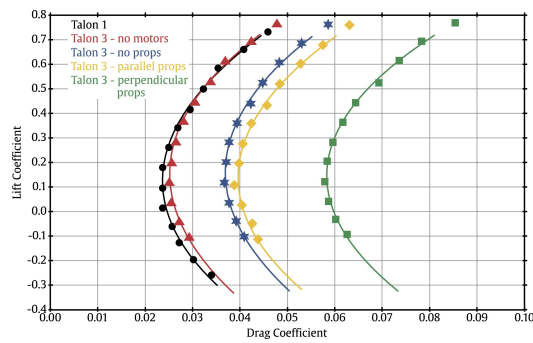


**Figure 8.14:** Forward flight drag polars with flow speed of 17.5 m/s for reference VTOL with various configurations of VTOL motors.

## 8.6. Tail Geometric Design

The vertical and horizontal tailplanes fulfill different functions than the wing, their purpose mainly center in static and dynamic, lateral and longitudinal stability, so their main requirements will be specified in Chapter 9. However, they do have a few requirements in the aerodynamic requirement, presented henceforth.

### Tail, Aerodynamic Requirements

**SYS-AERO-05** The horizontal tailplane shall exceed the wing angle of attack by 5 degrees.

**SYS-AERO-06** The horizontal tailplane shall show a smooth stall behavior.

**SYS-AERO-07** The horizontal tailplane span shall provide 1 m clearance between the booms.

**SYS-AERO-08** The tip chord of the vertical tailplanes must be equal to the tip chord of the horizontal tailplane.

In the geometric design of the tailplane, the process is simpler than for the wing. Given that it is not the main producer of lift (it produces negative lift, in fact), the additional wing parameters discussed in Figure 8.2 will not be considered. Instead, the design will consist in airfoil and aspect and taper ratio estimations, keeping the sweep at quarter chord  $\Lambda_{0.25c}$  at zero.

<sup>5</sup>URL: <https://www.sciencedirect.com/science/article/pii/S1270963820311111?via%3Dihub> [21/06/2022]

## Tail Airfoil

The airfoil of the tailplane is usually taken to be symmetric, as its design lift coefficient is dependent on the position of the center of gravity, and therefore should be able to be changed depending on the configuration. Looking back at Figure 8.3, there are many options for symmetrical airfoils, but the uncertainty of the final design  $C_l$  makes some 6-series airfoils, which have tight constraints for allowable lift coefficients, undesirable. Therefore, six airfoils were selected: three of them being NACA 4 digit airfoils with different thickness-to-chord ratios, and three 6-series airfoils with different thickness-to-chord ratios and high allowable lift coefficient ranges.

These airfoils and their characteristics are collected in Table 8.2. In this case, the driving design parameters are: the stall angle, as the horizontal tail should stall as late as possible to ensure recovery when the wing stalls; the stall behavior, as a smooth stall is more noticeable and less dangerous; the maximum lift coefficient, as it increases the range of possible centers of gravity; and lift-to-drag ratio since it saves on thrust and energy requirements. The winner of this trade-off is indisputably the NACA 0015 (Figure 8.15<sup>6</sup>), which will be used for both the horizontal and vertical tails, for simplicity and easier manufacturability.

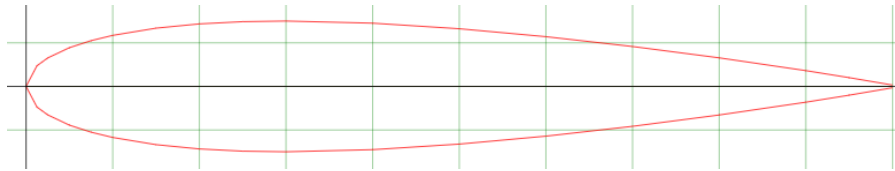


Figure 8.15: Normalized shape of the NACA 0015, where the centerline is highlighted (produced in XFLR5).

Table 8.2: Trade-off table of the NACA series airfoils for the tail, evaluated at a  $C_L$  of 0.5.

Criteria	$C_d$ (cruise)	$C_d$ parasite	$C_l/C_d$ (cruise)	$C_l$ max	$\alpha$ max	Stall behavior	Final trade-off score
Criteria Weights	0.1	0.1	0.2	0.2	0.2	0.2	1.0
NACA 0010	0.0081 (dg)	0.00289 (dg)	-54.1 (lg)	1.193 (lg)	13 (y)	abrupt (y)	3.8
NACA 0015	0.0095 (lg)	0.00397 (lg)	-50.8 (y)	1.273 (dg)	16.75 (dg)	smooth (dg)	4.4 (w)
NACA 0018	0.00985 (lg)	0.00985 (o)	-47.7 (o)	1.262 (dg)	16.25 (dg)	gradual (lg)	3.8
NACA 63012A	0.00856 (dg)	0.00856 (y)	-56.0 (dg)	1.034 (y)	11 (y)	abrupt (y)	3.6
NACA 63-015A	0.00815 (dg)	0.00815 (y)	-57.4 (dg)	1.148 (lg)	15 (lg)	gradual (lg)	4.2

## Tail Taper Ratio

The chosen tail configuration plays a very important role in the definition of the tail aspect and taper ratios. The inverse-U tail intersects the vertical and horizontal wings at their tips, so there is an inherent constraint that their tip chords must be equal to create a flush surface. Furthermore, the fact that the horizontal tailplane is supported on the extremes means that there is no structural reason for implementing a taper in the planform. This thesis is also supported by the fact that there will not be an induced angle of twist that could result in early tip stall. Furthermore, the vertical tails act as endplates, or some sort of winglets for the horizontal tail. This reduces the uneven downwash distribution typical of rectangular wings. In conclusion, the taper ratio for the horizontal wingtail will be 1, and therefore, the horizontal tail will be rectangular.

<sup>6</sup>URL: <http://airfoiltools.com/airfoil/details?airfoil=naca0015-il>

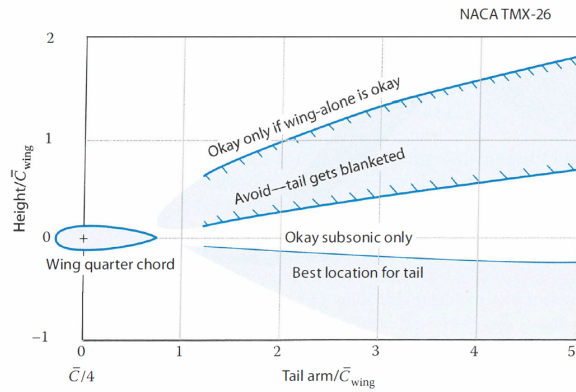


**Figure 8.16:** Blanketing effect depending on horizontal tail position.

In the case of the vertical tailplanes, the aspect ratio is not a design choice, since the sizing method is performed through statistical relationships that set the area of the vertical wings, and the root chord is fixed because of the assumption that the tip chords of both tails should be equal.

### Tail Aspect Ratio

The horizontal tail aspect ratio was sized according to recommendations in literature, where it was suggested that the aspect ratio of the horizontal empennage should be low, as then the stall angle is maximized, and the risk of deep stall (stall with no possible recovery) is minimized [32]. As a result, the suggested range of aspect ratios was 4-6, where the higher end of the spectrum was chosen (that is, 6), since it was advantageous for the stability calculations of Chapter 9.

The aspect ratio of the vertical tails, on the other hand, was suggested a range from 1.3 to 2.0 [34]. In the case of the inverted-U tail configuration, placing the horizontal wing too high up can cause blanketing in cases of high angle of attack, and thus make recovery impossible (deep stall), as depicted in Figure 8.16 [34]. As a result, the lower end of the spectrum was chosen; namely, the vertical tail has an aspect ratio of 1.3. In Table 8.3, the chosen taper and aspect ratios for the empennage are summarized.

**Table 8.3:** Aspect ratio and taper ratios of the vertical and horizontal wings of the empennage.

	Taper ratio ( $\lambda$ )	Aspect Ratio ( $AR$ )
Horizontal Wing	1	6
Vertical Wing	Assigned later	1.3

**Tail Incidence Angles** The tail incidence angles are fixed relatively easily. For the case of the horizontal tail, the incidence angle will be equal to the angle which produces the lift coefficient required to counteract the moment created by the wing. When this value is negative (i.e. the center of gravity is behind the aerodynamic center), this means that the stall angle of the horizontal wing is delayed with respect to the wing, which is beneficial since this means that recovery from stall will be less risky. For the twin vertical tails, Raymer [34] recommends 1 or 2 degrees of incidence to the left in single-engine aircraft (or single cruise propeller, in our case) to counteract the "p-effect" which is the yaw induced by the rotating propeller.

**Tail Aerodynamic Coefficients** For the static stability calculations of Chapter 9, it is important to define the  $C_{l_\alpha}$  of the horizontal tail as well. For this, the same DATCOM formula can be employed (Equation 8.8), albeit by multiplying the horizontal wing aspect ratio  $AR_h$  by a factor of 1.5, to account for the risk of deep stall of a high tail.

# Stability & Controllability Design

The stability and controllability of the UAV are assessed through the performance in two flight conditions: cruise flight and roll performance. Stability and control must be performed as an integrated design process, with the results of the sizing from the detailed design for aerodynamics. Stability and control curves are constructed in Section 9.1 and used to determine the longitudinal position of the wing and tail, as well as the tail area. Design of the aileron positioning and sizing are performed in Section 9.2. First, however, the requirements to be fulfilled by the stability and control design must be specified.

## Stability and Control Requirements

**SYS-STAB-01** The horizontal tail shall induce a negative slope of moment coefficient on the configuration as a whole.

**SYS-CON-01** The horizontal tail shall produce a moment around the center of gravity that equals or exceeds the moment caused by the tail-less aircraft in an opposite direction.

**SYS-CON-02** The ailerons shall allow the aircraft to roll 45 degrees in 1.4 seconds.

## 9.1. Static Longitudinal Stability & Control at Cruise Flight

The longitudinal stability of the aircraft is simply defined by the position of the center of gravity with respect to the neutral point. The neutral point is considered the position of the center of gravity where the pitching moment remains constant with changes of angle of attack, that is,  $C_{m_\alpha}$  is equal to zero (when its value is negative, the system is considered stable). In Figure 9.1, the neutral point and center of gravity positions are depicted for a wing and tail configuration. The static margin is defined as the longitudinal space that the gravity center could shift aft and still present stable behavior<sup>1</sup>.

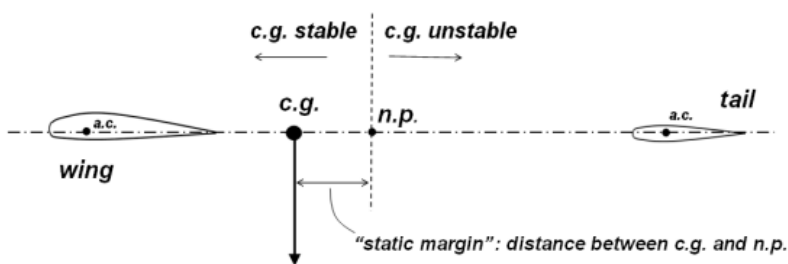


Figure 9.1: Illustration of the longitudinal stability of the aircraft

The position of the neutral point is given by the change in lift produced by the wing and horizontal tails when the angle of attack is changed, starting from equilibrium. Depending on the magnitudes of each lift, the neutral point will be closer or further from the aerodynamic center of the wing. By normalizing the expressions for lift (dividing by  $\frac{1}{2}\rho V^2 S$ ), accounting for the downwash of the flow on the tail ( $1 - \frac{dc}{d\alpha}$ ), the distance between the aerodynamic center of the wing and that of the tail ( $\frac{l_t}{c}$ ), and leaving a small static margin (S.M.) of 5% in case of unexpected weight shifts, Equation 9.1 is obtained.

The location of the aerodynamic center is attained in Section 8.4, the MAC was calculated in Section 8.2, Equations 9.2 and 9.3 use the DATCOM semi-empirical relationships [38] to determine the derivatives of

<sup>1</sup>URL: [https://ocw.tudelft.nl/wp-content/uploads/Hand-out-Stability\\_01.pdf](https://ocw.tudelft.nl/wp-content/uploads/Hand-out-Stability_01.pdf)

the lift coefficients (note that Equation 9.2 includes a factor of 1.5 on the aspect ratio to account for the high tail). Finally the distance between aerodynamic centers,  $l_h$ , was chosen to be three times the MAC ( $l_h = 2\bar{c}$ ). Since the tail is high, the relationship between the speed over the horizontal tail and the wing was considered to be  $\frac{V_h}{V} = 0.95$ , and the downwash gradient is given by Equation 9.4, according to semi-empirical relations given by the USAF Stability & Control DATCOM program [39]. These parameters will be used in the Scissor plot of Figure 9.2 in order to determine an optimal value of horizontal stabilizer area and its related center of gravity position.

$$\bar{x}_{cg} = \bar{x}_{ac} + \frac{C_{L\alpha_h}}{C_{L\alpha_{A-h}}} \left(1 - \frac{d\epsilon}{d\alpha}\right) \frac{S_h l_h}{S\bar{c}} \left(\frac{V_h}{V}\right)^2 - S.M. \quad (9.1) \quad C_{L\alpha_h} = \frac{2\pi 1.5 A_h}{2 + \sqrt{4 + \left(\frac{1.5 A_h \beta}{\eta}\right)^2 \left(1 + \frac{\tan^2 \Lambda_{0.5c_h}}{\sqrt{(1-M^2)}}\right)}} \quad (9.2)$$

$$C_{L\alpha_{A-h}} = C_{L\alpha_w} \left(1 + 2.15 \frac{b_f}{b}\right) \frac{S_{net}}{S} + \frac{\pi b_f^2}{2S} \quad (9.3) \quad \frac{d\epsilon}{d\alpha} = 4.44 K_{AR} K_{mr} K_\lambda \sqrt{\cos(\Lambda_{0.25})}^{1.19} \quad (9.4)$$

Equation 9.4 provides an estimate of the wing downwash according empirical factors defined in Equations 9.5 - 9.7. These are a function of the aspect ratio, taper ratio and sweep of the wing which all have defined values resulting from the aerodynamic design. In Equation 9.7, the normalized vertical ( $m$ ) and horizontal ( $r$ ) distance from wing to tail are used.

$$K_{AR} = \frac{1}{AR} - \frac{1}{1 + AR^{1.7}} \quad (9.5) \quad K_\lambda = \frac{10 - 3\lambda}{7} \quad (9.6) \quad K_{mr} = \frac{1 - \frac{m}{2}}{r^{\frac{1}{3}}} \quad (9.7)$$

The controllability requirement (**SYS-CON-01**) can be fulfilled when the moments in the aircraft are balanced. Starting from an expression of moment equilibrium such as Equation 9.8 and normalizing the moments, Equation 9.9 is obtained, which can be then rearranged to plot the center of gravity against the horizontal tail area ratio in the Scissor plot of Figure 9.2. In this case,  $C_{m,ac}$  was derived in Section 8.4,  $C_{L_{A-h}}$  is considered to be the same as the design lift coefficient  $C_{L_C}$ , and the lift coefficient of the tail is considered to be -0.5, as for the chosen airfoil, it allows for 10 degrees before stall if the aircraft pitches down (at which point the lift of the wing would be negative, so it is unlikely that this point will be reached), and for 20 degrees if it pitches up (at which point the wing would have already stalled, and the angle corrected through the elevator).

$$C_{m,ac} + C_{L_{A-h}} \frac{x_{cg} - x_{ac}}{\bar{c}} = C_{L_h} \frac{S_h l_h}{S\bar{c}} \quad (9.8) \quad \bar{x}_{cg} = \bar{x}_{ac} - \frac{C_{m_{ac}}}{C_{L_{A-h}}} + \frac{C_{L_h}}{C_{L_{A-h}}} \frac{S_h l_h}{S\bar{c}} \left(\frac{V_h}{V}\right)^2 \quad (9.9)$$

By combining the control and stability equations in a single graph, the range for center of gravity locations and tail area ratios relative to the wing which are both stable and controllable regions can be identified. This graph, depicted in Figure 9.2 and nicknamed "Scissor plot" for their intersecting straight lines, shows both the stability and controllability criteria when plotting the position of the center of gravity (measured from the leading edge of the MAC and normalized with respect to it) against the surface ratios of the horizontal stabilizer and the wing. The series called "neutral stability" is equivalent to the stability criterion without the static margin. Even though the position of the center of gravity will not supposedly change during operations (as the weight of the fuel constitutes approximately 0.45% of the maximum take-off weight), it was considered prudent to assume an allowable center of gravity range of 15% of the MAC, which resulted in the horizontal black line in Figure 9.2. This line specifies that the optimal surface ratio is a bit lower than 0.1, which means that the tail will not have to be very big, which is convenient.

Since an inverted U-tail is used, two vertical tails are present. This means that the surface area is divided over the two tails which have a tip chord equal to the horizontal tail. In order to calculate the surface area, the equation for tail volume coefficient was used (Equation 9.10). A value of 0.04 was used, based on a comparable UAV with boom and U-tail [40]. The calculated surface area still had to be divided by two to get the area for each tail. Then, using Equation 8.4, the span of each tail was calculated. Here, an aspect ratio of 1.3 was used<sup>2</sup>. Note that this aspect ratio is valid for only half a wing, so only the part above the boom. This

<sup>2</sup>URL: <https://aerotoobox.com/design-aircraft-tail/> [08/06/2022]

means that the calculated span is also for half a wing. The last step is to calculate the root chord, which was done with Equation 8.5.

$$C_{vv} = \frac{S_V l_V}{S b} \quad (9.10)$$

The relations for stability and control were implemented into the integrated design iteration described in Chapter 4, and is driven primarily by the wing aerodynamic design and the UAV center of gravity. In turn, the stability and control requirements drive the tail sizing.

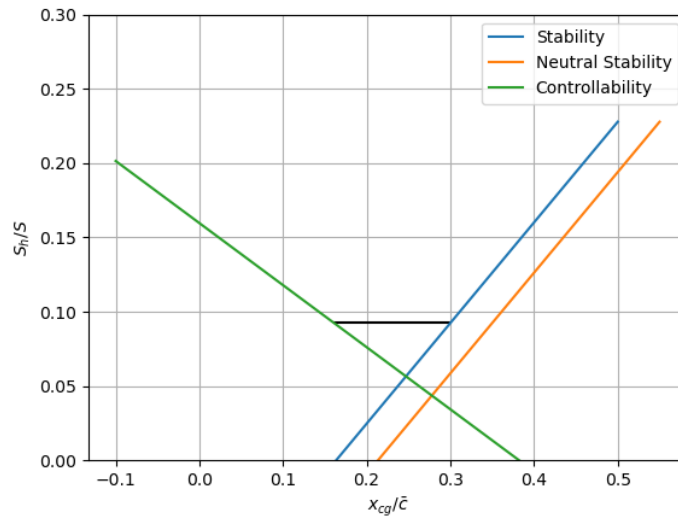


Figure 9.2: UAV controllability and stability scissor plot

## VTOL Flight Stability & Control

In addition to stability during cruise, so in horizontal flight, stability and controllability during vertical flight in VTOL and hover is required. For this, no dedicated analysis is performed in terms of control forces. However, in Chapter 5, it was accounted for this type of stability and controllability. Since a gyroscope is included in a the UAV, attitude and rotation determination during VTOL and hover is possible. So, by making use of gyroscope stabilization technology the UAV can be hold stable and controllable. The ESC's for each engine will play a crucial role in this system, controlling the speed of each engine independently.

### 9.2. Aileron Sizing

The aileron is a flight control surface, fundamental part of an aircraft's maneuverability. It is responsible for banking capabilities of the aircraft. The UAV is a surveillance mission which means that maneuverability is not a driving factor on the design during cruise (the flight section that could encounter fixed obstacles would be navigated through the VTOL propellers). Therefore, the aileron was designed to fulfill the basic requirements to make the aircraft roll along its longitudinal axis.

The sizing process is initiated by calculating the aileron effectivity which is the ratio of the aileron chord and the total local chord where the aileron is located.

Then, to calculate the control derivative, values specific for the wing were needed such as:  $C_{l_\alpha}$ , the zero drag coefficient as well as the surface area and the wingspan of the main wing. It was also necessary to use the chord length as a function of the wing span which was calculated geometrically.

$$C_{l_{\delta a}} = \frac{2c_{l_\alpha} \tau}{S_{ref} b} \int_{b_1}^{b_2} c(y) y dy \quad (9.11)$$

The roll damping coefficient is also needed for the sizing. It quantifies the aircraft's response against the banking movement of the airplane. To calculate the coefficient values, the same wing values and the chord length in function of the wing span needed for the control derivative were used.

$$C_{l_p} = -\frac{4(c_{l_\alpha} + c_{d_0})}{S_{ref} b^2} \int_0^{b/2} y^2 c(y) dy \quad (9.12)$$

The second-to-last step was to calculate the aircraft's steady roll rate. It measures at what rate the aircraft can change the roll attitude. It is the ratio between the control derivative and the roll damping coefficient multiplied by the total deflection of the airplane,  $\delta_a$ ; the cruising speed,  $V$ ; and the wingspan,  $b$ . For the total deflection, it was decided to choose a conservative 20 degrees for total deflection which is a commercial aircraft average [41]. Since the drone is not required to do aggressive movements or sudden maneuvers, the aileron deflection does not have to be of high magnitude.

$$P = -\frac{C_{l_{\delta a}} \delta_a}{C_{l_p}} \frac{2V}{b} \quad (9.13)$$

Finally, it was necessary to analyze the roll time. This was done by selecting a bank angle and dividing it by the aircraft steady roll rate. There are several categories for airplanes shown in Table 9.1. The category that the UAV lands in is class II which are the medium weight aircraft used for reconnaissance among others [35]. To be part of the class it is required for the aircraft to bank 45 degrees in 1.4 seconds which is the hard requirement to that sizes the location spanwise of the aileron.

**Table 9.1:** Aircraft classifications based on roll time performance.

Class	Roll performance
I	60 de in 1.3s
II	45 deg in 1.4s
III	30 deg in 1.5s
IVA	90 deg in 1.3s
IVB	90 deg in 1.0s
IVC	90 deg in 1.7s

The edges of the aileron are calculated with a different method for each. The outermost edge has a fixed value to be 10% offset from the wing tip because of vortex formation. The inner edge, on the other hand, is calculated by choosing the right value of  $C_{l_{\delta a}}$  to match the preferred category of Table 9.1. The depth of the aileron, so the dimension parallel to the wing chord length is equivalent to the distance from the trailing edge to the beginning of the rear spar which is equal to 35% of the tip chord length.

# Propulsion and Power Systems Design

The power required for the UAV determines the sizing of the propellers, the amount of hydrogen needed for the mission, the mass of the hydrogen tank, and the mass of the hydrogen fuel cell. This chapter first discusses the general equations to calculate the required power per flight stage in Section 10.1. In Section 10.2, the sizing of the propellers is explained. The positioning of the VTOL propellers is done in Section 10.3. Finally, the power and total energy needed for the specific mission of the UAV is given in Section 10.4.

## Propulsion and power requirements.

**SYS-POW-01** The VTOL propellers shall deliver enough thrust to take-off to an altitude of 50 m.

**SYS-POW-02** The fixed wing propeller shall deliver enough thrust to climb 560 m.

**SYS-POW-03** The fixed wing propeller shall deliver enough thrust to reach the maximum speed.

**SYS-POW-04** Enough hydrogen shall be carried aboard to complete a 2 hour mission with margin.

## 10.1. Propulsion

The power required is calculated for three fixed wing flight stages and three VTOL flight stages. The fixed wing flight stages are: cruise, sprint, and climb. The thrust to weight ratio is calculated for each flight stage, whereafter it is converted to power over weight ratio with Equation 10.1.  $\eta_p$  and  $V$  are the propeller efficiency and speed per flight stage, respectively. The cruise and sprint fixed wing flight stages are calculated with Equation 10.2, at desired cruise altitude differing only in speed.

$$P/W = \frac{(T/W)V}{\eta_p} \quad (10.1) \quad (T/W)_{cruise}^{FW} = \frac{0.5\rho V^2 C_{D_0}}{W/S} + \frac{2(W/S)}{\pi A e \rho V^2} \quad (10.2)$$

For the climb fixed wing stage Equation 10.3 is used. The climbing stage starts after the vertical take-off stage has reached an appropriate altitude. The climb speed  $V_c$  is determined with Equation 10.4.

$$(T/W)_{climb}^{FW} = \frac{R/C}{V_c} + \frac{0.5\rho V_c^2 C_{D_0}}{W/S} + \frac{2(W/S)}{\pi A e \rho V_c^2} \quad (10.3) \quad V_c = \sqrt{\frac{2(W/S)}{\rho_0} \sqrt{\frac{1}{3\pi A e C_{D_0}}}} \quad (10.4)$$

Secondly, the VTOL flight stages are vertical climb, hover, and vertical landing. Equation 10.5 [42] generates the thrust to weight ratio for the vertical take-off stage. In this equation, the ratio of the projected surface area,  $S_{proj}$  over the wing surface area,  $S$ , was taken to be 1.35 based on literature [43]. The thrust required for vertical climb is generated by the propellers used for the VTOL flight stage. The power required for this maneuver for a single propeller was calculated with Equation 10.7. In this equation,  $T$  is the required thrust per propeller needed for vertical climb,  $v_i$  is the air-induced velocity through the rotor disc, and FM is the Figure of Merit.

The thrust required during vertical climb can be determined by multiplying the thrust to weight ratio found during vertical climb by the weight of the UAV. The FM in Equation 10.6 is estimated from a regression model [42].

$$(T/W)_{climb}^{VTOL} = 1.2 \left( 1 + \frac{1}{W/S} \rho (R/C)^2 \frac{S_{proj}}{S} \right) \quad (10.5) \quad FM = 0.4742T^{0.0793} \quad (10.6)$$

First, the propeller disc area and induced velocity in hover must be known. The propeller disc area,  $S_{prop}$ , was calculated using Equation 10.8. DL is the disc loading for one propeller, which was determined using the wing loading and power loading diagrams. With this propeller disc area, the induced velocity in hover,  $v_h$  can be determined using Equation 10.9. Eventually, the air-induced velocity through the rotor disc during vertical climb,  $v_i$ , is calculated with Equation 10.10.

$$P_{req}^{VTOL} = \frac{T v_i}{FM} \quad (10.7)$$

$$S_{prop} = \frac{W_{TO}}{DL} \quad (10.8)$$

$$v_h = \sqrt{\frac{T}{2\rho S_{prop}}} \quad (10.9)$$

$$\frac{v_i}{v_h} = -\frac{(R/C)_{VTOL}}{2v_h} + \sqrt{\left(\frac{(R/C)_{VTOL}}{2v_h}\right)^2 + 1} \quad (10.10)$$

Additionally to the previous flight stages, the UAV must also be able to hover. When there is no wing area underneath the rotors of the UAV, it can be assumed that the thrust provided by the rotors is equal to the weight during hovering [44]. With this assumption, the power loading during hover, PL, can be determined with Equation 10.11. It should be noted that  $PL = W/P$  [44]. The Figure of Merit (FM) was again determined using the regression line; however, the thrust for hovering was now used.

$$PL_{hover}^{VTOL} = \frac{FM}{\sqrt{\frac{DL}{2\rho_0}}} \quad (10.11)$$

Lastly, the UAV also has to descend again to the ground station. The thrust needed to perform this maneuver has been calculated with Equation 10.12. Where  $W_o$  is the total weight,  $V_{LD}$  is the landing velocity,  $C_{D_{0,axial}}$  is the axial zero drag coefficient, equal to 2, and  $n$  is the number of propellers used for descent [43].

$$T_{LD}^{VTOL} = \frac{W_o - 0.5\rho V_{LD}^2 S C_{D_{0,axial}}}{n} \quad (10.12)$$

The power required by the propellers to generate this thrust during landing has been determined using Equation 10.13. Here,  $V_i$  is the axial descent induced velocity, determined using Equation 10.14 [43].

$$P_{LD}^{VTOL} = \frac{T_{LD}}{FM} (V_i - V_{LD}) \quad (10.13)$$

$$V_i = v_h(1.2 - 1.125x - 1.372x^2 - 1.718x^3 - 0.655x^4) \quad x = -\frac{V_{LD}}{v_h} \quad (10.14)$$

## 10.2. Propeller sizing

Now that the amount of thrust required during each flight stage is known, the VTOL and forward flight propellers can be sized. The propeller disc area for the VTOL propellers has been calculated with Equation 10.8, and the diameter of the propellers has been established by means of this disc area. This is the minimum diameter the propeller must have based on the disc loading constraints. With this diameter, a first estimate of the Rotations Per Minute (RPM) was found using regression. Equation 10.15 [42] has been used for this.

$$RPM^{VTOL} = 2762.786 D_{VTOL}^{-0.932} \quad (10.15)$$

Once these first estimates for the VTOL propeller were established, an estimate for the diameter of the forward flight propeller was made. This diameter was found using Equation 10.16 and Equation 10.17 [42]. The diameter found with these equations is about 9.43 inches. However, in a later stage, this diameter was set to 22.83 inches due to noise considerations. Since in Equation 10.18 the diameter and pitch must be given in inches, and commercially available propellers are usually expressed in inches, inches are used instead of meters to define the propeller diameter and pitch.

$$K_v = -0.228 \cdot 10^{-7} P^3 + 0.0003 P^2 + -1.101 P + 1685.676 \quad (10.16)$$

$$D^{FF} = 4.735 K_v^{-0.405} \quad (10.17)$$

The thrust generated by each propeller is based on the RPM and pitch of the propeller and the flight speed of the UAV. This thrust has been calculated using Equation 10.18<sup>1</sup>. For the VTOL propeller, an estimate of its pitch could be made using this equation. The thrust required for vertical take-off, the RPM estimate, and the climb rate were used as inputs in Equation 10.18. The rate of climb was used as the flight speed since the VTOL propellers are orientated horizontally on the UAV, and the incoming airflow will enter these propellers with the climb speed. It must be noted that these values are first estimates and that a commercially available propeller will be selected that has values close to these.

At this point, the pitch and RPM of the propeller for forward flight are still unknown. However, the pitch was set to a random value to estimate the RPM needed during cruise using Equation 10.18. An iteration was done to find an appropriate pitch and RPM value. A RPM value between 4000 and 6000 was desired since these are common RPM values. A high RPM value is namely undesired since it produces more noise. With the first estimate of a 9.43 inch diameter and 12 inch pitch, the propeller would need a RPM of about 6713 to generate the required thrust during cruise. With a pitch of 12 inches and a diameter of 22.83 inch, the propeller would need a RPM of 4532 during cruise, which is more desirable due to noise considerations.

$$F = 1.225 \frac{\pi(0.0254d)^2}{4} \left( (RPM_{prop} 0.0254 pitch \frac{1}{60})^2 - (RPM_{prop} 0.0254 pitch \frac{1}{60}) V_0 \right) \left( \frac{d}{3.29546 pitch} \right)^{1.5} \quad (10.18)$$

The first estimates of the propeller sizing based on the regression equations, Equation 10.15, Equation 10.16 and Equation 10.17, can be found in Table 10.1. Especially the size of the VTOL propeller is infeasible due to its large pitch. To decrease both the pitch and RPM, the propeller's diameter must be increased.

**Table 10.1:** First estimates of propeller sizing for VTOL and forward flight propellers based on regression

Flight Mode	Diameter [inch]	RPM [-]	Pitch [inch]
VTOL	12.17	8249	109
Forward flight	9.43	6713	12

### 10.3. Propeller positioning

An important consideration is the propeller positioning since they cannot interfere with the fuselage, the wing or one another. First, the x positions as in the reference frame in Figure 10.1, of the VTOL propellers have been determined. It is important that the VTOL propellers do not intersect with the wings of the UAV, so for safety, a propeller clearance,  $c_{prop}$ , of 0.1 m will be used. The x position of the two front VTOL propellers,  $x_{PF}$ , are determined using Equation 10.19 [45]. Where  $b_{HT}$  is the span of the horizontal tail,  $\Lambda_{LE_w}$  is the sweep of the leading edge of the wing, and  $D_{VTOL_{prop}}$  is the diameter of the VTOL propeller. It must be noted that the position of the leading edge at the wing root was taken as the null position, as opposed to the one depicted in Figure 10.1.

$$x_{PF} = \frac{b_{HT}}{2} \tan \Lambda_{LE_w} - \frac{D_{VTOL_{prop}}/2 - c_{prop}}{\cos \Lambda_{LE_w}} \quad (10.19)$$

The x position of the rear propellers,  $x_{PR}$  has been determined using Equation 10.20, where  $c_r$  is the root chord of the wing and  $\Lambda_{TE_w}$  is the sweep of the trailing edge of the wing [45].

<sup>1</sup>URL: <https://aviation.stackexchange.com/questions/51588/> [02/06/2022]

$$x_{PR} = c_r + \frac{b_{HT}}{2} \tan \Lambda_{TE_w} + \frac{D_{VTOL_{prop}}/2 - c_{prop}}{\cos \Lambda_{TE_w}} \quad (10.20)$$

The y positioning of the VTOL propellers was also determined. It has to be ensured that the VTOL propeller does not intersect with the propeller for the forward flight. Because of this, the y positing of the VTOL UAV is the radius of the forward propeller plus the radius of the VTOL propeller plus the propeller clearance. This is, however, the minimum y position the propellers can have. If the span of the horizontal tail is larger than this, then the y position of the VTOL propellers is half this span.

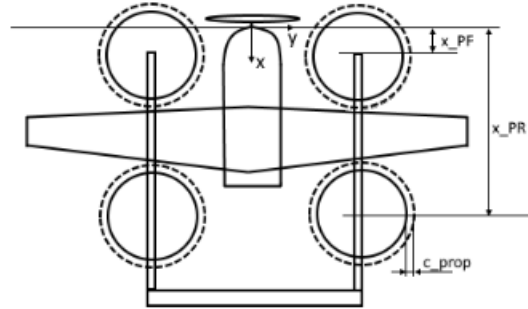


Figure 10.1: Top view of the UAV used for positioning of the VTOL propellers

## 10.4. Power & Energy

In order to size the hydrogen tank of the UAV, the total energy that the UAV needs during one flight must be known. With the values calculated in Section 10.1 and shown in Chapter 14, the energy per flight stage and thus the total energy needed for the mission is calculated. The results are shown in Chapter 14. The energy required during each flight stage has been calculated by multiplying the time the UAV is in that flight stage with the power required during that flight stage. A margin of power and energy has also been taken into account. This margin may be needed if the UAV needs to fly some extra kilometers unexpectedly. Since it is a margin, it was assumed that the UAV is already in the air when this margin may be needed. Thus only cruise and landing have been taken into account to calculate this margin for. The power required for this margin was taken to be the power required for cruise plus the power required for VTOL landing. The time is based on the time it takes to travel the maximum distance in a square to be monitored, which is its diagonal. In addition, some extra energy the UAV may need when it flies in, for example bad weather conditions or encounters high winds is five percent of the total energy required by the UAV. This was added to the total energy required as an extra margin.

### Hydrogen tank sizing

In this section, the hydrogen tank will be sized. The amount of hydrogen required can be calculated by means of the total power required. Equation 10.21 calculates this in terms of mass hydrogen required. The low heating value (LHV) of hydrogen, equal to 33.3 Wh/g, and  $\eta_{HFC}$ , the efficiency of the hydrogen fuel cell (HFC) is used for this calculation.

$$M_{Hydr} = \frac{E_{tot}}{LHV \eta_{HFC}} \quad (10.21)$$

The calculated mass is used for the sizing of the hydrogen tank. The size of the hydrogen tank was interpolated from the data of the Meyer HDRX-005 composite overwrapped pressure vessel<sup>2</sup>. Specifications of this hydrogen tank are specified in Table 10.2. The pressure of the UAV hydrogen tank was decided to be 300 bar, which is based on the Meyer data. Using this pressure, the mass of the hydrogen required could be determined from which the number of moles could also be determined. Subsequently, with the known cruise

<sup>2</sup>URL:<http://meyer.cd/copv/>[17/06/2022]

temperature, the volume required for the hydrogen was calculated using the ideal gas law Equation 10.22. With the calculated volume, the dimensions of the hydrogen tank have been calculated using interpolation of the Meyer hydrogen tank specifications.

$$PV = nRT \quad (10.22)$$

**Table 10.2:** Specifications of the Meyer hydrogen tank that is used to size the hydrogen tank of the UAV

Hydrogen tank	Capacity [L]	Working pressure [bar]	Nominal diameter [mm]	Nominal length [mm]	Weight [kg]	Material [-]
Meyer HDRX-005	0.5	300	80	190	0.42	Carbon

## Selected fuel cell

To provide the subsystems of the UAV with energy, a conversion from hydrogen to electricity must take place. A hydrogen fuel cell (HFC) is capable of doing so. The sizing of the HFC is contingent on the most power intensive stage of the mission. The maximum power condition occurs during vertical take-off, where the four VTOL motors operate at maximum rated power. Additionally, the payload must be supported at nominal power, as well as the avionics and communications. This value for power is used to select the fuel cell, with fuel cells rated for higher power tending to weigh substantially more. Hydrogen fuel cells typically provide both a maximum rated power, which represents the maximum power that can be sustained for long-term operations and a peak power. The peak power is typically several hundred of Watts higher than the continuous maximum rated power and can be sustained on the order of minutes without causing significant additional degradation to the HFC. Given the short duration of vertical take-off, the fuel cell peak power is used to select the fuel cell. A large range of lightweight fuel cells designed for aerial applications were found. The final fuel cell selected is presented in Section 14.1.

# Noise Considerations

This chapter will outline how the group has addressed the issue of noise production of the UAV. Firstly, a short introduction to the related theory will be given in Section 11.1, followed by an investigation into propeller noise in Section 11.2 and the effect of this noise on wildlife in Section 11.3. Lastly, the airframe noise will be addressed in Section 11.4.

## Noise, Sustainability Requirements

**SYS-SUSN-01** The system shall provide a noise reduction of 6dB compared to commercially available drones, measured at ground level (thus a noise output of 75dB).

## 11.1. Background Sound Theory

Sound is a longitudinal wave consisting of variations in pressure within a medium. This wave has an amplitude and a frequency, which both affect how different entities perceive the sound. For the purposes of this report, the unwanted sound produced by the UAV is the most important. To measure this, the Sound Pressure Level (SPL) is used. This compares the effective sound pressure to the reference effective pressure. Sometimes, the Overall Sound Pressure Level (OSPL or OASPL) will be used. This is obtained by integrating the SPL along with the hearing frequency range.

The UAV will be treated as a point source for sound, meaning the wavefronts are spheres. This is an acceptable assumption as the UAV is small relative to its environment. In addition, the worst scenario in terms of sound directionality will be taken in all situations. This means that despite the sound emission being non-uniform, the direction with the highest SPL will be taken as the SPL for all directions. As this section is intended to be a first estimation, the effect of wind will not be taken into account. Furthermore, given the scale of the surveillance area being relatively small per UAV, the shadow zone created by the variations in pressure with altitude has been treated as out of scope. Lastly, the periodic (tonal) sound is of the greatest interest to the project. Considering that the broadband noise will not be highly noteworthy, it will be neglected in the analysis.

## 11.2. Propeller Noise

The main source of noise from the UAV comes from the propellers. This is due to the high rotational speed of their blades and their size. This produces three types of noise: tonal noise, broadband noise, and narrow-band noise. Tonal noise is its periodic part, which is characterized by a pulse that is repeated in time. It occurs with a frequency of  $1/BN$ , known as the blade-passing frequency (BPF), where  $B$  is the number of blades of the propeller and  $N$  is the rotational speed in revolutions per second. Usually, these tones are not pure, meaning they are composed of several frequencies, or harmonics, which are integer multiples of the BPF.

Broadband noise is that which spreads over all frequencies and is random in nature. It is not very loud when put in comparison with tonal noise. Finally, narrow-band random noise is almost periodic; rather than being concentrated at specific frequencies, it is spread out around them. The main component of noise in propellers however is tonal noise [46]. Therefore, in this section, the tonal noise of propellers is analyzed.

First, with Equation 11.1, the OSPL produced by the propellers is calculated.

$$\text{OSPL}_{\max} = 83.4 + 15.3 \log_{10} P_{br} - 20 \log_{10} D + 38.5 M_t - 3(B - 2) + 10 \log_{10} N_p \quad (11.1)$$

In this equation,  $P_{br}$  is the engine power in kW,  $D$  is the diameter of the propeller in meters,  $M_t$  is the Mach

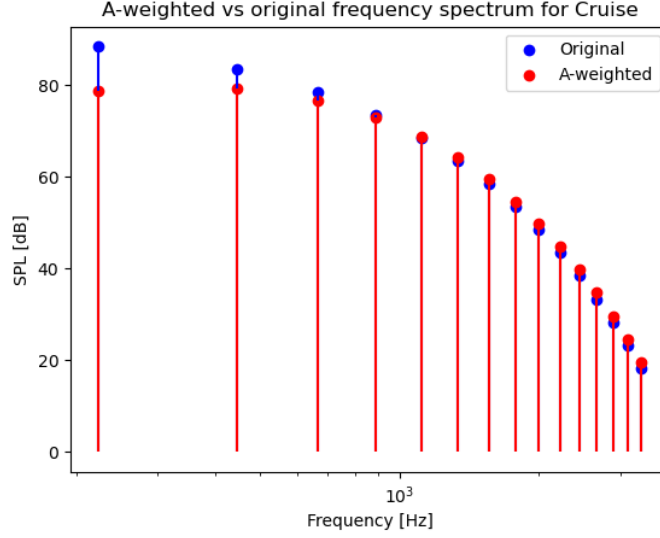


**Figure 11.1:** Sound pressure level [dB], as a function of the frequency for the propeller during cruise, measured at 1 meter of distance. The original SPL is shown in blue, and the A-weighted SPL is shown in red.

number at the tip of the blade, given by Equation 11.2,  $B$  is the number of blades per propeller and  $N_p$  the number of propellers.

$$M_t = \frac{\pi D n_p}{c \cdot 60} \quad (11.2)$$

with  $n_p$  the propeller rotational speed in RPM and  $c$  the speed of sound. To be able to extract useful information from this OSPL, it is transformed into the frequency domain. To do this, only the harmonics are looked at. It is known that there will be a higher peak in SPL at the BPF and the consecutive peaks, at integer multiples of the BPF, possessing a lower SPL. Therefore, to obtain the value of the higher peak, Equation 11.3 and Equation 11.4 are combined to form Equation 11.5. Equation 11.3 is the definition of OSPL [47].

$$\text{OSPL} = 10 \log_{10} \sum_{i=1}^n 10^{\text{SPL}(f_i)/10} \quad (11.3)$$

$N$  is taken as the number of harmonics we want to take into account. A value of 15 is considered since the consecutive harmonics have very low values for SPL. Most of the energy is accumulated at the first harmonic, for the following harmonics a decrease of 5 dB is observed per harmonic [48]. Therefore, the SPL of each of the harmonics can be expressed as:

$$\text{SPL}_i = \text{SPL}_1 - 5 \cdot (i - 1) \quad (11.4)$$

Where  $i$  represents the number of harmonics and  $\text{SPL}_{1st}$  is the SPL of the first harmonic. Therefore, making use of Equation 11.1, Equation 11.3 and Equation 11.4 the sound pressure level for the first harmonic can be obtained.

$$\text{SPL}_1 = \text{OSPL}_{\max} - 10 \log_{10} \left( \sum_{i=1}^n 10^{5(i-1)/10} \right) \quad (11.5)$$

In Figure 11.1, the values for the SPL at different frequencies can be observed for the propeller used during cruise. The blue dots are the original values, and the red dots are those obtained by A-weighting the SPL. This is done to express the relative SPL as perceived by the human ear. There is a limited amount of information regarding how noise affects animals, other than some standalone articles which look into some specific animals' hearing capabilities. For example, elephants can hear very low frequencies [49], but it is not known how certain frequencies affect them. Therefore, it was decided to assume that the same data that is used to assess the disturbance of humans applies to that of animals. There are also other weighting

methods available, like B- or C-weighting, which are more suitable for the hearing range of animals. However, A-weighting was chosen because more data was available to help decide whether the drone would disturb or not. Weighting consists of adding a factor that decreases or increases the SPL, depending on the frequency<sup>1</sup>. It is decreased for those frequencies that affect fewer humans and the other way around. This factor is calculated using Equation 11.6, and is added to the SPL from Equation 11.4 to obtain the red dots on Figure 11.1.

$$\Delta L_A = -145.528 + 98.262 \log_{10} f - 19.509 (\log_{10} f)^2 + 0.975 (\log_{10} f)^3 \quad (11.6)$$

Furthermore, other factors decrease the noise the propellers produce; here, two will be discussed, the distance to the observer and the atmospheric absorption. First, the distance to the observer leads to the addition of the factor calculated using Equation 11.7 [46]. With this, the SPL has decreased by 6 dB each time the distance to the observer is doubled.

$$\Delta L_r = -20 \log_{10} (r) \quad (11.7)$$

where  $r$  is the distance. Second, the atmospheric absorption is dependant on the frequency mainly, but also on temperature, pressure and relative humidity. It attenuates more at higher frequencies than it does at lower frequencies. The effect of this absorption leads to the addition of another factor, calculated with Equation 11.8 [50].

$$\Delta L_\alpha = -\alpha \cdot r (r) \quad (11.8)$$

where  $r$  is the distance in km and alpha is calculated in Equation 11.9 in dB/km.

$$\alpha = f^2 \left[ \left( \frac{1.84 \times 10^{-11}}{\left(\frac{T_0}{T}\right)^{\frac{1}{2}} \frac{p_s}{p_0}} \right) + \left(\frac{T_0}{T}\right)^{2.5} \left( \frac{0.10680 e^{-3352/T} f_{r,N}}{f^2 + f_{r,N}^2} + \frac{0.01278 e^{-2239.1/T} f_{r,O}}{f^2 + f_{r,O}^2} \right) \right] \quad (11.9)$$

where  $f$  is the frequency,  $T_0$  is the reference temperature of 20 °C in kelvin,  $T$  the atmospheric temperature,  $p_s$  is the local atmospheric pressure in kPa,  $p_{s0}$  is the reference pressure of 1 atm in kPa and  $f_{r,N}$  and  $f_{r,O}$  are relaxation frequencies, which have to do with the vibration of nitrogen and oxygen molecules. They are given by Equation 11.10 and Equation 11.11.

$$f_{r,N} = \frac{p_s}{p_{s0}} \left(\frac{T_0}{T}\right)^{\frac{1}{2}} \times \left(9 + 280 H e^{-4.17[(T_0/T)^{1/3} - 1]}\right) \quad (11.10)$$

$$f_{r,O} = \frac{p_s}{p_{s0}} \left(24.0 + 4.04 \times 10^4 H \frac{0.02 + H}{0.391 + H}\right) \quad (11.11)$$

where  $H$  is the percentage of molar concentration of water vapor in the atmosphere, equal to  $\rho_{sat} r_h p_0 / p_s$ . Here,  $\rho_{sat} = 10^{C_{sat}}$ , with  $C_{sat} = -6.8346(T_0/T)^{1.261} + 4.6151$  and  $r_h$  is the relative humidity in percentage.

Therefore, taking into account all of the factors mentioned above, the OSPL can be calculated for the different times in flight using Equation 11.12. During cruise flight, a value of less than 35 dB, measured from the ground, is desired. This is because the ambient background noise there is at night-time in the rural is on average 35 dB, and therefore, sound pressure levels below that are not heard<sup>2</sup>. Figure 11.2 shows the values at each of the moments of a typical flight. Here, the blue line indicates the OSPL measured from an observer at the ground, and the black line (horizontal line at 80dB OSPL) represents the minimum value for OSPL that is considered when calculating the SEL. The indent in the OSPL at half of the flight time is due to the change from VTOL to cruise propellers. Therefore, this graph only analyses the take-off and landing phases, and the dip in the middle represents the entire cruise phase of the flight.

$$L_A = 10 \log_{10} \sum_{i=1}^N 10^{\frac{\text{SPL}(i) + \Delta L_A(i) + \Delta L_r + \Delta L_\alpha(i)}{10}} \quad (11.12)$$

<sup>1</sup>URL: <https://www.sciencedirect.com/topics/engineering/a-weighting> [14/06/2022]

<sup>2</sup>URL: <https://www.airboredrones.co/drone-noise-levels/> [15/06/2022]

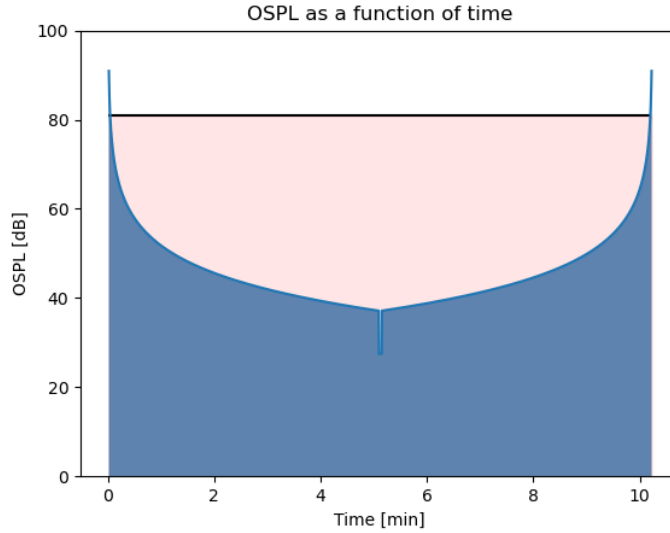


**Figure 11.2:** OSPL as a function of time, for the UAV take off and landing phases

Here, it is not taken into account that the transition to forward flight occurs at 50 meters. However, this would not affect the calculations since, at this height, the OSPL does not sum towards the SEL. This is because, at 50 meters, the value of the OSPL is lower than the 10 dB less than the maximum threshold for measuring the sound disturbance.

### 11.3. Consequences of Noise Pollution on Wildlife

As stated before, it is difficult to estimate when or if the wildlife will be affected by the drone. Therefore, the same data that is used to measure the annoyance of human beings because of noise is used. The sound exposure level (SEL) indicates the impact the drone has. It takes into account both the SPL and the duration of the exposure. It is calculated using Equation 11.13.

$$SEL = 10 \log_{10} \left[ \frac{1}{T_1} \int_0^T 10^{\frac{L_A(t)}{10}} dt \right] \quad (11.13)$$

where  $T_1$  is equal to 1,  $T$  is the integration time in seconds, in this case, the whole duration of the flight, and  $L_A(t)$  is calculated using Equation 11.12. Furthermore,  $L_A(t)$  is only accounted for values that are higher than 10 % lower than the maximum  $L_A(t)$ , since these have the most impact on the SEL. Therefore, only a few seconds after take-off and before landing are relevant for the calculation of SEL.

Following, the day-night average is calculated. This is the most frequently used metric to represent the noise exposure level; it provides a way to describe the noise exposure over a period of 24 hours, introducing weights to account for the moment of the day it occurred on. For noise that occurs during the night (22:00-7:00), a weight of 10 dB is added. For non-stationary noise events, like in this case, where the UAV only produces significant levels of noise at take-off and landing, it is very convenient to use the SEL to calculate it. The day-night average level can therefore be calculated using Equation 11.14.

$$L_{DN} = 10 \log_{10} \left[ \frac{1}{86400} \sum_{i=1}^N 10^{(SEL_i + W_i)/10} \right] = -49.4 + 10 \log_{10} \left[ \sum_{i=1}^N 10^{(SEL_i + W_i)/10} \right] \quad (11.14)$$

where  $SEL_i$  is the value for each of the events, and  $W_i$  is its corresponding penalty in dB [47]. In this case, where the UAV surveils 4 squares of 5 km<sup>2</sup>, 8 flights are performed per UAV per day. Since each flight would take a maximum of 2 hours, in the night period, only 4 flights could take place. The  $L_{DN}$  is then calculated taking a weight of 10 dB for 4 flights and 0 dB for the other 4 flights.

Once this is calculated, an estimation of the disturbance of wildlife can be made. For this, Figure 11.3 is used. Here, it can be seen how up until 40 dB of noise very few people are highly annoyed by the noise

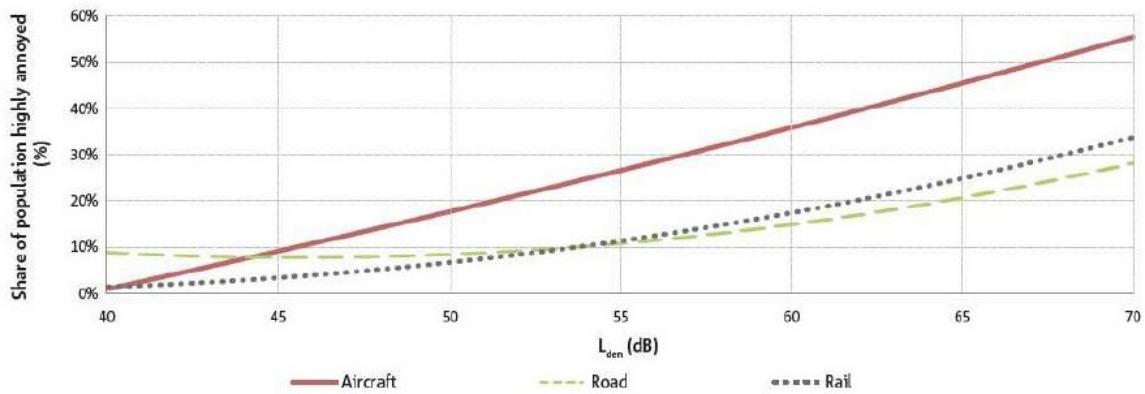


**Figure 11.3:** Percentage of highly annoyed people by different noise sources as a function of the day-night average level [47].

produced by an aircraft. Namely close to 1 %. Moreover, for 45 dB of noise, this is 10 %. This means it is desired that the day-night average level stays as low as possible, preferably below 45 dB.

### 11.4. Airframe Noise

In general, with propeller aircraft, the airframe noise is negligible. This will also be assumed for this project. However, some explanation as to why this is acceptable will be given. Firstly, airframe noise is mostly made up of broadband noise, and is created as a result of turbulence of the flow around the surfaces of the aircraft [47]. When control surfaces, high lift devices, or the landing gear are deployed, this noise can become influential. The airframe noise is proportional with either  $V^5$  for non-compact noise sources or  $V^6$  for compact sources [47]. The size and velocity of jet airliners, where this noise source can become significant, are larger than that of the UAV. Considering that the group is ignoring broadband noise for the propellers and that the velocity of the UAV is very low compared to a traditional aircraft, the airframe noise can be completely neglected.

# Structural Design

This chapter focuses on the design of the main structures of the UAV. Section 12.1 presents an analysis of the candidate materials ending with the selection of one material, Section 12.2 performs a sizing of the wing box and tail. The design of the fuselage, booms and landing gear is provided in Section 12.3.

## 12.1. Material Selection process

In accordance with selection methods from literature [51, 52], the material selection starts with the identification of a material index. After comparing the material indices of different material families, the best materials are identified. Then a literature study on the recyclability of the best candidates is carried out to make sure the requirement on sustainability is met. Lastly the exact material with specific material properties is chosen.

### Material Families Considerations

The material selection process begins with a comparison of the material properties according to a selected material index. A material index is needed when a single material property is not, in itself, representative of the loading scenario. In order to formulate a material index, the function of the structural member that is being designed needs to be established. Subsequently, the performance objectives, for example minimum weight and maximum stiffness, is established together with design constraints, for example minimum stiffness required. From these two, the material index is formulated using theoretical structural analysis equations. To simplify the designing process, manufacturing costs and ease of recyclability one single material will be chosen for the entire airframe. This material is chosen based on the critical load cases that the wing is subjected to. For a subsonic aircraft with VTOL capabilities and an unpressurized fuselage, the wing loads are considered the critical ones. All the materials selected to be compared are feasible materials for the design of all the main airframe components.

The function of the designed structural member is therefore to be an appropriate aircraft wing with the performance objective of resisting high bending loads, experiencing the smallest strain possible for the least weight possible. Constraints are varied but affect the selection in a less direct manner. Relevant aspects to be considered are recyclability, ease of design, manufacturing and maintenance costs. From the performance objectives, two material indexes can be formulated. Equation 12.1 shows the material index for a light and stiff beam, where  $E$  is the Young's modulus of the material,  $\rho$  the density and  $\phi^e$  is the shape factor for elastic bending. Mean while, Equation 12.2 shows the material index for a light and strong beam, where  $\sigma$  is the failure strength considered [51].

$$M_{beam(light,stiff)} = \frac{(\phi^e E)^{\frac{1}{2}}}{\rho} \quad (12.1)$$

$$M_{beam(light,strong)} = \frac{\sigma^{\frac{2}{3}}}{\rho} \quad (12.2)$$

These material indexes can be directly computed for each material family or used together with material property charts to isolate search areas for the material families. The graphical method was preferred to the analytical one. Figure 12.1 and Figure 12.2 are material charts relating respectively E-modulus to the density and strength to the density. According to the method, the best performing materials according to both material indexes are selected to be later compared. The charts show a straight continuous red line for the desired material index. Within the highest performing materials found around these lines, only some are considered in the selection. The reason is because some materials are either unfeasible for aerospace structural design, for example foams and ceramics, or not used for UAV applications for reasons unrelated to structural design like titanium due to production costs. The circles on the charts show the material families that promise a good performance as well as seeming feasible. These material families are: steel alloys, aluminium alloys, carbon fiber reinforced polymers (CFRPs), glass fiber reinforced polymers (GFRPs) and

wood. However the latter only shows sufficient performance when load is applied along the grain direction. With the exception of steel, which is already under-performing compared to other materials, all of these materials are used in aeronautical design.

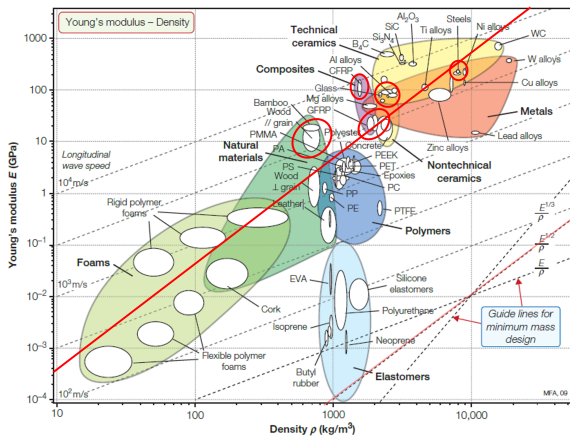


**Figure 12.1:** Material chart relating Young's modulus to density [51]. The line chosen to isolate the best performing material related to the material index  $E^{1/2}/\rho$  is highlighted with a continuous red line. The materials taken into consideration are circled in red.

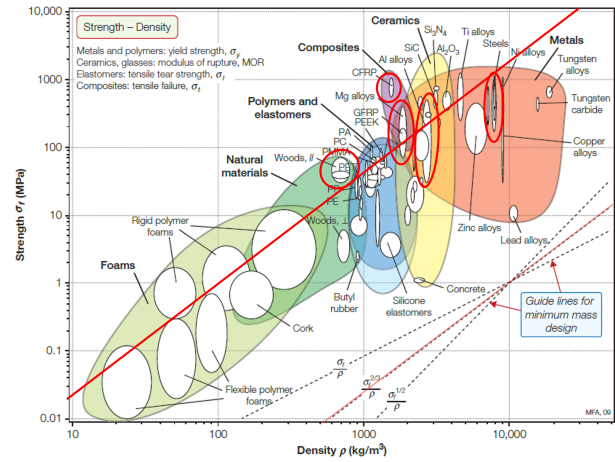


**Figure 12.2:** Material chart relating strength ("yield strength for metals and polymers, compressive strength for ceramics, tear strength for elastomers, and tensile strength for composites") to density [51]. The line chosen to isolate the best performing material related to the material index  $\sigma^{2/3}/\rho$  is highlighted with a continuous red line. The materials taken into consideration are circled in red.

Once the material families are chosen, the relevant material properties are collected, in Table 12.1, to calculate the material index ranges corresponding to the different families. Properties in material families can span relatively high ranges, for example different aluminum alloys can have differences in strength of more than one order of magnitude.

**Table 12.1:** Comparison of material properties of five aerospace material families. Wood data is provided for loading both longitudinally and perpendicularly to the grain direction. The properties of the composites are average values for quasi-isotropic plies. The minimum values do not include any shape factor while the maximum values are multiplied by the maximum shape factor. No shape factor are considered for strength [51].

	$\rho$ [Mg/m <sup>3</sup> ]		E [GPa]		$\sigma$ [MPa] <sup>1</sup>		$(\phi^e)$
	min	max	min	max	min	max	max <sup>2</sup>
Steel(s)	7.6	8.1	189	217	170	1150	65
Al alloys	2.5	2.9	68	82	30	500	44
CFRP	1.5	1.6	69	150	550	1050	39
GFRP	1.75	1.97	15	28	110	192	39
wood (long)	0.6	0.8	6	20	30	70	5
wood (trans)	0.6	0.8	0.5	3	2	6	5

<sup>1</sup> Yield strength for metals, tensile strength for composites and wood;

<sup>2</sup> Upper limits of achievable empirical shape factors.

The comparison between the different families is carried out by plotting the performance ranges as shown in Figure 12.3, Figure 12.4 and Figure 12.5 based on the data from Table 12.1. Figure 12.3 shows the performance according to  $M_{beam(light,stiff)}$  with a shape factor of 1. CFRPs, wood and Al alloys are the clear three best performing materials, in this order. Figure 12.4 shows the same three best performing materials, for the  $M_{beam(light,strong)}$  index, however, aluminium performs better than wood. Figure 12.3 was obtained multiplying the maximum value of the range of each material family with the maximum empirical shape factor, in Table 12.1, to have a better depiction of  $M_{beam(light,stiff)}$  with varying shape factors. This plot is a more appropriate means of comparison since these materials are hardly ever unshaped in their application. However, it is relevant to notice that the procedure followed serves as a general indication since inside

material families, not all the members can achieve the same shape factors. It is also important to remember that the highest shape factors are less common due to their niche applications and higher manufacturing costs. The introduction of the shape factor makes wood the worst choice while aluminium becomes the second best option. The overall outcome of the analysis is that the material families offering the best properties are CFRPs, aluminium alloys and wood. These are also some of the most common aircraft structural components materials, confirming the validity of the selection process.

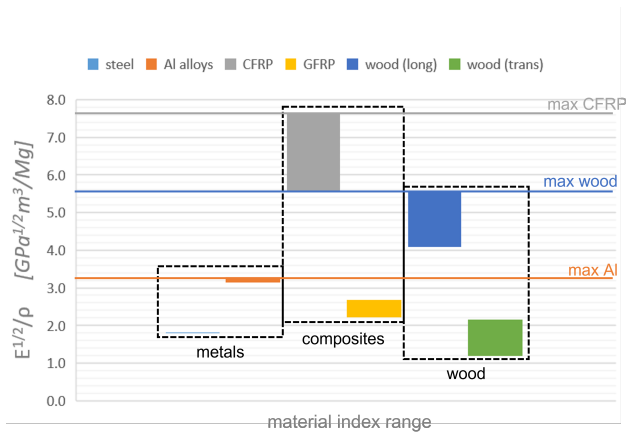


**Figure 12.3:** Comparison of material index  $E^{1/2}/\rho$  ranges between material families. The maximum performance of the best three materials (CFRP, wood and Al alloys) is highlighted with an horizontal line.

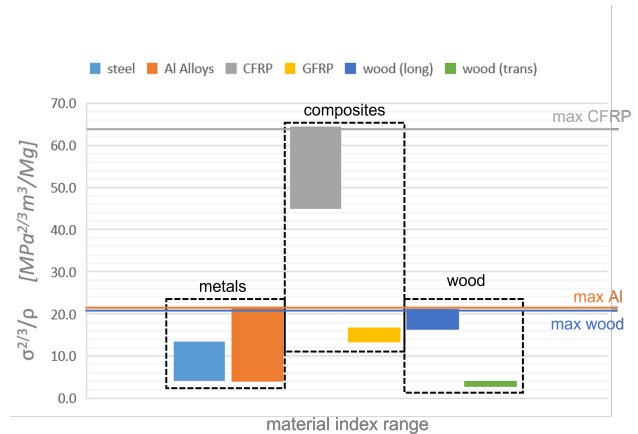


**Figure 12.4:** Comparison of material index  $\sigma^{2/3}/\rho$  ranges between material families. The maximum performance of the best three materials (CFRP, wood and Al alloys) is highlighted with an horizontal line.

Literature indicates that due to the anisotropic nature of composites, "direct comparison of material properties between aluminum alloys and composites is not possible" and it should be made case by case for specific structural applications [53]. For this reason, the choice will be made based on other considerations that are not directly related to the mechanical properties.

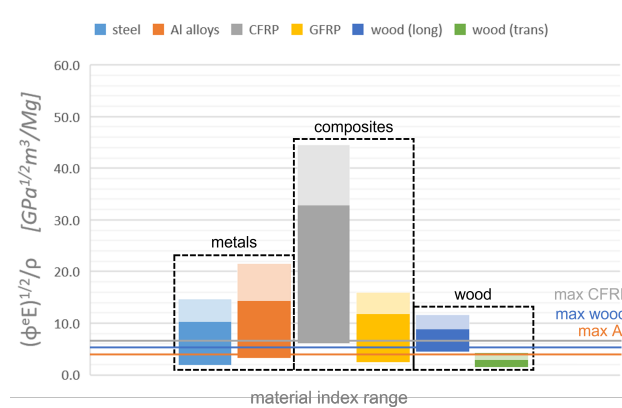


**Figure 12.5:** Comparison of material index  $\phi^e E^{1/2}/\rho$  ranges between material families. The maximum performance of the best three materials (CFRP, wood and Al alloys) without taking into account the shape factor (same number as Figure 12.3) is highlighted with an horizontal line. The largest 0.25% of each range is shaded to highlight the fact that those values are achieved at high, less common, shape factors.

## Material Recyclability Considerations

One of the requirements having direct impact on the structural design of the UAV is SYS-SUSM-01. Since the first two candidates of the previous analysis are a family of composites (CFRPs) and one of metals (aluminium alloys), the recyclability considerations are naturally gravitating around the differences between these two material families to identify the best one regarding this aspect.

## **Material, Sustainability Requirements**

**SYS-SUSM-01** At least 75% of the aircraft parts should be recyclable/reprocessable.

Composite materials are by definition composed of more than one material. This heterogeneous nature is at the base of the difficulty in their recycling process. Fiber reinforced composites used in the aerospace sector are especially problematic to recycle due to thermoset nature of the matrices. This is due to the high level of cross-linking, that is itself at the base of the desired properties of high thermal stability and chemical resistance. Currently, the reprocessing methods employed industrially imply either down recycling or loss of the matrix to recover the reinforcing fibers. In the first case the product is ground into pieces resulting in loss of continuity of the fibers and loss of directionality. Therefore, the product obtained after the process has material properties considerably lower than the initial. In the second case, methods like pyrolysis or solvolysis allow to dispose the matrix and recover the fibers. However, the process is energy intensive and the fibers recovered, when used again in a compound, "exhibited a marked decrease in nearly all properties except modulus". A solution to the problems of recyclability of the matrices could be offered by matrices with (thermally or chemically) reversible bonds, yet this concept has not gone any further than the academic environment. Due to the "inability of the industry to utilise the individual components that make up the composite materials", most of CF reinforced composites end up in landfill at end-of-life [54, 55, 56].

Metals recycling is more established in the industry and stretches far beyond the aerospace sector. Yet, recycling of aluminium alloys within the aerospace industry comes with its challenges. The first challenge is related to the availability of aluminium alloys coming from retired aircraft, undesired for newly built airframe due to the existence of better performing alloys. An other problem is related to the sorting of the alloys before scrapping and melting of the parts to be recycled. The properties of the alloys are given by precise percentages of specific metals dispersed in the aluminium lattice. The combination of unknown quantities of different alloys together with small uncontrolled quantities of other metals would result in a product with unpredictable properties (in between those of the initial alloys), undesirable and inconsistent on a large scale. Automatic sorting is already industrially employed but presorting would reduce the small amounts of undesirable alloying elements that get mixed in a batch. With the necessary alloy contamination precautions, the aluminium alloy can be re-used. Recycled aluminium containing mixtures of different alloys can be employed in non-critical aircraft components as long as the properties are known. The recycling process does not result in the 100% of the input material becoming viable for new applications since 10 to 35% of the material is inevitably lost due to the nature of the melting process [57, 55, 56].

Conclusions can be drawn regarding the better material choice based on recyclability considerations. Building with CFRPs especially designed for recycling would be possible yet this is an option that relies on a technology that has not reached industrial manufacturing. Considering methods implying the discarding of the matrix is also not an option since the matrix would be disposed, not reprocessed. Thermoplastic based CFRPs have not been investigated as they are not common in aeronautical structural applications. However, the main factor discouraging the use of CFRPs is that even if in principle fibers could be recovered, it seems like there is not demand for recycled fibers and the material would be disposed regardless. For this reasons, aluminium alloys are chosen over CFRPs for their recyclability. In the case of aluminium, recycling is established and the process requires only 5% of the energy required to produce virgin aluminium and results in 4% of the emissions.

## **Final Material Selection**

Due to the previous investigation of recyclability in Figure 12.1, aluminium alloys have been chosen over CFRPs. Different aluminium alloys have specific mechanical and manufacturing properties that are optimised to fit specific functions. As already anticipated in Section 12.1, the one material chosen will be used for the design of the entire airframe. For this reasons, considerations regarding production and material properties other than strength and modulus are taken in consideration. Table 12.2 shows three alloys that have sufficient strength, are obtained by means of wrought manufacturing and can be heat treated, together

with their respective properties and usual applications.

**Table 12.2:** Compositions, mechanical properties and typical applications of common aluminium alloys (adapted from [52]).

Al Alloy	Composition (wt%) <sup>1</sup>	$\sigma_{failure}$ [MPa]	$\sigma_y$ [MPa]	Typical Applications
2024	0.12 Cu, 1.5 Mg, 0.6 Mn	470	325	Aircraft structure, truck wheels, rivets, screw machine products
6061	1.0 Mg, 0.6 Si, 0.30 Cu, 0.20 Cr	240	145	Trucks, canoes, railroad cars, furniture, pipelines
7075	5.6 Zn, 1.0 Mg, 0.30 Cu, 0.20 Cr	570	505	Aircraft structural part and other

<sup>1</sup> The balance of the composition is aluminium

The 2xxx series is characterised by good machinability, relatively high strength and fatigue strength, corrosion resistance with cladding. The 6xxx series is characterised by "good formability and weldability and corrosion resistance". The 7xxx series is characterised by relatively high strength, high toughness and good machinability. [58] Although Al7075 has a higher yield strength, which produces a lighter design, the performance of Al2024 in strength is deemed sufficiently high with the additional advantage of corrosion and fatigue resistance. Al6061 is therefore chosen as the material used for the airframe.

**Table 12.3:** Material properties of Al6061.

Al Alloy	$\rho$ [kg/m <sup>3</sup> ]	$\sigma_y$ [MPa]	E [GPa]
2024	2710	325	70

## 12.2. Wing and Tail Structural Design

An overview of the structural components of the wing is presented below. The loads on the wing are analyzed for cruise and VTOL operation, and the maximum stresses and primary failure modes are used to size the wingbox structure. The assumptions taken for the subsequent design of the wing structure are outlined in Section 12.2. The operation of the wing in the context of the UAV mission, and the resulting loading diagrams are given in Section 12.2. Finally, the sizing of the wingbox is presented in Figure 12.2.

### Assumptions and Requirements

#### Wing, Structural Requirements

- SYS-STRUCT-01** The wing shall withstand a positive maximum load factor of 2.5 without failure.
- SYS-STRUCT-02** The wing shall withstand a positive ultimate limit load factor,  $n_{ult}^+$  of 3.75 without failure.
- SYS-STRUCT-03** The wing shall withstand a negative ultimate limit load factor,  $n_{ult}^-$  of 1.5 without failure.
- SYS-STRUCT-04** The wing structure shall have a minimum design safety factor  $K_{safety}$  of 1.5.
- SYS-STRUCT-05** The wing structure shall not yield or buckle under maximum design loads.

The assumptions required to model the loading of the wing and size the structure are given below:

- The wing behaves in bending as an ideal cantilevered beam. This is valid because the wing is clamped at the fuselage attachment, limiting deflection and twist.
- Any local failure is treated as global failure of the wingbox.
- The wingbox is assumed to be symmetric, and therefore the product second moment of area  $I_{xy}$  is zero. This assumption neglects the variation in moment of inertia resulting from the airfoil contour, which is valid as the contribution of the wingbox to moment of inertia is substantially larger.
- The deformation of the wing is continuous. This is valid while no failure occurs.

- Ideal fastening is assumed. The design of fasteners is beyond the scope of this design, but would be sized at further stage of the design. The assumption of ideal fasteners implies transfer of loads creates no variation in stresses, which is valid because proper production lead to minimal increases in peak stresses, which are compensated for with the design safety factor .
- The wingbox is modeled as a thin walled structure for shear calculations. This is valid because the skin thickness is substantially smaller than the wingbox geometry.
- The wingbox is modelled as rectangular. This is valid, because the placement of the spars within the airfoil leads to a minimal angle between the front and rear spar. Moreover, calculations for moment of inertia assume the average spar height, making the impact of this assumption minimal.
- It is assumed that shear loads are carried only by the spars. This assumption is conservative, and leads to slightly over-designed spars as the shear contribution of the skin and stringers are neglected. This is reasonable, because the contribution of skin to the moment of inertia  $I_{xx}$  is extremely small due to the low thickness.
- The skin panels are assumed to be rectangular to allow for the use of sheet buckling formulas. This is valid, as the taper ratio is relatively low, and the plates are segmented by ribs.
- The skin of the wing is assumed to be clamped at the spars and spar caps, and hinged where a stringer is attached, and at the ribs.
- The wingbox, formed by the skin and spars, is assumed to carry the torsional loads, and act as a closed section.
- Bending loads are considered to be carried by the spars and skin.
- The maximum VTOL loads and forward flight loads are considered separately, and not superimposed. This is valid, because transition occurs at low velocities, while maximum loading conditions for both VTOL and forward flight occur at high maneuvering speeds.
- VTOL climb is assumed to be symmetric and purely vertical translation.

## Operation and Loads

The operation of the UAV is divided into two disparate flight modes: VTOL flight, where all lift is propulsively generated, and forward flight, where aerodynamic lift is employed.

The internal loads are plotted spanwise for a half-wing. The force diagram for vertical forces shown in Figure 12.6 indicates the loads acting on the wing. These include the downwards-acting weight of the wing, which is subtracted from the upwards-acting distributed load from the lift, shown in orange for clarity. Two point loads are also illustrated, one at the base representing the half-weight of the UAV, and mass of the boom carrying the VTOL motors. The resulting shear and moment diagrams are also plotted. The peak values for shear force and moment are later used in Figure 12.2 to size the wingbox structure, in combination with the ultimate limit load factors  $n_{ult}$ . Similarly, Figure 12.7 shows the spanwise variation in longitudinal forces. As the propellers for forward flight are attached to the fuselage, the only longitudinal force results from aerodynamic drag, which is calculated from the wing analysis performed in Section 8.1. Finally, the torsion is plotted spanwise in Figure 12.8, resulting from the aerodynamic moment about the airfoil.

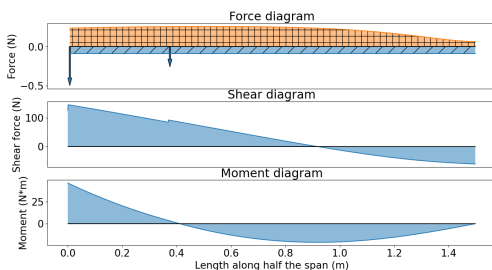


**Figure 12.6:** Vertical forces applied, and shear and moment load diagrams for cruise flight, where  $L/W = 1$ .

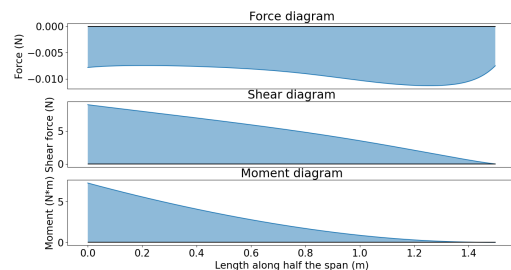


**Figure 12.7:** Horizontal forces applied, and shear and moment load diagrams for cruise flight, where  $L/W = 1$ .

The vertical loads during VTOL operation at wide-open throttle (WOT) are given below in Figure 12.9. Note that other loads are not shown, as VTOL climb was assumed to be only vertical, meaning no significant horizontal forces are considered.

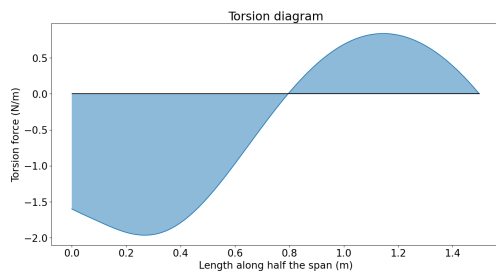


Figure 12.8: Torsion load diagram

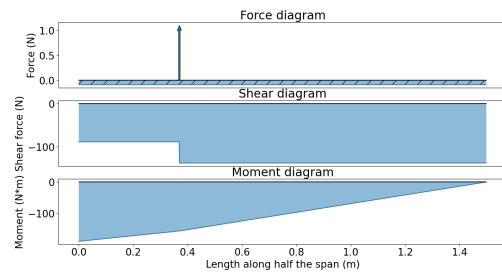


Figure 12.9: Force, shear and moment load diagrams for operation at WOT, with thrust over weight equal to 2.

The magnitude of loads resulting from VTOL at a T/W equal to 2 exceeds cruise loads, but each of the cruise loads are larger when the ultimate load factor  $n_{ult}^+ = 4.75$  is applied. Therefore, the loading resulting from the ultimate positive and negative load factors will be used for the design of the wing.

## Stress Analysis and Wing Structural Design

The wing structure is designed according to the maximum loads identified in Section 12.2. An overview of the approach taken in the design is provided below, before the structural sizing is further described.

A simple rectangular wingbox was designed. Initially, only a skin was sized, with a constant thickness, and a taper ratio matching the wing. The predominant loads acting on the wing are bending and shear about the vertical axis, as a consequence of the lift, which greatly exceed the bending and shear about the horizontal axis, as shown in Section 12.2. This led to the development of thicker rectangular spars to carry bending loads. Moreover, the thickness of the skin required to prevent buckling was prohibitive, and therefore ribs were added, as well as a single stringer on the upper skin and spar caps at the wingtips to reduce torsional deformation. A minimum gauge of 0.2 mm was used according to manufacturing specifications for the aluminium alloy employed for the wing structure<sup>1</sup>. As a result, the outboard section of the final wingbox design has a margin of safety (MOS), defined as the ratio of ultimate load and limit design load, which far exceeds the design requirements.

First, a single rib was placed on each wing-half, and is placed at the location of the existing hardpoint for the boom carrying the VTOL propellers, to facilitate the efficient transfer of loads to the wing box structure during take-off and landing. However, as it became clear that buckling was the dominant failure mode, an additional 5 ribs were added along each wing-half. The placement of these ribs significantly decreases the effective sheet length of the wing skin, increasing the magnitude of the critical buckling stress. The design for each structural component, consisting of the sizing for corresponding failure modes is given below. The relations used for consider bending failure, shear failure, bending failure, torsional failure, buckling failure, and combined failure [59, 60, 61]. A render of the wingbox is shown in Figure 12.10. Note that the structural calculations assume a rectangular wingbox as explained in Section 12.2, while the render shows a slightly trapezoidal wingbox.

<sup>1</sup>URL: <https://www.alumeco.com/knowledge-technique/tolerances/plates-and-sheets-cold-rolled> [15/6/2022]

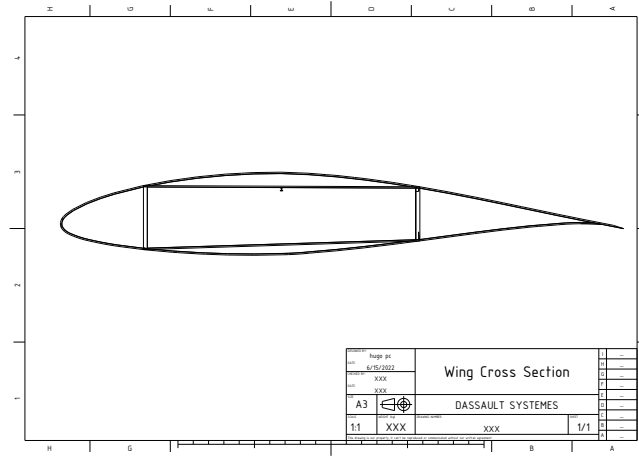


Figure 12.10: Wingbox cross-section.

The bending stress due to pure bending due to lift about the x-axis is given by Equation 12.3. This equation was used to size the spars according to bending loads during initial iterations. The stress resulting from combined bending due to moments from lift about the x-axis and drag about the y-axis is given by Equation 12.4. This was used to verify the performance of the wingbox, but the contribution from bending about the y-axis is nearly negligible. This is because the magnitude of drag is significantly smaller than that of lift, and the wingbox moment of inertia  $I_{yy}$  is larger than  $I_{xx}$  due to the larger dimension of the chord compared to the airfoil thickness.

$$\sigma_z = -\frac{M_x y}{I_{xx}} \quad (12.3)$$

$$\sigma_z = -\frac{M_x y}{I_{xx}} + \frac{M_y x}{I_{yy}} \quad (12.4)$$

The maximum positive and negative moments identified in Section 12.2 occur at the wing root. Therefore, the initial wingbox sizing will be performed for the root. The cross section of the wingbox varies along the span to fit the airfoil dimensions, but the skin thickness remains constant, to increase the manufacturability of the wing. It was subsequently verified that the margin of safety (MOS), defined as the ratio between design limit load, considering safety factor  $K_{\text{safety}}$ , and actual load, is greater than one for the entire length of the wing. The MOS is one at the root where the wingbox is sized and grows quadratically along the span.

The shear stress due to torsion in a closed section is given by Equation 12.5, where  $t$  is the minimum thickness of the section, and  $A_{\text{bound}}$  is the area enclosed by the section. The shear stress due to pure shear is given by Equation 12.6. Shear stress is maximum at the furthest distance from the neutral axis, where  $Q$ , the first moment of area, is maximum.

$$\tau = \frac{T}{2tA_{\text{bound}}} \quad (12.5)$$

$$\tau = -\frac{V_y Q}{I_{xx} t} \quad (12.6)$$

## Spars

The spars are assumed to carry the entire shear load, due to the minimal contribution of the upper and lower skin the wingbox moment of inertia  $I_{xx}$ , due to their low thickness. First the required spar thickness is calculated using Equation 12.3 and Equation 12.7. This is done by calculating the required moment of inertia  $I_{xx}$  to achieve a maximum axial stress  $\sigma_z$  proportional to  $1 / K_{\text{safety}}$  times the yield strength of the aluminium alloy used in both the upper and lower skins using Equation 12.3. Then, thickness is calculated from Equation 12.7 given the required moment of inertia, according to the height of the spars in the wingbox.

$$I_{xx\text{spar}} = \frac{1}{12} t_{\text{spar}} h_{\text{spar}}^3 \quad (12.7)$$

Additionally, the required spar thickness according to the critical shear stress for buckling in spars is checked using Equation 12.8. The value for the shear buckling coefficient,  $k_s$  is given by Figure 12.11, with hinged edges assumed for the spars. This is because the edges are free to rotate if the wingbox is subject to asymmetric loading. The critical value for shear buckling is compared to the actual shear, adjusted for the safety factor  $K_{\text{safety}}$ . If the value  $\tau_{cr}$  is too low, and shear buckling is found to occur, the spar thickness is increased. Therefore, the spar thickness is determined by whichever the maximum required thickness resulting from Equation 12.7 and Equation 12.8. This was typically the thickness required for bending, as the critical stress for shear buckling was very large compared to the slender profile of the airfoil.

$$\tau_{cr} = \frac{\pi^2 k_s E}{12(1-\nu^2)} \left( \frac{t}{h_{\text{spar}}} \right)^2 \quad (12.8)$$

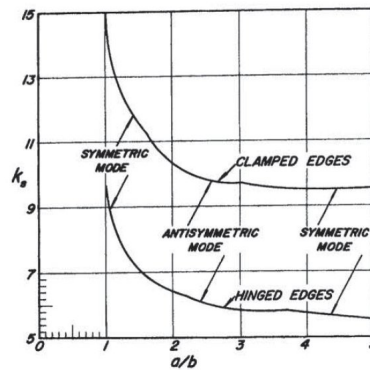


Figure 12.11: Shear buckling coefficient  $k_s$  in thin sheet [62].

### Upper and Lower Skin

The critical buckling stress for a thin panel is given by Equation 12.9. Sheet buckling is an unstable mode of failure, and therefore is not driven by material strength, but rather stiffness. The Young's modulus  $E$  describes the effect of the material stiffness. The critical buckling stress is highly dependent on the clamping of the sheet, as well as aspect ratio, which is described by the buckling coefficient  $K_c$ , with values shown in Figure 12.12 [63]. Finally, the ratio of sheet thickness  $t$  to the effective sheet width  $2w_s$  drives the buckling failure stress. The effective sheet width is defined by the distance between stringers minus  $w_e$ , which describes the effective stiffened sheet panel area by the stringer. However, only a single stringer was used in the upper sheet for the final wingbox design, and its small size limited the effect of the sheet stiffened by the stringer. Therefore the stiffening contribution of the stringer was neglected, and  $2w_s$  was taken to be the distance from the spar to the stringer for the upper skin. For the lower skin,  $2w_s$  was the entire skin width between the spars. This is because no stiffener was required for the lower skin due to the decreased magnitude of the negative ultimate load factor  $n_{\text{ult}}^-$ .

$$\sigma_{cr} = K_c \frac{\pi^2 E}{12(1-\nu^2)} \left( \frac{t}{2w_s} \right)^2 \quad (12.9)$$

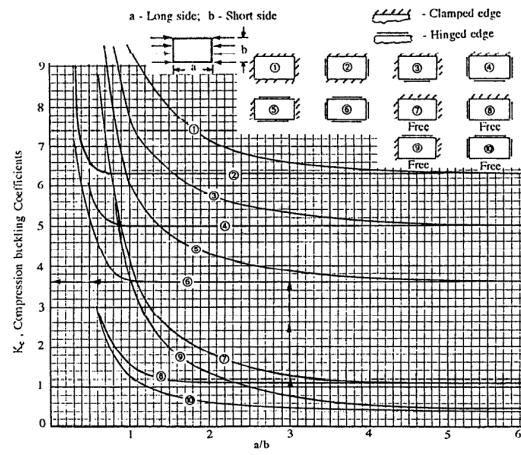


Figure 12.12: Buckling coefficient  $K_c$  in thin sheet.

## Stringers

A single stringer was added to the upper skin, to reduce the sheet aspect ratio and reduce the skin thickness required to fulfill the buckling requirement. The critical column buckling stress for a slender column is given by Equation 12.8, where  $K$ , the end-fixity coefficient, results from the boundary conditions of the column.  $K$  is 4 if both ends are clamped, and equal to 1 if both ends of the stringer are pinned [59]. A value of  $K = 1$  was used, with the stringers assumed as pinned at the wing root, and at ribs, limiting the effective length. In addition to buckling, crippling failure is considered. The ratio of critical crippling stress to yield stress for a plate is given by Equation 12.11, which resembles the equation for critical buckling stress, with the addition of semi-empirical adjustment factors  $\alpha$ , and  $n$ . For aluminium alloys,  $\alpha$  and  $n$  are equal to 0.8 and 0.6 respectively [59]. The crippling stress for the entire I-stringer is then the area-weighted average of crippling stressed for the three plates forming the I-beam, given by Equation 12.12, where  $A_i$  is the area of each plate minus the corners.

$$\sigma_{cr} = \frac{K\pi^2 EI}{AL^2} \quad (12.10)$$

$$\frac{\sigma_{cc}^{(i)}}{\sigma_y} = \alpha \left( \frac{K_c}{\sigma_y} \frac{\pi^2 E}{12(1-\nu^2)} \left( \frac{t}{2w_e} \right)^2 \right)^{1-n} \quad (12.11) \quad \sigma_{cc} = \frac{\sum(\sigma_{cc}^{(i)} A_i)}{\sum A_i} \quad (12.12)$$

No trade-off was performed for the stringer design, given the low relative importance of this design decision. An I-section was chosen for the stringer, due to the efficient performance in bending and strong precedence for use in aerospace applications. The moment of inertia for a constant thickness I-stringer with thickness  $t$ , flange width  $a$ , and web height  $h$  is given by Equation 12.13, following thin-walled assumptions. The thickness  $t_{str}$  and web height  $h_{str}$  were chosen at a ratio of 1:10, satisfying the requirement to use the thin-walled assumption. Then, the flange width  $a_{str}$  is calculated to provide the required moment of inertia to prevent stringer buckling or crippling at the maximum axial load in the upper skin defined in the skin sizing. If buckling is critical, cross sectional area is required, and therefore, Equation 12.14 is required calculate the required flange width. However, in this case, crippling was critical, and this was not needed.

$$I_{stringer} = \frac{h_{str}^3 \cdot t_{str}}{12} + \frac{t_{str}^3 \cdot a_{str}}{12} + a_{str} \cdot t_{str} \cdot \left( \frac{h_{str}}{2} + \frac{t_{str}}{2} \right)^2 \quad (12.13) \quad A_{stringer} = t_{str}(2a_{str} + h_{str}) \quad (12.14)$$

## Integrated Wingbox

Given the design of the spars, skin, and stringer, performance failure modes of the integrated wingbox structure must be verified. First, the maximum shear stress due to torsion, given by Equation 12.5 is checked. The maximum torque and corresponding shear stress from aerodynamic torsion is calculated. However, the largest torsional load on the wing occurs in the case of max thrust from both forwards VTOL propellers,

and no thrust from the rear propellers, in the case of an aggressive maneuver. The shear stress resulting from this torque is calculated. The magnitude of shear stresses from torsion were below 20% of the yield shear stress, reflecting that the buckling stress requirement drove the design.

Finally, combined failure is considered. The Tresca failure criteria is used. The three axial stresses  $\sigma_1$ ,  $\sigma_2$ , and  $\sigma_3$  are calculated according to Mohr's circle. Then, maximum shear stress is identified from Equation 12.16 - Equation 12.18. This value is compared to the value for the failure shear stress given by Equation 12.15. As was the case with torsion, the Tresca failure stress is extremely high compared to the maximum stress experienced, meaning buckling failure in the skin is most critical for the design of the wingbox.

$$\tau_{\text{fail}} = \frac{\sigma_{\text{yield}}}{2} \quad (12.15)$$

$$\tau_{\text{max}_1} = \frac{\sigma_1 - \sigma_2}{2} \quad (12.16)$$

$$\tau_{\text{max}_2} = \frac{\sigma_2 - \sigma_3}{2} \quad (12.17)$$

$$\tau_{\text{max}_3} = \frac{\sigma_1 - \sigma_3}{2} \quad (12.18)$$

Using inputs from Chapter 12, the final design of the wingbox is presented. In Section 14.1, the component masses for the final wingbox are given in Table 14.4. The skin thickness, spar thickness, and stringer dimensions are provided in Chapter 4. Using inputs from Chapter 12, the final design of the wingbox is presented. Table 14.4 gives the component masses for the final wingbox. The skin thickness, spar thickness, and stringer dimensions are provided in Chapter 4.

## Tail Sizing

The structural sizing of the vertical and horizontal tail is performed in the same manner as the wing sizing as described in Figure 12.2, but with a lower level of detail. The inverted U-tail was treated as two vertical tails and a horizontal planform for the purpose of sizing calculations. No stringers were required due to the small dimensions, which reduced the prevalence of buckling failure. Also, the loads considered were scaled according to the maximum lift of the tail. The final tail mass is provided in Section 14.1.

## 12.3. Fuselage, Booms and Landing Gear Design Sizing

The sizing of the fuselage, the booms and the landing gear was carried out based on very simple preliminary considerations with the intention to produce predictions for dimensions and weight but did not undergo a detail design similar to the one of the wing box. First the fuselage design is explained, followed by the sizing of the booms and the landing gear.

### Fuselage Sizing

The fuselage design starts by placing the aircraft payload, cruise propulsion system and power system in longitudinal order, such that the required diameter of the fuselage would be minimized. For simplicity, the shape of the fuselage is assumed circular, however, the exact cross-section is not deemed relevant at this stage of the design. This is reflected in the renders of the concept shown in Section 14.1. The estimates on weight and size are not expected to change considerably with a more optimized cross-section.

The length of the fuselage ( $l_f$ ) was obtained by placing the motor, payload (with a specific arrangement allowing cameras and LiDAR to hang close to the nose), fuel cell and fuel tank along a longitudinal axis. Aligning their largest dimension in the longitudinal direction the smallest fuselage radius ( $r_f$ ) could be obtained. The sum of the masses of those same components altogether is the mass of the systems contained in the payload (with the addition of the propeller).

The fuselage mass ( $m_f$ ) is obtained by summing the weight of the cylindrical section and the two half-spherical heads as shown in Equation 12.19. The fuselage mass is computed by computing the volume of

the skin, then multiplying it by the density of the chosen material, Al2024. The skin thickness of the fuselage ( $t_f$ ) was chosen to be 2 mm for a conservative estimate.

$$m_f = m_{cylinder} + 2m_{head} = \rho_{Al6061} \left[ l_f \cdot 2\pi r_f \cdot t_f + 2 \cdot \frac{4}{3} \pi \cdot r_f^3 - 2 \cdot (r_f - t_f)^3 \right] \quad (12.19)$$

## Boom Sizing

The sizing of the booms was carried out based on a relation for boom sizing from literature. [64] The function of the booms is double: connecting the VTOL engines to the rest of the airframe and transferring the loads from the empennage to the wing. The booms are therefore first sized to allow for the VTOL propellers' clearance from the fuselage and the front propeller. The length of the boom ( $l_{boom}$ ) is then compared with the aerodynamic tail arm ( $l_h$ ) and increased in case lower in size. Equation 12.20 shows the regression formula from literature to calculate the mass of the boom system (both booms). The variable  $m_{cant}$  represents the ideal weight at the end of a cantilever beam if the boom would be idealized as such.

$$m_{Booms}[lbs] = (0.14 * l_{boom}[ft] * m_{cant}[lbs]) \quad (12.20)$$

## Landing Gear Sizing

The landing gear design consisted of a set of 4 struts of semi-circular cross-section. As a design choice, their attachment on the booms is located right below the VTOL motors. Such positioning provides the maximum ground stability without extending the booms further the length designed to satisfy VTOL engine positioning and empennage positioning. With such a cross-section, it is possible to fold the landing gear struts below the booms minimizing frontal cross-section, and therefore, drag.

The height of the landing gear needs to provide ground clearance for the cruise propeller and the payload (camera system and LiDAR). The largest dimension to be cleared is multiplied by a factor of 1.25 and chosen as landing gear height. The cross-section of each strut is sized such that with the failure of deployment of two struts, the two remaining would still be able to sustain the weight of the UAV with a load factor of 2 without yielding. From the minimum area necessary to satisfy this design principle and the required height, the weight can be computed.

# Iterative Design Process

As a follow up from Chapter 4, this chapter deals with the dependencies found within the different design groups in Section 13.1. In Section 13.2, the verification and validation processed were documented.

## 13.1. Iteration Dependencies

In order to come up with a feasible design, each department individually developed a Python script to calculate a set of relevant parameters. The values used for each script were either labeled as constants and saved in a separate file, or as inputs, calculated by other departments. Since the number of inputs and outputs involved in the code is high, Table 13.1 was made, containing the name of all of the variables, a description, the name of the department from which program they come, i.e., outputs, and for which department it is used, i.e., inputs. Having an overview of all of the variables that are used is very useful. It is also used as a verification tool by checking that all of the variables are being used in some department, or that the correct department is using the appropriate inputs.

The code was written by compiling the work of the different departments in a loop. This was done following the order discussed in Chapter 4, with a slight modification: the aircraft configuration department was joined together with the structures department. Therefore, two separate scripts were written, one dedicated to the wing structure and one dedicated to the mass estimation of several components and center of gravity estimation.

Mission profile and payload sizing were sized independently from the loop since they come directly from requirements and are not influenced by the other subsystems. The only parameter that could change, depending on the values from the noise department, was the cruise altitude. Therefore, the parameter was changed after each iteration if the noise constraints were not met. The order of the main loop is then as follows:

1. Aerodynamics
2. Stability and controllability
3. Propulsion
4. Power and energy
5. Noise
6. Aircraft configuration + Structures and materials

Thanks to changing the order of the departments in the loop, only a few variables were necessary to initiate the program. By looking at the order of the departments, and their inputs and outputs from Table 13.1, it can be seen that the two variables that compose the initial values are the take-off mass and the fuselage width. In this way, it is easier to analyze how much the initial conditions influence the converged result.

It is set up so that, given the set of initial values, several iterations are performed until the system's weight does not change more than 0.01% from iteration to iteration. Since the fuel cells selected come from a database, if the results diverge, an error pops up when the power required is higher than that provided by the fuel cells found.

**Table 13.1:** All input and output variables for the UAV design iteration. The input and output columns indicate which department uses them and which one calculates them, respectively. The departments are mission profile (MPROF), power (POW), noise (NOI), aerodynamics (wing design, WDES), stability and controllability (stability, STAB, and aileron design, AIL), structures and materials (structures, STRU, and wing structure, WSTRU) and propulsion (PROP).

Variable	Description	Inputs	Outputs	Units
$h_{cruise}$	Cruise altitude	POW, NOI, WDES	NOI	m
$b$	Wing span	STAB, AIL, WSTRU, STRU	WDES	m
$b_h$	Span of horizontal stabilizer	STRU, WSTRU	STAB	m
$b_v$	Span of vertical stabilizer	WSTRU	STAB	m
$C_L$	Lift coefficient of the wing at cruise	STAB	WDES	-
$c_r$	Root chord of main wing	STRU, WSTRU	WDES	m
$c_{r_h}$	Root chord of horizontal stabilizer	WSTRU	STAB	m
$c_t$	Tip chord of main wing	WSTRU	WDES	m
$d_{cruise}$	Diameter of cruise propeller	NOI, STRU	PROP	m
$d_{VTOL}$	Diameter of VTOL propellers	NOI, STRU	PROP	m
$diam_{h_2,tank}$	Diameter of H2 tank	STRU	POW	m
$dim1_{fc}$	Dimension 1 of fuel cel system	STRU	POW	m
$dim2_{fc}$	Dimension 2 of fuel cel system	STRU	POW	m
$dim3_{fc}$	Dimension 3 of fuel cel system	STRU	POW	m
$b_f$	Fuselage width	STAB	STRU	m
$l_h$	Tail arm	STRU	STAB	m
$length_{h_2,tank}$	Length of H2 tank	STRU	POW	m
hor. tail mass	Mass of horizontal tail	STRU	WSTRU	kg
tot $H_2$ mass	Mass of hydrogen needed	STRU	POW	kg
$motor_{cruise}$ mass	Mass of cruise motor	STRU	PROP	kg
$motor_{VTOL}$ mass	Mass of VTOL motor	STRU	PROP	kg
power system mass	Mass of power subsystem	STRU	POW	kg
$prop_{cruise}$ mass	Mass cruise propeller	STRU	PROP	kg
$props_{VTOL}$ mass	Mass VTOL propeller	STRU	PROP	kg
vert. tail mass	Mass of vertical tail	STRU	WSTRU	kg
wing mass	Mass of the wing	STRU	WSTRU	kg
MAC	Mean aerodynamic chord	WSTRU, STAB, STRU	WDES	m
$P_r$ cruise	Power required for cruise	POW	PROP	W
$P_r$ descent	Power required for descent	POW	PROP	W
$P_r$ cruise climb	Power required for cruise climb	POW	PROP	W
$P_r$ VTOL	Power required for VTOL	POW	PROP	W
$P_r v_{max}$	Power required for $v_{max}$	POW	PROP	W
$\rho_{cruise}$	Rho at altitude	PROP	WDES	$kg/m^3$
RPM <sub>cruise</sub>	RPM cruise propeller	NOI	PROP	1/min
RPM <sub>VTOL</sub>	RPM take-off propellers	NOI	PROP	1/min
S	Surface area wing	STAB, PROP, AIL, WSTRU	WDES	$m^2$
$\Lambda_{LE}$	Sweep angle of leading edge	STRU	WDES	deg
$\Lambda_{TE}$	Sweep angle of trailing edge	STRU	WDES	deg
$W_s$	Wing loading	PROP	WDES	$N/m^2$
TOM	Maximum take-off mass	PROP, WDES, WSTRU	STRU	kg
front props <sub>VTOL</sub> pos	Position of the propellers y wise	WSTRU	STRU	m

It also helped to know which variables are needed to start the program.

## **13.2. Verification and Validation**

During the development of the final design for the UAV, models were built to simulate the various systems and their functions. It is vital throughout this process to guarantee the validity of the results obtained with the models. For this reason, multiple verification and validation methods were used to evaluate and potentially rectify the models. The models used during the preliminary design of the concepts were created in python to facilitate the iteration process. The following subsections will give an overview of the steps taken to verify and validate the models.

### **13.2.1. Model Verification**

Verification is the process used to ensure that a product or model meets the requirements that the designers set. Multiple techniques can be used to verify: inspection, demonstration, test, and analysis. The implementation of the scripts into the main loop occurred as follows. First, the individual departments developed their own code. Second, the code was written into the required format to be included in the main loop. Since the two processes are done by different people, it was possible to perform verification at different levels while implementing the code.

After the development of the individual codes, the models were verified using both inspection and analysis. The model inspection entailed reviewing the formulas and checking their correct input in the code. This was done by the member who worked on that code, as they were more familiar with it. The computations integrated into the model were also reproduced on paper for verification using analysis. This process ensured that, similarly to inspection, the equations were inputted correctly. The hand computation of the equations used in the model proved to be more effective at raising alerts as sanity checks since small details are challenging to spot.

Consequently, the code was verified while it was reformatted into the correct structure. The primary method used for verification was the use of unit tests. Unit tests are designed to test small portions of the code to ensure correct functioning and integration. A unit test can, for example, be used to compare the output of a specific function to another value determined by hand computation, or check that the relation between input and output is correct. For each model, a file for unit testing was created, verifying each function independently.

Furthermore, by implementing the code into the loop, verification by inspection was performed. This was done in this stage since once a new code was implemented into the main loop, composed of previously verified scripts, it is easier to spot a value that is away from what is expected. Finally, after all the scripts were integrated, the behavior of the whole system was analyzed. For this, multiple iterations were done, and the inputs and outputs of the departments were plotted as a function of the iteration number. This helped to monitor if the design was converging or diverging and which of the variables was causing it. In addition, extreme value testing was performed at this stage.

In retrospect, the methods used for verification of the models, as well as the workflow implemented, proved to be efficient and will be used as a basis for future verification procedures.

### **13.2.2. Model Validation**

Validation is the process used to make sure the product or model fulfills its intended purpose. Validating a model relies on making sure the final results correspond to the physical process described by the model. There are multiple methods that can be used to validate a model; these include but are not limited to experience, analysis, and comparison. Similarly to the verification organization, the validation was conducted by several people at different moments in time.

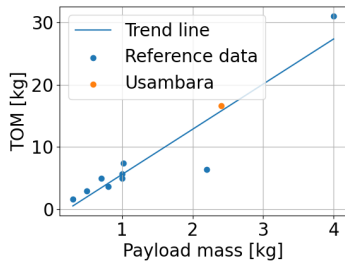


Figure 13.1

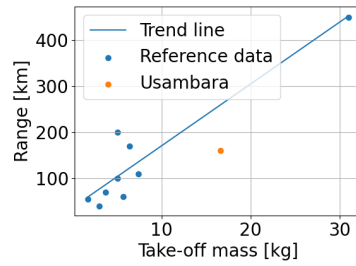


Figure 13.2

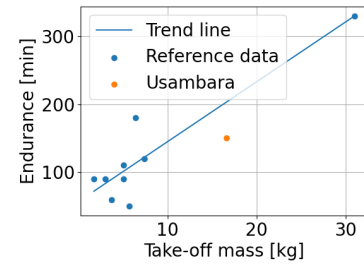


Figure 13.3

The primary validation technique used was comparison. The method is based on comparing the results obtained by the model to verified data from tests or independent models. Throughout the creation of the models, sanity checks were carried out at different stages by comparing obtained results with data from existing UAVs. This allowed the validation of intermediate steps, possibly raising alerts in case the result would greatly deviate from literature values. These alerts permitted the models to be corrected in a timely manner reducing the workload at the end. Once the model was completed, a final validation was carried out comparing the final obtained results with known UAV parameters.

For the final comparison, data from several UAVs was gathered, including maximum take-off mass, range, endurance, and payload mass. With this, three linear regression analyses were performed, take-off mass against payload mass (Figure 13.1), range against take-off mass (Figure 13.2), and endurance against take-off mass (Figure 13.3). The first figure helps to appreciate how the take-off mass over payload mass ratio for the UAV is very close to that of the reference data. However, in the following two figures, it can be seen how the UAV underperforms compared to the reference data. The values for the range over take-off mass as well as for endurance over take-off mass are lower than for the reference data, which indicates that the group has been conservative while designing. It is therefore expected that the UAV actually performs better than it is expected now when the design is refined.

After these validation tasks, some recommendations are made in order to verify the model further. It is recommended that another model is done for this aircraft, or use an already existing one, to validate the results obtained. In addition, a scaled model could be built to test the actual characteristics of the UAV.

### 13.2.3. Sensitivity Analysis

Once the verification and validation tasks were performed, a sensitivity analysis was carried out. This is a tool used to check how target variables are affected based on the changes of other variables or inputs. In order to achieve this, sensitivity analyses are performed at two separate levels; by changing the initial conditions or by changing other parameters.

First, the initial conditions are tested. There are only two initial conditions that can be changed, as explained at the beginning of this chapter; these are the take-off mass and the fuselage width. Therefore, the main loop is run at different values for these initial conditions for 15 iterations to assess how the final take-off weight of the UAV was affected.

Figure 13.4 shows the take-off mass as a function of the iteration number for different values for the initial weight. It can be seen with this how the code produces a convergent design for all the tested conditions below 22 kg. For an initial mass of 22 kg or more, the design does not converge. The graph shows some interesting results that give information about how the system behaves. For initial weights of 17 kg or below, the design converges to a 16.6 kg UAV. However, for higher initial weights, still below 22 kg, the design converges to higher weight options. This is because for high initial weights, the power required is very high, and a fuel cell that covers those needs is selected, not allowing for any more decrease in weight. This figure

helps to see how the chosen final design, presented in Chapter 14, is the most desirable since it possesses the lowest weight design. Furthermore, the figure illustrates how the final weight is quite sensitive to the initial weight value.

Figure 13.5 presents the take-off mass as a function of the iteration number for different values of the initial fuselage width, with an initial mass of 15 kg. In contrast with the previous figure, it is observed that the output is much less sensitive to the initial value of the fuselage width. The results diverge slightly after the first two iterations but still converge to the same design.

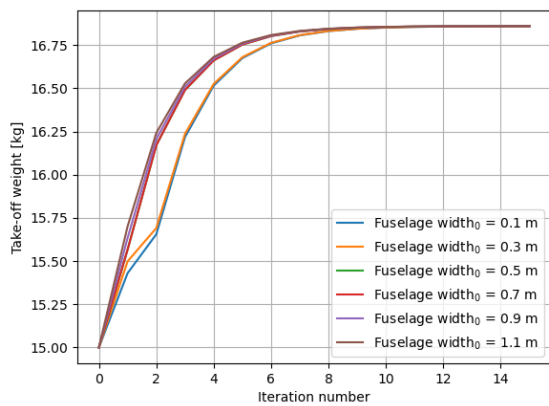


**Figure 13.4:** Change on the take-off mass with respect to the iteration number for different values of the initial mass.

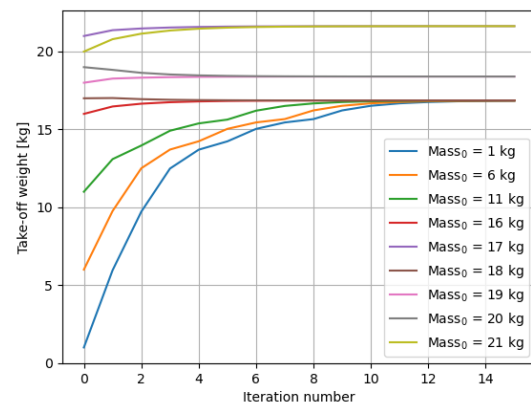


**Figure 13.5:** Change on the take-off mass with respect to the iteration number for different values of the fuselage width.

Second, two different parameters were changed to see how the weight of the final design would change. During the integration of the code, it was noticed how the convergence or divergence of the result was heavily determined by the mass of the power subsystem and the wing structure. It was therefore decided that it was a good idea to perform a sensitivity analysis changing these two parameters.

A power scaling factor was first defined. This represents the value by which the power required by the propulsion system is multiplied. This means that for a scaling factor of 0.5, the power needed is divided by two. This would be equivalent to increasing the power density of the fuel cells used and also helps to visualize how the design could be different in the coming years as fuel cells raise their popularity within the UAV segment and their power density increase. Figure 14.1 shows how the take-off mass, power required, and mass of hydrogen change with the power scaling factor. From it, it can be seen how by decreasing the factor, i.e. increasing power density, the converged design becomes more stable since it changes less with decreasing power. Furthermore, as a power scaling factor of 1.1 is reached, the design starts to diverge. By taking a look at where in the plot the current design is positioned, i.e. 1.0 scaling factor, it can be seen that this is an unstable area, where a slight change in the power can lead to a significant change in the mass, even to divergence. This occurs mainly because the main loop uses a database with fuel cells and hydrogen tanks, which, as their peak power or mass of hydrogen stored is not enough, their weight increases substantially. This can be appreciated in the figure; the horizontal black lines in the power required plot indicate the maximum peak power of a fuel cell in the database, and the hydrogen mass required indicates the maximum capacity of one of the tanks. It can therefore be seen that a more significant increase in take-off mass occurs when these two limits are reached.

Second, a wing mass scaling factor was secondly defined. Similar to the power scaling factor, the wing mass scaling factor is multiplied by the wing structural mass. Figure 13.7 shows how the take-off mass, power required, and hydrogen mass change with this factor. This serves to illustrate how the converged design would behave in case different types of stiffening elements were used since these would increase or decrease the mass slightly. It was observed during the production of this figure that if the same range of factors used was the same as for the power scaling factor figures, they were almost identical. However,

a smaller range was considered since this range made more sense. The black horizontal lines here also represent the maximum peak power and hydrogen storage capacity and are also followed by an increase in take-off mass.

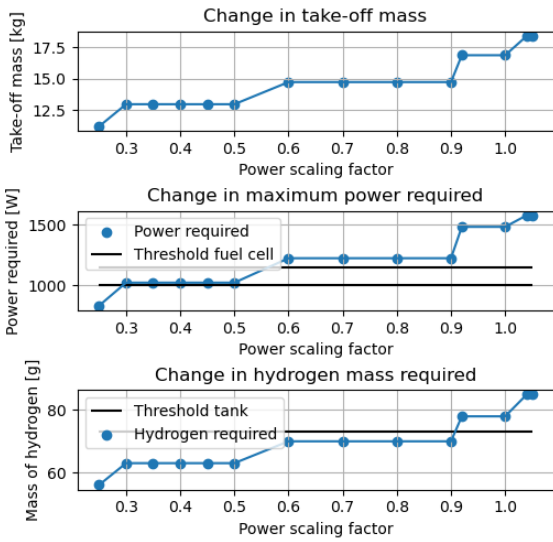


**Figure 13.6:** Change in take-off mass, power required and hydrogen mass with respect to the power scaling factor. The black horizontal lines in the power plot represent peak power, and in the hydrogen mass plot, the maximum hydrogen storage capacity. The maximum scaling factor before the design diverges is 1.09.

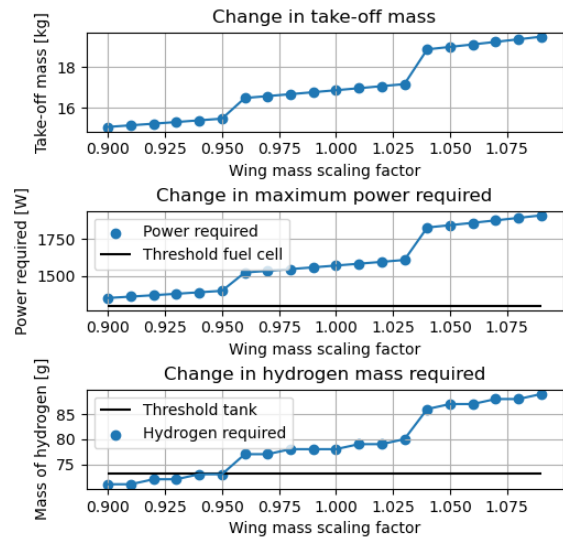


**Figure 13.7:** Change in take-off mass, power required and hydrogen mass with respect to the wing mass factor. The black horizontal lines in the power plot represent peak power, and in the hydrogen mass plot, the maximum hydrogen storage capacity. The maximum scaling factor before the design diverges is 1.09.

# Complete Final Design

The aim of this chapter is to present the final design of the UAV and its characteristics. The values of the final design found by the iterations are stated in Section 14.1. The budget breakdown of the mass and power of the final UAV design is presented in Section 14.2. The plan of how the design should be produced is addressed in Section 14.3. An analysis on the performance of the final design is presented in Section 14.4. The reliability, availability, maintenance and safety of the UAV are evaluated in Section 14.5. A compliance matrix which shows if the design meets the specific requirements set is shown in Section 14.6. Lastly, the post design risk of the UAV are analyzed in Section 14.7.

## 14.1. Finalized Design

At the end of the iteration process, a converged final design was achieved. This final design can be viewed in Figure 14.1.

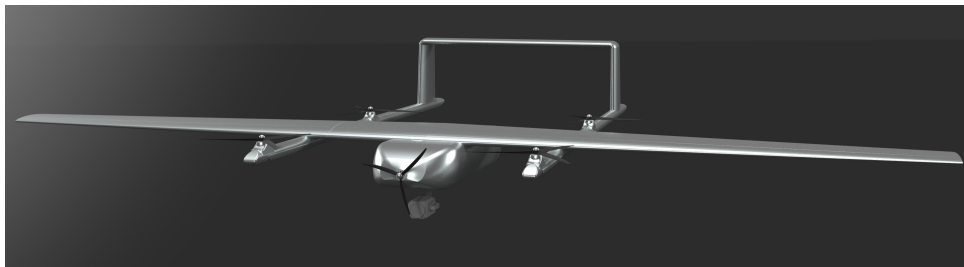


**Figure 14.1:** Visualization of the final design of the designed UAV

In order to have a clear overview several tables summarizing the UAV design are provided. Table 14.1 and Table 14.2 contain information regarding wing shape, size and performance. Table 14.3 summarizes horizontal and vertical tail planform parameters. Table 14.4 and Table 14.7 provide information on the weight of specific wing structural elements, the tail, the size of the booms and of the fuselage, further general design parameters like VTOL propeller positioning. Table 14.6 contains power system data (including the specific fuel cell<sup>1</sup> and the tank selected<sup>2</sup>), Table 14.8 propulsion system data while Table 14.5 contains some noise parameters are provided in their relevant section.

**Table 14.1:** Wing planform parameters and size.

Parameter	Value [unit]
S	1.3 [ $m^2$ ]
b	3.2 [m]
AR	6 [-]
$c_r$	0.57 [m]
$\lambda$	0.8 [-]
Dihedral	0 [deg]
MAC	0.42 [m]
Airfoil	NACA 64 <sub>2</sub> 415
$\Lambda_{c/4}$	0 [deg]
$\Lambda_{LE}$	0.054 [deg]
W/S	129 [ $N/m^2$ ]

**Table 14.2:** Wing aerodynamic performance data.

Parameter	Value [unit]
$C_{l_{max}}$	1.26 [-]
$C_L^1$	0.45 [-]
$C_{L\alpha}$	4.98 [ $rad^{-1}$ ]
$C_{m,ac}$	-0.085 [-]
$C_{m\alpha}^2$	0.87 [ $rad^{-1}$ ]
$C_D^1$	0.017 [-]
$C_{D0}^3$	0.010 [-]

<sup>1</sup> Cruise value;

<sup>2</sup> wing and fuselage, no tail included;

<sup>3</sup> wing and tail contributions only.

**Table 14.3:** Vertical and horizontal tail planform parameters and size.

Parameter	Value [unit]
$l_h$	0.85 [m]
$S_h$	0.12 [ $m^2$ ]
$AR_h$	6 [-]
$S_h S$	0.10 [-]
$b_h$	0.84 [m]
$c_{r_h}$	0.14 [m]
$c_{t_h}$	0.14 [m]
$S_v$	0.10 [ $m^2$ ]
$AR_v$	1.3 [-]
$b_v$	0.35 [m]
$c_{r_v}$	0.40 [m]
$c_{t_v}$	0.14 [m]

<sup>1</sup>URL:[https://www.h3dynamics.com/\\_files/ugd/c65691\\_7699e151793045e5b91fad3408a1b7e.pdf](https://www.h3dynamics.com/_files/ugd/c65691_7699e151793045e5b91fad3408a1b7e.pdf) [17/06/2022]

<sup>2</sup>URL:<http://meyer.cd/copv/> [17/06/2022]

**Table 14.4:** Wing structural components characteristics.

Parameter	Value [unit]
skin mass	2.98 [kg]
spars mass	0.72 [kg]
stringers mass	0.36 [kg]
ribs mass	0.38 [kg]
spar caps mass	0.06 [kg]
total mass	4.50 [kg]

**Table 14.5:** Noise data.

Parameter	Value [unit]
$h_{cruise}$	610 [m]
SPL at $h_{cruise}$	27.25 [dBA]
SEL at $h_{cruise}$	74 [dBA]
$L_{DN}$	41 [dBA]

**Table 14.7:** Main aircraft components size and mass. Propellers location.

Parameter	Value [unit]
wing mass	4.5 [kg]
hor. tail mass	0.7 [kg]
vert. tail mass	0.6 [kg]
TOM	16.8 [kg]
cg pos <sup>1</sup>	0.71 [m]
$x_c$ cg pos	0.25 [-]
fuselage size <sup>2</sup>	0.15 · 1.27 [m]
booms length	2.15 [m]
outboard boom pos <sup>3</sup>	0.42 [m]
front props <sub>VTOL</sub> pos <sup>1</sup>	0.19 [m]
rear props <sub>VTOL</sub> pos <sup>1</sup>	1.23 [m]
prop <sub>VTOL</sub> clearance <sup>4</sup>	0.1 [m]
$l_f/d$ <sup>5</sup>	8.7 [-]

<sup>1</sup> From the nose of the aircraft;

<sup>2</sup> diameter x length;

<sup>3</sup> from the longitudinal axis;

<sup>4</sup> from the wing and from the cruise propeller;

<sup>5</sup> aircraft fuselage finess ratio.

**Table 14.6:** Power system specifications.

Parameter	Value [unit]
tot energy flight	1175 [Wh]
tot H <sub>2</sub> mass	0.08 [kg]
H <sub>2</sub> tank size <sup>1</sup>	0.14 · 0.55 [m]
H <sub>2</sub> tank mass	1.6 [kg]
H <sub>2</sub> tank volume	0.5 [L]
H <sub>2</sub> tank $p_{operative}$	300 [bar]
H <sub>2</sub> tank brand and model	Meyer HDRX-005
H <sub>2</sub> tank material	CFRP
fuel cell $P_a$	1500 [W]
fuel cell size <sup>2</sup>	0.30·0.15·0.12 [m]
fuel cell mass	2.8 [kg]
fuel cell brand and model	Aerostak 1500
power system mass	5.5 [kg]

<sup>1</sup> Diameter x length of the cylindrical tank;

<sup>2</sup> length x width x depth of the H<sub>2</sub> fuel cell.

**Table 14.8:** Propulsion system required power outputs, propeller and motor characteristics.

Parameter	Value [unit]
$P_r$ VTOL	1482 [W]
$P_r$ hover	985 [W]
$P_r$ descent	741 [W]
$P_r$ cruise	455 [W]
$P_r v_{max}$	681 [W]
$P_r$ cruise climb	656 [W]
$d_{VTOL}$	0.86 [m]
RPMS <sub>VTOL</sub>	4400 [ $min^{-1}$ ]
props <sub>VTOL</sub> tot mass	0.52 [kg]
motor <sub>VTOL</sub> mass	0.29 [kg]
$d_{cruise}$	0.52 [m]
RPMS <sub>cruise</sub>	3850 [ $min^{-1}$ ]
prop <sub>cruise</sub> mass	0.08 [kg]
motor <sub>cruise</sub> mass	0.15 [kg]

## 14.2. Mass and Power Budget Breakdown

In this section, different budgets are created. First, a mass budget is made. Subsequently, a power budget is given. These budgets give more information to where in the system most resources are dedicated to. This means that most costs of the system are driven by the biggest components in the budgets. So by identifying them, more information is available on the distribution of the budget and potential pitfalls.

### Mass budget

In order to obtain more information about the distribution of weight over the UAV, a mass budget has been made which can be seen in Table 14.9. It shows that the wing and power systems make up a great part of the MTOW. Since the UAV has a long endurance, a lot of power is required. Also, long and slender wings allow

for more endurance, causing the need for a lot of bending stiffness in the structure and thus adding wing weight. The systems are very light. However, this is due to the components chosen to be included in this category. Most of the systems are namely included in other categories, like propulsion, power and payload. In essence, only small electronics and cables are included in the systems, justifying the small mass. Moreover, Figure 14.2 shows the distribution of weight over the categories as percentage of MTOW.

In addition to the expected masses, contingencies are given. At this point of the design, all the calculated masses are still conceptual. In order to avoid unexpected changes of the masses, and thus introducing additional costs, contingencies are taken into account. Since the wing weight is dependent on the weight of other components as well, this contingency is the highest. Moreover, the payload contingency is only 5% since the payload consists mostly of off the shelf components.

**Table 14.9:** UAV mass budget

Component	Mass [kg]	Percentage of MTOW [%]	Contingency [%]
Wing	4.50	26.71	20%
Empennage	1.16	6.88	10%
Booms + landing gear	1.72	10.21	10%
Fuselage	1.76	10.45	10%
Systems	0.05	0.30	10%
Payload	2.36	14.01	5%
Power system (Including fuel)	4.49	26.65	10%
Propulsion system	0.81	4.81	10%
<b>Total</b>	<b>16.85</b>	<b>100</b>	

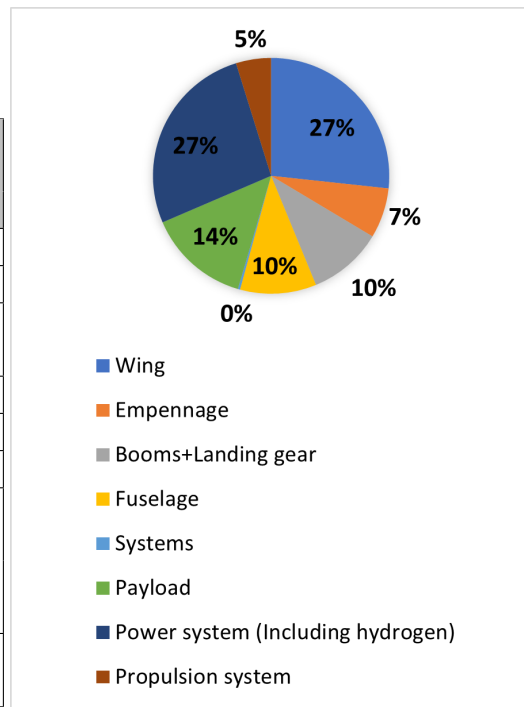


**Figure 14.2:** UAV mass breakdown in % of MTOW

## Power budget

Just like the mass budget, a power budget is required. This is given in Table 14.10. Note that this power budget is only for cruise, since during VTOL, the payload is not operational and the propulsion system is very power consuming. As can be seen in Table 14.10, the propulsion system forms the majority of required power during cruise. However, the power required for payload and avionics are also not negligible, as a consequence of the relatively high power needed to record and transmit videos. Moreover, the contingencies are given.

**Table 14.10:** UAV cruise flight power budget

Component	Power [W]	Percentage of total power [%]	Contingency
Payload	55	10.15	5%
Propulsion system	455.37	84.07	15%
Avionics	31.30	5.78	10%
<b>Total</b>	<b>541.67</b>	<b>100</b>	

The selected fuel cell according to the sizing described in Section 10.4 is provided below. The Aerostak 1500 hydrogen fuel cell system was chosen as the lightest hydrogen fuel cell which provided the 1586 W of required peak power during vertical take-off<sup>3</sup>. The Aerostack 1500 HFC consists of a 54 cell stack. Technical

<sup>3</sup>URL:[https://www.h3dynamics.com/\\_files/ugd/c65691\\_7699e151793045e5b91fad3408a1b7e.pdf](https://www.h3dynamics.com/_files/ugd/c65691_7699e151793045e5b91fad3408a1b7e.pdf) [17/06/2022]

specifications of the Aerostak 1500 are stated in Table 14.11.

**Table 14.11:** Technical specifications of the Aerostak 1500 hydrogen fuel cell system, which will be equipped to the designed UAV

Hydrogen fuel cell system	Rated power [W]	Peak power [W]	Dimensions [mm]	Weight [kg]
Aerostak 1500	1500	1700	302 x 120 x 145	2.8

### 14.3. Production Plan

Figure 14.3 displays the manufacturing, assembly and integration plan (MAI Plan), in other words the production plan, of the UAV. Here, the blue blocks represent raw materials or half fabricates being used to produce parts. The yellow blocks represent simple parts or products to be used in bigger structures. The green block represent those bigger structures. Red blocks are components that are bought as a whole because it is a lot more convenient to buy them instead of producing them yourself. The purple block is the final product, Usambara.

Most of the produced parts will be made from aluminium 6061 sheets, which are first cut to the correct dimensions and then bent to obtain the right shape. Note that the wing ribs will have holes and flanges, which are made by punching and deep drawing respectively. For the hinges supporting moving parts, a very complex shape is required. That is why casting is the preferred method for those parts. Note that this is also the most expensive production method compared to the others. In order to obtain the final UAV, all the parts and structures are welded, soldered, riveted and bonded together.

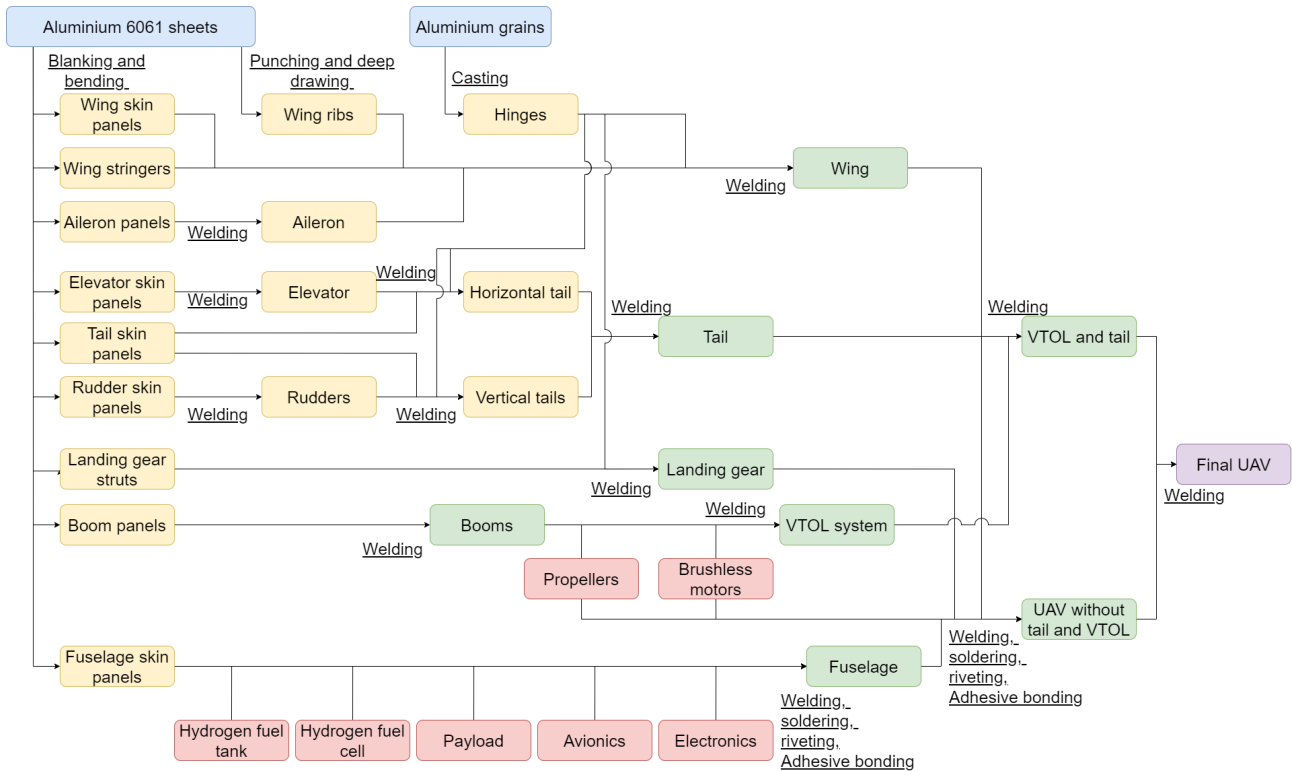


**Figure 14.3:** Flow diagram of manufacturing, assembly and integration plan of the UAV

Moreover, Figure 14.4 displays the MAI Plan for the ground station. As the ground station design is still very preliminary, so is the MAI Plan. However, a rough estimation of the materials, off the shelf components and processes required to manufacture the ground station can already be made as shown.

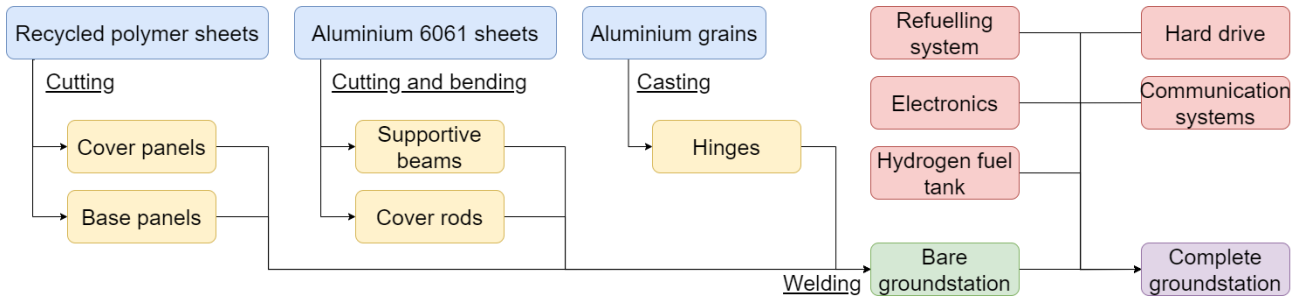


**Figure 14.4:** Flow diagram of manufacturing, assembly and integration plan of the ground station

## 14.4. Performance Analysis

This section provides a summary of various performance parameters of the final UAV design. Table 14.12 provides data on the maximum and minimum capabilities of the UAV while Table 14.13 summarizes the regular mission parameters coming either from decisions taken in Chapter 6 or from performance calculations. A brief comparison of the performance of the aircraft with other existing drones is provided from the graphs in Section 13.2.

**Table 14.12:** Maximum and minimum performance considerations.

Parameter	Value [unit]
max range	160 [km]
max endurance	2:30 [hr:min]
max speed	26.4 [ms]
max operative ceiling <sup>1</sup>	840
max surface covered per flight	35 [km <sup>2</sup> ]
max flights per day <sup>2</sup>	11 [-]
max $w_{ct}$ at $h_{cruise}$	277 [m]
min $w_{ct}$ at $h_{cruise}$	38 [m]
max $w_{ct}$ at 120 m	54 [m]
min $w_{ct}$ at 120 m	8 [m]
min px swath width $h_{cruise}$ <sup>3</sup>	0.06 [m]
max $px_{pp}$ at $h_{cruise}$	196 [-]
SPL at max ceiling	24 [dBA]
max SPL at ground station	91 [dBA]

<sup>1</sup> In order to still be able to provide more than  $px_{pp}$ ;

<sup>2</sup> for a single drone;

<sup>3</sup> ground width that each pixel covers;

**Table 14.13:** Regular flight performance data.

Parameter	Value [unit]
operative range	160 [km]
operative endurance	2 [hr]
cruise speed	22.22 [m]
$h_{cruise}$	610[m]
surface covered per flight	35 [km <sup>2</sup> ]
flights per day	8 [-]
operative swath width	38 [m]
operative px swath width	0.06 [m]
SPL at $h_{cruise}$	27 [dBA]
$px_{frame}$	1920 x 1080 [-]
drone number for surveilled area <sup>1</sup>	18 [-]

<sup>1</sup> Number of drones required to cover a 50x50 area as stated in the requirements.

With respect to noise considerations, the SPL at cruise was found to be 27 dBA. In Chapter 11 it was discussed that the UAV would be considered silent if the noise level was kept under 35 dBA. This is because the background noise in a rural environment is found to be between 35 and 45 dBA, therefore, with the current noise at cruise of the UAV, the noise produced is well below this threshold and would therefore barely be heard, if at all. However, a bigger problem is how the UAV disturbs the wildlife around it when take-off and landing takes place. To measure how much noise the wildlife was to be exposed to, the day-night average level of noise was computed. The result shows a value of 41 dB, which looking at Figure 11.3 gives a percentage of human population highly annoyed of below 3 %. It is therefore concluded that the UAV does not disturb the wildlife surrounding it.

## 14.5. Reliability, Availability, Maintenance, Safety

To define the characteristics of a product a RAMS analysis allows to specify different aspects of the system. RAMS stands for Reliability, Availability, Maintenance and Safety. These four attributes are directly related with the way a product is used to fulfill its mission and are intrinsically related with the requirements of the UAV. During the design procedure of the aircraft these aspects were continuously taken into consideration to create an optimal craft that would be able to fully fulfill the requirements set.

Each of the RAMS characteristics led to adjustments of the creation process of the UAV:

- **Reliability:** is based on the aircraft being able to perform the mission it was designed for. This can be described with the use of the failure rate for example, however this would require a higher level analysis of the craft design. For this reason the concept was created with the idea to maximize its reliability. One of the major considerations that was applied throughout the design process was to produce a UAV with a low level of complexity. This was decided early on with the objective to reduce the possibility of failure due to the use of complex systems. One example of a design decision made resulting from this consideration was to use a dual system for the propulsion system. Indeed using separate systems for the VTOL and cruise propulsion led to a reduced intricacy of the UAV, compared to using a complex propulsion system consisting of a rotating motor to switch from a VTOL to cruise configuration. Furthermore another method used, to increase reliability, was the over-sizing of certain components in order to assure a superior reliability. For example when designing the wing structure a load factor of 3.75 was set to assure the compliance of the design with an added safety margin.
- **Availability:** is the ability of the UAV to perform its mission successfully when placed in an environment. When designing the aircraft a case study was used, where a surveillance mission must be carried out in the Kruger National Park. This allowed certain challenges specific to the environment of operation to be brought to light impacting the design process. The environment impact on the UAV and the mission was decided to be reduced. From this aspect came out the principle of protecting the UAV in between surveillance missions as well as in case of harsh climate conditions. To achieve this the ground station, in addition to being a communication and refueling station, would serve as a shield for the UAV by fully sealing the craft inside the ground station.
- **Maintenance:** refers to the ability to quickly and easily maintain the UAV. This has the objective of maximizing the availability of the craft for which the opposite would increase costs. In order to reduce the time and complexity of maintenance for the aircraft a modular design was created, in case of a particular part failure it would then be simple to change a smaller portion of the craft. Another aspect that helps the maintenance is that the UAV is made from off the shelf components, as well as simple structures that are simple to manufacture. This has the benefit of allowing the easy acquisition of additional parts when required for maintenance.
- **Safety:** is based on the principle that the aircraft should not bring harm to humans nor to its operational environment during its life cycle. One of the major aspects of safety for this UAV is to protect the environment and limit the disturbance of the wildlife. In order to limit the disturbance that the UAV has, the sound emission was an important aspect continuously kept in mind. For this reason the propulsion system, being the most impactful on noise, was studied extensively and designed for optimal noise reduction. Another way the aircraft could disturb the environment is with polluting emissions. Since the power system uses a hydrogen fuel cell the emissions have been reduced to zero. Moreover a risk coming from flying a drone over natural environments is the possibility of hurting the wildlife in the event of a crash. Considering the aircraft is used for surveillance purposes stability is prioritized over maneuverability which is also in consequence reducing the risk of crashing.

## 14.6. Compliance Matrix

Table 14.14 shows the system requirements from Table 2.1. With the values achieved by Usambara, and the margin on the requirements, it was checked if the requirements are met.

**Table 14.14:** Requirement compliance matrix

Identifier	Requirement	Usambara	Margin	Compliance	Verification
<b>Performance</b>					
SYS-PER-01	The system shall surveil an area of 50 km x 50 km at least twice a day.	50x50 km	0	Yes	Table 6.2
SYS-PER-02	The UAV shall reach a cruise speed of at least 80 kmh.	80 km/h	0	Yes	Section 10.1
SYS-PER-03	The UAV shall have an endurance of at the least 2 hrs.	2 h	0	Yes	Section 10.4
SYS-PER-04	The UAV shall have a minimum cruise altitude of 120 m.	610 m	+490 m	Yes	Designed for this altitude
SYS-PER-05	The system shall be able to reach any location within its monitoring zone in less than 2 minutes.	2 min	0	Yes	Table 6.2
SYS-PER-06	The UAV shall have a maximum take-off and landing distance of 25 m.	0	-25	Yes	UAV has VTOL
SYS-PER-07	A single UAV shall be able to monitor an area of at least 5 km <sup>2</sup> in one single flight.	5 km <sup>2</sup>	0 km	Yes	Table 6.2
SYS-PER-08	The UAV shall have a minimum range of 150 km.	150 km	0	Yes	Section 10.4
<b>Movement</b>					
SYS-MOV-01	The UAV shall fly and manage recharging/refueling autonomously.	-	-	Yes	Autopilot present
SYS-MOV-04	The UAV shall be able to carry out regular operations with headwinds of up to 5.7 m/s.	4.2 m/s	0	No	Maximum speed is 95 km/h
SYS-MOV-05	The UAV shall be flight statically stable.	-	-	Yes	Chapter 9
SYS-MOV-06	The UAV shall be flight dynamically stable through control mechanisms.	-	-	No complete analysis	More detailed design required
SYS-MOV-07	The system shall detect poachers with a maximum rainfall of 7.6 mm/h.	-	-	No complete analysis	Tests are required
SYS-MOV-08	The system shall detect poachers within fog of maximum CAT II fog <sup>4</sup> .	-	-	No complete analysis	Tests are required
<b>Detection</b>					
SYS-DET-01	The system shall allow detection of a wildfire affecting an area larger than 100 m <sup>2</sup> .	100 m <sup>2</sup>	0	Yes	Chapter 5
SYS-DET-02	During daytime, the system shall allow detection of litter covering a ground area no smaller than 2 m <sup>2</sup> .	2 m <sup>2</sup>	0	Yes	Chapter 5
SYS-DET-03	The UAV cameras shall be able to provide footage of human figures with a resolution no-lower than 30 pixels.	100 pxl	+70	Yes	Chapter 5
<b>Communication</b>					
SYS-COMM-01	The system shall have an alert response time of maximum 5 seconds.	Instant	5 seconds	Yes	Chapter 5

<sup>4</sup>URL:<https://www.flir.com/discover/rd-science/can-thermal-imaging-see-through-fog-and-rain/>

SYS-COMM-02	The UAV shall provide its position to the ground station at a data rate of 1.02 Mbps or more.	1.02 Mbps	0	yes	Chapter 5
SYS-COMM-03	The aerial vehicle shall provide a continuous data budget of at least 21.4 Mbps downlink.	25 Mbps	+3.6	Yes	Chapter 5
SYS-COMM-04	The system shall receive a continuous data budget of at least 2 Mbps uplink.	25 Mbps	+23	Yes	Chapter 5
SYS-COMM-05	The ground station shall record the received livestream data.	-	-	Yes	Chapter 5
<b>Safety &amp; Reliability</b>					
SYS-SR-01	The system shall abide by the relative EASA regulations (excl. altitude).	-	-	No	Fit in specific category, which is still under development
SYS-SR-02	The system shall be 90% reliable for 500 hours of operational time.	-	-	No complete analysis	Tests are required
<b>Sustainability: Noise</b>					
SYS-SUSN-01	The system shall provide a noise reduction of 6dB compared to commercially available drones, measured at ground level (thus a noise output of 75dB).	41 dB	18	Yes	Chapter 11
<b>Sustainability: Materials</b>					
SYS-SUSM-01	The UAV shall consist of 75% of recyclable or processable materials (excluding sensors).	75%	0 %	Yes	Section 12.1
<b>Sustainability: Emissions</b>					
SYS-SUSEM-01	The UAV shall not emit carbon oxides, nitrogen oxides nor particulates during operation.	0	0	Yes	Hydrogen powered
<b>Sustainability: Ecosystem</b>					
SYS-SUSEC-02	In the case of an accident, the UAV shall not release polluting substances.	-	-	Yes	Hydrogen powered
<b>Maintenance</b>					
SYS-MAI-01	The payload shall be easily replaceable by trained staff.	-	-	Not tested	Operation has to clarify

## 14.7. Post Design Risk Analysis

After finalizing the design the risk associated with post-design and operation need to be identified to ensure the minimization of unexpected problems occurring later on. The aim of this section is to show the risk analysis for the post design activities. Firstly, all the risks are identified and assessed based on their likelihood and estimated impact. Then a mitigation strategy is presented to reduce the medium-high and medium risks.

### Risk Assessment

The post-design risks identified by the team are outlined in Table 14.15. The risks have been divided into three different categories. These categories are: Operational, external, production. These categories cover the post design stages.

**Table 14.15:** Risk list and breakdown of the values

Identifier	Risk	Likelihood	Estimated Impact	Total Value
Operational				
R-OP-01	Maintenance is not performed regularly.	3	4	12
R-OP-02	Maintenance is not performed correctly.	4	4	16
R-OP-03	Autonomous refuelling fails.	2	3	6
R-OP-04	Leakage during refuelling.	2	4	8
R-OP-05	Failed delivery of hydrogen to ground station.	4	3	12
R-OP-06	Alert/detection system failed.	2	4	8
R-OP-07	Wildlife heavily disturbed by implementation of ground station.	2	3	6
External				
R-EX-01	Hydrogen price increases.	2	3	6
R-EX-02	Demand is overestimated.	4	3	12
R-EX-03	Demand is underestimated.	2	2	4
Production				
R-PRO-01	Production falls behind.	3	4	12
R-PRO-02	Aluminum price increases.	4	3	12
R-PRO-03	Off the shelf parts are not available.	4	4	16
R-PRO-04	Production cost is higher then expected.	3	3	9

The ranking system for the likelihood and estimated impact is as described in Section 2.2, with the last column being the multiplication of the likelihood and estimated impact. Table 14.16 visualizes the severity of the risks. The table is color labelled as explained in Section 2.2.

The lowest level risks do not require a mitigation strategy, since they are very unlikely to affect the project significantly. The medium-low risk will not need a mitigation strategy as well. The level of these risks is still too low to have a significant effect on the project. From the medium level risks onward, a mitigation strategy will be necessary. These risks may affect the project in such a way that setbacks may occur, therefore for a risk that ranks 10 or higher a mitigation assessment is performed.

**Table 14.16:** Risk matrix

		Likelihood				
		Low	Medium Low	Medium	Medium High	High
Estimated Impact	<b>Negligible</b>					
	<b>Marginal</b>		R-EX-03			
	<b>Moderate</b>		R-OP-03, R-OP-07, R-EX-01,	R-PRO-04	R-OP-05, R-EX-02, R-PRO-02	
	<b>Critical</b>		R-OP-04, R-OP-06,	R-OP-01, R-PRO-01	R-OP-02, R-PRO-03	
	<b>Catastrophic</b>					

### Medium-High Risks

**R-OP-02 *Maintenance is not performed correctly.*** If the maintenance is not performed correctly, a higher chance of failure during flight can be expected. This would be detrimental to the mission. Correct maintenance can be improved with an in-depth course for the maintenance of the UAV should be given with a small test at the end to check for missed knowledge.

**R-PRO-03 *Off the shelf parts are not available.*** If the manufacturer of the off shelf parts can not deliver on time, a delay in the production of the UAV can occur. This risk can be mitigated by purchasing more off the shelf parts than needed.

**Medium Risks**

**R-OP-01 *Maintenance is not performed regularly.*** If the maintenance is not performed regularly, fatigue or small cracks are detected later than desired, which could result in the earlier failure of the UAV. It is recommended to set up a maintenance schedule and follow up on this schedule.

**R-PRO-01 *Production fails behind.*** Due to the staff’s sickness or the failure to deliver materials, production can fail. A schedule should be made beforehand detailing the change in production should an employee fall sick. Materials should be bought in a small excess in case of a failed delivery.

**R-OP-05 *Failed delivery of hydrogen to ground station.*** Once again, extra hydrogen should be stored in the event of a failed delivery so the UAV can keep operating.

**R-EX-02 *Demand is overestimated.*** Due to a miscalculation, the expected demand for the UAV can be overestimated. It is recommended to produce the UAV per application, not to overproduce.

**R-PRO-02 *Aluminum price increases.*** If the aluminum price suddenly increases and an application for a UAV has already been accepted, the overall profit could decrease. A small margin should be put on the market price to ensure small deficiencies can be compensated.

Table 14.17 shows the mitigated risks.

**Table 14.17:** Mitigated Risk matrix

		Likelihood				
		Low	Medium Low	Medium	Medium High	High
Estimated Impact	<b>Negligible</b>					
	<b>Marginal</b>		R-EX-03		R-PRO-03, R-OP-05, R-EX-02, R-PRO-02	
	<b>Moderate</b>		R-OP-03, R-OP-07, R-EX-01, R-OP-02,	R-PRO-04, R-OP-01, R-PRO-01		
	<b>Critical</b>		R-OP-04, R-OP-06,			
	<b>Catastrophic</b>					

# Economic Considerations

The aim of this chapter is to present the economic considerations of the project. A market analysis is presented in Section 15.1. In Section 15.2 an estimate of the costs of the product has been made. This estimation is based on unit costs estimates for the different subsystems. The return on investment will be presented in Section 15.3.

## 15.1. Market Analysis

In order to produce a successful product that meets the needs of all stakeholders, a market analysis is necessary. It provides insight into the technology trend and what issues need to be resolved with the UAV. Most importantly, it allows the product to be competitive, both in performance and price. First, the types of UAVs are investigated. Second, the competitors of the UAV are gathered. Third, the different segments will be explained. Fourth, the potential customers are analyzed, and finally a SWOT analysis has been made.

### Types of Unmanned Aerial Vehicles

An unmanned aerial vehicle is a transportation medium that operates without an onboard crew or passengers, guided by remote control, autonomously, or both<sup>1</sup>. It is segmented based on application, region, and type<sup>2</sup> which will be further discussed later on in the report. It can, however, also be described using Figure 15.1, which shows both the supply and demand sides<sup>3</sup>. Here, the squares represent the different segments in the market, on the supply side by type and the demand side by application or sector.

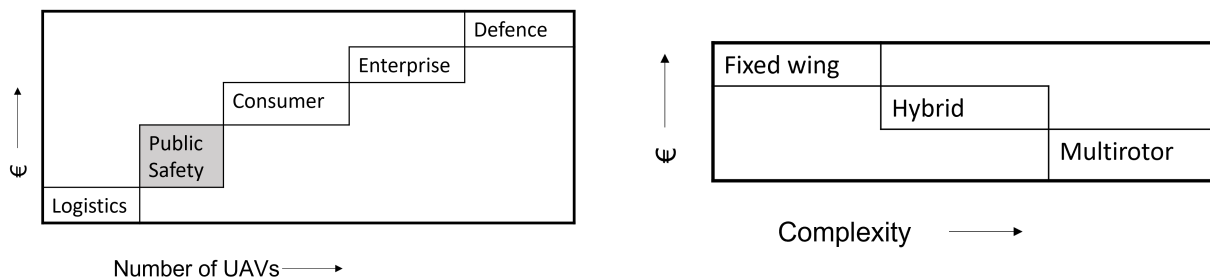


**Figure 15.1:** Supply (left) and demand (right) representation of the UAV market.

### Competitors

Understanding the current potential competitors of our product in the market is a key factor for discovering market niches or room for development. In Table 15.1, some major competitors are gathered and described, and some of their major characteristics, like endurance and speed, are highlighted.

<sup>1</sup>URL: <https://www.britannica.com/technology/unmanned-aerial-vehicle> [25/05/2022]

<sup>2</sup>URL: <https://www.mordorintelligence.com/industry-reports/drones-market#:~:text=The%20Drones%20Market%20is%20segmented,Middle%2DEast%20and%20Africa> [26/04/2022].

<sup>3</sup>URL: <https://www.alliedmarketresearch.com/unmanned-aerial-vehicle-market-A09059> [26/04/2022]

**Table 15.1:** Competitors in UAV general sector.

Name	Current state	Characteristics	Endurance [min]	Cruise speed [km/h]	Control	Weight [kg]
SenseFly eBee	Company that produces drones used for detecting sites with waste to be able to clean it, identifying turtles floating in the sea, etc <sup>4</sup> .	V-shape. Autonomous-flying Wind resistance: 46 km/h	45 - 90	40 - 110	Agile	1.3 - 1.6
AVY	Company that produces drones specialized in quick responses in cases of emergency, delivery of blood samples, vaccines and other logistics <sup>5</sup> .	Autonomous flying Wind resistance: 46.3 km/h	55	90	Agile	12
The Drone Bird Company	Company that uses drones shaped like birds for surveillance and to keep other birds out of the airport's airspace <sup>6</sup> .	Bio-inspired, shaped as birds Flapped drones	90	43	Very stable and slow	0.5 (max payload)
Ukrspec Systems	Company specialized in drones, some are electric, some use combustion. They make use of a catapult to let their drones take off <sup>7</sup> .	8 engines Multirotor design Autonomous flying	50	11	Very stable	6.8
DJI	This company specializes in high quality camera drones, but they can be equipped with other sensors, such as thermal cameras. They can also incorporate Real-Time Kinematic positioning (RTK) <sup>8</sup> .	Quadcopters Wind resistance: 36-54 km/h	30-55	25	Agile	6.8
Height Technologies	This company develops military drones with advanced capabilities for defense, public safety, and commercial use <sup>9</sup> .	Multirotor design Wind resistance: 46.3 km/h	40-90	60-75	High stability but highly stable	11-4

<sup>4</sup>URL: <https://www.sensefly.com/drones/compare-drones/> [26/04/2022]

<sup>5</sup>URL: <https://avy.eu/stories/> [26/04/2022]

<sup>6</sup>URL: <https://www.thedronebird.com/aves/> [26/04/2022]

<sup>7</sup>URL: <https://ukrspecsystems.com/drones/pc-8-4> [26/04/2022]

<sup>8</sup>URL: <https://www.dji.com/nl> [26/04/2022]

<sup>9</sup>URL: <https://heighttechnologies.com/products/mi-2/> [26/04/2022]

Helvetis	This start-up develops long-range UAVs with focus on mapping and military applications. However, it runs on fuel <sup>10</sup> .	Hybrid VTOL fixed wing	480	140	Stable	"Light-weight"
Azur drones	This company present an innovative solution design to strengthen the security over sensitive sites. They offer a quick response <30 seconds <sup>11</sup> .	Fully autonomous Multicopter design	25	50	Agile	0.375
Eye Above	Company that develops a fixed wing STOL UAV to prevent poaching in Africa, similar to our mission need statement <sup>12</sup> .	Fully autonomous Two VTOL and Two Thrust propellers	180-420	57	Stable, agile	6.6

Due to this quantitative and qualitative comparison, it is now possible to create a market map where two important characteristics are plotted against each other to illustrate gaps in the market or tendencies in behavior. In this case, it was chosen to plot two driving parameters: endurance and cruise speed. In Figure 15.2, the competitors have been plotted in points, lines, or rectangles corresponding to performance values given as a specific value or a range of values. The requirements for cruise speed and endurance define the no-design zone in red, with the white space corresponding to the desired design space. For illustration, the configurations of the different options are depicted at the top of the figure.

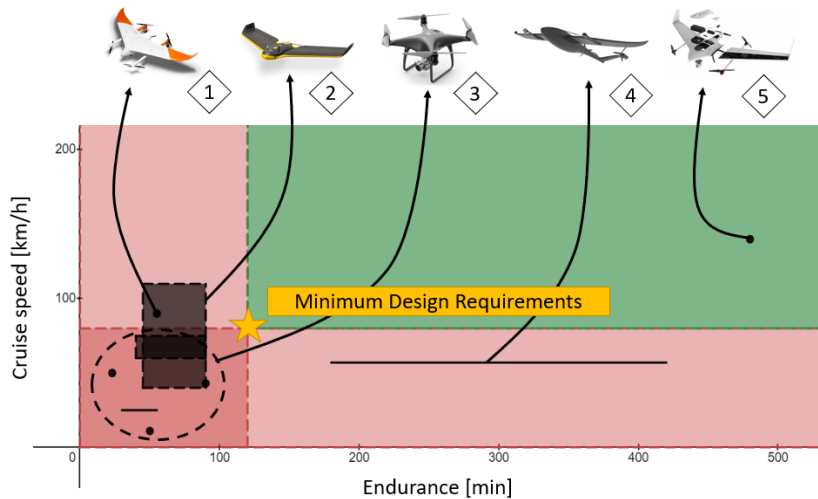


**Figure 15.2:** Market positioning map of the UAV market with the user mission requirements for speed and endurance. Competitors: 1 -Avy Area 3<sup>13</sup>. 2 - Sensefly<sup>14</sup>. 3 - DJI Phantom pro 4<sup>15</sup>. 4 - Eyeabove<sup>16</sup>.5 - Helvetis<sup>17</sup>.

<sup>10</sup>URL: <https://helvetis.com/> [26/04/2022]

<sup>11</sup>URL: <https://www.securify.se/azur-drones> [26/04/2022]

<sup>12</sup>URL: <https://theeyeabove.co.za/> [26/04/2022]

As Figure 15.2 depicts, most of the current market options do not fulfill both of the requirements at the same time, which may indicate that the UAV technology is not sufficiently mature yet, or that no products have been designed for the specific requirements needed. Moreover, the only drone that fulfills both requirements, Helvetis, is a start-up without a working product. This may be due to either one of the identified reasons. Because of this, it may be more likely that other companies, such as AVY or SenseFly eBee will approach a more desirable design configuration.

## Segments

The drone market was valued at 17.1 billion in 2020 and is projected to more than double to 39.8 billion by 2030, as shown in Figure 15.3<sup>18</sup>. This market can be segmented by type, region and application.

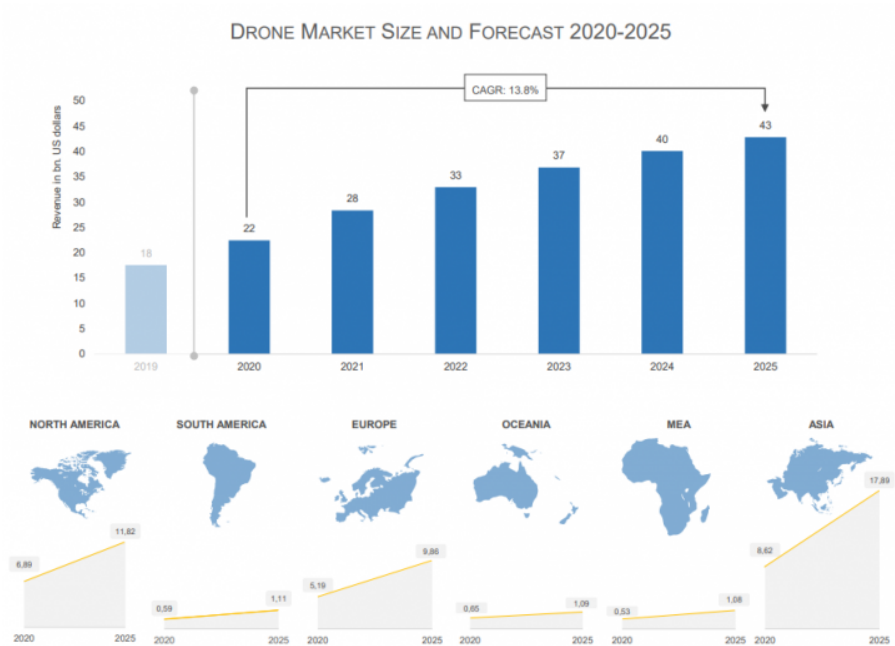


Figure 15.3: The drone market around the world

Firstly, the market is segmented by type in fixed-wing, rotatory blade, or hybrid. Figure 15.4<sup>19,20</sup> shows the market share per product type. The type of drone that is chosen in different situations depends largely on the conditions. In case large maneuverability and relatively slow speeds are desired, a rotatory blade design is preferred. However, as speed increases, the drag becomes too high for this type of drone, and therefore the battery size must increase, leading to significant weight increase. Therefore, fixed wing or hybrid configurations are selected for large distances and high speeds.

<sup>13</sup>URL: <https://avy.eu/our-integrated-solution/new-aera/> [05-16-2022]

<sup>14</sup>URL: <https://www.sensefly.com/> [05-15-2022]

<sup>15</sup>URL: <https://www.dji.com/nl/phantom-4-pro?site=brandsite&from=nav> [05-16-2022]

<sup>16</sup>URL: <https://theeyeabove.co.za/> [05-16-2022]

<sup>17</sup>URL: <https://helvetis.com/vtol-uav-isr/> [05-16-2022]

<sup>18</sup>URL: <https://droneii.com> [28/04/2022]

<sup>19</sup>URL: <https://www.mordorintelligence.com/industry-reports/uav-payload-and-subsystems-market> [28/04/2022]

<sup>20</sup>URL: <https://www.expertmarketresearch.com/reports/commercial-drone-market> [04/05/2022]

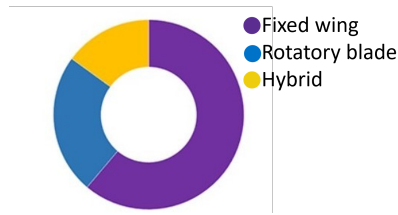


Figure 15.4: UAV Payload Market - Revenue (%) 2019.

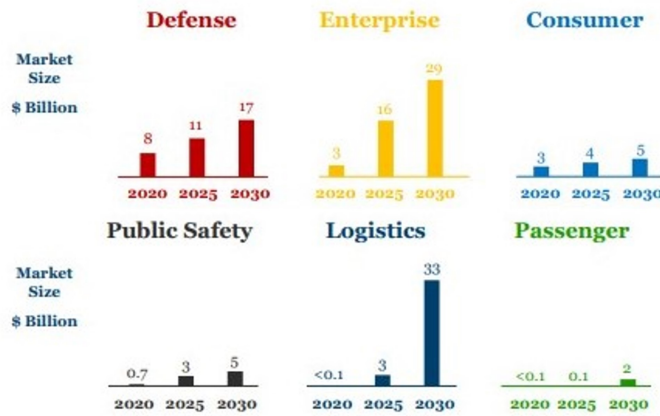


Figure 15.5: Projection of market share per drone application until 2027 [65].

Secondly, the market can be segmented by region: Europe, Asia, Oceania, Africa, North America, and South America. North America and Asia make up two-thirds of the global market share, as of 2019<sup>21</sup>. In 2018, North America had a slightly bigger share, however it has been eclipsed by the size of the Asian market due to rapid growth of the Chinese, Japanese, and Indian markets. Figure 15.3 shows the current size of the market per region and also an estimation of the size by 2025. All the regions are thought to double or almost double their market size in the half decade from 2020 to 2025.

Finally, the market can be segmented by application into defense, enterprise, consumer, public safety, logistics, and passenger UAVs<sup>22</sup>. Figure 15.5 shows the size of each of the markets per application and the expected growth by the year 2030. UAVs provide the capability for high accuracy and long-distance strikes without endangering the lives of operators, making UAVs a popular tool in combat scenarios. This, coupled with the significant government spending on military development, makes the defense sector the largest market share, with 53% of the UAV market. The enterprise segment is composed of hardware, software, and service companies that create products for industrial or commercial applications. It is the segment growing the fastest at the moment, and its largest segments are construction, built inspection, and agriculture. It is expected that by the year 2030, it will share 35.8% of the market. Furthermore, the logistics segment is forecast to take the largest share of drone market in the next ten years, with a share of 40.7% [65].

One facet of this forecast growth comes from the potential for drones to be used quick and cheap delivery services. With current delivery techniques, sending a package through, for example, FedEx Express costs around 30 euros and takes one day or more, or with Amazon Prime, 7-8 euros. The price of delivering with drones is currently about 60 euros, and it takes about 30 minutes. However, it is estimated<sup>23</sup> that the cost in the next decade will go down to around 4 euros. The development of the drone economy will make the costs of each drone go down, and automation capabilities also help decrease production costs, and ultimately further the fall in UAV prices.

## Customers

It is very important to analyze the potential customers of the product in order to design for their needs; in the end, without customers, there are no sales. The product will most probably be equipped with at least one camera to be able to detect poachers, wildfires, and litter. Therefore, once the cameras are installed, what they are used for can be changed easily, and the range of potential customers increases. Several groups of customers have been identified.

First, natural parks are thought to be the primary potential customer. With the large amounts of poaching happening, parks are interested in preventing this from happening. Since the project is aimed at designing

<sup>21</sup>URL: <https://www.mordorintelligence.com/industry-reports/utility-drone-market>

<sup>22</sup>URL: <https://levitatecap.com/levitate/wp-content/uploads/2020/12/White-Paper-v4.pdf> [28/04/2022]

<sup>23</sup>URL: <https://levitatecap.com/levitate/wp-content/uploads/2020/12/White-Paper-v4.pdf> [page 130 18/04/2022]

a UAV for surveillance of large areas to protect against poaching, wildfires, and littering, it is thought that natural parks are the target customer. In addition, the drone is designed to not disturb the wildlife by being a zero emission option with lower noise than other commercially available options. Some examples of these are the Kruger National Park in South Africa (19500 km<sup>2</sup>), the Serengeti National Park in Tanzania (14800 km<sup>2</sup>), the Ranthambore National Park in India (1350 km<sup>2</sup>), Veluwe in The Netherlands (1000 km<sup>2</sup>) or Torres del Paine in Chile (1800 km<sup>2</sup>).

Furthermore, it is thought that governments can also make use of the product, since it provides with surveillance capabilities and allows for the protection of specific areas of interest. As an example, worldwide, about 880 million US dollars have been spent on drones to inspect areas affected by fire<sup>24</sup>. In addition, non-profit organizations are also considered as potential customers. Their interest in natural habitat preservation fits perfectly with the objective of the product. As examples, WWF are putting in much effort to try to close markets that sell elephant tusks<sup>25</sup>. Deals could be made with this organization in order to help them stop the poaching activities the tusks come from. The Jane Gooddall Institute is an NGO that to ensures that her vision and life's work continue to mobilize the collective power of individual action to save the natural world. They have spent 13 million US dollars in 2019 on conservation tasks<sup>26</sup>. For protection and data gathering tasks they are using satellite observations that have a resolution of 60 cm<sup>27</sup>. Since the product will have much better resolution than theirs, they could become potential customers. Finally, another group of customers that may be interested in the product are research groups.

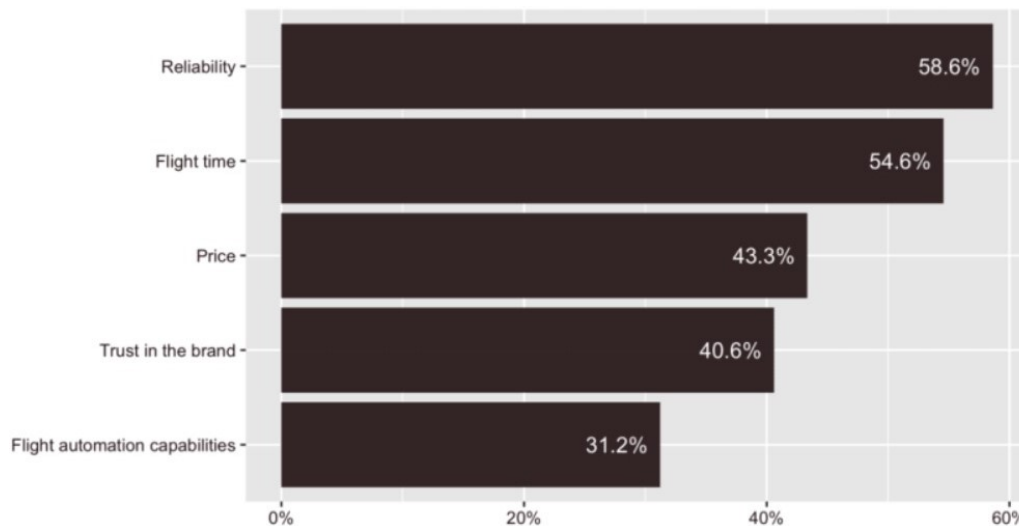


**Figure 15.6:** Primary purchasing factors for drones, "Which factors are most important when selecting a drone?"

For all four segments, five key factors have been identified as the main ones that drive the purchase choice. These can be found in Figure 15.6<sup>28</sup>. First among these factors is reliability, which is defined as "the ability of a system or component to function under stated conditions for a specified period of time"<sup>29</sup>. Therefore, it is important that during the design phase, an emphasis is placed on the reliability of the design. It can also be noted how price is not the driving factor in most of the cases, but rather the confidence in the product and its ease of operation. This suggests that ensuring delivery of a product is then ideal to offer to the potential customers, since it provides a reliable and low noise zero emission option, which flies autonomously and with a larger endurance than most commercially available options.

<sup>24</sup>URL: <https://www.dronefly.com/firefighting-drones-drones-in-the-field-infographic> [28/04/2022]

<sup>25</sup>URL: <https://www.worldwildlife.org/species/elephant> [04/05/2022]

<sup>26</sup>URL: <https://www.influencewatch.org/non-profit/jane-goodall-institute/> [04/05/2022]

<sup>27</sup>URL: <https://www.janegoodall.org/earth-observation/> [4/05/2022]

<sup>28</sup>URL: <https://www.thedronegirl.com/2021/05/03/reliability-drone-buying-decision/> [18-04-2022]

<sup>29</sup>URL: [https://en.wikipedia.org/wiki/Reliability\\_engineering](https://en.wikipedia.org/wiki/Reliability_engineering) [28/04/2022]

## SWOT Analysis

The ultimate objective of a market analysis is to increase the chance of success of the project by reducing the risks and uncertainties. To conclude, a SWOT analysis was performed which helps to discern the different advantages and disadvantages that the UAV market presents for those companies that are willing to invest in it. By analyzing the nature of this market, and its trends over time, it is possible to gather the market's Strengths, Weaknesses, Opportunities, and Threats. In Figure 15.7, these attributes are listed.

	Helpful	Harmful
Internal origin	<p><b>STRENGTHS</b></p> <ul style="list-style-type: none"> <li>• Cheap; drones are not usually very expensive for their value</li> <li>• Versatile; it caters to many different industries</li> <li>• Replacing outdated and expensive technology (helicopters or cranes for video, etc.)</li> <li>• Many different designs that fit different purposes</li> </ul>	<p><b>WEAKNESSES</b></p> <ul style="list-style-type: none"> <li>• Market is not mature</li> <li>• Technology needs development</li> <li>• Components might be more expensive as they are minoritarian</li> <li>• Tight regulations hold for design and operations</li> </ul>
External origin	<p><b>OPPORTUNITIES</b></p> <ul style="list-style-type: none"> <li>• Since it is young, there are plenty of market gaps.</li> <li>• Involved companies are relatively small; no dominant players</li> <li>• Market is expanding rapidly</li> <li>• New concepts are being constantly developed</li> </ul>	<p><b>THREATS</b></p> <ul style="list-style-type: none"> <li>• Future regulations could harm its versatility</li> <li>• Homebuilt models might reduce demand</li> <li>• Market might become more homogeneous as it grows</li> </ul>

**Figure 15.7:** Table depicting the SWOT analysis of the UAV market.

Through Figure 15.7, the UAV market can be described as young and progressing towards maturity. Furthermore, entering the market at this stage seems easy, since the competition consists of relatively small companies (with significant exceptions, such as DJI). Even though quadcopters are famous configurations for UAV, new concepts are being constantly developed to cater other market segments, leading to further market expansion. However, the current design liberty might be hampered as the technology becomes more known and legislation becomes more precise and restrictive.

This gives the team an opportunity to prepare a design procedure with little capital and from scratch, trying with known and less developed configurations in the hopes of developing a vehicle that fulfills every requirement.

## 15.2. Cost Analysis

In this section, a cost estimate for the system will be made. The total system costs can be defined as the sum of non-recurring costs and recurring costs, or development and manufacturing costs respectively. The methodology used to define these costs is based on a unit cost estimate for the different subsystems [66]. The unit costs are retrieved from normalized data of a Boeing 777-200. With some adaptations which will be explained later in this section, this data can be used as an estimate for the UAV costs as well. Moreover, since the unit costs were originally given in 2002 dollars/pounds, a conversion to 2022 EUR/kg was made<sup>30</sup>.

<sup>30</sup>URL: <https://www.inflationtool.com/us-dollar>[06-13-2022]

The proportions of these unit costs dedicated to different departments are also given as a percentage, of which the sum is 100%. These departments are engineering, manufacturing engineering, tool design, tool fabrication and support for the development and labor, materials and other for the manufacturing. The share of costs taken by these departments, together with the unit costs of the subsystems can be seen in Figure 15.8. Note that the width of the departments represent the percentage of the costs it takes. It can also be seen in the figure that the recurring costs are multiplied with the amount of UAV's produced. At the moment, it is assumed that only one UAV is being produced.

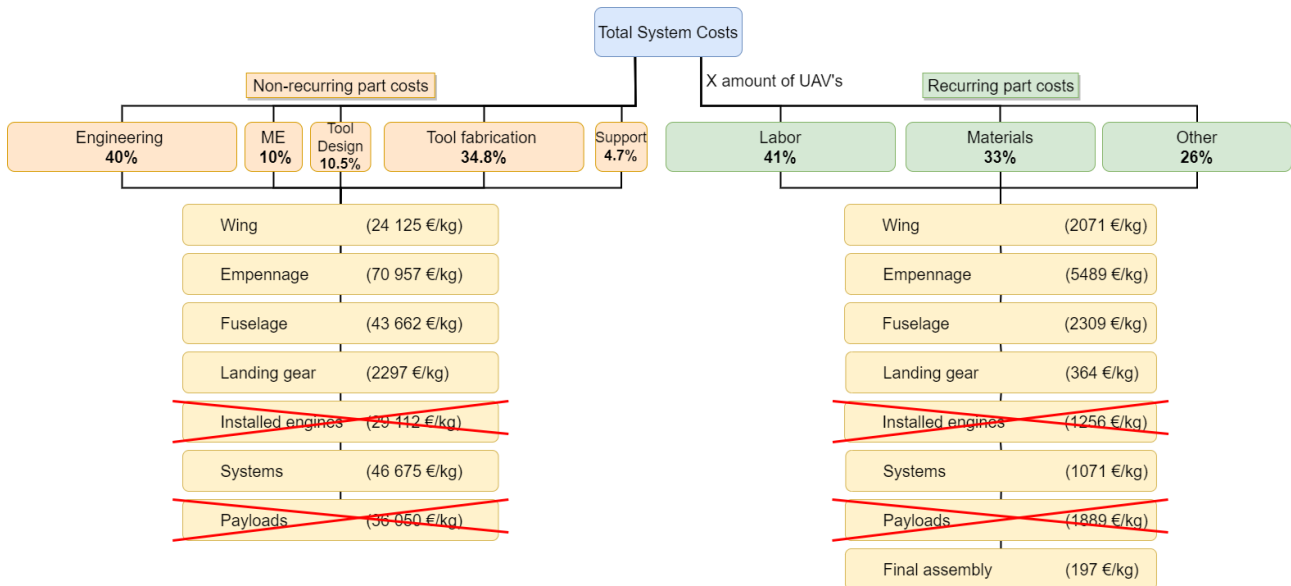


**Figure 15.8:** Cost breakdown for development and manufacturing costs per kg in 2022 EUR

It can be seen in Figure 15.8 that the installed engines and payloads are crossed out. The reason is that these components are off the shelf, meaning that the development and manufacturing of these components is done by another party. The price of these components can thus directly be related to the purchase price. These costs are given in Table 15.2. As for the other components, some changes have to be made. Since the data is based on a Boeing 777-200, costs for some parts of the UAV can have a very different nature. First of all, the wing. The wing of the UAV has to support the weight of four engines, the booms and the tail. Moreover, during VTOL a point load is induced while a distributed load is present during cruise. This all causes extra complications which has to be accounted for, this means a 10% increase in non-recurring costs will be set. Subsequently, the empennage will have the same value since the design and construction of an inverted U-tail compared to a conventional tail is not more complicated. As for the fuselage, a 70% decrease in non-recurring costs and 80% decrease in recurring costs will be set. This is due to the fact that the fuselage for the UAV is tremendously less complicated than for a Boeing 777-200. First of all, the fuselage does not have any passengers. Together with the fact that the UAV does not fly at high altitudes this means that the fuselage does not have to have climate control like pressurization. Furthermore, design for seats, luggage, crew, facilities and center of gravity shifts is not required. This makes the development easier, as with manufacturing. For the landing gear, simple retractable struts are used. Unlike a complicated landing gear for the Boeing 777-200, which has wheels, dampers and multiple hinges, the landing gear for the UAV is relatively simple. This was estimated to result in a 50% reduction in development costs is used and a 70% reduction in manufacturing costs. Lastly, the systems are considered. The requirements for the flight systems of the UAV are more comprehensive since it is VTOL and autonomous. On the other hand, like explained before, there is no need for climate control and a cockpit. Considering both sides, a decrease of 10% and 20% for the non-recurring and recurring costs respectively is used.

**Table 15.2:** Cost of off the shelf components used for the UAV

Off the shelf components					
	Amount	Total [EUR]		Amount	Total [EUR]
<b>Sensors</b>			<b>Propulsion &amp; Power</b>		
Cameras		14999	Fixed wing propeller		50
LiDAR		8079	VTOL propeller	x4	200
Bird repeller speaker		89	HFC		10,852
PIR	x2	40	Hydrogen tank		1729
Autopilot		5750	Fixed wing motor		320
GNSS antenna		190	VTOL motor	x4	1602
Transceiver		3000			
Antenna for UAV	x2	9			
<b>Total</b>		<b>€32157</b>	<b>Total</b>		<b>14,753</b>
<b>Aggregate Total</b>			<b>46,910</b>		

Now, with the mass budget given in Chapter 14, the costs of each part can be calculated to obtain all the costs. This is done by using the modified values of Figure 15.8 as explained previously. Together with the off the shelf components as given in Table 15.2, a complete picture can be made. This total cost breakdown can be found in Table 15.3. As can be seen, the development costs are a lot higher than the manufacturing costs, which also makes sense looking at the unit costs in Figure 15.8. Next to this, the manufacturing costs of the systems seem to be very cheap. This is due to the fact that most of the systems are already accounted for in the payload, power and propulsion categories. The resulting weight of the MTOW is used to calculate the remaining systems. However, they only include some electronics and cables. Note that the development and manufacturing costs of the ground station are not presented, this is due to the large contingencies being present in the design. As explained in Section 14.3, the ground station design is still very conceptual and to a very broad level of detail. However, the costs for the ground station will in all probability not blow up the total costs because of the simplicity compared to the UAV.

**Table 15.3:** Final development and manufacturing cost breakdown for the UAV

	Development costs [EUR]	Manufacturing costs [EUR]	Purchase price [EUR]
Wing	~165,000	~ 12,250	-
Empennage	~82,000	~ 6,400	-
Fuselage	~23,000	~ 800	-
Landing gear	~2,500	~ 160	-
Systems	~ 2,200	~ 40	-
Final assembly	-	~ 3,200	-
Payload	-	-	~ 32,000
Propulsion	-	-	~2,200
Power	-	-	12,600
<b>Total</b>	<b>~ 274,700</b>	<b>22,850</b>	<b>47,000</b>
<b>Grand total</b>	<b>274,700</b>	<b>69,850</b>	

Figure 15.9 shows the manufacturing costs of each component as percentage of the total manufacturing costs. Note that the payload makes up a great part of the costs, since expensive equipment needs to be bought. Landing gear and systems are displayed as 0% of total costs due to rounding, however, their costs are provided in Table 15.3.

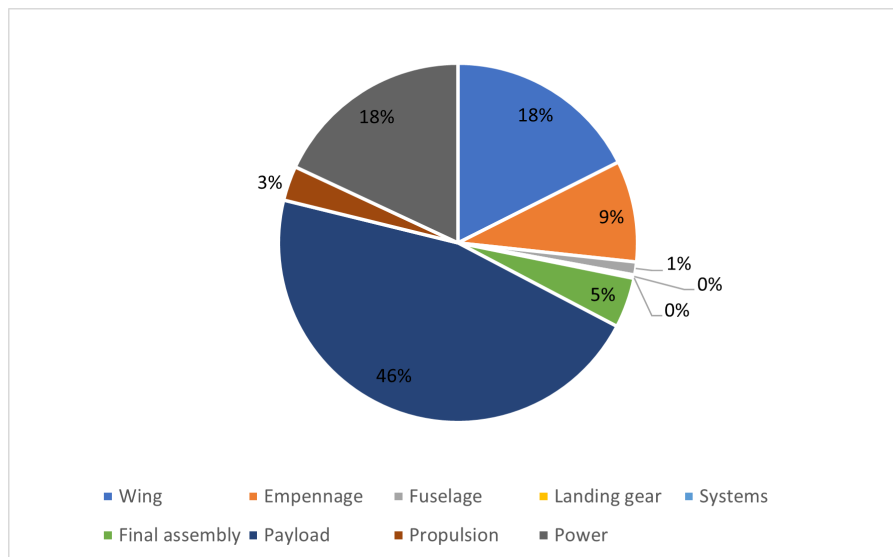


**Figure 15.9:** UAV manufacturing costs breakdown in % of total

### 15.3. Return on Investment

The final product to be developed and sold will be a hydrogen fixed wing VTOL UAV with an accommodating ground station to handle the wildlife surveillance autonomously. The hydrogen UAV will be able to fly around ten times a day due to its quick refueling, and as the UAV can cover at least 35.3 km<sup>2</sup> in one flight it will be able to survey 141.2 km<sup>2</sup> in a day. Resulting in a product of one UAV and one ground station per 141.2 km<sup>2</sup>.

The Return on Investment is based on the product of one UAV and one ground station, and can be established with six parameters: The market price, the market volume, the achievable market share, the development cost, the production cost, and the operational cost.

- First, the market price of the product. The market price is based on the budget from the client, which is 100,000 euro per UAV and 50,000 euro per ground station.
- Second, the achievable market share. As seen in Figure 15.2 the hydrogen UAV, which can be seen as a star on the map, meets the requirements of the client with only one other competitor. However, this competitor does not meet the sustainability requirements, leaving the hydrogen UAV in its own specific niche.
- Third, the production cost consist of the cost for the material and sensors of the product and the cost to produce the product. To produce the product an approximate of 5 high-level engineers are needed to produce one UAV in one week.
- Fourth, the operational cost, which encompasses the cost for the placement and construction of the ground station and possible setting-up of the UAV.

#### Market Share

The world is transitioning to a sustainable society with production, materials, and fuel becoming the focus of the change. Many UAVs are powered electrically when carrying a lightweight payload. However, UAVs that carry heavier payloads can also be powered by gasoline or a hybrid method in order to overcome the weight to power ratio caused by batteries. Hydrogen-powered fuel cells for UAVs is a relatively new technology that can tackle both the sustainable and weight issues given its great energy density and water exhaust.

The commercial market for surveillance UAVs is projected to be \$15 billion while 30% of the drones by 2022 are expected to be hydrogen powered<sup>31</sup>. It is a relatively new technology that is more beneficial in terms of

<sup>31</sup>URL: <https://www.haskel.com/en-us/blog/hydrogen-powered-drones-fuel-cell-technology-solves-flight-range> [15-06-2022]

range, sustainability and versatility. Considering the market value and equating the 30% yields \$4.5 billion dollars. The market has ten key companies producing UAVs and it is almost equally segmented in market share. Therefore, assuming the hydrogen UAV is able to perform optimally, it can be estimated that it can have an equal share as the other companies.

The amount of UAVs needed is heavily dependent on the customer. For example, for national parks, this amount depends both on the budget and on the size of the area needed to be covered. Kruger National Park is the reference for the project and its area coverage is 19,485 km<sup>2</sup> while each drone can cover 35 km<sup>2</sup>. Given the hefty costs of the drones with the base, it is expected for two drones a year to be bought by each customer until completion of the desired surveillance area. Along with national parks, the capabilities of the drone can also be of the interest of any other department in need of surveillance. With the fixed costumers ordering drones twice a year and the rest of other applications for the UAV, it can be estimated that the market share is around 9.1%.

## Market Volume

Given the available information, the market volume estimation is based on the United States national parks and scaled down by a factor of 0.896 to account for the economic capabilities of the countries that suffer the most from poaching and lack of infrastructure. The scale factor was calculated by dividing the estimated annual budget for an African park, which is \$381 million<sup>32</sup>, by the American park budget of \$425 million annually<sup>33</sup>.

A recently new initiative in the United States's national parks consists of drones being flown in the area for surveillance and after six years, they have flown around 250 missions<sup>34</sup>. Per year that is roughly 42 drones but multiplied by the scale factor it yields an estimate of 38 drones per year. Multiplying the number by two, since two per year are estimated given national park cuts, it yields 76. Assuming that the rest of the continents in the world have an equal amount of drones, 76, the total drones annually needed is estimated to be 422. The estimated products to be sold are also stated in Table 15.4 and the return on investment is stated in Table 15.5.

**Table 15.4:** Products to be sold

Estimation future product sold	
Market volume	422
Market share	9.1%
Estimate of to be sold products	38 products

**Table 15.5:** Return on Investment

Return on Investment	
Sold products	38
Market price per product	100,000 euro
Total price for sold products	3,800,000 euro
Total investment cost	€2,929,000
<b>Return on Investment</b>	<b>29.7%</b>

The value of the return on investment is promising in terms of the UAV's position in the market. If each year it makes 29.7% of what it invested in profit, it is a successful product that can be continued.

<sup>32</sup>URL: <https://www.pnas.org/doi/10.1073/pnas.1805048115> [15-06-2022]

<sup>33</sup>URL: <https://smartasset.com/taxes/the-economics-of-national-parks> [15-06-2022]

<sup>34</sup>URL: <https://www.federaltimes.com/management/2018/09/07/taking-to-the-skies-inside-the-world-of-national-park-ser> [06-2022]

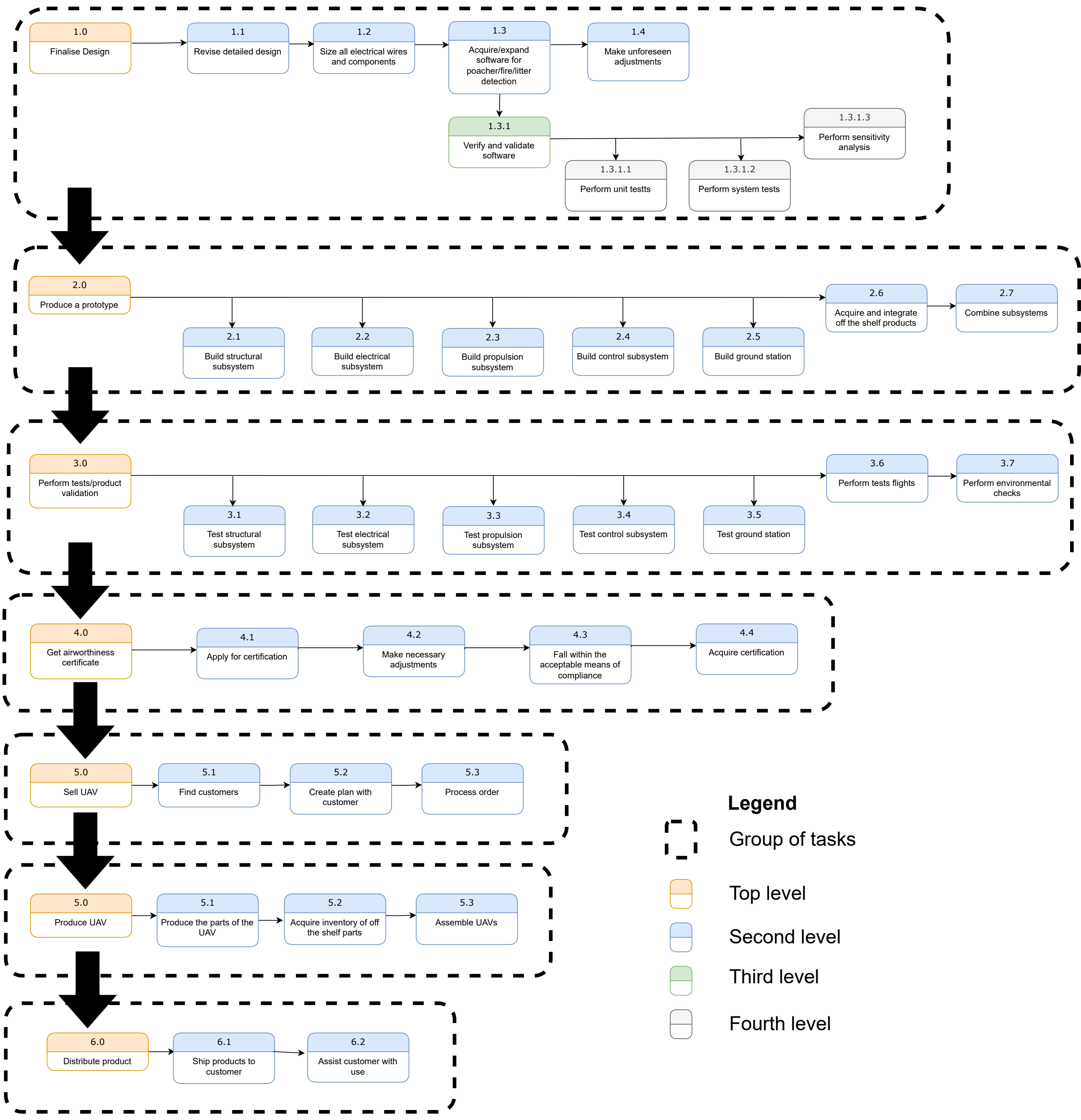
## Project Design and Development Logic

The DSE is a preliminary phase in the design process. Many other activities remain to be completed for the success of the project.

For this reason, this chapter presents how the DSE group 11 intends the continuation of the design and development process to be carried out. It is important to note that as this process has not been done before by the authors, that this is an estimation based purely on expectations rather than experience. As can be seen in the flow diagram of activities, the design must first be finalized. This will include things such as electrical wiring plans, detailed production method descriptions and the sizing of components outside the scope of the current report. Furthermore, this includes the integration of software into the system. This is not discussed in this report as the goal is currently to make a viable UAV design. This software must also be verified and validated.

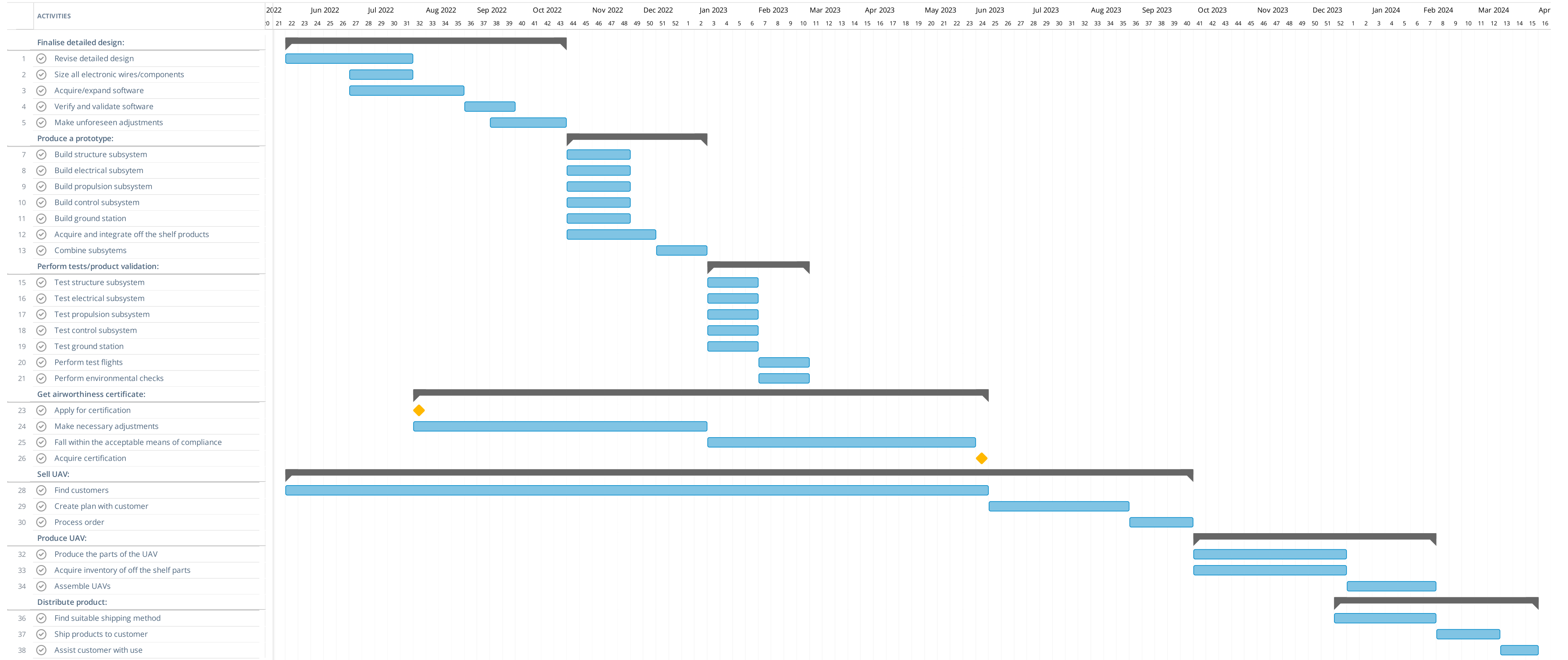
Next, a prototype can be produced. This includes the construction of all of the subsystems as well as the purchasing of the off the shelf parts. This is followed by integrating them and seeing if it in fact does work. At this stage all of the subsystems can also be tested individually in addition to being tested together. Finally, the UAV can be checked against the expected environmental conditions and a flight test can be completed.

The last big step is applying for certification. Despite the system being much less complex than an airliner, it is nevertheless still complex and the certification process could take a lot of time. The group however feels that with the detail of the design, there should be no major issues. Once this has happened, the selling, production, and distribution can occur, leading to the customer having the product and a success of the project. To show the time frame the group expects this process to follow, a Gantt chart with the major tasks is also included. With this estimation, the customer could have the product by March 2024. This is however significantly dependent on whether or not the product can be certified in a timely manner.



# USAMBARA Project Gantt Chart

Read-only view, generated on 15 Jun 2022



## Conclusion

The objective of this report was to design a zero-emissions, low-noise, unmanned, autonomous aerial surveillance system to monitor wildlife and the environment, for a cost of less than 100,000 and 50,000 euros per vehicle and ground station respectively. Four different configurations were evaluated for this design and a trade-off between them was made. The winner of the trade-off has been developed into further detail. This development entails a conceptual design of all the subsystems present in the unmanned aerial vehicle (UAV) and the integration between them. This conceptual design was mainly driven by its requirements on range and endurance, for 150 km and 2 hrs respectively.

A vertical take-off and landing (VTOL) UAV has been designed. To monitor wildlife and the environment, this UAV will be equipped with the Zenmuse H20N, which has two thermal cameras and two visual cameras. Machine learning software programs will use these cameras footage to detect poachers, wildfires and litter in the monitored area. The UAV has an autopilot, the Autopilot 1x, that allows the UAV to fly autonomously during its whole operation and avoid obstacles and birds using LiDAR sensors, and a bird repellent system. During flight, the UAV will use four rotors, with a propeller diameter and pitch of 0.8 m and 12 inches respectively, to take-off vertically, hover and land vertically. During cruise, the UAV will use its fixed wings of a wing span of 3.197 m and a surface area of 1.277 m<sup>2</sup>, to generate lift and will use a propeller with a diameter of 0.521 m and a pitch of 15 inches to generate the required thrust. The propellers have such large diameters and pitch to ensure little RPM are needed to generate the required thrust, little RPM is desired since that generates less noise. The propeller noise generated during cruise has a sound pressure level of 27.249 dBA measured from the ground. The ambient background noise in the area at night is 35 dBA on average, and thus the noise of the UAV can not be heard from the ground. To provide stability during flight, the UAV has an inverted U-shaped tail connected to the wings with two booms. To provide enough stiffness for the structure of the UAV while still making sure the UAV is as light weighted as possible the airframe of the UAV will be made from Al6061 alloy. Lastly, to make sure the UAV has zero-emissions during flight it is powered by hydrogen. The UAV will thus have a hydrogen tank with a diameter of 0.143 and a length of 0.546 kept at 300 bar. The power required by the UAV will be generated from a hydrogen fuel cell system that has a stack of 54 hydrogen fuel cells that produce power from the hydrogen in the hydrogen tank. The mass and power budgets of the designed UAV are shown in Table 17.1 and Table 17.2. The production cost per UAV was estimated to be 70,000 EUR.

**Table 17.1:** UAV mass budget

Component	Mass [kg]	Percentage of MTOW [%]
Wing	4.50	26.71
Empennage	1.16	6.88
Booms + landing gear	1.72	10.21
Fuselage	1.76	10.45
Systems	0.05	0.30
Payload	2.36	14.01
Power system (Including hydrogen)	4.49	26.65
Propulsion system	0.81	4.81
<b>Total</b>	<b>16.85</b>	<b>100</b>

**Table 17.2:** UAV power budget for cruise.

Component	Power [W]	Percentage of total power [%]
Payload	55.00	10.15
Structure	-	-
Propulsion system	455.37	84.07
Fuel system (Incl. fuel)	-	-
Avionics	31.30	5.78
Landing gear	-	-
<b>Total</b>	<b>541.67</b>	<b>100</b>

After each flight the UAV will return to its ground station. This ground station serves as a docking point for the UAV and a refueling point. The ground station will have two hinged hatches that can open when the UAV takes off or lands. The ground station has these, so the UAV is completely covered from the outside elements when stationed at the ground station. Curious animals or weather effects will not reach the UAV while stationed at ground. The ground station will also have a rotating landing pad. This pad can rotate, so the UAV can be positioned adequately for the refueling operation. During refueling, a pipe will connect to the UAVs hydrogen tank with a quick disconnect and will refuel the tank with the use of pressure differences. The ground station will has a surface area of about 30 m<sup>2</sup> to make sure the UAV completely fits within the ground station. The ground station will be constructed out of recycled polymer, which is strong against the elements while still being able to protect the UAV from all the environmental conditions and curious wildlife. A visualization of the UAV at the ground station can be seen in Figure 17.1.

Regarding the detection of threats, it is recommended to work with one of the software projects as mentioned in Section 6.2 or with a University researching AI detection programs. The data collected by the Usambara can be used to develop the detection programs further. Although, due to requirements, Usambara reaches quite a high cruise speed, it is recommended to lower this requirement for a better chance of using AI detection programs to spot threats.

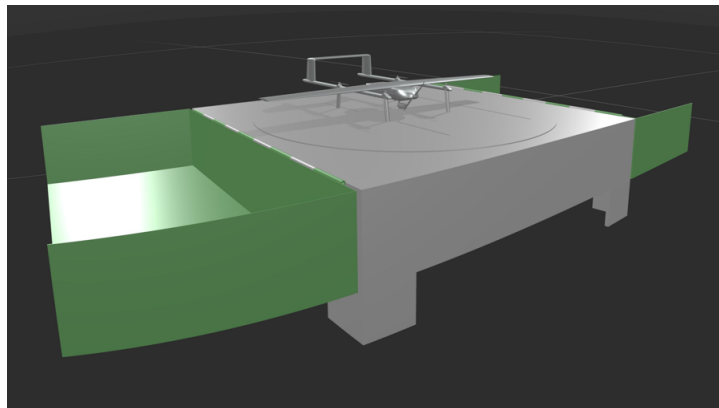


**Figure 17.1:** First design of ground station for the UAV

# References

- [1] E. Gill. Verification and Validation for the Attitude and Orbit Control System. lecture slides, AE3212-II, Delft University of Technology. Mar. 2022.
- [2] H. Chassagnette et al. “Midterm Report, Unmanned Wildlife Surveillance Drone”. Autonomous Quiet Aerial Surveillance System For Protecting Wildlife And Environment Spring DSE, Faculty of Aerospace Engineering, Delft University of Technology, unpublished. May 2022.
- [3] E. Erkut and M. Tarimcilar. “On Sensitivity Analysis in the Analytic Hierarchy Process”. In: *IMA Journal of Mathematics Applied in Business & Industry* 3 (Feb. 1991), pp. 61–83.
- [4] S. Oğuztimur. “Why Fuzzy Analytic Hierarchy Process Approach For Transport Problems?” In: 51st Congress of the European Regional Science Association: New Challenges for European Regions and Urban Areas in a Globalised World. European Regional Science Association (ERSA). 2011.
- [5] H. Chassagnette et al. “Baseline Report, Requirements and concepts for the design of an autonomous wildlife surveillance system”. Autonomous Quiet Aerial Surveillance System For Protecting Wildlife And Environment Spring DSE, Faculty of Aerospace Engineering, Delft University of Technology, unpublished. May 2022.
- [6] E. Bondi. “SPOT Poachers in Action: Augmenting Conservation Drones With Automatic Detection in Near Real Time”. In: 2008 IEEE Aerospace Conference. Vol. 32. 1. DOI: 10.1109/ AERO.2008.4526559. AIEE, Apr. 2018.
- [7] P. Rudol and P. Doherty. “Human Body Detection and Geolocalization for UAV Search and Rescue Missions Using Color and Thermal Imagery”. In: 2008 IEEE Aerospace Conference. DOI: 10.1109/ AERO.2008.4526559. IEEE, Apr. 2018.
- [8] C. Manore, P. Manjunath, and D. Larkin. “Maximizing object detection using sUAS”. In: Thirteenth International Conference on Machine Vision. Vol. "11605. SPIE, Feb. 2021.
- [9] E. Bondi. “SPOT Poachers in Action: Augmenting Conservation Drones With Automatic Detection in Near Real Time”. In: 2008 IEEE Aerospace Conference. Vol. 32. 1. DOI: 10.1109/ AERO.2008.4526559. AIEE, Apr. 2018.
- [10] F. Hossain, Y. Zhang, and M. Tonimal. “Forest fire flame and smoke detection from UAV-captured images using fire-specific color features and multi-color space local binary pattern”. In: *Journal of Unmanned Vehicle Systems* 8.4 (2020).
- [11] R. Caponi et al. “Thermodynamic modeling of hydrogen refueling for heavy-duty fuel cell buses and comparison with aggregated real data”. In: *International Journal of Hydrogen Energy* 46.35 (May 2021), pp. 18630–18643. DOI: [10.1016/j.ijhydene.2021.02.224](https://doi.org/10.1016/j.ijhydene.2021.02.224).
- [12] K. Reddi et al. “Impact of hydrogen SAE J2601 fueling methods on fueling time of light-duty Fuel Cell Electric vehicles”. In: *International Journal of Hydrogen Energy* 42.26 (June 2017), pp. 16675–16685. DOI: [10.1016/j.ijhydene.2017.04.233](https://doi.org/10.1016/j.ijhydene.2017.04.233).
- [13] R. H. Liebeck. “Design of the Blended Wing Body Subsonic Transport”. In: *Journal of aircraft* 41 (Feb. 2004), pp. 10–25.
- [14] J. S. M. Ali and M. M. Saleh. “Experimental and Numerical Study on the Aerodynamics and Stability Characteristics of a Canard Aircraft”. In: *Journal of Advanced Research in Fluid Mechanics and Thermal Sciences* 53 (2019), pp. 165–174.
- [15] JOUAV. OUAV successfully delivered the first hydrogen-powered vertical take-off and landing (VTOL) fixed-wing UAV. May 2021.
- [16] F. Götten et al. “Full configuration drag estimation of short-to-medium range fixed-wing UAVs and its impact on initial sizing optimization”. In: *CEAS Aeronautical Journal* (2021).
- [17] G. Nugroho, G. Zuliardiansyah, and A. Rasyiddin. “Performance Analysis of Empennage Configurations on a Surveillance and Monitoring Mission of a VTOL-Plane UAV Using a Computational Fluid Dynamics Simulation”. In: *Aerospace MDPI* (2022).
- [18] S. Almeida and A. Danna. High Endurance Rapidly Deployable Collaborative UAS (HERD-CU) Critical Design Document. Sept. 2021.
- [19] N. Levin and M. Staleman. Interview with CEO Robert Miller of Eye Above Anti-Poaching Drone Project. May 2022.
- [20] P. Rajendran et al. “Electric Propulsion System Sizing for Small Solar-powered Electric Unmanned Aerial Vehicle”. In: *International Journal of Applied Engineering Research* 11 (Sept. 2016), pp. 9419–9423.

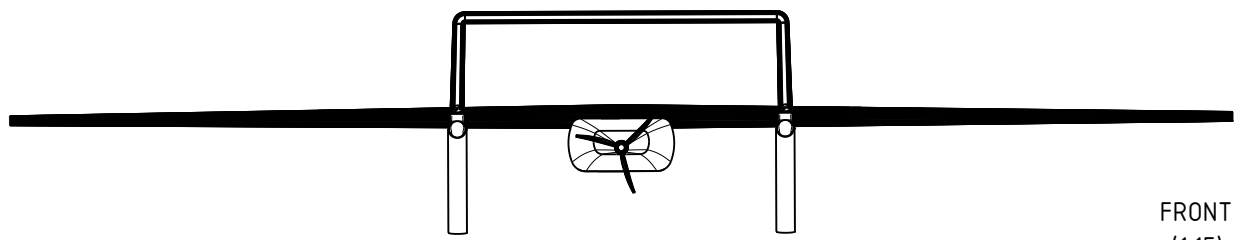
- [21] B. Smith et al. “eVTOL Rotor Noise in Ground Effect”. In: Center for Mobility with Vertical Lift (MOVE) (2021).
- [22] A. Saeed et al. “A survey of hybrid Unmanned Aerial Vehicles”. In: Progress in Aerospace Sciences 98 (2018). DOI: <https://doi.org/10.1016/j.paerosci.2018.03.007>.
- [23] M. Rehan et al. “Vertical take-off and landing hybrid unmanned aerial vehicles: An overview”. In: The Aeronautical Journal (2022), pp. 1–41. DOI: [10.1017/aer.2022.29](https://doi.org/10.1017/aer.2022.29).
- [24] S. Pedro et al. “Design and performance quantification of VTOL systems for a canard aircraft”. In: The Aeronautical Journal 125.1292 (2021), pp. 1768–1791. DOI: [10.1017/aer.2021.63](https://doi.org/10.1017/aer.2021.63).
- [25] Y. Govdeli, A. Tran, and E. Kayacan. “Multiple Modeling and Fuzzy Switching Control of Fixed-Wing VTOL Tilt-Rotor UAV”. In: Fuzzy Techniques: Theory and Applications. 2019, pp. 270–284. ISBN: 978-3-030-21920-8.
- [26] E. Cetinsoy et al. “Design and construction of a novel quad tilt-wing UAV”. In: Mechatronics 22.6 (2012). Special Issue on Intelligent Mechatronics (LSMS2010 & ICSEE2010), pp. 723–745. ISSN: 0957-4158. DOI: <https://doi.org/10.1016/j.mechatronics.2012.03.003>.
- [27] K. Masuda and K. Uchiyama. “Robust Control Design for Quad Tilt-Wing UAV”. In: Aerospace 5.1 (2018). ISSN: 2226-4310. DOI: [10.3390/aerospace5010017](https://doi.org/10.3390/aerospace5010017).
- [28] A. Reyes. “Design and development of an UAV with hybrid flight capabilities”. MA thesis. Center for Research in Optics, Aug. 2018.
- [29] A. Bacchini et al. “Impact of lift propeller drag on the performance of eVTOL lift+cruise aircraft”. In: Aerospace Science and Technology 109 (2021), p. 106429. ISSN: 1270-9638. DOI: <https://doi.org/10.1016/j.ast.2020.106429>.
- [30] Y. Rahman et al. “Design and Fabrication of Small Vertical-Take-Off-Landing Unmanned Aerial Vehicle”. In: MATEC Web Conf. 152 (2018). DOI: [10.1051/mateconf/201815202023](https://doi.org/10.1051/mateconf/201815202023).
- [31] J. D. Gage. Deep-Sea Biology: A Natural History of Organisms at the Deep-Sea Floor. Cambridge University Press, 1991.
- [32] M.H.Sadraey. “Aircraft Design A Systems Engineering Approach”. In: John Wiley & Sons (2013).
- [33] L. Cistriani. “Falco UAV Low Reynolds Airfoil Design and Testing at Galileo Avionica”. In: UAV Design Processes / Design Criteria for Structures (2007), pp. 1–24.
- [34] D. P. Raymer. Aircraft design: A conceptual approach. 3rd ed. American Institute of Aeronautics and Astronautics, 1999.
- [35] R. Vos, J. Melkert, and B. Zanderben. Aerospace Design and Systems Engineering Elements I-AE1222-II (slides). 2019.
- [36] S. HOERNER. FLUID-DYNAMIC DRAG Practical Information on AERODYNAMIC DRAG and HYDRO-DYNAMIC RESISTANCE. second. 1992.
- [37] Z. Sahwee. “Drag Assessment of Vertical Lift Propeller in Forward Flight for Electric Fixed-Wing VTOL Unmanned Aerial Vehicle”. In: IOP Electronic (2019).
- [38] F. Oliviero. Requirement Analysis and Design principles for A/C stability & control (Part 1) (slides). 2022.
- [39] W. Morales and J. Pertierra. “CFD-Based Method for Validation of DATCOM and Potential Flow Stability and Control Derivatives”. In: (2021).
- [40] K. Darlami et al. “Design and Analysis of Twin-Vertical-Tailed Fixed-Wing Unmanned Aerial Vehicle”. In: Journal of Automation and Automobile Engineering 5.3 (2020), pp. 12–30.
- [41] Y. Gao, G. An, and C. Zhi. Test Techniques for Flight Control Systems of Large Transport Aircraft. Science Direct, 2021.
- [42] J. An et al. “Advanced Sizing Methodology for a Multi-Mode eVTOL UAV Powered by a Hydrogen Fuel Cell and Battery”. In: Aerospace 9.2 (2022). ISSN: 2226-4310. DOI: [10.3390/aerospace9020071](https://doi.org/10.3390/aerospace9020071).
- [43] N. Pynaert. “A methodology for design, analysis and optimization of a vertical take-off system for rigid-wing airborne wind energy systems”. MA thesis. Delft University of Technology, Jan. 2020.
- [44] A. Kamal and A. Ramires-Serrano. “Design methodology for hybrid (VTOL + Fixed wing) unmanned aerial vehicles”. In: Aeronautics and Aerospace Open Access Journal (2018).
- [45] M. Tyan et al. “Comprehensive preliminary sizing/resizing method for a fixed wing - VTOL electric UAV”. In: Aerospace Science and Technology (2017).

- [46] B. Magliozzi. *Aeroacoustics of Flight Vehicles: Theory and Practice*. Volume 1: Noise Sources. 1991. Chap. Propeller and Propfan Noise.
- [47] D. Simons and M. Snellen. Course AE4431, Aircraft Noise and Emissions. Aug. 2021. Chap. Introduction to general acoustics and aircraft noise.
- [48] J. Michael. *Aircraft Noise*. Cambridge Aerospace Series. Cambridge University Press, 1989. DOI: [10.1017/CB09780511584527](https://doi.org/10.1017/CB09780511584527).
- [49] R. Heffner and H. Heffner. "Hearing in the elephant (*Elephas maximus*): absolute sensitivity, frequency discrimination, and sound localization". In: *Journal of comparative and physiological psychology* 96.6 (1982), pp. 926–944.
- [50] K. Attenborough. "Sound Propagation in the Atmosphere". In: Jan. 2014, pp. 117–155. DOI: [10.1007/978-1-4939-0755-7\\_4](https://doi.org/10.1007/978-1-4939-0755-7_4).
- [51] M. F. Ashby. *Materials Selection in Mechanical Design*. fourth. Elsevier, 2011.
- [52] W. Callister and D. Rethwisch. *Materials Science And Engineering - An Introduction*. seventh. John Wiley and Sons Ltd, Feb. 2006.
- [53] Y. Yılıkçı and F. Findik. "A Survey of Aircraft Materials: Design for Airworthiness and Sustainability". In: *Periodicals of Engineering and Natural Sciences (PEN)* 1 (June 2013). DOI: [10.21533/pen.v1i1.13](https://doi.org/10.21533/pen.v1i1.13).
- [54] Y. Yongxiang et al. "Recycling of composite materials". In: *Chemical Engineering and Processing: Process Intensification* 51 (2012). Delft Skyline Debate, pp. 53–68. DOI: <https://doi.org/10.1016/j.cep.2011.09.007>.
- [55] B. Wang et al. "Readily recyclable carbon fiber reinforced composites based on degradable thermosets: a review". In: *Green Chem.* 21 (21 2019), pp. 5781–5796. DOI: [10.1039/C9GC01760G](https://doi.org/10.1039/C9GC01760G).
- [56] W. Post et al. "A Review on the Potential and Limitations of Recyclable Thermosets for Structural Applications". In: *Polymer Reviews* 60.2 (2020), pp. 359–388. DOI: [10.1080/15583724.2019.1673406](https://doi.org/10.1080/15583724.2019.1673406).
- [57] J. Gronostajski, H. Marciniak, and A. Matuszak. "New methods of aluminium and aluminium-alloy chips recycling". In: *Journal of Materials Processing Technology* 106.1 (2000), pp. 34–39. ISSN: 0924-0136. DOI: [https://doi.org/10.1016/S0924-0136\(00\)00634-8](https://doi.org/10.1016/S0924-0136(00)00634-8).
- [58] Y. Kaushik. "A Review on use of Aluminium Alloys in Aircraft Components". In: *i-manager's Journal on Material Science* 3 (Dec. 2015), pp. 33–38.
- [59] J. Melkert and C. Rans. Buckling, AE2135-I Structural Analysis Design (slides). 2021.
- [60] J. Melkert and C. Rans. Shear, AE2135-I Structural Analysis Design (slides). 2021.
- [61] J. Melkert and C. Rans. Torsion, AE2135-I Structural Analysis Design (slides). 2021.
- [62] S. Gupta et al. "Designing of an aircraft based on preliminary mission requirement - 2". In: (Apr. 2018). DOI: [10.13140/RG.2.2.28985.26727](https://doi.org/10.13140/RG.2.2.28985.26727).
- [63] M. Niu. *Airframe Stress Analysis and Sizing*. second. Hong Kong Conmilet Press LTD., 1997.
- [64] J. Gundlach. "Designing Unmanned Aircraft Systems (A Comprehensive Approach)". In: 697 (2012). DOI: [10.2514/4.868443](https://doi.org/10.2514/4.868443).
- [65] C. Dario. *The Future of the Drone Economy*. white paper. Levitate Capital. Dec. 2021.
- [66] J. Markish. *Valuation Techniques for Commercial Aircraft Program Design*. 2002.

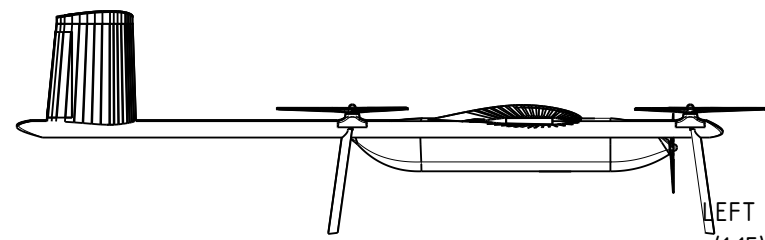
# A

## Catia Technical Drawings

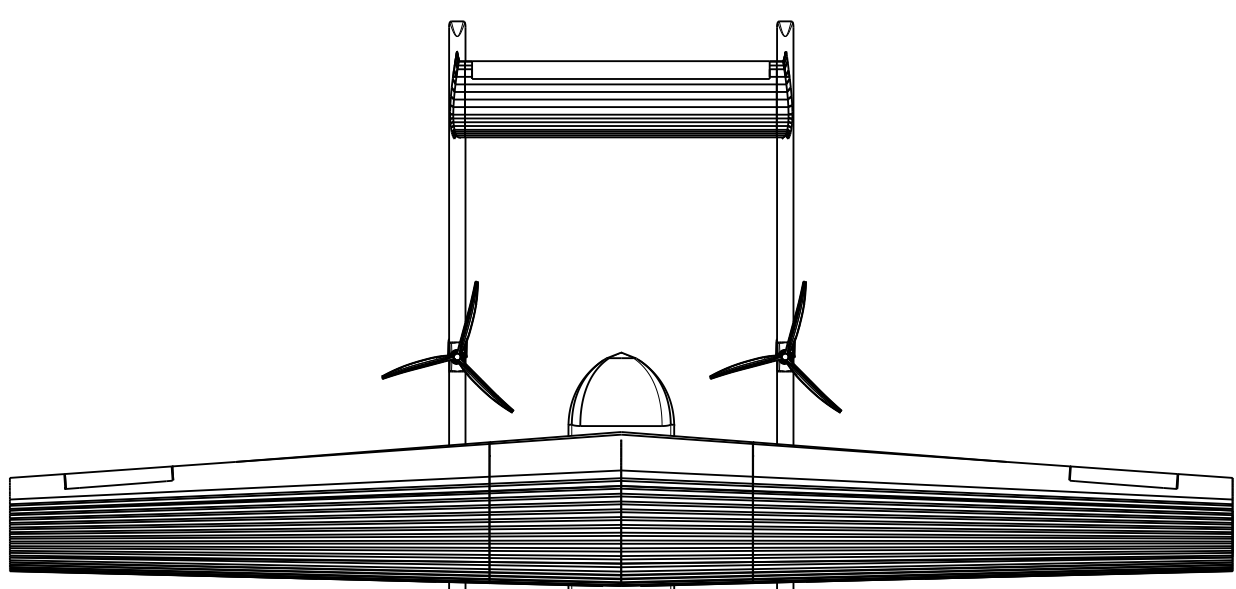
In this Appendix draft drawings of the UAV and the Ground station and their various components can be found.



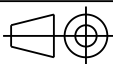
FRONT  
(1:15)



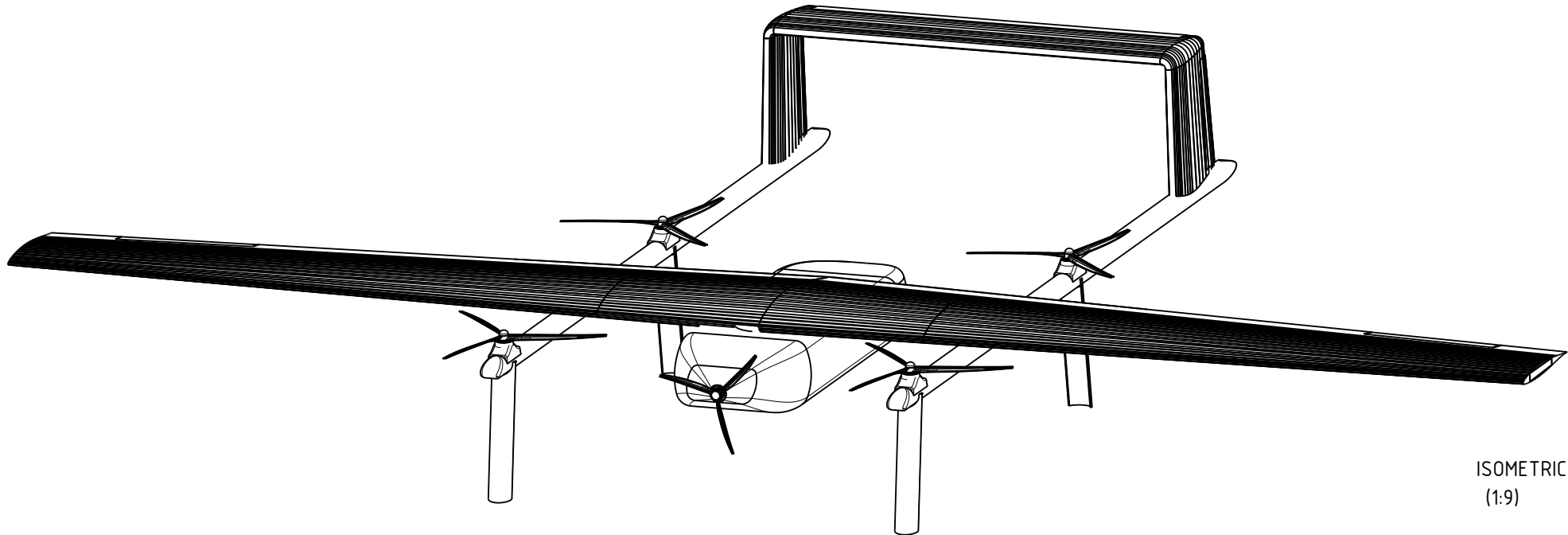
LEFT  
(1:15)



TOP  
(1:15)

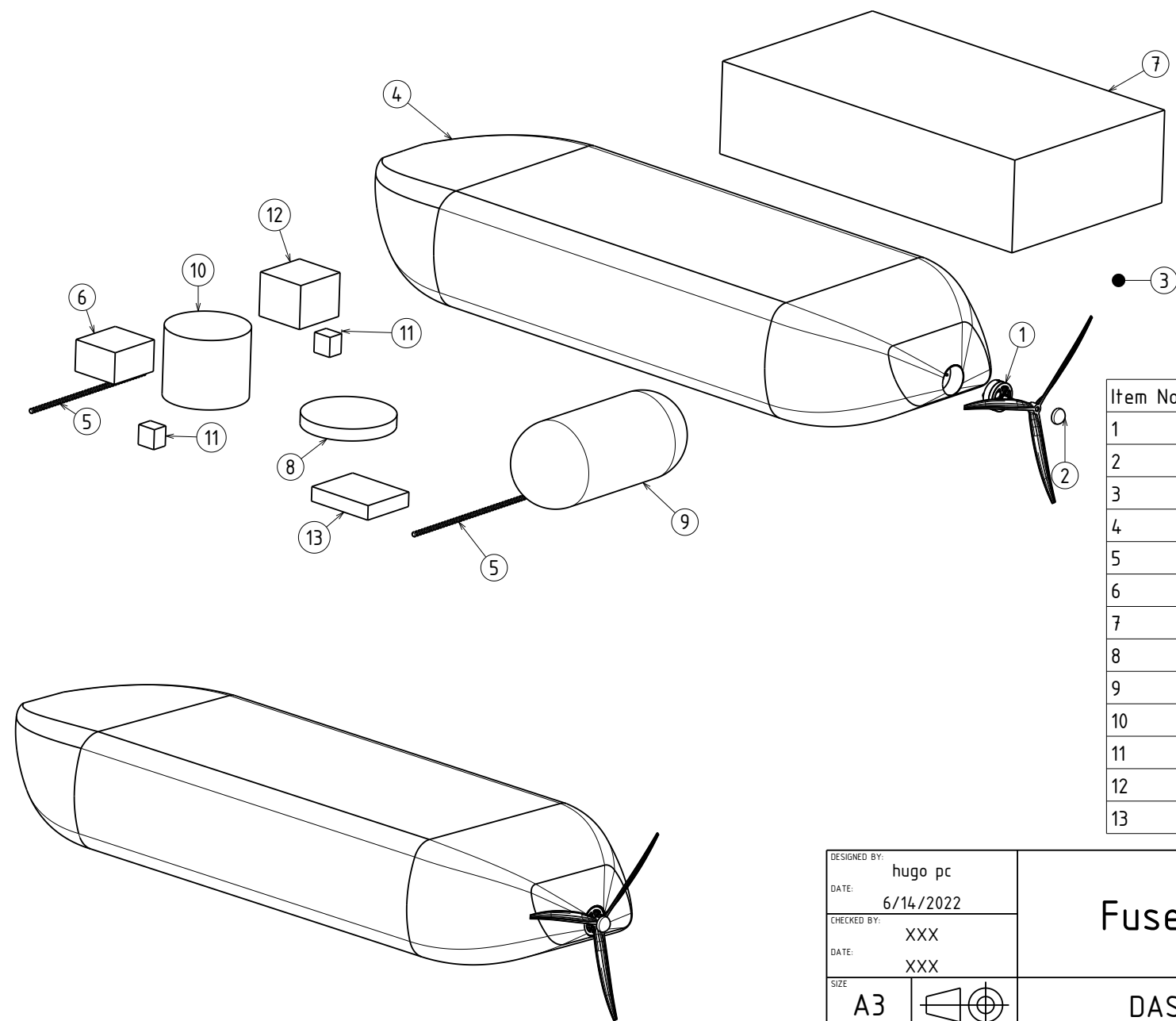
DESIGNED BY: hugo pc		<h1>Usambara</h1>	I	—
DATE: 6/14/2022			H	—
CHECKED BY: XXX		<h2>DASSAULT SYSTEMES</h2>	G	—
DATE: XXX			F	—
SIZE: A3		<h3>DASSAULT SYSTEMES</h3>	E	—
SCALE: 1:15	WEIGHT (kg): XXX		D	—
DRAWING NUMBER: XXX		C	—	
		B	—	
		A	—	
		SHEET 1/6		

This drawing is our property; it can't be reproduced or communicated without our written agreement.



ISOMETRIC  
(1:9)

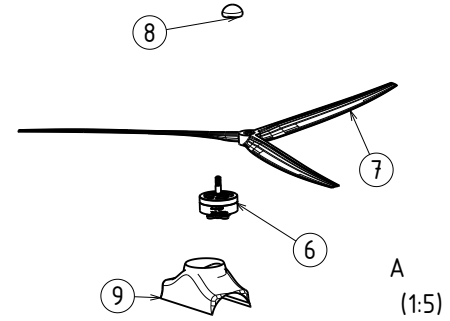
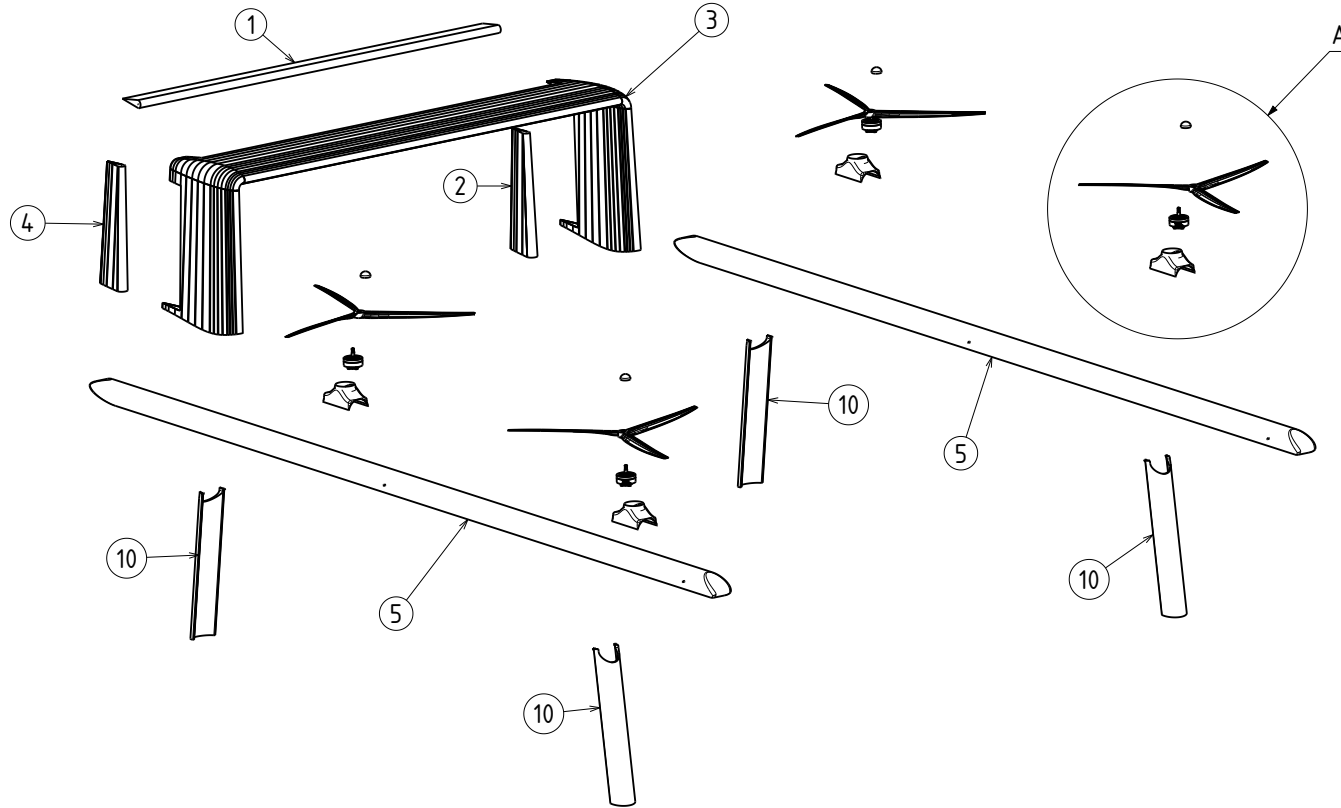
DESIGNED BY: hugo pc		<h1>Usambara</h1>		I	—
DATE: 6/14/2022				H	—
CHECKED BY: XXX				G	—
DATE: XXX		<h2>DASSAULT SYSTEMES</h2>		F	—
SIZE: A3				E	—
SCALE: 1:10	WEIGHT (kg): XXX			D	—
DRAWING NUMBER: XXX		SHEET: 2/6		C	—
This drawing is our property; it can't be reproduced or communicated without our written agreement.				B	—
				A	—



Item No.	Quantity	Title
1	1	BH_Avenger_3008-1300KV
2	1	Cap
3	1	Propeller
4	1	Fuselage
5	2	Antenna
6	1	Autopilot
7	1	Fuel Cell
8	1	GPS
9	1	H2 Tank
10	1	Lidar
11	2	PIR
12	1	Speaker
13	1	Tranceiver

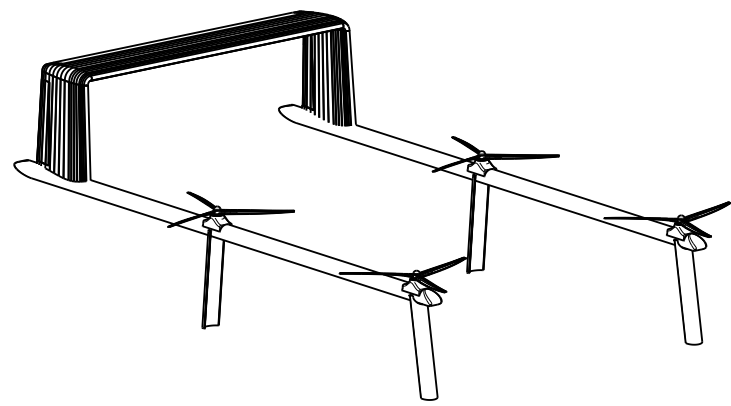
DESIGNED BY: hugo pc		<h1>Fuselage Assembly</h1>		I	—
DATE: 6/14/2022				H	—
CHECKED BY: XXX		<h2>DASSAULT SYSTEMES</h2>		G	—
DATE: XXX				F	—
SIZE: A3		<h3>3/6</h3>		E	—
SCALE: 1:15	WEIGHT (kg): XXX			D	—
DRAWING NUMBER: XXX		SHEET: 3/6		C	—
This drawing is our property; it can't be reproduced or communicated without our written agreement.				B	—
				A	—

ISOMETRIC  
(1:10)



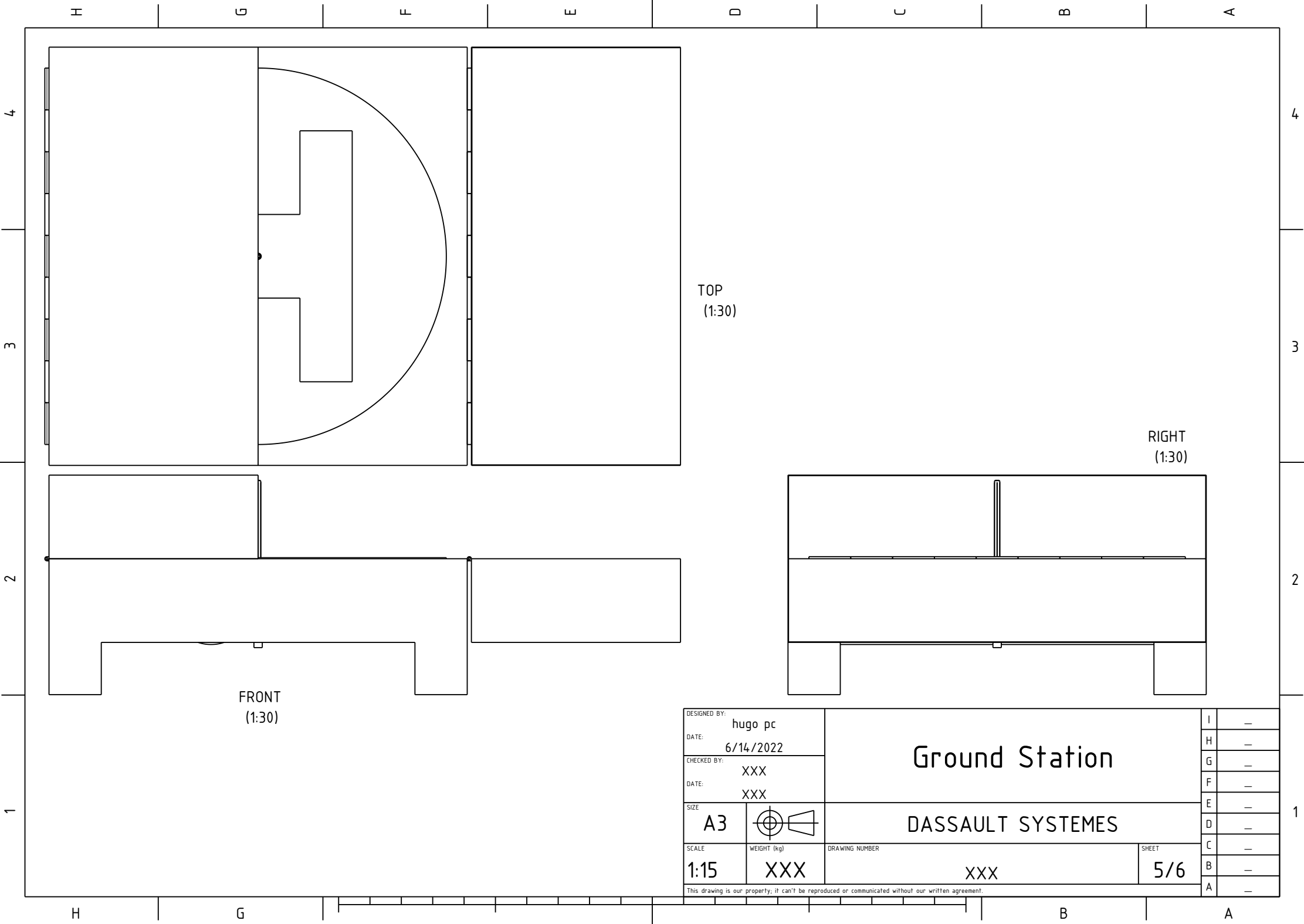
Item No.	Quantity	Title
1	1	Tail Assembly
2	2	boom assembly

Item No.	Quantity	Title
1	1	Tail control surface
2	1	Tail vertical control surfaces
3	1	tail design
4	1	Symmetry of Tail vertical control surfaces
5	2	Boom
6	4	BH_Avenger_3008-1300KV
7	4	Propeller
8	4	Cap
9	4	Motor mount
10	4	Landing gear V2



ISOMETRIC  
(1:15)

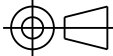
DESIGNED BY: hugo pc		<h1>Tail + Boom Assembly</h1>	I	—
DATE: 6/14/2022			H	—
CHECKED BY: XXX		<h2>DASSAULT SYSTEMES</h2>	G	—
DATE: XXX			F	—
SIZE: A3		<h3>4/6</h3>	E	—
SCALE: 1:15			WEIGHT (kg): XXX	D
DRAWING NUMBER: XXX		C	—	
SHEET: 4/6		B	—	
This drawing is our property; it can't be reproduced or communicated without our written agreement.		A	—	



TOP  
(1:30)

RIGHT  
(1:30)

FRONT  
(1:30)

DESIGNED BY: hugo pc		<h1>Ground Station</h1>	I	—
DATE: 6/14/2022			H	—
CHECKED BY: XXX		<h2>DASSAULT SYSTEMES</h2>	G	—
DATE: XXX			F	—
SIZE: A3		<h3>DASSAULT SYSTEMES</h3>	E	—
SCALE: 1:15	WEIGHT (kg): XXX		D	—
DRAWING NUMBER: XXX		C	—	
		B	—	
		A	—	
		SHEET: 5/6		

This drawing is our property; it can't be reproduced or communicated without our written agreement.

H G F E D C B A

4

3

2

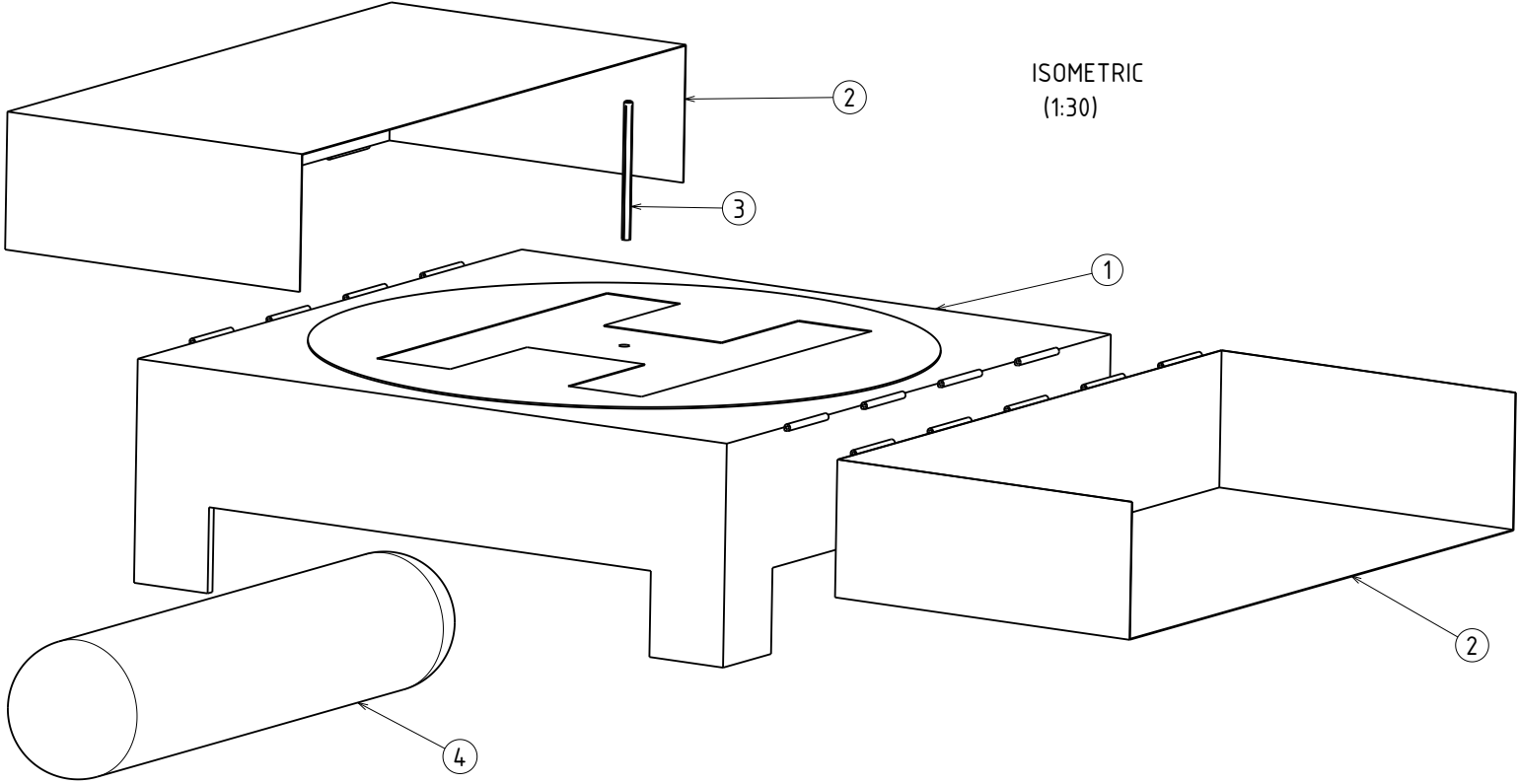
1

4

3

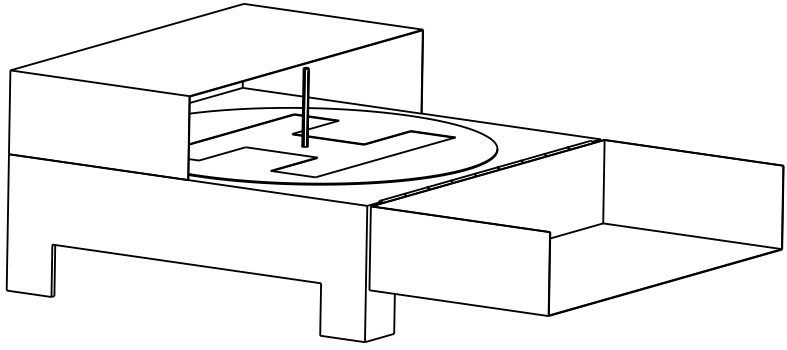
2

1



ISOMETRIC  
(1:30)

Item No.	Quantity	Title
1	1	Ground Station Base
2	2	Ground Station door
3	1	Refuelling rod
4	1	External tank



ISOMETRIC  
(1:50)

DESIGNED BY: hugo pc		<h1>Ground Station</h1>	I	—
DATE: 6/14/2022			H	—
CHECKED BY: XXX		<h2>DASSAULT SYSTEMES</h2>	G	—
DATE: XXX			F	—
SIZE: A3		<h3>6/6</h3>	E	—
SCALE: 1:50			WEIGHT (kg): XXX	D
DRAWING NUMBER: XXX		C	—	
SHEET: 6/6		B	—	
This drawing is our property; it can't be reproduced or communicated without our written agreement.		A	—	

H G F E D C B A

H G F E D C B A

4

4

3

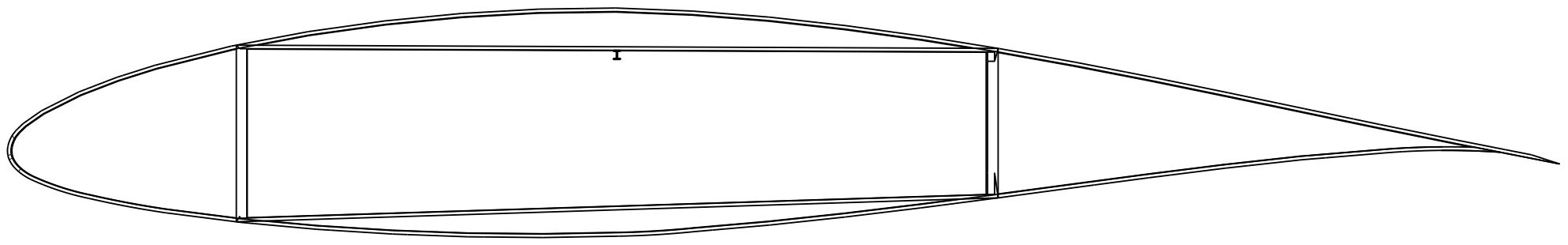
3

2

2

1

1



DESIGNED BY: hugo pc		Wing Cross Section		I	-
DATE: 6/15/2022				H	-
CHECKED BY: XXX		DASSAULT SYSTEMES		G	-
DATE: XXX				F	-
SIZE: A3		DASSAULT SYSTEMES		E	-
SCALE: 1:1	WEIGHT (kg): XXX			D	-
DRAWING NUMBER: XXX		SHEET: 1/1		C	-
This drawing is our property; it can't be reproduced or communicated without our written agreement.				B	-
				A	-

H G F E D C B A